

12-2019

## Relevance of FGFR1 and its Isoforms in Prostate Cancer Bone Metastases

Estefania Labanca

Follow this and additional works at: [https://digitalcommons.library.tmc.edu/utgsbs\\_dissertations](https://digitalcommons.library.tmc.edu/utgsbs_dissertations)



Part of the [Translational Medical Research Commons](#)

---

### Recommended Citation

Labanca, Estefania, "Relevance of FGFR1 and its Isoforms in Prostate Cancer Bone Metastases" (2019). *The University of Texas MD Anderson Cancer Center UTHealth Graduate School of Biomedical Sciences Dissertations and Theses (Open Access)*. 987.  
[https://digitalcommons.library.tmc.edu/utgsbs\\_dissertations/987](https://digitalcommons.library.tmc.edu/utgsbs_dissertations/987)


This Dissertation (PhD) is brought to you for free and open access by the The University of Texas MD Anderson Cancer Center UTHealth Graduate School of Biomedical Sciences at DigitalCommons@TMC. It has been accepted for inclusion in The University of Texas MD Anderson Cancer Center UTHealth Graduate School of Biomedical Sciences Dissertations and Theses (Open Access) by an authorized administrator of DigitalCommons@TMC. For more information, please contact [digitalcommons@library.tmc.edu](mailto:digitalcommons@library.tmc.edu).

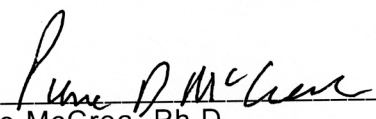
RELEVANCE OF FGFR1 AND ITS ISOFORMS IN PROSTATE CANCER BONE  
METASTASES

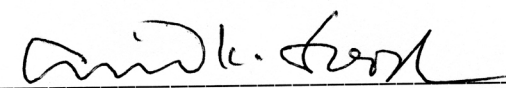
by

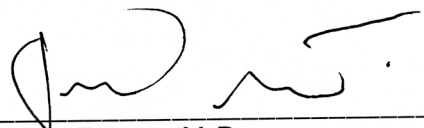
*Estefania Labanca, B.S.*


APPROVED:

  
\_\_\_\_\_  
Nora Navone, M.D., Ph.D.  
Advisory Professor

  
\_\_\_\_\_  
Pierre McCrea, Ph.D.

  
\_\_\_\_\_  
Anil Sood, M.D.

  
\_\_\_\_\_  
Juan Fueyo, M.D.

  
\_\_\_\_\_  
Fen Wang, Ph.D.

APPROVED:

\_\_\_\_\_  
Dean, The University of Texas  
MD Anderson Cancer Center UTHealth Graduate School of Biomedical  
Sciences



RELEVANCE OF FGFR1 AND ITS ISOFORMS IN PROSTATE CANCER BONE  
METASTASES

A

DISSERTATION

Presented to the Faculty of

The University of Texas

MD Anderson Cancer Center UTHealth

Graduate School of Biomedical Sciences

in Partial Fulfillment

of the Requirements

for the Degree of

DOCTOR OF PHILOSOPHY

by

Estefania Labanca, B.S.  
Houston, Texas

December, 2019

*"Dans la vie, rien n'est à craindre, tout est à comprendre.*

*On ne fait jamais attention à ce qui a été fait; on ne voit que ce qui reste à faire"*

Marie Curie

*Nothing in life is to be feared, it is only to be understood.  
One never notices what has been done; one can only see what remains to be done.*

## **Dedication**

*To my family.*

*A special mention to Mateo and Sofia,  
who are in my heart every single day  
even though we are kilometers away.*

## **Acknowledgments**

I would like to acknowledge my mentor Dr. Navone for welcoming me into her laboratory and for her confidence in my potential and constant guidance throughout this entire journey. I am thankful for your trust, freedom and support in me to take risks and search new challenges, “one step at a time”. Not only I have learnt outstanding science from your vast experience, but I have been instructed and inspired in many aspects of life.

I sincerely thank my Advisory Committee members Dr. McCrea, Dr. Sood, Dr. Fueyo, Dr. Wang and Dr. Gallick (who followed my progress until the very last day), for their valuable input in research and in my development as a scientist. Thank you for getting involved with the project, for suggesting alternatives, providing feedback and challenging me endlessly to produce the best outcomes. I extend my gratitude to the additional candidacy exam members, Dr. Rowley and Dr. Mattox. I feel privileged to have had you as part of such fruitful experience. I thank Dr. Friedl and his laboratory for allowing me as a rotation student. I have acquired substantial experience in such a short time.

I would like to acknowledge MD Anderson UTHealth GSBS for providing me the opportunity to perform my studies in such a prestigious institution. I am grateful to all the members of the school, for their great predisposition in actively and patiently answering all my questions time after time and always available to help with any issue that might come across. I also thank the course instructors and lecturers for their inspiring presentations. Thank you to the generous donors that have encouraged my training during these years, the Haar Family and Dr. T.C. Hsu family and friends.

I thank the members of GU Oncology for constituting a great team, for opening the doors of their laboratories and offices with a welcoming smile; and the collaborators that have been instrumental to this project, Dr. Broom, Dr. Chinnaiyan, Dr. Kundra, Ravoori,

Dr. Corn, Dr. Troncoso, Dr. Logothetis and Dr. Gueron (for the trust, bringing out the best of me), for their efforts and assistance. I also acknowledge additional collaborators for taking the time to share their expertise. Thank you all for the fruitful interactions that have enriched my training. I apologize to those that I could not mention specifically. Also, thanks to the Laboratory of Inflammation and Cancer (UBA) for continuously lending a hand.

I am most thankful to current and past members of Dr. Navone's group, Jun, Peter, Mike, Justin, Leah, Xinhai, Jiabin. I am pleased to have shared day by day with such amazing people. I wouldn't have made it without your ceaseless help and hard-work.

I thank all my friends, from Houston (that helped call it home throughout these years) as well as from Argentina who have always been there, for listening, for the support and for the best times shared. Thank you to all my family and extended family for demonstrating motivated interest and being proud of my endeavors. And thanks Preta.

Finally, I would like to thank you Tano for cheering for me, for your comforting hugs in times of need, for celebrating every accomplishment more than myself, and for believing I can achieve whatever I propose myself and more. I extend my immense gratitude to my brother, my sister and my parents, for their immeasurable generosity and love. You have been the power engine and the pillars standing behind all my personal and academic development and education from the very beginning, as well as an example of the strength it requires to not give up and go on. Any acknowledgment is not enough for how grateful I am. A special grand shout-out to my mom, for going above and beyond, for being an outstanding referent, for your comforting and knowledgeable advise in every instance and step of the way, and for transmitting your passion, dedication and your confidence in me. Thank you all for making this journey with me, sharing victories and defeats, feeling that you were close every step of the way, in spite of the distance.

## **Abstract**

### **RELEVANCE OF FGFR1 AND ITS ISOFORMS IN PROSTATE CANCER BONE METASTASES**

Estefania Labanca, B.S.

Advisory Professor: Nora Navone, M.D., Ph.D.

The fibroblast growth factor receptor (FGFR) 1 is implicated in prostate cancer (PCa) progression. Various FGFR1 isoforms have been described and we demonstrate here that the well-characterized FGFR1  $\alpha$  and  $\beta$  isoforms are correlated with the expression of different genes and pathways in human PCa. Direct injection of PC3 PCa cells overexpressing FGFR1 isoforms into the femur of mice resulted in enhanced tumor growth and reduction in bone volume when compared with PC3 expressing empty vector. However, only PC3 overexpressing FGFR1  $\beta$  was associated with increased osteoclast parameters, suggesting that each isoform may mediate diverse biological effects (similar findings were obtained when using C4-2B PCa cell line). Also, PC3 PCa cells overexpressing FGFR1  $\alpha$  injected intracardially significantly reduced mouse survival ( $P = 0.0001$ ) and PCa cells overexpressing FGFR1  $\alpha$  and  $\beta$  increased the incidence of bone metastases ( $P = 0.00005$  and  $P = 0.025$  compared to controls). Accordingly, immunohistochemical analysis of castration-resistant human PCa bone metastases revealed a significant enrichment of FGFR1 expression compared with treatment-naïve, non-metastatic primary tumors ( $P = 0.0007$ ). Importantly, we demonstrate by RPPA analysis that FGFR1 induces expression of the anchoring filament protein  $\alpha$ -catenin 1

(LAD1) in PC3 cells. Furthermore, *LAD1* gene amplification and LAD1 expression were significantly enriched in castration-resistant human PCa bone metastases ( $P < 0.0001$  and  $P = 0.0048$  respectively) suggesting that LAD1 is implicated in FGFR1-mediated metastases.

In summary, our studies indicate that FGFR1 drives the PCa metastatic phenotype, thus further supporting the development of FGFR blockade as a therapy for metastatic PCa. Our results also suggest that new FGFR1 signatures define pathway activation and this knowledge will help identify markers of pathway inhibition in human PCa. Finally, our findings implicate, for the first time, LAD1 in the metastatic phenotype of a subpopulation of men with PCa.

## Table of Contents

<b>Approval Sheet.....</b>	<b>i</b>
<b>Title Page .....</b>	<b>ii</b>
<b>Quote.....</b>	<b>iii</b>
<b>Dedication.....</b>	<b>iv</b>
<b>Acknowledgments.....</b>	<b>v</b>
<b>Abstract.....</b>	<b>vii</b>
<b>List of Illustrations.....</b>	<b>xii</b>
<b>List of Tables.....</b>	<b>xv</b>
<b>Abbreviations .....</b>	<b>xvi</b>
<b>Chapter 1: INTRODUCTION.....</b>	<b>1</b>
Overview of prostate gland and prostate cancer .....	2
Heterogeneity and classification of PCa .....	5
The clinical challenge of PCa treatment-resistance.....	8
Cancer progression to established metastases.....	9
Overview of bone biology and bone metastasis .....	13
Models of metastasis .....	19
The FGF signaling axis.....	20
Role of FGF signaling in bone.....	25
FGF axis in PCa.....	29
FGF family implications in the pathogenesis of PCa bone metastases .....	30
Hypothesis and Aims .....	33



<b>Chapter 2: METHODS</b>	<b>36</b>
BIOINFORMATICS ANALYSIS	37
Data mining from the Prostate Adenocarcinoma Project of The Cancer Genome Atlas (PRAD-TCGA)	37
cBioPortal	38
Ingenuity Pathway Analysis (IPA)	38
IN VITRO EXPERIMENTS	38
Cell lines	38
Plasmid amplification and purification	39
Transfections and transductions	40
Cell treatment	42
Cell sorting	42
Western blot analysis	43
Reverse phase protein array (RPPA)	44
Immunocytochemistry	45
ANIMAL STUDIES	45
Intrabone injection	46
Left ventricle intracardiac Injection	49
Bone histomorphometric analysis	51
Magnetic resonance imaging (MRI)	51
Bioluminescence imaging	52
CLINICAL CORRELATES	52
Immunohistochemistry (IHC) in tissue specimens obtained from human PCa samples	52

STATISTICS .....	54
<b>Chapter 3: RESULTS .....</b>	<b>55</b>
Different human PCa tissue samples express different FGFR1 isoforms.....	56
FGFR1 isoforms are associated with the expression of different genes in human PCa .....	57
FGFR1 alters the bone phenotype induced by PCa cells in tumor-bearing femurs ....	64
FGFR1 isoforms significantly increase PCa bone metastases <i>in vivo</i> .....	74
FGFR1 expression is significantly increased in human PCa bone metastases.....	80
FGFR1 isoforms induce the expression of laminin 1, an anchoring filament protein, in PCa PC3 cells.....	83
<b>Chapter 4: DISCUSSION .....</b>	<b>88</b>
Future Directions.....	93
<b>APPENDIX I.....</b>	<b>99</b>
FGF axis implications in bone metastases of other cancers .....	99
<b>APPENDIX II.....</b>	<b>102</b>
<b>APPENDIX III.....</b>	<b>103</b>
<b>APPENDIX IV .....</b>	<b>104</b>
<b>Bibliography.....</b>	<b>119</b>
<b>Vita.....</b>	<b>142</b>

## List of Illustrations

Figure 1. Diagram of human male anatomy illustrating prostate and surrounding organs and prostate zones.....	3
Figure 2. Types of cells within human prostatic ducts and acini and stages in PCa progression.....	4
Figure 3. A model of PCa progression.....	5
Figure 4. Representative diagram depicting Gleason score.....	6
Figure 5. Spiral model of PCa progression.....	8
Figure 6. The metastatic cascade.....	10
Figure 7. Bone structure.....	15
Figure 8. The bone remodeling cycle.....	16
Figure 9. The vicious cycle of bone metastasis.....	18
Figure 10. Paracrine FGF signaling pathways.....	22
Figure 11. FGF23 endocrine and autocrine/paracrine actions.....	23
Figure 12. Representation of FGFR1 isoforms.....	24
Figure 13. FGFR1 is implicated in PCa bone metastases.....	31
Figure 14. pcDNA3.1+P2A-eGFP vector map.....	41
Figure 15. CMV-Luciferase (firefly)-2A-RFP lentiviral particles.....	42
Figure 16. Method used for intrafemoral injection of cancer cells in mice.....	48
Figure 17. Representative image illustrating method used for intracardiac injection of cancer cells in left ventricle of mice.....	50
Figure 18. Heatmap of the 2,000 genes most highly correlated with FGFR1 isoforms $\alpha$ and $\beta$ in PRAD-TCGA dataset.....	58
Figure 19. Proportion of FGFR1 isoforms-associated pathways.....	60

Figure 20. Most significantly FGFR1 $\alpha$ - and $\beta$ -associated pathways in PRAD-TCGA dataset.....	61
Figure 21. FGFR1 and P-MAPK expression in PCa cells.....	63
Figure 22. Heatmap depicting RPPA results of C4-2B–FGFR1 sublines.....	64
Figure 23. PC3-FGFR1 sublines intrabone injection.....	65
Figure 24. X-ray analysis of mouse femurs injected with PC3-FGFR1 sublines.....	66
Figure 25. MRI analysis of mouse femurs injected with PC3-FGFR1 sublines.....	67
Figure 26. $\mu$ CT analysis of mouse femurs injected with PC3-FGFR1 sublines.....	68
Figure 27. Bone histomorphometry analysis of mouse femurs injected with PC3-FGFR1 sublines.....	70
Figure 28. C4-2B–FGFR1 sublines intrabone injection.....	71
Figure 29. MRI analysis of mouse femurs injected with C4-2B–FGFR1 sublines.....	72
Figure 30. $\mu$ CT analysis of mouse femurs injected with C4-2B–FGFR1 sublines.....	73
Figure 31. Bone histomorphometry analysis of mouse femurs injected with C4-2B–FGFR1 sublines.....	74
Figure 32. Kaplan-Meier survival curves of mice injected intracardially with PC3-FGFR1 $\alpha$ and PC3 control cells.....	75
Figure 33. PC3 sublines injected into the heart of SCID mice.....	76
Figure 34. Rate of bone metastases of PC3-FGFR1 sublines after intracardiac injection into SCID mice.....	77
Figure 35. Examples of histological validation of PC3-FGFR1 sublines bone metastases.....	78
Figure 36. Rate of bone metastases of C4-2B–FGFR1 sublines after intracardiac injection into SCID mice.....	79

Figure 37. Analysis of bioluminescent-positive areas produced by intracardiac injection of C4-2B-FGFR1 sublines.....	80
Figure 38. FGFR1 expression in human PCa.....	81
Figure 39. FGFR1 expression in human prostate tissue.....	82
Figure 40. FGFR1 expression in human PCa bone metastasis.....	83
Figure 41. Heatmap depicting RPPA results of PC3-FGFR1 sublines.....	84
Figure 42. Network identified by IPA using RPPA results of PC3-FGFR1 $\alpha$ -induced genes.....	85
Figure 43. LAD1 expression in PC3-FGFR1 sublines.....	86
Figure 44. <i>LAD1</i> genetic alterations in human prostate adenocarcinoma.....	86
Figure 45. LAD1 expression in human PCa.....	87
Figure 46. A schematic model depicting FGFR1 as a driver of PCa metastatic progression.....	93

## List of Tables

Table 1. List of the 20 genes most highly correlated with FGFR1 $\alpha$ and $\beta$ isoforms in PRAD-TCGA dataset.....	54
---	----

## Abbreviations

AACR	American Association for Cancer Research
aa	amino acids
AKT	protein kinase B
AR	androgen receptor
ATCC	American Type Culture Collection
BCA	bicinchoninic acid
BMP	bone morphogenic proteins
BMU	basic multicellular units
BS	bone surface
BSA	bovine serum albumin
BSP	bone sialoprotein
BV	bone volume
CDH1	E-cadherin
CDH11	OB-cadherin [osteoblast]
CMV	cytomegalovirus
CRPC	castration-resistant prostate cancer
μCT	microcomputed tomography
CTC	circulating tumor cells
CTSK	cathepsin K
DHT	dihydrotestosterone
Dmp1	dentin matrix acidic phosphoprotein 1
DMSO	dimethyl sulfoxide
DNA	deoxyribonucleic acid
DTC	disseminated tumor cells
DTT	dithiothreitol
ECL	enhanced chemiluminescence
<i>E. coli</i>	<i>Escherichia coli</i>
EDTA	ethylenediaminetetraacetic acid
EGTA	ethylene glycol tetraacetic acid
EMT	epithelial to mesenchymal transition
ES	enrichment score

ET1	endothelin 1
FACS	fluorescence-activated cell sorting
FBS	fetal bovine serum
FDA	Food and Drug Administration
FDR	false discovery rate
FFPE	formalin-fixed, paraffin-embedded
FGF	fibroblast growth factor
FGFR	fibroblast growth factor receptor
FGFRL1	FGFR-like 1
FITC	fluorescein isothiocyanate
FRS2 $\alpha$	fibroblast growth factor receptor substrate 2 $\alpha$
FWER	family-wise error rate
GEM	genetically engineered mice
GLS	Glutaminase
GR	glucocorticoid receptor
GSEA	Gene Set Enrichment Analysis
HE	hematoxylin and eosin
HER2	human epidermal growth factor receptor 2
HMW-FGF2	high molecular weight fibroblast growth factor 2
HR	hormone receptors
HRP	horseradish peroxidase
HS	heparan sulfate
HSC	hematopoietic stem cell
HSPG	heparan sulphate proteoglycan
IACUC	Institutional Animal Care and Use Committee
Ig	immunoglobulin
IGF-1	insulin-like growth factor-1
IHC	immunohistochemistry
IL	interleukin
IPA	Ingenuity Pathway Analysis
IVIS	In Vivo Imaging System
LAD1	ladinin 1
LB	Luria-Bertani



LMW-FGF2	low molecular weight fibroblast growth factor 2
MAPK	mitogen-activated protein kinase
MRI	magnetic resonance imaging
mRNA	messenger ribonucleic acid
NES	normalized enrichment score
NIH	National Institutes of Health
Nom. p-val	nominal <i>P</i> value
NSCLC	non-small cell lung cancer
OB	osteoblast
OC	osteocalcin
Oc	osteoclast
Oc.S	osteoclast surface
OPG	osteoprotegerin
OPN	osteopontin
PBS	phosphate-buffered saline
PCa	prostate cancer
PCF	Prostate Cancer Foundation
PDX	patient-derived xenografts
PIN	prostatic intraepithelial neoplasia
PLC $\gamma$	phospholipase C $\gamma$
PRAD-TCGA	Prostate Adenocarcinoma Project of The Cancer Genome Atlas
PSA	prostate-specific antigen
PTH	parathyroid hormone
PTHrP	parathyroid hormone-related protein
RANKL	receptor activator for nuclear factor- $\kappa$ B ligand
RHCL	Research Histology Core Laboratory
RNA	ribonucleic acid
RPKM	reads per kilobase per million
rpm	revolutions per minute
RPPA	reverse phase protein array
Rsv	Rous sarcoma virus
RT-qPCR	real time quantitative polymerase chain reaction
RTU	ready-to-use

RUNX2	Runt-related transcription factor 2 RUNX2
S1P	sphingosine 1-phosphate
SAIF	Small Animal Imaging Facility
SCLC	small cell lung cancer
SD	standard deviation
SDS	sodium dodecyl sulfate
SDS-PAGE	sodium dodecyl sulfate -polyacrylamide gel electrophoresis
SOC	Super Optimal broth with Catabolite repression
SV40	simian virus 40
STAT	signal transducer and activator of transcription
SU2C	Stand Up To Cancer
TBS-T	tris-buffered saline-Tween 20
TCGA	The Cancer Genome Atlas
TE	Tris- ethylenediaminetetraacetic acid
TGF $\beta$	transforming growth factor beta
TKI	tyrosine kinase inhibitor
TNBC	triple-negative breast cancer
TRAP	tartrate-resistant acid phosphatase
tRNA	transfer RNA
TV	tissue volume
UICC	Union for International Cancer Control
VEGF	vascular endothelial growth factor
Wnt	Wingless-related integration site

# **Chapter 1: INTRODUCTION**

This chapter is partly based upon “Navone N.M. and E. Labanca, 2017. Modeling Cancer Metastasis. In: Patient-Derived Xenograft Models of Human Cancer. Molecular and Translational Medicine. Humana Press, Cham. Y. Wang, D. Lin, and P.W. Gout, editors. pp. 93-114”, with permission from Springer International Publishing AG 2017, Springer Nature. License number: 4654420161143.

## **Overview of prostate gland and prostate cancer**

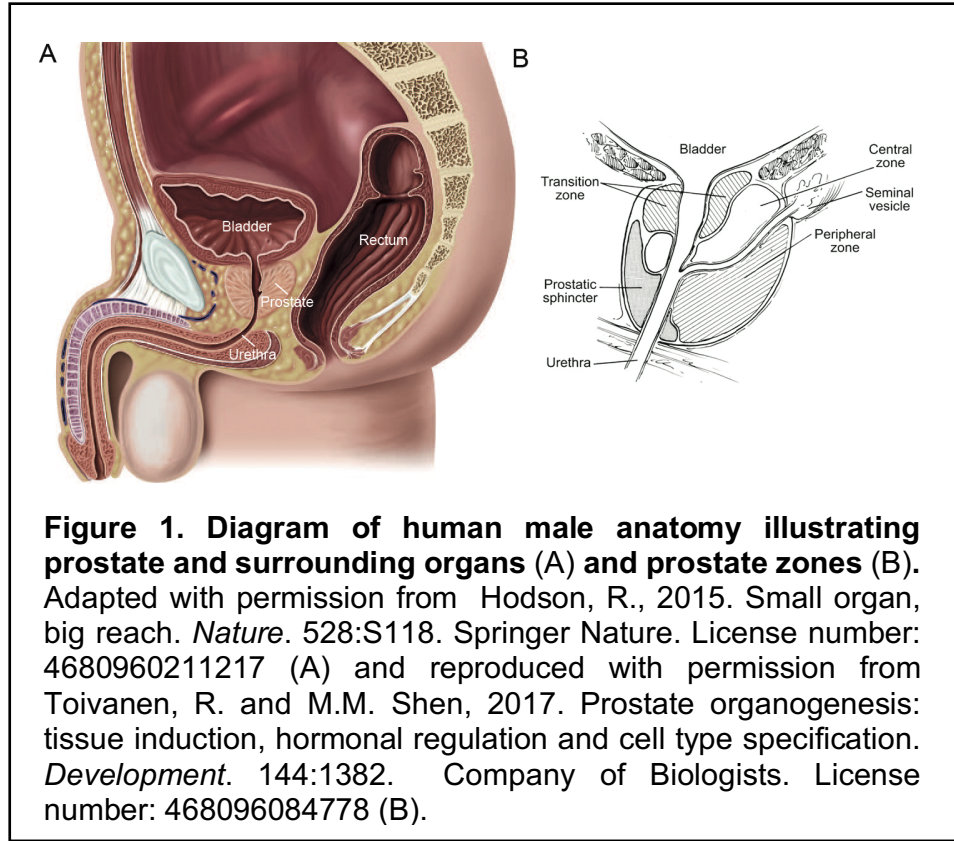
Located below the bladder and surrounding the prostatic urethra, the prostate is a small accessory gland of the male reproductive system (Fig. 1A). Its main role is to secrete fluids that protect the sperm.

Male sex hormones, androgens, including testosterone and dihydrotestosterone (DHT), contribute to prostate growth, in particular, by regulating survival and proliferation of prostate cells. Size increases of this gland can be associated to several prostate conditions: inflammation, benign prostatic hyperplasia, or cancer (Hodson, 2015).

Prostate cancer (PCa) is the second leading cause of cancer deaths in men in the United States (Siegel et al., 2018) and among the most commonly diagnosed cancer worldwide (Bray et al., 2018). Genetic and non-genetic components can be associated to this disease; the major risk factors being age and ethnicity (Cuzick et al., 2014).

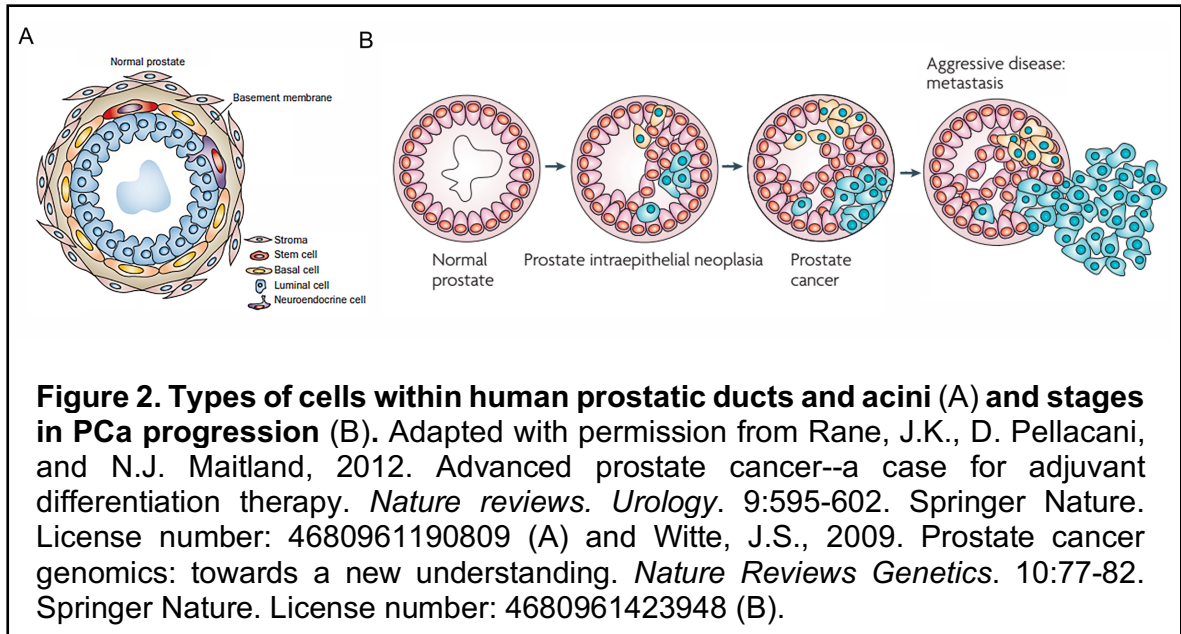
Among the secretion products of the prostate is the prostate-specific antigen (PSA), whose serum levels are currently used as a marker for PCa or other prostate abnormalities, since PSA blood levels vary specifically with perturbations of the gland (Balk et al., 2003). PSA expression is also androgen-regulated (Kim and Coetzee, 2004).

Different anatomic regions, or zones, can be distinguished in the prostate: central, transition and peripheral (Fig. 1B). Most PCa begin in the peripheral zone.



Histologically, the normal human prostate is composed of prostatic glands embedded in a non-glandular stroma (Fig. 2A). The glandular component is comprised by ducts and acini. Each glandular lumen of the ducts and acini is surrounded by an epithelium layer of secretory cells. These cells express androgen receptor (AR), are androgen-dependent and produce the molecules that are secreted as part of the seminal fluids (e.g. PSA).

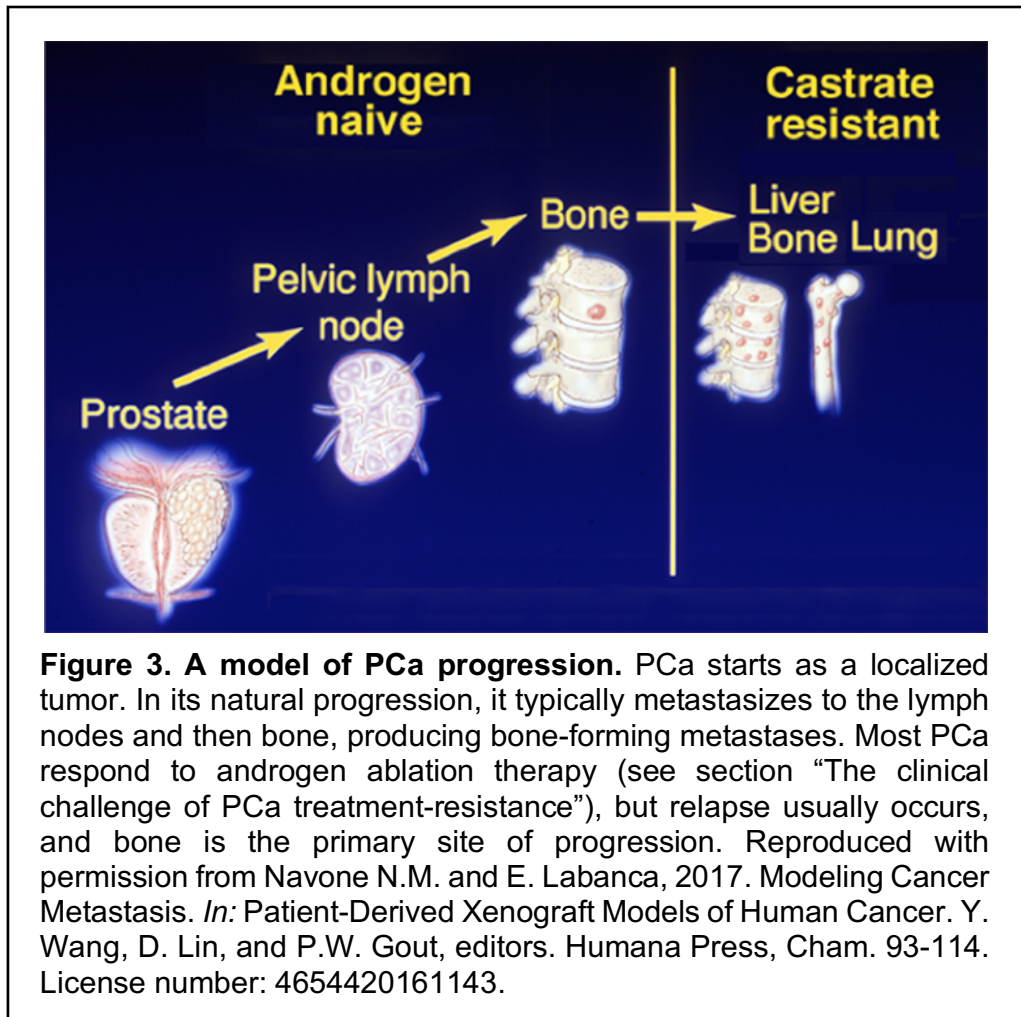
A layer of basal cells encloses these secretory luminal cells. Neuroendocrine cells, androgen-independent, and rarely, stem cells, that are AR-negative, can be found intercalated in the stratum of basal cells. A basement membrane surrounding the basal cells delimits them from the stroma. The non-glandular stroma is mainly fibromuscular stroma, and includes nerves, blood vessels and other components.



A pre-malignant lesion may present as dysplasia, or abnormal growth of cells. In PCa, the prostatic intraepithelial neoplasia (PIN) is the most accepted presumed precursor of PCa (De Marzo et al., 2016; Haffner et al., 2016; Zhou, 2018). However, it is the high-grade PIN (characterized by cells that share many genetic and molecular similarities with cancer cells) which is believed to have clonal, temporal, and spatial relationships with invasive PCa. The transition between high-grade PIN and invasive PCa is believed to result from invasion through the basement membrane into the stroma (localized and locally advanced PCa), which can eventually disseminate to other organs resulting in metastasis (Wang et al., 2018) (Fig. 2B).

In most cases, PCa is an indolent, or slow-growing disease that does not spread; thus, the survival rate is high for the early stages. However, the 5-year survival rate drops from nearly 100% to 29% when the disease has disseminated beyond the local

site (Siegel et al., 2017). Metastatic PCa cells spread through the blood and lymph to lymph nodes and bone primarily (Fig. 3).

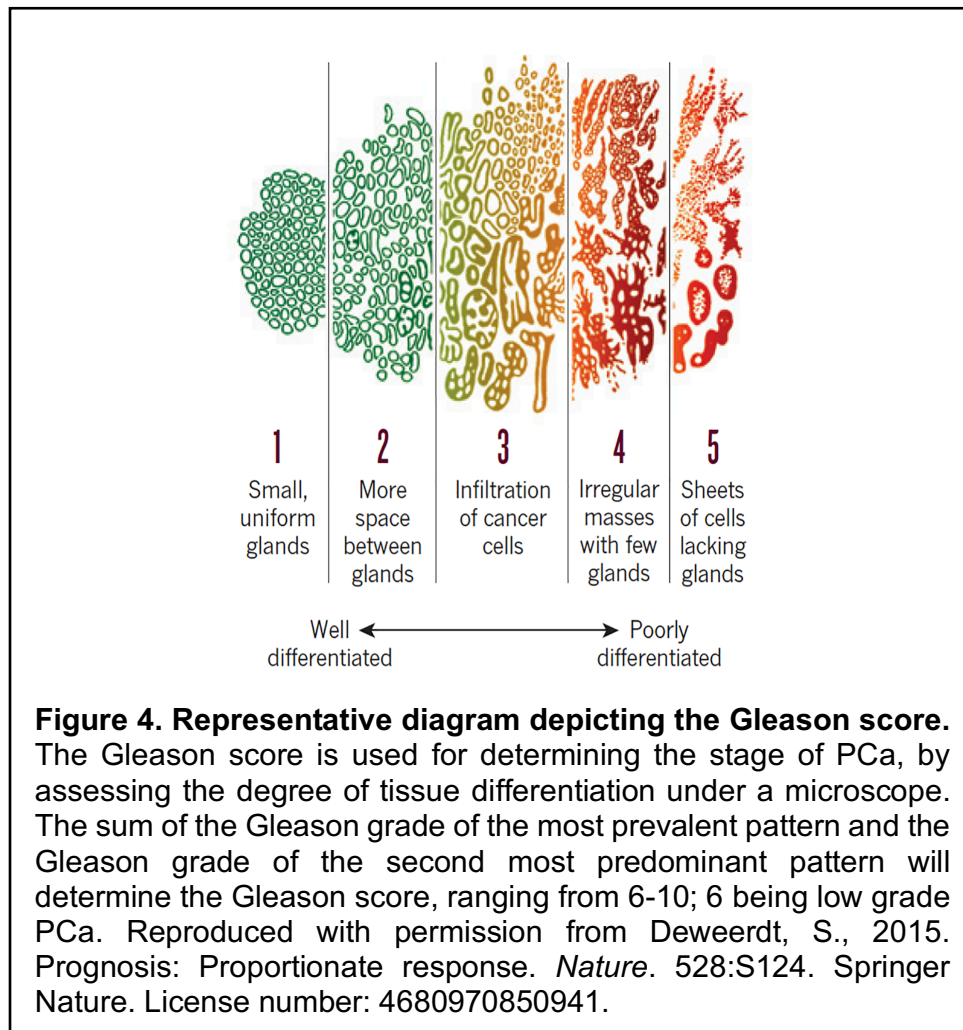


### Heterogeneity and classification of PCa

Solid tumors are typically heterogeneous. The existence of a wide variety of clinical scenarios, from indolent to lethal, evidence the characteristic heterogeneity of PCa.

Morphologically, most PCa are adenocarcinomas, and they are classified using the Gleason score (Union for International Cancer Control, UICC), which is based on the appearance of the tumor under the microscope (Gleason, 1966) (Fig. 4). Because

different areas within a tumor typically have a different Gleason score, which outlines a spatial heterogeneity, the pathologists report the Gleason sum score which considers the two more prevalent scores within the tumor.



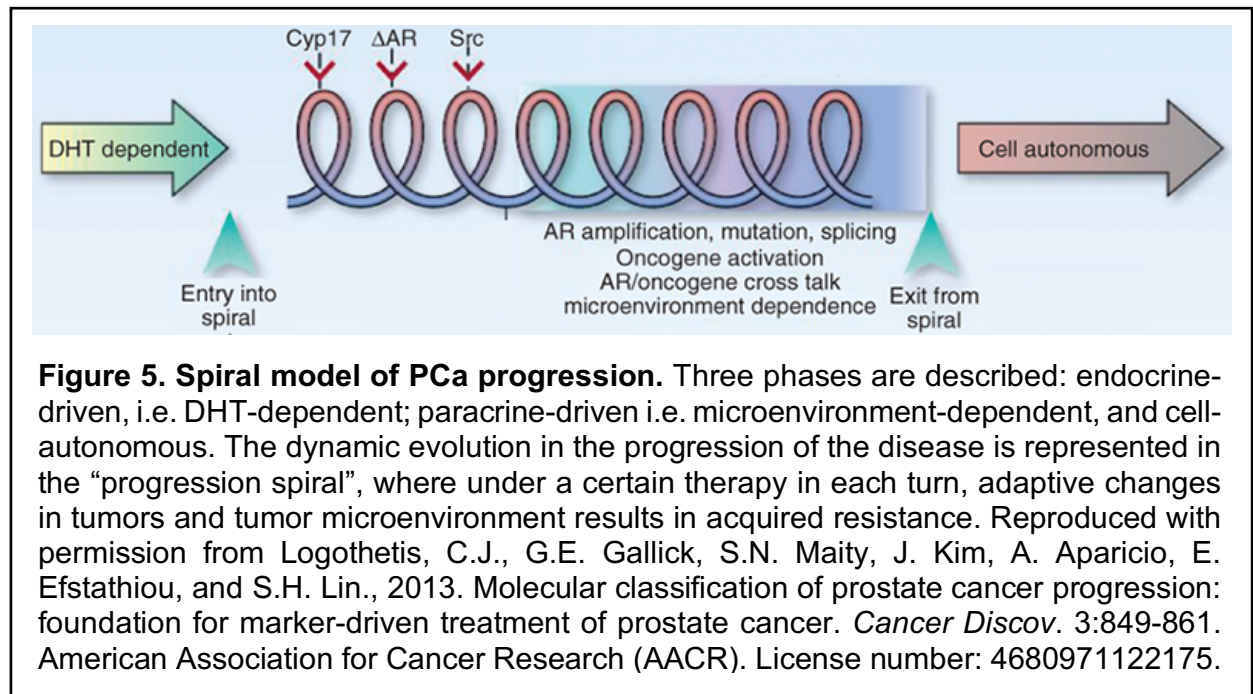
Clinically, the progression from localized and hormone-naïve PCa to castration-resistant PCa (CRPC) may be accompanied by phenotypic divergence. In addition to the classic CRPC metastatic phenotype consisting of osteoblastic bone metastases, high levels of PSA, and responsiveness to androgen deprivation therapy (ADT), the existence of clinically aggressive variants of PCa are increasingly recognized in the clinic, especially



after the introduction of the highly potent AR pathway inhibitors, enzalutamide and abiraterone. Use of these inhibitors is also correlated with an increasingly prevalent morphology and immunohistochemical acquired neuroendocrine-like phenotype (Beltran et al., 2014). The clinical phenotype of these aggressive variants is characterized by the development of rapidly progressive disease involving visceral metastases and hormone refractoriness. Importantly, clinically defined aggressive variants are estimated to account for 40% of lethal PCa (Beltran et al., 2014).

The clinical course of PCa from diagnosis to death has been classified as a series of clinical stages or treatment statuses (e.g., extent of the local disease, hormonal status, absence or presence of detectable metastases on an imaging study). These clinical stages and treatment statuses together with PSA blood levels are used to monitor disease progression and response to treatment. However, investigators have proposed a new molecular classification of PCa that incorporates AR signaling, oncogenes/tumor suppressors, and the tumor-bone microenvironment in the disease model (Logothetis et al., 2013) (Fig. 5). This proposed classification, reflecting the dynamic evolution in the progression of the disease, may facilitate the implementation of current and emerging therapies.

Studies have suggested the existence of clonal evolution of metastases as well as genetic and epigenetic diversity of primary and metastatic clones (de Bruin et al., 2014; Turajlic and Swanton, 2016). This clonal diversity may be reduced or enhanced at both primary and metastatic sites by systemic treatment. The spiral model proposed by (Logothetis et al., 2013) (Fig. 5) reflects the temporal heterogeneity that supports the emergence of pre-existing subclones under selection pressures. Underlining these features is the molecular genetic and epigenetic heterogeneity, that will result in different transcription and metabolic programs (Dagogo-Jack and Shaw, 2017).



### The clinical challenge of PCa treatment-resistance

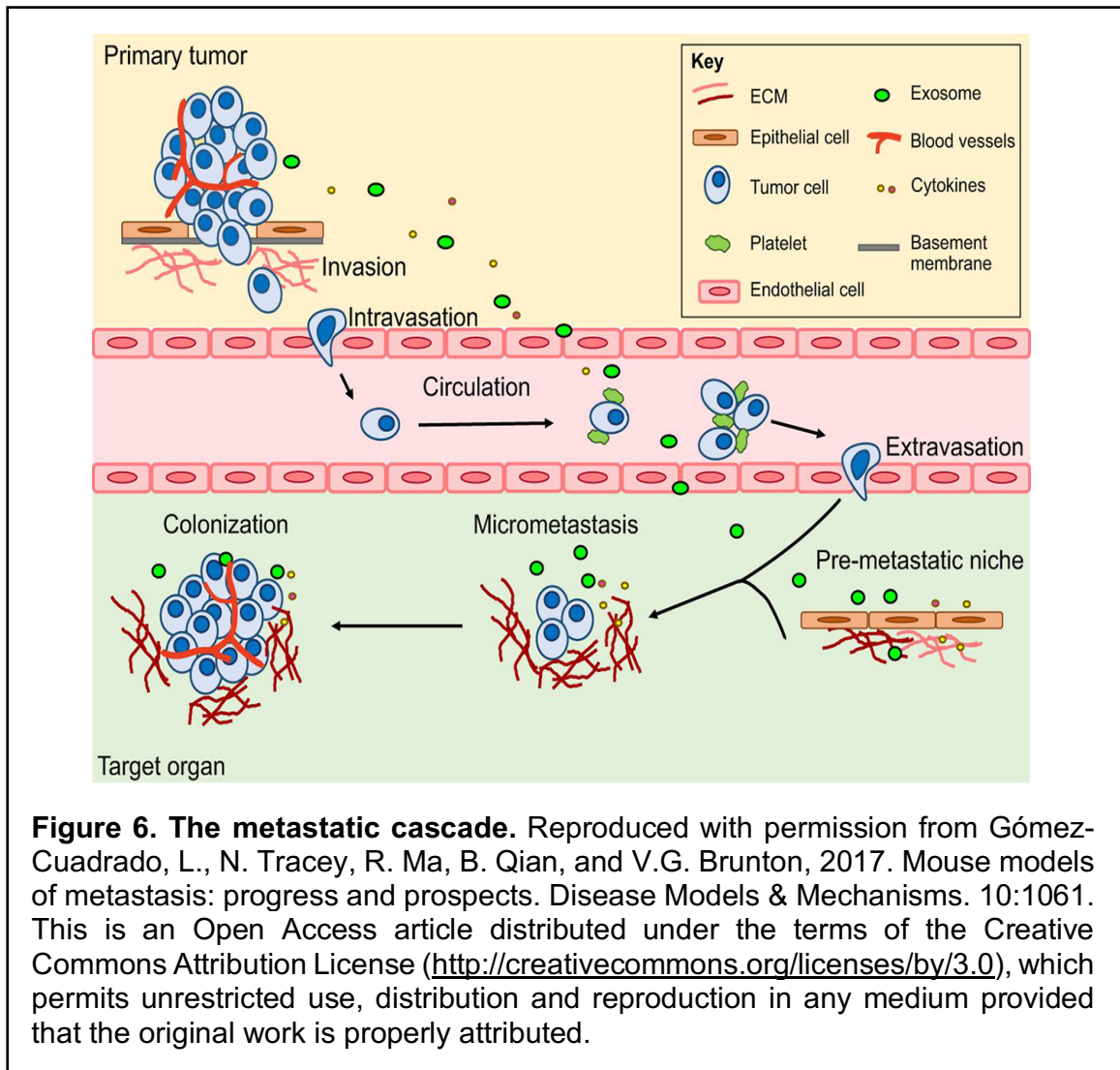
When tumor cells spread and grow in sites noncontiguous to the organ of origin, primary site, and become metastatic, cancer enters a treatment-resilient stage. At this stage, the prospects for a cure using conventional therapy (e.g., surgery, radiotherapy) are greatly reduced. Patients with advanced metastatic PCa have several treatment options, but none of them are curative. Since PCa cells use androgens as fuel to grow, hormone or androgen deprivation (e.g., leuprolide and bicalutamide) is the most effective and first-line therapy, but growth of the cancer resumes over time in most cases, and the disease progresses to CRPC (Watson et al., 2015). Although new-generation drugs for ADT are available and also effective (e.g., abiraterone and enzalutamide), resistance to these therapies eventually emerges. Since there is no available chemotherapy and/or targeted therapy that is curative, disease recurrence and death after several different treatment modalities occur in most cases (Loberg et al., 2005; Watson et al., 2015).

## **Cancer progression to established metastases**

The invasive phenotype, defined by the ability to actively breach or cross tissue barriers, including the bone marrow (Kohrman and Matus, 2017), distinguishes benign from malignant neoplasms (cancer) and is manifested throughout the metastatic process.

Metastases result from a multi-step cascade that cancer cells must undergo to establish tumors at distant sites. In brief, these steps include escape of cancer cells from the primary tumor by local invasion of the surrounding extracellular environment, degradation, and passage through a basement membrane, followed by intravasation into the blood or lymphatic system, survival in circulation (hematogenous and/or lymphatic), arrest at a distant organ (involving lodging in a distant capillary bed), extravasation out of the blood vessel, survival in the new environment, and invasion and proliferation in what is now a foreign cellular microenvironment (establishment of a secondary tumor at a distant site) (reviewed in Talmadge and Fidler, 2010 (Fig. 6)).

The cascade of events that lead to metastatic dissemination starts long before a tumor is clinically detected at a distant site (Hong et al., 2015; Turajlic and Swanton, 2016). Metastatic dissemination possibly continues throughout the progression of the disease. Therefore, the need for precise understanding of the molecular mechanisms underlying each step in the metastatic process is imperative. Longitudinal analyses of human cancer progression in addition to laboratory-based studies have demonstrated the anarchic evolution of metastases, which in some cases caused local recurrence, whereas others had cross-metastatic site seeding (Crockford et al., 2014; Hong et al., 2015; Turajlic and Swanton, 2016). In fact, one study demonstrated the presence of metastatic and primary tumor clones in blood even years after removal of the primary tumor, supporting the concept of the anarchic evolution of metastases (Hong et al., 2015).



The development of metastases constitutes a complex and demanding process cancer cells must overcome to successfully colonize remote organ sites (Massague and Obenauf, 2016; Sethi and Kang, 2011; Talmadge and Fidler, 2010; Turajlic and Swanton, 2016; Valastyan and Weinberg, 2011). Tumor cells must have or acquire specific traits, including restructuring of the cytoskeleton along with transcriptional and epigenetic changes. Furthermore, invasive cells can adopt different morphogenetic programs. When invasive cancer cells utilize a mesenchymal invasion program, the switch from epithelial to mesenchymal cell phenotype is often referred to as epithelial to mesenchymal transition

(EMT) (Kohrman and Matus, 2017). Recently reported evidence indicated that cells are in cell-cycle arrest when they enter an invasive state. This cell-cycle arrest state is frequently associated with the invasive phenotype acquired via EMT (Hagedorn et al., 2013; Kohrman and Matus, 2017; Matus et al., 2010; Matus et al., 2015). The transition to a different morphogenetic program is influenced by the tumor microenvironment.

Stephen Paget's 1889 work proposed that metastasis depends on a cross-talk between cancer cells (the "seeds") and specific organ microenvironments (the "soil"). This hypothesis has been used to account for the non-random and cancer specific distribution of metastases. Furthermore, the concept of the selective nature of metastasis was supported by experimental evidence (Hart and Fidler, 1980). A detailed analysis of experimental metastases in syngeneic mice indicated that mechanical arrest of tumor cells in the capillary bed of distant organs did indeed occur but that subsequent cell proliferation and growth into secondary lesions were influenced by specific organ cells (Hart and Fidler, 1980).

PCa is one of the most striking examples of the selectivity of cancer cells for specific sites of metastasis. Indeed, as PCa progresses, greater than 80% of tumors will develop bone metastases, and the majority will be bone-forming (Catalona, 1994; Cook and Watson, 1968; Hess et al., 2006; Loberg et al., 2005). Other malignancies have a lower, though still significant, incidence of bone metastases, namely breast (50%-60%) (Hess et al., 2006), thyroid (40%), renal (35%), lung (35%), liver (13%), and rectal (10%) carcinoma (Freeman et al., 2015; Hess et al., 2006). Additionally, multiple myeloma, a B cell malignancy, is the second most common haematological malignancy and, characteristically, involves bone during progression (Panaroni et al., 2017). Yet, only PCa has bone as a single, dominant metastatic site (Hess et al., 2006). Also, it was recently

reported that targeting bone metastases in PCa with a bone homing  $\alpha$ -emitting radiopharmaceutical lengthens survival (Parker et al., 2013). Taken together these clinical observations point to a central role of bone metastases in PCa progression.

Following local progression, cancer cells will in some cases acquire traits that allow them to escape the local site and disseminate, eventually, via the blood stream (circulating tumor cells [CTCs]). Once they reach a distant site, they are known as disseminated tumor cells (DTCs). In this context, it is important to distinguish between trafficking cells (cells that are moving freely in organs' blood vessels and capillary beds, not yet growing or invading) and cells that are arrested at certain sites. Currently, there are two lines of thought to explain the process by which a cancer cell will get arrested at certain organ sites but not others: active or passive arrest. Passive arrest is when cancer cells get mechanically trapped in the capillary beds of distant organs, and active arrest is when cancer cells specifically migrate and stay in certain organs by, for example, receptor-mediated tropism. It is worth noting that normal bone houses the hematopoietic stem cell (HSC) niche, which comprises hematopoietic and mesenchymal cell populations, which provide homing signals to HSCs and regulate HSC self-renewal (Taichman et al., 2010). It has been suggested that DTCs can precondition the metastatic niche and compete with and occupy the HSC niche to facilitate metastasis (Decker et al., 2016; Shiozawa et al., 2011).

Arrested cancer cells at organ sites (DTCs) will generally undergo a period of dormancy prior to the development of either micrometastases (metastases composed of small groups of cancer cells that cannot be detected by current diagnostic procedures) or established metastases. The mechanism that makes the cell leave the dormant state and start growing is ill-defined and a subject of intense study. It has been proposed that there

are signals and factors from the metastatic/HSC niche, including c-Myc, vascular endothelial growth factor (VEGF) and fibroblast growth factor (FGF) 2, that can play a role in exiting dormancy (Decker et al., 2016; Shiozawa et al., 2011).

## **Overview of bone biology and bone metastasis**

The human skeleton is constituted of rigid, dense connective tissues, bones, and semi-rigid connective tissue, cartilage. Among its central functions are supporting the body, enabling locomotion, protecting soft tissues, minerals (calcium and phosphate) storage and hematopoiesis within the bone marrow cavity (J. Gordon Betts, 2013).

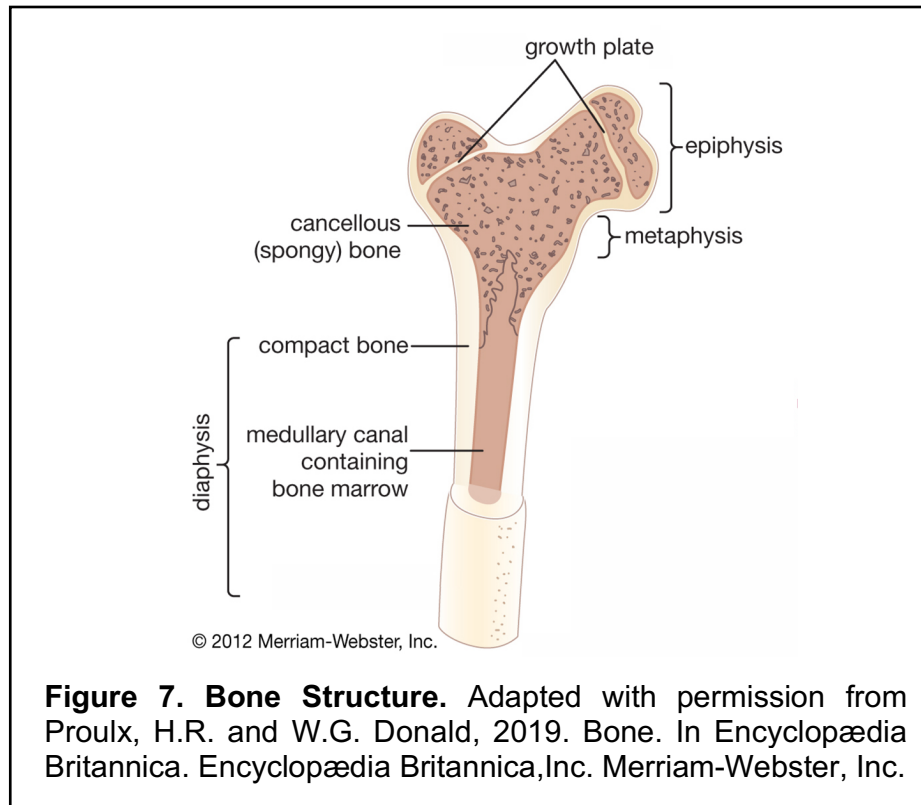
Bone formation in the embryo involves the conversion of preexisting mesenchyme into bone tissue (Gilbert, 2000). Briefly, embryonic skeletogenesis starts with mesenchymal condensation in all prospective bones. The bone tissue is then formed by two different mechanisms: endochondral (axial and appendicular bones) and intramembranous ossification (flat bones of the face, most of the cranial bones, and the clavicles). During endochondral ossification, condensation leads to the formation of a complete cartilaginous skeleton that will eventually be replaced by bone (Rodan, 2003). In intramembranous ossification, mesenchymal condensation is followed directly by ossification centers. Cells then assume osteoblastic features and start depositing bone matrix (consisting of collagen fibers and calcium-derived mineral, hydroxyapatite, mainly) that will go on to mineralize and form the bones (Rodan, 2003). The commitment of mesenchymal stem cells and differentiation into osteoblasts requires expression of Runt-related transcription factor 2 (RUNX2) and Osterix, master transcription factors that regulate several genes in osteoblasts, such as type I collagen, bone sialoprotein (BSP), osteopontin (OPN), transforming growth factor beta (TGF $\beta$ ), and osteocalcin (OC). The

regulation of bone formation involves several factors, including TGF $\beta$ s, bone morphogenic proteins (BMPs), FGFs, and Wingless-related integration site (Wnt) signaling, all of which were shown to regulate cell differentiation and survival in a spatiotemporal manner (Berendsen and Olsen, 2015; Ornitz and Marie, 2015; Sims and Martin, 2014; Takarada et al., 2016). In summary, a network of signaling molecules governs bone morphogenesis. Among them, FGF and their receptors were identified as relevant players in bone formation (Shahi et al., 2017), and some functional redundancies and complementary roles between different FGFRs throughout osteogenesis have been determined (Karuppaiah et al., 2016).

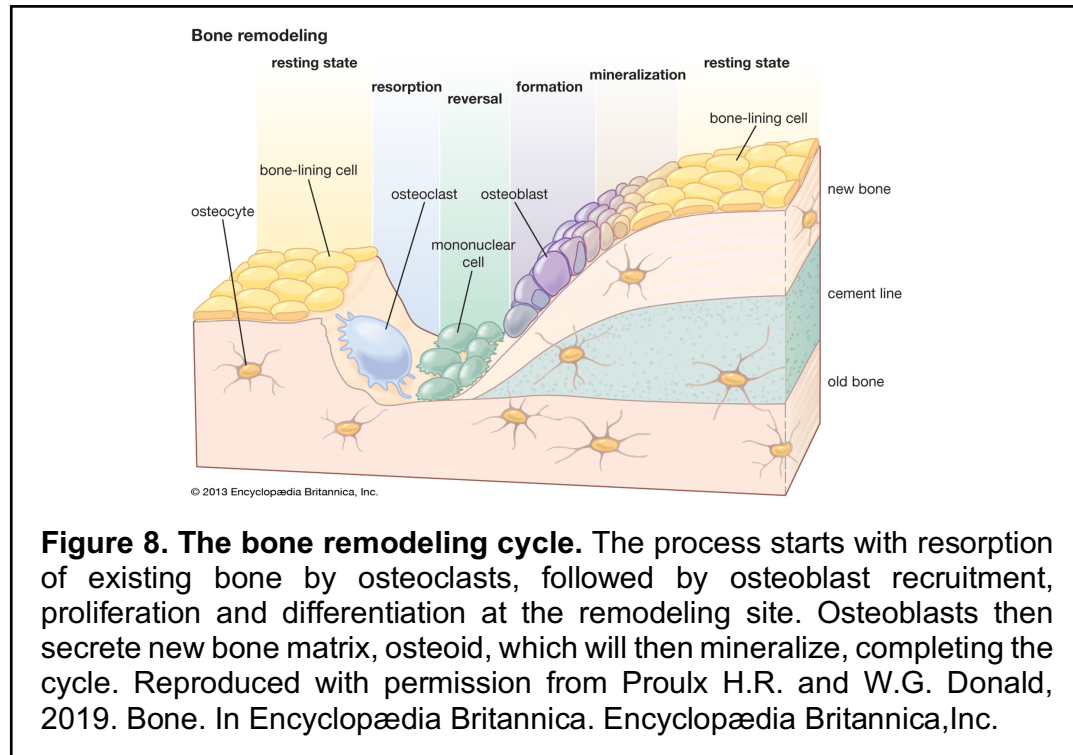
Two types of bone can be distinguished: compact or cortical bone, constituting the dense outer layer of bones, and trabecular, cancellous or spongy bone, constituting the internal area of the bones. The latter is porous and, given the higher remodeling surface, metabolically more active (J. Gordon Betts, 2013).

Structurally, different parts can be distinguished in long bones (Fig. 7). The diaphysis constitutes the cylindrical shaft that runs between the two bone ends. It holds the medullary cavity inside, occupied by bone marrow, and surrounded by walls of compact bone. Towards each of the bone ends, there is the epiphysis, occupied with trabecular bone. Between these two parts, the metaphysis can be found, which contains the growth plate in actively growing bones. In developed bones, only a scar line of it is left. All parts are highly innervated by blood vessels and nerves (J. Gordon Betts, 2013).





The bone is a highly dynamic organ. During adulthood, bone undergoes continuous remodeling via resorption and replacement at basic multicellular units (BMUs) (Fig. 8). This process of bone remodeling is critical for bone homeostasis in response to structural and metabolic demands, and is strictly controlled through a complex cell communication network involving signals between cells of the osteoblastic and osteoclastic lineages at each BMU (Sims and Martin, 2014). Many factors mediating stimulatory and inhibitory signals contribute to coupling the processes of bone formation, mediated by osteoblasts, and resorption, mediated by osteoclasts, including oncostatin M, parathyroid hormone-related protein (PTHrP), sclerostin, matrix-derived TGF $\beta$ , insulin-like growth factor-1 (IGF-1), cardiotrophin-1, Sema4D/3B, sphingosine 1-phosphate (S1P), ephrinB2 and ephrinB4, receptor activator for nuclear factor- $\kappa$ B ligand (RANKL), Sema3B, Wnt5a, osteoprotegerin (OPG), and T cell-derived interleukins (IL).



More recently, evidence indicates that bone-forming mature osteoblast and bone-resorptive mature osteoclast functions are also regulated via direct cell–cell contact between these cell types (Benayahu et al., 2019; Chen et al., 2018; Furuya et al., 2018).

These pathways and bona fide cell-to-cell interactions in bone are hijacked by cancer cells during the metastatic process. Indeed, it has been proposed that tumor cells can acquire features exclusive to cells from the microenvironment (i.e., osteomimicry) (Huang et al., 2005). Consequently, the arrival and growth of cancer cells in the bone will disrupt bone homeostasis. Depending on the specific interaction that occurs between cancer cells and bone cells, bone metastases can be osteoblastic (e.g., PCa) or osteolytic (e.g., multiple myeloma). If the balance between bone formation and bone resorption is shifted towards increased bone formation, the bone lesion will be seen as radiodense in the X-ray analyses. These are the so-called osteoblastic lesions. When the balance is

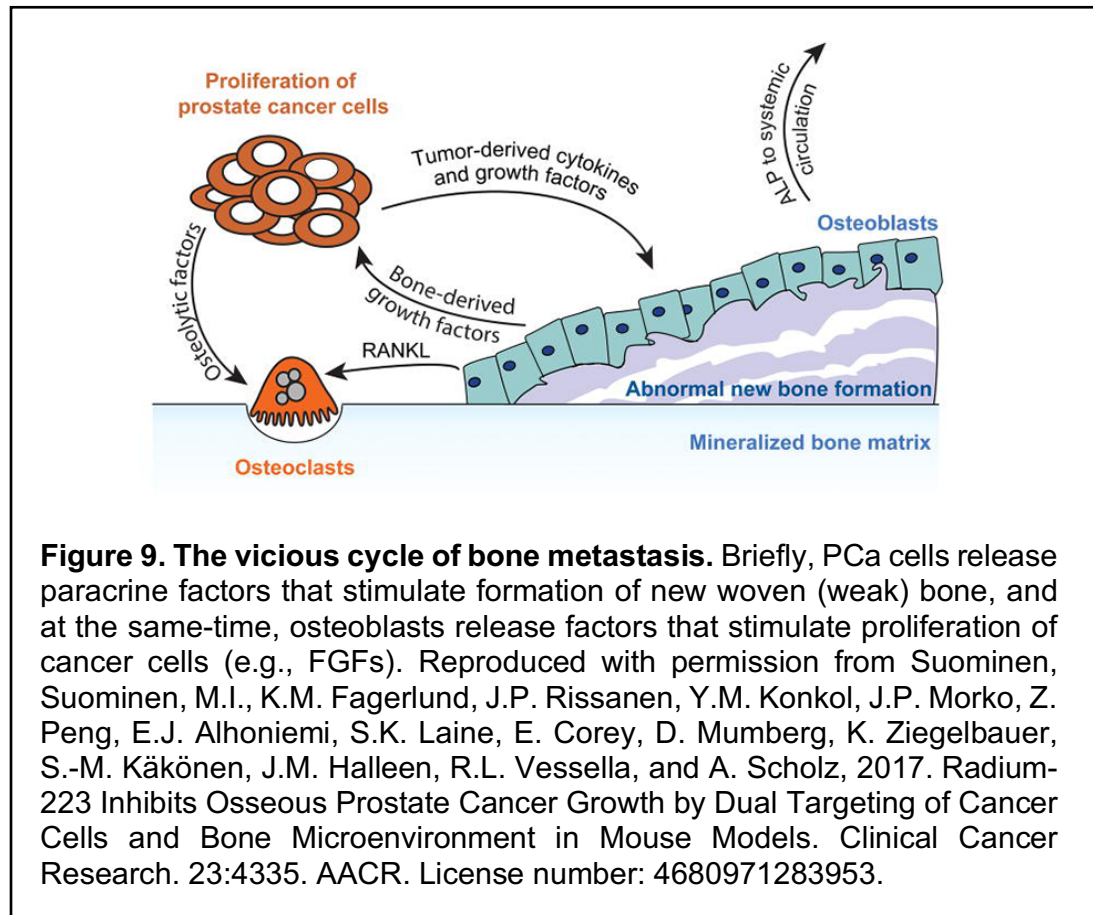
shifted towards bone resorption (as a consequence of osteoclast activation), the bone lesion will be seen as radiolucid in the X-ray analyses. These are the so-called osteolytic lesions. In many instances, the lesions can be mixed blastic-lytic. Nonetheless, both components (osteolytic and osteoblastic) are generally present at different levels in any type of bone metastasis.

In this context, a positive feedback loop or “vicious cycle” mediated by soluble factors released by cancer cells and the bone is implicated as a means of survival and growth in the bone microenvironment (Fig. 9). Authors originally described this cycle in the interaction of breast tumor cells with bone cells (Ell and Kang, 2012; Kozlow and Guise, 2005). Researchers proposed that tumor cells, osteoblasts, osteoclasts, and bone matrices are the four components of the vicious cycle necessary for the initiation and development of bone metastases (Kozlow and Guise, 2005).

Among the factors implicated in osteoclast activation by cancer cells in osteolytic metastases, either directly or via activation of osteoblasts, are RANKL, PTHrP, and IL-6. Conversely, gene expression in tumor cells is modified by factors released from the bone matrix by osteoclast-mediated resorption that promote tumor cell proliferation and survival.

Among the factors mediating aberrant formation of new bone by osteoblasts in osteoblastic metastases, are IGFs, BMPs, FGF, endothelin 1 (ET1), and Wnt ligands secreted by tumor cells. In a reciprocal fashion, osteoblast activation is suggested to produce factors that favor the growth of PCa cells (Lee et al., 2015a; Lee et al., 2015b; Li et al., 2008; Logothetis et al., 2008; Yang et al., 2001). Since the osteolytic component is present as well in the osteoblastic lesions, the release of factors embedded in the bone

matrix (e.g., IGF, TGF $\beta$ ) by the bone resorption process will, in turn, support cancer growth.



As described above, bone is the most common and often the only site of PCa progression (Logothetis et al., 2013). Accordingly, bone-related complications (primarily bone pain, fractures, and spinal cord compression) are the main causes of morbidity and mortality in PCa (Ottewell et al., 2014). A consistent hallmark of PCa lethal progression to bone is the development of osteoblastic metastases (Bubendorf et al., 2000), indicating that PCa–bone interaction may mediate PCa growth in bone (Croucher et al., 2016; Logothetis et al., 2018). Therefore, identifying the molecular pathways involved in the

development of bone metastases and PCa growth after dissemination to and in the bone will lead to the development of therapeutic opportunities for secondary prevention.

### **Models of metastasis**

*In vivo* studies modeling metastases in mice may involve the entire metastatic process when cells are injected orthotopically (in the site of origin of the cancer), and metastatic spread is monitored macroscopically or by labeling the input cells with a transgene-expressing luciferase, which enables them to be tracked *in vivo* (termed “spontaneous” metastasis). The ability of cells to reach specific organs, via the blood vessels, and grow can be studied with intracardiac injection of cancer cells into the left ventricle (termed “experimental” metastasis). In this scenario, the initial steps of metastasis are bypassed. Finally, the interaction of cancer cells with the host cells at the metastatic site can be studied using direct injection of the cancer cells into the organ subject of study. This strategy does not provide information about the metastatic process but does provide important information on tumor-microenvironment interactions that lead to tumor growth at the metastatic site. In particular, bone metastases of PCa are sites of treatment resistance; thus, this approach is useful in preclinical studies for assessment of impact on not only tumor volume but also PCa cell-bone interaction. Cancer-induced bone remodeling generates high heterogeneity of bone lesions. Histomorphometry of undecalcified bone provides an accurate measure of tumor-induced bone reaction and treatment effects on normal bone and tumor-induced bone reaction. Metastatic lesions in the bone are believed to grow in the medullary cavity first. These measurements are usually performed in the mid-cancellous region of the distal metaphysis of the femur.

These experimental procedures have strengths and shortcomings, and determining the value of each of these methods comes down to the scientific question that is being addressed and how well the methods for answering the question were selected. For example, intracardiac injection of cancer cells into the left ventricle will provide important evidence regarding the preferred site of metastasis of a given cell line and how this tropism can be altered by genetically manipulating the injected cells. However, the effects of genetic manipulation of the injected cells in the initial steps of metastasis cannot be studied using intracardiac injection. Also, the effects of genetic manipulation of the injected cells on tumor-stroma interaction at the metastatic site cannot be accurately assessed because the pattern of metastasis is unpredictable. A more informative method for the latter would be direct injection of a cells into the metastatic site because the subject of the study is controlled. For preclinical/co-clinical studies, direct injection of cells into the organ of interest is preferred if the purpose of the study is to identify means of controlling the growth of established metastases. If the goal is to prevent the development of metastases, either orthotopic or intracardiac injection would be adequate.

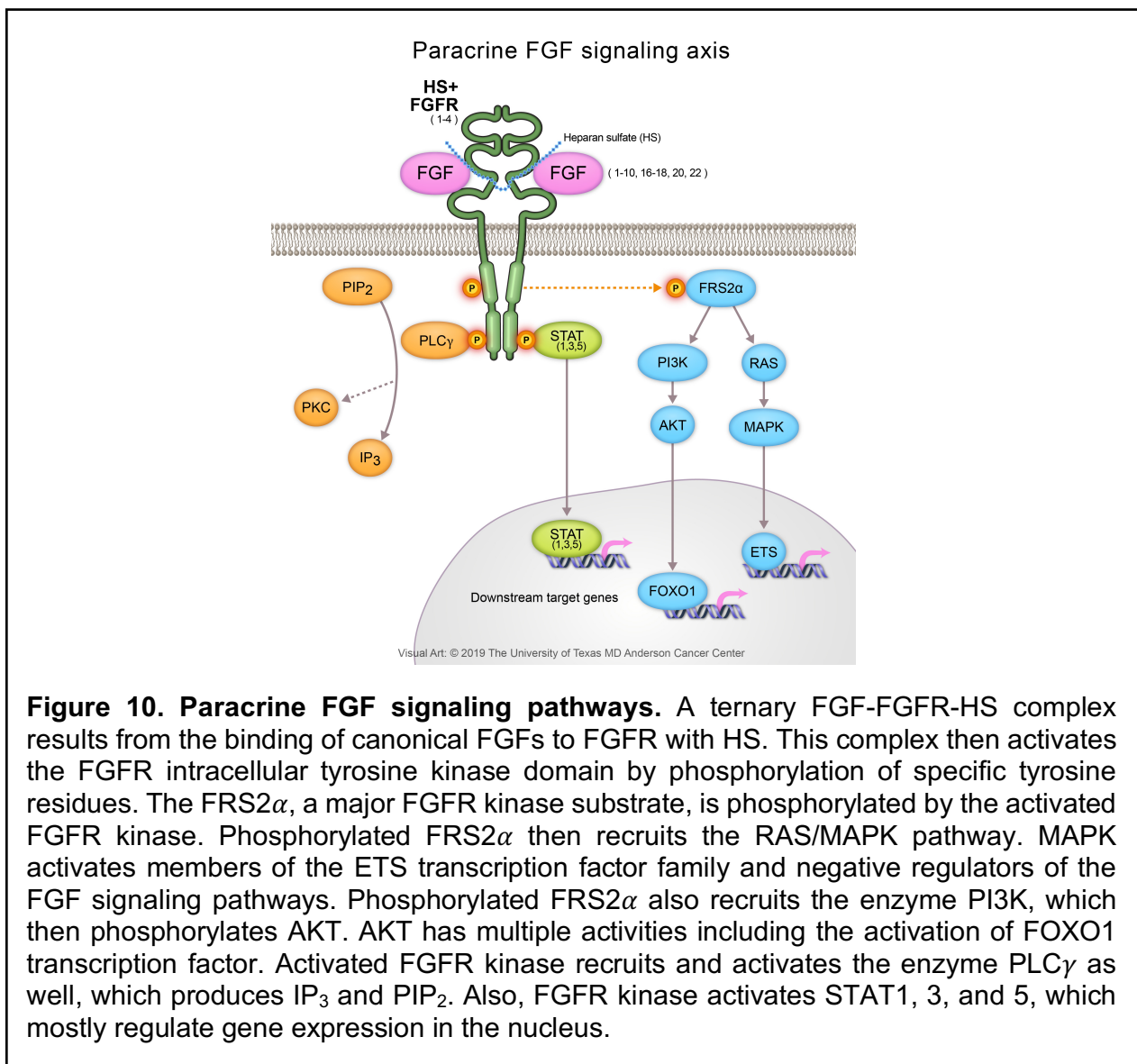
### **The FGF signaling axis**

The contribution of bone metastases to the clinical morbidity of solid tumors has prompted efforts to better understand the mechanism of cancer metastases to bone. As a result, many factors implicated in bone metastases have been identified. Prominent among these areas of study is the FGF signaling axis, which has been shown to be central to the metastatic progression in bone of some tumors, including PCa. While in other

tumors, there is still insufficient evidence to implicate the FGF axis in its progression to bone metastases.

The FGF axis is a highly conserved complex signaling pathway that typically mediates epithelial–stromal cell interactions and is central to prostate and bone development (Lin and Wang, 2010; Su et al., 2014). In humans, the axis consists of 18 receptor-binding ligands (FGFs), 4 transmembrane receptor tyrosine kinases (FGFRs), and their isoforms. The various FGFs are classified in canonical (paracrine), hormone-like (endocrine), and intracellular (intracrine).

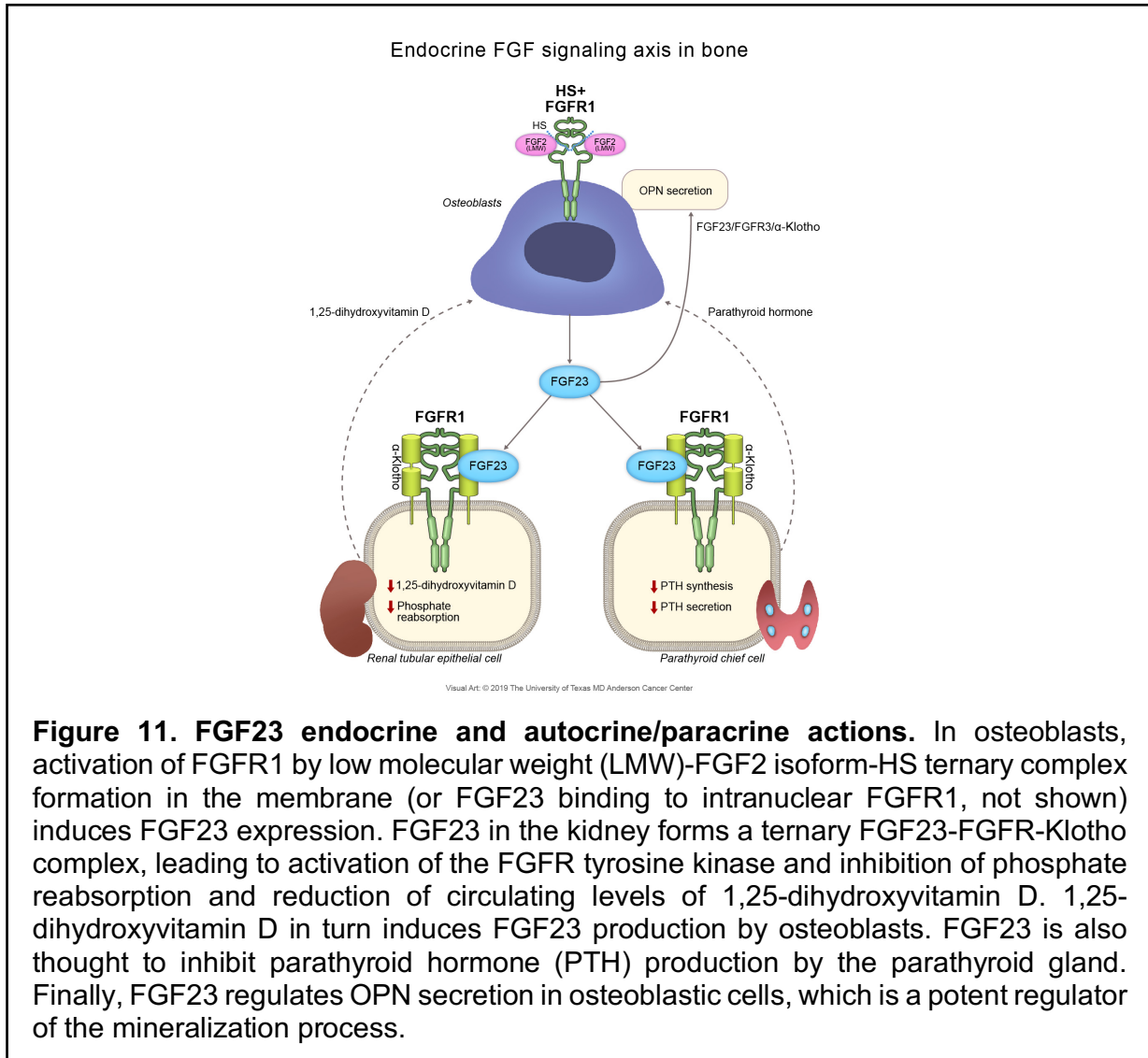
The interaction in the paracrine signaling requires heparan sulfate (HS), which leads to activation of the FGFR kinases. Current evidence indicates that FGFR kinase activation is followed by phosphorylation of FGFR substrate 2 $\alpha$  (FRS2 $\alpha$ ), recruitment of phospholipase C $\gamma$  (PLC $\gamma$ ), and activation of downstream cascades and networks (e.g., mitogen-activated protein kinase [MAPK], protein kinase B [AKT], signal transducer and activator of transcription [STAT]) (Ornitz and Itoh, 2015) (Fig. 10). FGFR signaling can be modulated by different mechanisms including negative regulators (e.g., Sprouty) and receptor internalization and degradation (Ornitz and Itoh, 2015).



In addition to the paracrine canonical FGFs, there are three FGFs, namely FGF19, 21, and 23, that function as endocrine factors and are believed to require protein co-factor  $\alpha$ Klotho,  $\beta$ Klotho, or the Klotho-related protein for receptor binding and activation due to their lower affinity for HS (Ornitz and Itoh, 2015) (Fig. 11). Also, the intracrine FGF subfamily, FGF11-14, encodes intracellular FGFs, which are non-signaling proteins that



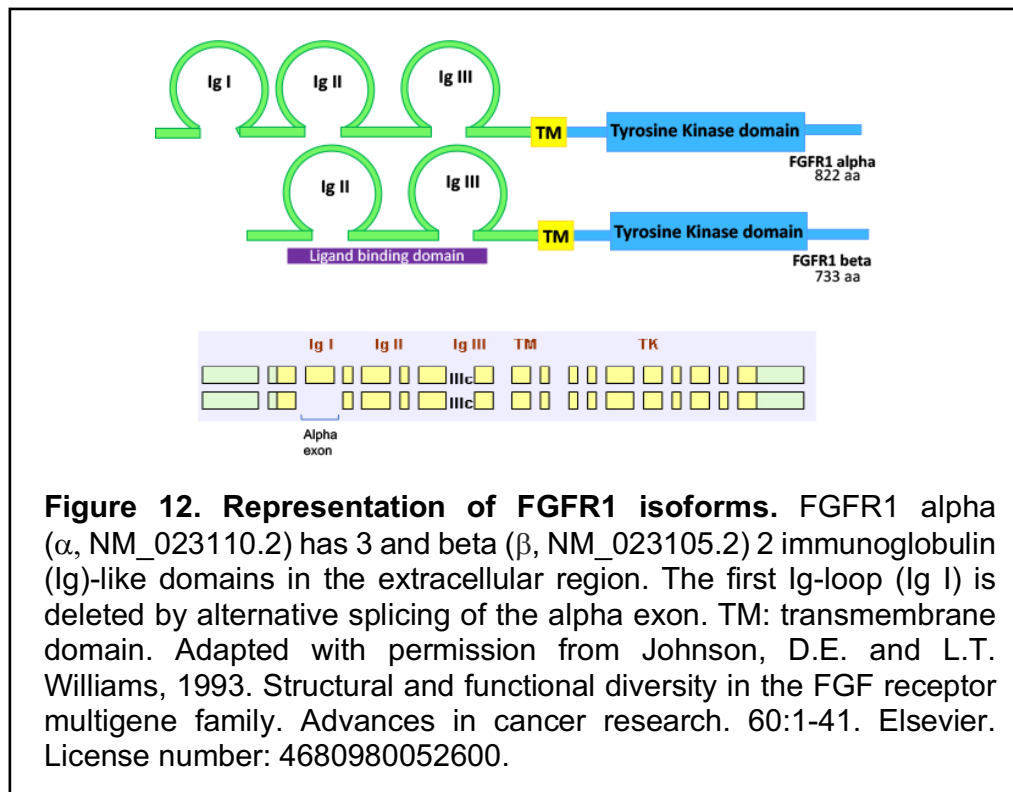
serve as cofactors for voltage-gated sodium channels and other molecules (Ornitz and Itoh, 2015).



The complexity of this axis is further increased by the possibility of FGFRs to undergo alternative splicing, producing isoforms with differential ligand specificity and spatial lineage expression, as well as the complexity of HS members (Gong, 2014; Li et

al., 2016). Lastly, an additional member of the family is FGFR-like 1 (FGFRL1) or FGFR5, which lacks the cytoplasmic tyrosine kinase domain (Kahkonen et al., 2018).

In particular, the FGFR1 extracellular, ligand-binding, region comprises two or three Ig-like domains which result from alternative splicing of the  $\alpha$  exon leading to FGFR1  $\alpha$  (containing the  $\alpha$  exon) and  $\beta$  (lacking the  $\alpha$  exon) isoforms (Fig. 12). This does not affect ligand binding, but can lead to enhanced ligand affinity in the FGFR1  $\beta$  isoform, possibly due to partial loss of auto-inhibition. Expression of both isoforms is detected in most tissues, being  $\alpha$  predominant in general, and expressed during embryogenesis in the mice, and  $\beta$  expressed after birth (Wan et al., 2014).



These isoforms are of interest in cancer as they have been associated with pancreatic cancer, breast cancer, bladder cancer and glioblastoma (Bruno et al., 2004; Luqmani et al., 1995; Tomlinson and Knowles, 2010; Vickers SM, 2002; Wendt et al., 2014; Zhao et al., 2019). Furthermore, it has been reported that changes in the expression ratio of these simultaneously expressed splice variants in cancer could modulate responses to either autocrine or paracrine factors (Luqmani et al., 1995).

Of note, these are only some of the many isoforms that have been identified for FGFR1. For instance, lack of the exon coding for the transmembrane domain can result in soluble receptor forms. Additionally, other isoforms can result from alternative exon usage of the exon coding for a region of the IgIII, generating IIIb and IIIc isoforms (Gong, 2014). Interestingly, previous reports from our group determined that the FGFR1 IIIc isoform is prevalently expressed in PCa compared to IIIb (Wan et al., 2014).

Once activated, FGF signaling regulates a plethora of cellular biological processes: mitogenesis, differentiation, angiogenesis, survival, and motility/invasiveness, among others (Li et al., 2016; Ornitz and Marie, 2015). The FGF pathway plays a central role in various processes that include embryonic and organ development, wound healing and carcinogenesis (Corn et al., 2013; Teven et al., 2014). In particular, the FGF axis is integral to normal bone development and function (Li et al., 2016; Ornitz and Marie, 2015).

### **Role of FGF signaling in bone**

The discovery that FGFR mutations are associated with specific skeletal abnormalities in humans has established the relevance of this pathway in bone development and homeostasis (Ornitz and Marie, 2015). These include congenital

FGFR2 mutations in humans associated with craniosynostosis (Karuppaiah et al., 2016) and bent bone dysplasia among other skeletal disorders, implicating this receptor in bone development (Neben et al., 2017). However, the effects of FGF/FGFR signaling in osteogenesis are complex, as they depend on which FGFs and FGFRs are expressed, the stage of maturation of the target cells, and the microenvironment (e.g., availability of HS). Studies using genetically engineered mice (GEM) have provided some understanding of the role of the FGF axis in bone biology (Jacob et al., 2006).

Briefly, the data resulting from conditional knockout of *Fgfr1* in the osteoprogenitor lineage suggest that FGFR1 promotes the differentiation of mesenchymal progenitors into preosteoblasts, while inhibiting their proliferation (Jacob et al., 2006; Xiao et al., 2014; Zhang et al., 2014), and inhibits the maturation and mineralization of osteoblasts (Jacob et al., 2006; Su et al., 2014). Likewise, *Fgfr2* inactivation in mice suggest that this receptor is also involved in postnatal bone growth (Karuppaiah et al., 2016), although the underlying mechanism is not clear. *Fgfr1* and *Fgfr2* have considerable overlap in their expression patterns and their double deletion in mice resulting in severe postnatal growth defects and impaired longitudinal bone growth, embodies the important role for FGF signaling in bone formation after birth (Karuppaiah et al., 2016).

As for FGFR3, gain-of-function mutations result in achondroplasia and related chondrodysplastic disorders, as a consequence of suppressing pre-pubertal skeletal growth. Further, in mice studies, chondrogenesis was observed as a result of an inhibitory activity of FGFR3, expressed on growth plate chondrocytes (Ornitz and Marie, 2015). Although much is known about the signals downstream of FGFR3 in chondrocytes, the mechanisms that regulate FGFR3 expression and activation, and that coordinate osteogenesis and chondrogenesis are poorly understood (Ornitz and Marie, 2015).

The specific roles of FGF ligands in bone biology post birth are not completely understood. Cell-based and GEM studies implicate FGF2 (one of the most studied FGF ligands) in osteogenesis (Montero et al., 2000; Su et al., 2014). However, different FGF2 isoforms (low molecular weight [LMW] and high molecular weight [HMW]) seem to have opposite effects on bone mass (Xiao et al., 2018; Xiao et al., 2010). Moreover, both, LMW- and HMW-FGF2 induce FGF23 promoter activity (Han et al., 2015). FGF23, expressed mainly by osteoblasts and osteocytes (Martin et al., 2011), controls phosphate homeostasis and bone mineralization via endocrine actions in its main target organ, the kidney, after formation of the ternary FGF-FGFR-Klotho complex (Feng et al., 2013; Quarles, 2012). There is also evidence suggesting the existence of a PTH–bone feedback loop in which PTH stimulates FGF23 bone-expression and FGF23 inhibits PTH production by the parathyroid gland (Quarles, 2012) (Fig. 11). Finally, FGF23 also locally regulates bone mineralization acting through FGFR3 in a Klotho-independent manner. In this case, FGF23 regulates OPN secretion in osteoblastic cells, which is a potent regulator of the mineralization process (Murali et al., 2016) (Fig. 11).

Combined *in vitro* and *in vivo* studies suggest that FGF-ERK1/2 signaling regulates the expression of dentin matrix acidic phosphoprotein 1 (Dmp1), critical for proper bone mineralization in osteocytes. Once activated, the mechanism of FGFR signaling down-regulation involves ubiquitin ligase c-CBL and is prevalent in osteoblasts, thus highlighting the important role of this adaptor protein in the control of osteoblastogenesis (Ornitz and Marie, 2015).

FGF signaling interacts with other pathways involved in osteogenesis most notably with BMPs and the Wnt canonical pathway. Briefly, *in vitro* and *in vivo* studies indicate that FGFs enhance canonical BMP2 signaling and induce  $\beta$ -catenin nuclear

accumulation in osteoblasts, thus regulating the fate and differentiation of mesenchymal stem cells (Miraoui and Marie, 2010; Ornitz and Marie, 2015).

Furthermore, FGF2 is necessary for the positive effects of PTH on osteoblast proliferation and differentiation (Ornitz and Marie, 2015); and, in turn, PTH stimulates Fgf2, Fgfr1, and Fgfr2 in osteoblasts.

The FGF axis regulates bone remodeling by regulating osteoclast activation and function, as well. FGF2 induces osteoclast precursor proliferation and stimulates bone resorption through the activation of FGFR1 and MAPK. FGF18 can induce RANKL and cyclooxygenase-2 expression in osteoblasts, which in turn will induce osteoclast formation and function. *In vivo* studies indicate that FGFR1 and FGFR3 contribute to osteoclast activity (Ornitz and Marie, 2015). Further, mice with *Fgfr1* inactivation in osteoclast and osteoclast precursors are normal at birth but have abnormal bone remodeling and increased bone mass (Lu et al., 2009).

In summary, it is clear that the FGF axis is a key player in osteogenesis. Furthermore, it is equally clear that its function is multifaceted and highly context-dependent, with the effects of particular components, as well as interacting proteins, varying according to the specific microenvironment and stage of bone development. Numerous downstream signaling cascades triggered by the interaction between FGFs and FGFRs in association with other pathways regulate the different steps in osteoblast maturation (Ornitz and Marie, 2015).

Overall, the above-mentioned studies emphasize the complexity of bone formation dynamics, which require a tight, regulated, fine-tuned coordination of pathways and processes, including the fundamental role of the FGF axis and its crosstalk with other signaling cascades.

Finally, FGF/FGFR is a target in the treatment of bone-associated diseases. A feature of particular importance is that FGF activation mediates angiogenesis and osteogenesis, two closely related processes of bone formation (Charoenlarp et al., 2017; Shahi et al., 2017). Hence, the relevance of its therapeutic application in cancers involving bone.

### **FGF axis in PCa**

Besides androgen signaling, epithelial-mesenchymal interactions regulate prostate gland homeostasis and development. FGFs partly mediate this interaction; in particular FGF2, 7, 9 and 10 are expressed in the stromal, and their receptors in the epithelial compartment.

Alterations in the FGF pathway have been implicated in different types of cancer, including breast, bladder, lung and PCa (Wesche et al., 2011). Aberrant FGF expression in prostate stroma or epithelium can lead to PIN and is involved in the early stages of PCa development; in particular, through a paracrine fashion. Also, increased levels of FGF in the epithelial prostate cells also contribute to aberrant growth by autocrine signaling. Furthermore, PCa progression and EMT have been shown using an inducible FGFR1 prostate mouse model, and its inhibition by conditional inactivation of FGFR1 or FRS2 $\alpha$  in the TRAMP mouse model (SV40 T antigen-expressing transgenic adenocarcinoma of the mouse prostate) (Corn et al., 2013). Finally, several FGFs and FGFR1 mainly have been found overexpressed in human prostate tumors, in many cases, associated to more aggressive grade and clinical stage (Corn et al., 2013).

## **FGF family implications in the pathogenesis of PCa bone metastases**

Alterations in the FGF/FGFR axis found in cancer result either from activating mutations of receptors or from overexpression of ligand or receptors (see Appendix I: “FGF axis implications in bone metastases of other cancers: breast, lung, bladder cancer and multiple myeloma”). Not all alterations in the FGF axis in cancer emerge from genomic alterations (e.g., PCa).

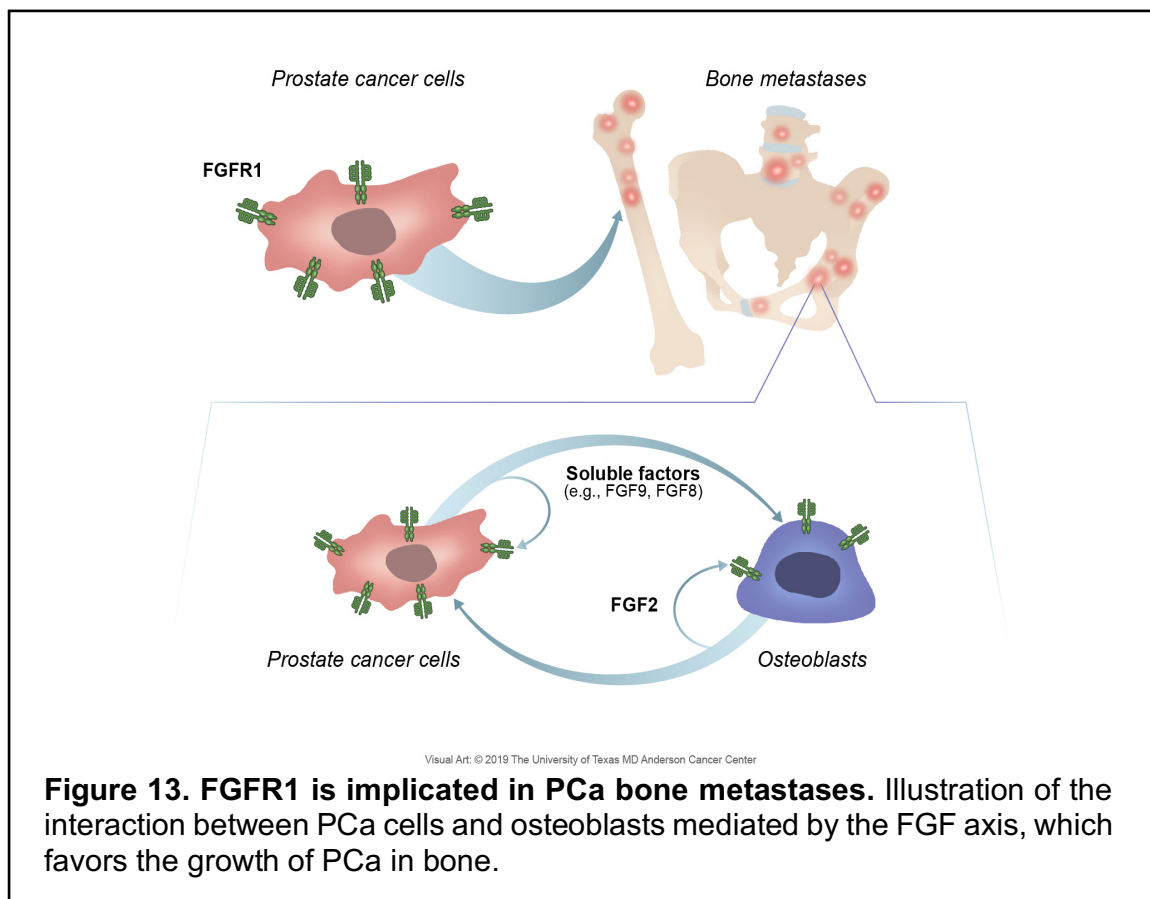
FGF axis abnormalities in PCa have been associated with receptor or ligand overexpression (Wang et al., 2019), but mutations of FGF axis components have been detected in only a small fraction of PCa.

Previous reports implicate the FGF axis in PCa development and progression (Corn et al., 2013; Teishima et al., 2019). Given the role of the FGF axis in bone biology, aberrant FGF signaling activation in bone cells would upset the bone homeostasis. Studies conducted by our laboratory and others indicate that PCa cells can alter the bone microenvironment by triggering the expression of FGFs (in particular FGF9 and FGF8) (Li et al., 2008; Valta et al., 2008). Indeed, expression of FGF8 and FGF9 is significantly increased in human PCa bone metastases compared with the primary site (Li et al., 2008; Valta et al., 2006). Further, ectopic expression of FGF8 and FGF9 in PCa cells promotes, while blocking FGF9 reduces, the growth of PCa cells in bone (Huang et al., 2015; Li et al., 2008; Valta et al., 2008). These evidences implicate FGF8 and FGF9 in the pathogenesis of PCa bone growth.

Our laboratory also reported that blockade of FGFRs with dovitinib (TKI258, Novartis Pharmaceuticals), a receptor tyrosine kinase inhibitor with potent activity against FGFR and VEGFR, has clinical activity in a subset of men with CRPC and bone metastases (Wan et al., 2014) (Fig. 13). Our findings not only identify the FGF axis as a



candidate target for therapy, but also implicate the FGF axis in a positive feedback loop between PCa cells and bone cells; and suggest that FGFR1-mediated autocrine and paracrine signals in PCa cells enable PCa growth in bone. In support of this, recent reports indicate that the FGF axis may underlie CRPC progression (Bluemn et al., 2017) and resistance to cabozantinib (c-MET and VEGFR2 inhibitor) treatment (Varkaris et al., 2016), further underpinning the importance of developing FGFR blockade as therapy or secondary prevention for PCa.



Furthermore, a previous report from our group showed that FGF2 expression is increased in tumor-associated bone cells in an experimental model (Wan et al., 2014). Results of a recent study indicate that high FGF2 levels in osteoblasts (secondary to

Tgf $\beta$ 2 loss) promote PCa bone metastases in mice (Meng et al., 2018). Prostate stromal cells express biologically relevant levels of FGF2, and therefore the increase in FGF2 in the bone microenvironment may promote PCa cell growth by providing a similar niche (Kwabi-Addo et al., 2004; Pecqueux et al., 2018). Together, these studies suggest that loss of Tgf $\beta$ 2 expression in osteoblasts enables FGF2-mediated cross-talk with PCa cells and promotes bone metastasis (Meng et al., 2018). In support of these studies, it has been shown that loss of Tgf $\beta$ 2 occurs in the bone marrow of 77% of bone-involved PCa cases examined. Further, knockout of Tgf $\beta$ 2 in mouse stromal fibroblasts results in earlier tumor development in intratibially-injected mice (Li et al., 2012).

Lastly, a study using experimental systems indicates that deletion of FRS2 $\alpha$  in human or mouse PCa cells results in reduced angiogenesis and impaired tumor growth in bone (Liu et al., 2016). These results are in alignment with the known role of the FGF axis in angiogenesis attributed to the mitogenic effect on endothelial cells.

Together, the evidence discussed further suggests that FGF signaling mediates autocrine and paracrine signals between PCa cells and bone cells.

## Hypothesis and Aims

Bone metastases remain a major therapeutic challenge.

FGFR1 is implicated in PCa pathogenesis and FGFR blockade has shown clinical activity in advanced, metastatic disease. However, the specific mechanism by which the FGF axis, FGFR1 in particular, mediates PCa growth in bone remains poorly understood.

In this study, we have found that various FGFR1 isoforms are detected in PCa tissue specimens.

The overall goal of this proposal is to investigate the molecular and clinical implications of FGFR1/FGFR1 isoforms expression in the pathogenesis of PCa bone metastases.

*We hypothesize that FGFR1 induces PCa progression to bone metastases. We further propose that the two best characterized FGFR1 isoforms, alpha and beta, activate different genes and pathways in PCa cells, and that this may partly explain PCa heterogeneity and pattern of progression.*

We will test these hypotheses in the following Specific Aims:

### **Aim 1. Assess the role of FGFR1 isoforms in the metastatic potential and growth pattern in bone in PCa.**

Given that FGF signaling is a key mediator of bone formation and that FGFR1 is involved in PCa progression, we propose that FGFR1 isoforms accelerate the bone metastatic phenotype of PCa cells. We will

(a) evaluate the metastatic dissemination mediated by FGFR1 isoforms after intracardiac injection of PCa cells in mice, and

(b) the induction of PCa growth in bone by direct injection of PCa cells into the femur of mice.

## **Aim 2. Study the signaling cascade induced by FGFR1 isoforms.**

We hypothesize that FGFR1 alpha and beta trigger activation of different associated gene signatures that modulate malignancy. We will

(a) mine the TCGA PCa datasets to examine FGFR1 molecular correlates, and

(b) determine the activation of downstream targets in PCa cells expressing FGFR1 isoforms by Western blot and reverse phase protein array (RPPA). To identify candidate genes enriched in FGFR1-mediated metastasis, we will then assess the expression of FGFR1-associated proteins/phospho-proteins in human PCa metastases specimens by immunohistochemistry (IHC).

## **Aim 3. Analyze clinical correlates of FGFR1 and its isoforms in human PCa.**

Since we detected various FGFR1 alternative splice variants in PCa samples, we will test our postulate that PCa tumors are heterogeneous in FGFR1 levels throughout disease progression and that FGFR1 is enriched in PCa metastases.

We will assess the expression of FGFR1 in clinical samples reflecting the progression of the disease by IHC.

Dissecting the role of FGFR1 isoforms in PCa bone metastases will significantly contribute to the identification of men with FGFR1 activation as candidates for FGFR1 blockade, to develop new therapies targeting FGF signaling, and to identify predictive biomarkers of response to this treatment.

## **Chapter 2: METHODS**

This chapter is partly based upon “Navone N.M. and E. Labanca, 2017. Modeling Cancer Metastasis. In: Patient-Derived Xenograft Models of Human Cancer. Molecular and Translational Medicine. Humana Press, Cham. Y. Wang, D. Lin, and P.W. Gout, editors. pp. 93-114”, with permission from Springer International Publishing AG 2017, Springer Nature. License Number: 4654420161143.

## **BIOINFORMATICS ANALYSIS**

### **Data mining from the Prostate Adenocarcinoma Project of The Cancer Genome Atlas (PRAD-TCGA)**

The human RNA sequencing data from the PRAD-TCGA data portal site (<http://cancergenome.nih.gov/>), which has gene expression data from 476 prostate tumor samples and normal adjacent tissue (last access: December 2018) measured by massively parallel sequencing (IlluminaHiSeq), was used. The dataset was mined for expression of FGFR1 isoforms and their molecular correlates. The search was performed using the specific sequence of each of the FGFR1 isoforms ( $\alpha$ , NM\_023110.2; and  $\beta$ , NM\_023105.2). To perform the analyses, a FGFR1 score was defined as the ratio of FGFR1  $\alpha$  to the sum of FGFR1  $\alpha$  and FGFR1  $\beta$  (Ryan et al., 2012). A high FGFR1 score indicates prevalence of FGFR1  $\alpha$  and a low FGFR1 score indicates prevalence of FGFR1  $\beta$ . Expression of genes and pathways associated with FGFR1 score was also assessed, using Gene Set Enrichment Analysis (GSEA) (Subramanian et al., 2005). BIOCARTA, KEGG, NABA, PID, REACTOME, SA, SIG, and ST pathway databases were used. We prioritized those pathways that had a  $P < 0.002$  and an absolute value of normalized enrichment score (NES)  $> 1.78$ .

## **cBioPortal**

The cBio Cancer Genomics Portal (<http://cbioportal.org>, open source cancer genomics data platform created by Memorial Sloan-Kettering Cancer Center) was used to analyze genetic alterations in the *LAD1* gene in PCa (Cerami et al., 2012; Gao et al., 2013). The criteria used in order to include datasets in our analysis were the following: (1) type of cancer: prostate (adenocarcinoma); (2) the study must be published; and (3) the study must consist of > 300 samples.

## **Ingenuity Pathway Analysis (IPA)**

Data were analyzed and a network was generated through the use of IPA (QIAGEN Inc., <https://www.qiagenbioinformatics.com/products/ingenuity-pathway-analysis>) (Kramer et al., 2014).

## ***IN VITRO* EXPERIMENTS**

### **Cell lines**

Two human prostate carcinoma derived cell lines were used in the studies:

- PC3: PCa cell line which does not express AR and is therefore hormone insensitive. It was established from a bone metastasis of a prostatic adenocarcinoma. Its pattern of growth in bone is osteolytic.
- C4-2B: a subline of the human prostate adenocarcinoma LNCaP obtained from a bone metastasis in male nude mice, which expresses AR.



PC3 and C4-2B cells were purchased from the American Type Culture Collection (ATCC) and were maintained in RPMI 1640 (Sigma-Aldrich) supplemented with 10% fetal bovine serum (FBS) (Sigma-Aldrich) and 1% penicillin and streptomycin (Sigma-Aldrich). All cell lines and sublines were grown in a 37°C incubator with a humidified 5% CO<sub>2</sub> atmosphere and split using Trypsin 0.25%, ethylenediaminetetraacetic acid (EDTA) 0.1% (Corning) upon reaching 80% confluency. For all experiments, cell line passage number was kept to higher than 2 and smaller than 20 after thawing. All cell lines and sublines were routinely tested for mycoplasma contamination using the Universal Mycoplasma Detection Kit (ATCC).

Cell lines stocks were prepared in culture medium supplemented with 45% FBS and 10% dimethyl sulfoxide (DMSO) (Sigma-Aldrich) and cryopreserved in liquid nitrogen. Freezing was done at a controlled slow cooling rate using freezing containers (i.e., CoolCell (Corning) or Mr Frosty (Nalgene)) in -80°C freezer, followed by transfer to liquid nitrogen storage. Thawing of cryotubes (Nunc) was performed at 37°C directly from liquid nitrogen preservation, followed by a wash to eliminate DMSO and placed in the growth conditions described above.

### **Plasmid amplification and purification**

Plasmids amplification was performed by bacterial transformation of DH5 $\alpha$  competent *E. coli* (Invitrogen). Briefly, 1-5  $\mu$ L of DNA were added to 50  $\mu$ L of bacteria, incubated on ice for 30 minutes and heat-shocked at 42°C for exactly 30 seconds. 250  $\mu$ L of Super Optimal broth with Catabolite repression (SOC) media (Invitrogen) were then added and cells were incubated on a 37°C shaker for 1 hour. After incubation, 50-200  $\mu$ L

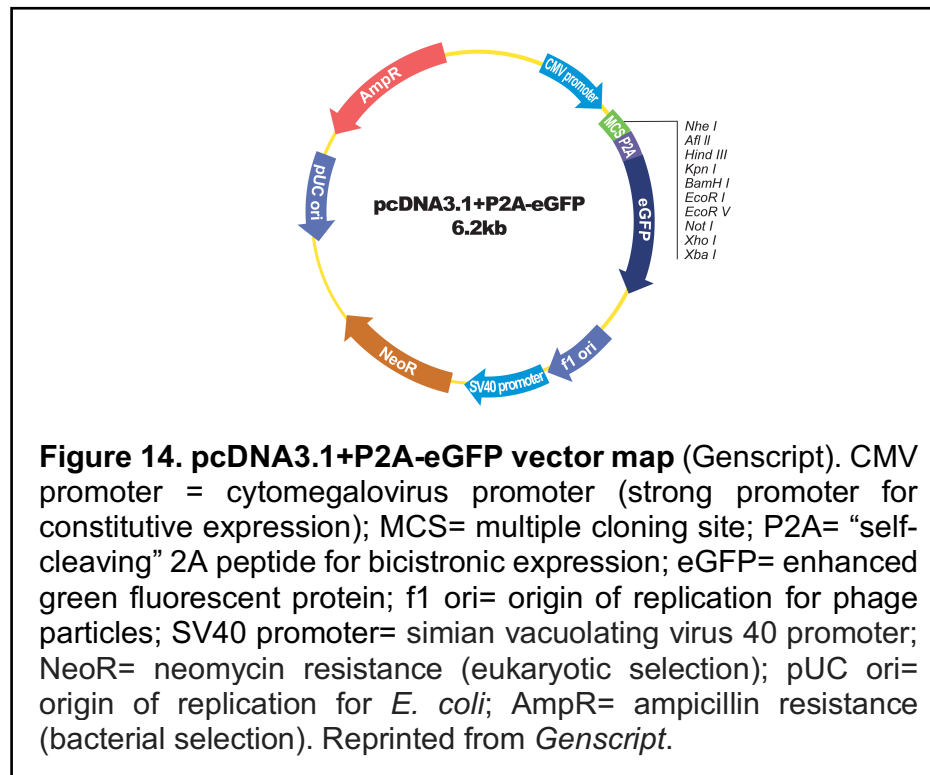
(at least two different volumes) were spread on a prewarmed Luria-Bertani (LB) agar plate containing the corresponding antibiotic and incubated at 37°C overnight.

Colonies were picked the next morning and grown in 2 mL of LB broth (Corning) with the corresponding antibiotic for 4 hours on a shaker at 37°C, then transferred to 100 mL LB broth containing antibiotic for overnight incubation on a shaker at 37°C. One mL bacterial stocks were prepared with 25% glycerol (from a 50% glycerol stock prepared in H<sub>2</sub>O) and stored at -80°C. Bacterial cells were harvested by centrifugation at 6,000 x g for 15 minutes at 4°C and plasmids purified using the EndoFree Plasmid Maxi kit (QIAGEN). Plasmid DNA pellet was resuspended in 500 µL water or Tris-EDTA (TE) buffer and quantified by pipetting 2 µL in the Take3 Micro-Volume Plate (BioTek) followed by absorbance measurement at 260 nm performed in the Synergy HTX multi-mode microplate reader (BioTek). Volumes were adjusted accordingly for Midi and Mini preps based on manufacturer's instructions. Ten µL of vectors at a 100 ng/µL concentration were sequenced at the Sequencing and Microarray Facility, MD Anderson Cancer Center, Houston, TX, using 10 µL of 1 pmol/µL of custom primers or primers provided by the Core.

### **Transfections and transductions**

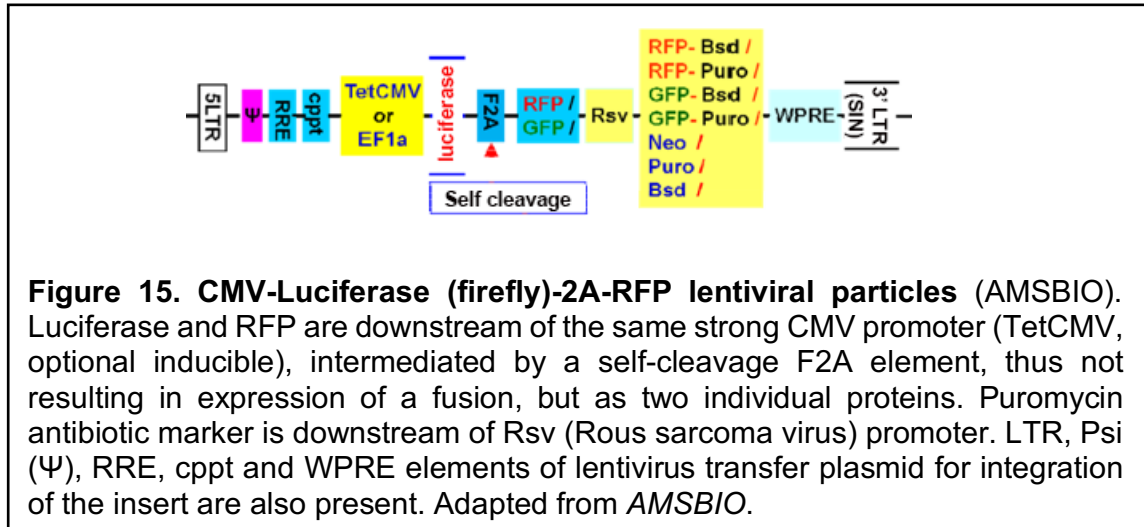
FGFR1  $\alpha$  and  $\beta$  sublines were developed from parental cell lines by stably transfecting them with pcDNA3.1-FGFR1 $\alpha$ -P2A-eGFP (PC3-FGFR1  $\alpha$  and C4-2B-FGFR1  $\alpha$ ) or pcDNA3.1-FGFR1 $\beta$ -P2A-eGFP (PC3-FGFR1  $\beta$  and C4-2B-FGFR1  $\beta$ ) plasmids (GenScript) (Fig. 14). Control sublines (transfected with empty vectors, PC3-V and C4-2B-V) were also generated. Transfections were performed using Lipofectamine 3000 Transfection Reagent (Invitrogen) or Fugene HD (Promega). Briefly,

2.5 µg (when using Lipofectamine 3000) or 3 µg (when using Fugene HD) of DNA were added to 70-90% confluent cells in a 6-well plate, according to the manufacturer's instructions. Transfected cell lines were selected by both, treatment with G418 (500 µg/mL, Geneticin, Sigma-Aldrich) and subsequent cell sorting for GFP expression by fluorescence-activated cell sorting (FACS) at the Flow Cytometry and Cellular Imaging Core Facility at MD Anderson Cancer Center, Houston, TX, as described in "Cell sorting" section. The optimal antibiotic selection concentration was determined by performing a dose response curve for each wild-type cell line.



Luciferase(luc)-expressing sublines of C4-2B–FGFR1  $\alpha$ ,  $\beta$ , and V were also generated, by infecting them with CMV-luciferase (firefly)-2A-RFP lentiviral particles (LVP324,  $\sim 1 \times 10^7$  IFU/mL, AMSBIO) (Fig. 15) according to the manufacturer's

instructions, followed by selection with 1 µg/mL puromycin (Thermo Scientific). Briefly, 50 µL of ready to use pre-made lentivirus were added into each well of a 24-well-plate with cells 50%-75% confluent. Fluorescence microscopy, FACS and luciferase *in vitro* assays were used to visualize positive transduction rate.



## Cell treatment

PC3 and C4-2B stably expressing FGFR1 isoforms or empty vector controls were serum-starved for 3 hours, and 50 ng/mL heparan sulphate proteoglycan (HSPG, Sigma-Aldrich) were added during the last hour of starvation. Then, 100 ng/mL of FGF2 or FGF9 (Peprotech), prepared from a 100 µg/mL stock, were added for 45 minutes to activate FGFR pathway. Cells treated with vehicle were used as controls.

## Cell sorting

GFP positive cells were sorted in Beckman Coulter MoFlo Astrios, Becton Dickinson FACS Aria II or FACS Aria Fusion Cell Sorter (Flow Cytometry and Cellular

Imaging Core Facility, MD Anderson Cancer Center, Houston, TX). Unlabeled parental cell lines were used as negative controls, and all samples were filtered through 35  $\mu$ m cell strainer cap tubes (Falcon) prior to running in the sorter to obtain single cell suspensions. Cell aggregates were excluded by singlet cell population gating. Fluorescein isothiocyanate (FITC) channel (green, 488 nm excitation/ 530 nm emission wavelength) was applied. The top percentage (5%-10%) of fluorescent cells was collected.

### **Western blot analysis**

Cells were harvested at the end of treatment in lysis buffer containing 1% Triton X-100, 50 mM HEPES pH 7.4, 150 mM NaCl, 1.5 mM  $MgCl_2$ , 1 mM ethylene glycol tetraacetic acid (EGTA), 100 mM NaF, 10 mM Na pyrophosphate, 1 mM  $Na_3VO_4$ , 10% glycerol, and freshly added protease and phosphatase inhibitor cocktail tablets (Roche). Protein concentration was measured using bicinchoninic acid (BCA) Protein Assay Kit (Pierce) and read in Synergy HTX multi-mode reader (BioTek). Immunoblot analysis was performed using standard procedures as previously described (Wan et al., 2014). Briefly, 20 to 30  $\mu$ g of denatured, reduced total cell lysates (using sample buffer containing 200 mM Tris-Cl pH 6.8, 8% sodium dodecyl sulfate (SDS), 0.4% bromophenol blue, 40% glycerol and 400 mM dithiothreitol (DTT), and boiled for 5 minutes) were loaded in equal amounts into a 4-20% gradient Tris-Glycine gel (Novex), separated by SDS-polyacrylamide gel electrophoresis (SDS-PAGE), and then transferred into a 0.2  $\mu$ m nitrocellulose membrane (Thermo Scientific). Blocking was done in either 5% milk or 5% bovine serum albumin (BSA) in tris-buffered saline-Tween 20 (TBS-T) (0.1% Tween 20), according to the manufacturer's instructions. The following antibodies were used: for

FGFR1 detection, anti-FGFR1 (Cell Signaling Technology, rabbit monoclonal, clone D8E4); for p-MAPK detection, Path Scan Multiplex Western Cocktail I against p-p44/42 MAPK (Erk1/2) (Cell Signaling Technology, rabbit monoclonal); for laminin 1 detection, anti-LAM1 (Sigma-Aldrich, rabbit polyclonal); and for GAPDH, anti-GAPDH (Cell Signaling Technology, rabbit monoclonal, clone 14C10). As secondary antibody, goat anti-rabbit IgG, horseradish peroxidase (HRP)-conjugated antibody (Cell Signaling Technology) was used, followed by chemiluminescence detection using enhanced chemiluminescence (ECL) Prime Western Blotting Detection Reagents (Amersham GE Healthcare). Images were acquired using either the ChemiDoc MP digital Imaging system (Bio-Rad) or a film developer, with Amersham Hyperfilm MP High performance autoradiography film (GE Healthcare) or Carestream® Kodak® BioMax® MR film (Kodak).

### **Reverse phase protein array (RPPA)**

RPPA analysis was performed at the Functional Proteomics RPPA Core Facility at MD Anderson Cancer Center, Houston, TX. Briefly, sample preparation consisted of harvesting cells using lysis buffer as previously described (see “Western blot analysis” section). They were then diluted to a concentration of 1.5 µg/µL and mixed accordingly with 4X sample buffer (40% glycerol, 8% SDS, 0.25 M Tris, pH 6.8), to which β-mercaptoethanol was added (1:10 ratio) before use. 80 µL of each sample (five replicates per group) were submitted to the RPPA Core Facility and run using a set of 295 (set 143 for C4-2B sublines) and 447 (set 160 for PC3 sublines) validated antibodies (Tibes et al., 2006) to explore expression/activation levels of signaling proteins following a previously described protocol (Pin et al., 2014). The list of antibodies used can be found at <https://www.mdanderson.org/research/research-resources/core-facilities/functional->

[proteomics-rppa-core/antibody-information-and-protocols.html](http://proteomics-rppa-core/antibody-information-and-protocols.html). The criteria for selection of candidate proteins was done by prioritizing those exhibiting an adjusted *P* value (*P* value corrected by the number of antibodies used to eliminate false positives) cutoff at 0.01 and fold change of 50% or more.

The heatmap depicting RPPA results using C4-2B was provided by the Functional Proteomics RPPA Core. The heatmap depicting results of PC3 sublines was generated as previously described (Broom et al., 2017).

### **Immunocytochemistry**

For immunocytochemistry analysis of FGFR1 expression in PC3 and C4-2B transfected cells, cultured cells were trypsinized, collected, fixed in 4% paraformaldehyde and pelleted. Liquid low melting point agarose (Sigma-Aldrich) was then mixed with pelleted cells and embedded in paraffin. Fixed and paraffin-embedded cell blocks were sectioned and sections were stained with anti-FGFR1 antibody (Cell Signaling Technology, rabbit monoclonal, clone D8E4) as described in “Immunohistochemistry in tissue specimens obtained from human PCa” section.

### **ANIMAL STUDIES**

All practices involving laboratory animals were approved by the Institutional Animal Care and Use Committee of MD Anderson, Houston, TX, under the regulation of the Animal Welfare Committee (IACUC), and conformed to the National Institutes of Health (NIH) Policy on Humane Care and Use of Laboratory Animals.

## **Intrabone injection**

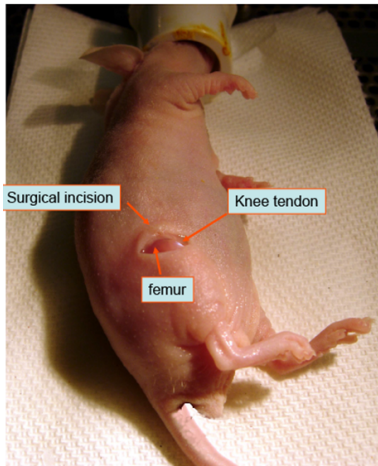
For intrabone assays,  $1 \times 10^6$  C4-2B-FGFR1  $\alpha$ ,  $\beta$ , or empty vector cells, or  $0.5 \times 10^6$  PC3-FGFR1  $\alpha$ ,  $\beta$ , or empty vector cells were injected into the distal end of femurs of 6- to 8-week-old male severe combined immunodeficiency CB17.SCID mice (Charles River Laboratories) ( $n = 6$  per group) as previously described (Li et al., 2008).

Briefly, cells in culture were trypsinized and collected by spinning in a centrifuge at 1,000 rpm for 5 minutes at room temperature. After PBS wash, cell concentration was adjusted by adding 1X PBS as needed to produce a final suspension containing  $0.5 \times 10^6$  or  $1 \times 10^6$  cells (according to the subline) per 5  $\mu$ L, and placed on ice in preparation for cell implantation into mice. Animals were anesthetized by administering isoflurane according to training in the Institution's Department of Veterinary Medicine and using an approved inhalation-induction-vapor recovery apparatus. Isoflurane was administered at concentrations of 4–5% for induction and 2–3% for maintenance of anesthesia. With the mouse placed in the left lateral decubitus position, hair was shaved over the distal right femur, and the surgical field (lateral side of the distal end of the femur) sanitized by spraying it with 70% ethanol. After gently finger flipping a few times a tube containing the prepared and iced cell suspension to remix, 15  $\mu$ L were aspirated into a sterile, glass-tight 25- $\mu$ L Hamilton syringe with a 28.5-gauge needle. The Hamilton needle has been previously cut to a length of 2.5–3.0 cm and sharpened, polished to make a smooth blunt end using a Dremel 10.8-V cordless rotary tool and 541 aluminum oxide grinding wheel. With sharp 9-cm straight scissors, a 0.5-cm skin incision was made on the lateral side of the distal end of the femur. Holding the femur and tibia with eye forceps, bone was exposed, and a track through the cortical bone into the bone marrow cavity was manually



created by drilling a hole with a sterile 28.5-gauge needle (attached to an insulin syringe) into the femur until the marrow cavity was reached and keeping the needle direction parallel to longitudinal axis of femur. The needle was gently removed, followed by insertion of the 28.5-gauge needle attached to the Hamilton syringe containing the tumor cell suspension through the established needle track into the bone marrow cavity, and 5  $\mu$ L of the cell suspension were slowly injected into the cavity. The needle was carefully removed and the injection area sprayed with 70% ethanol. The skin wound was closed with one or two surgical clips. The mouse was observed for 24 hours after the implantation procedure for any apparent physiologic disturbances, such as infection or inability to walk. Wound clips were removed in the usual manner at 10–14 days after the implantation procedure (Fig. 16).

Anesthetize 5- to 6-week-old mice that are to receive tumor cells



Hold femur and tibia with eye forceps and select puncture point



Drill a hole in lateral side of distal end of femur with needle till marrow cavity is reached. Keep the needle direction parallel to longitudinal axis of femur



Gently insert needle attached to Hamilton syringe containing tumor cell suspension through the established needle track into the bone marrow cavity and slowly inject cell suspension



Carefully remove needle. Clean injection area and close skin wound with one or two surgical clips



**Figure 16. Method used for intrafemoral injection of cancer cells in mice.** Note: *in vivo* studies performed in this work were done using male SCID mice, following the exact same procedure represented in this figure for male athymic nude mice. Adapted with permission from Navone N.M. and E. Labanca, 2017. Modeling Cancer Metastasis. *In* Patient-Derived Xenograft Models of Human Cancer. Y. Wang, D. Lin, and P.W. Gout, editors. Humana Press, Cham. 93-114. License Number: 4654420161143.

All mice were monitored by X-ray imaging (Faxitron) in the Small Animal Imaging Facility (SAIF) at MD Anderson Cancer Center, Houston, TX. Quantification of the radiolucent areas of the X-ray analyses was obtained as the ratio of radiolucent area to the total tissue area (whole bone) using the BioQuant Osteo software. Magnetic resonance imaging (MRI) was performed at the end of the study. Animals were euthanized after eight weeks for C4-2B and after four weeks for PC3 tumor-bearing mice. In each case, tumor-bearing femurs and contralateral normal femurs were collected and analyzed by high resolution microcomputed tomography ( $\mu$ CT) (SCANCO, Baylor College of

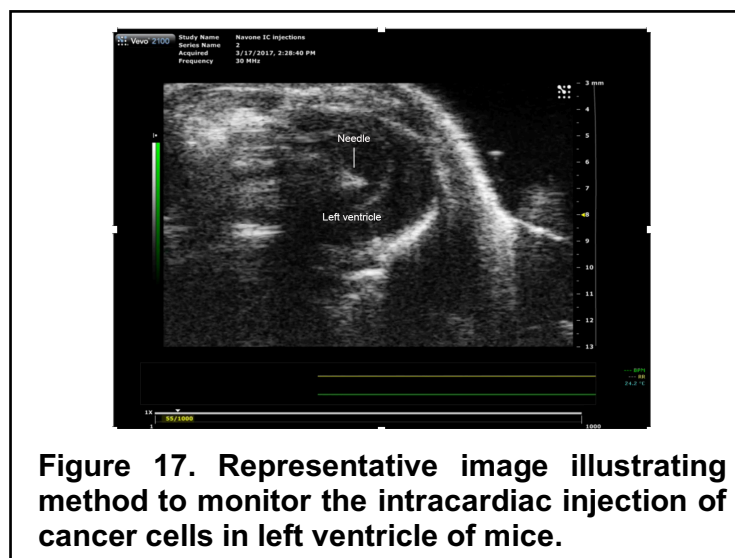
Medicine, The Bone Disease Program of Texas, Houston, TX). Femurs were subsequently fixed, decalcified in 10% EDTA pH 7.2 solution (changed daily), and processed for histologic analysis (Research Histology Core Laboratory (RHCL) at MD Anderson Cancer Center, Houston, TX) and bone histomorphometric analysis (Bone Histomorphometry Core Laboratory, The Bone Disease Program of Texas) as previously described (Li et al., 2008).

### **Left ventricle intracardiac Injection**

For intracardiac injection,  $1 \times 10^6$  PC3- or C4-2B-FGFR1  $\alpha$ ,  $\beta$  or corresponding empty vector cells were injected into the left ventricle of 6- to 8-week-old male CB17.SCID mice (Charles River Laboratories) (n = 12 per group) guided by ultrasound imaging (SAIF, MD Anderson Cancer Center). This system allows for the monitoring of precise intracardiac injection of tumor cells.

Briefly, cells in culture were trypsinized and collected by spinning in a centrifuge at 1,000 rpm for 5 minutes at room temperature. After PBS wash, cell concentration was adjusted by adding 1X PBS as needed to produce a final suspension containing  $1 \times 10^6$  cells per 100  $\mu$ L and placed on ice in preparation for cell implantation into mice. Animals were anesthetized using isoflurane as described above. All of the hair around the entire chest area was removed prior to the injection using hair removal cream. With the mouse placed symmetrically in supine position (dorsal side down), limbs were fixed to the imaging table with tape; the surgical field (chest) was sanitized by spraying it with 70% ethanol, and dried with sterile gauze, followed by application of ultrasound gel in the area. The transducer was mounted in the holder and the position adjusted until the left ventricle

could be visualized. After gently finger flipping a few times the tube containing the cell suspension and making sure it was free of aggregates to prevent embolic obstruction, 200  $\mu$ L were aspirated into a syringe with a 26.5-gauge needle and the syringe was secured on the syringe mount. The needle was adjusted until the tip came clearly visible in the field of view (Fig. 17). Guided by ultrasound imaging, cell mixture was slowly injected. Once the injection was completed, the needle was withdrawn, the transducer set aside and the tape removed from the mouse. The animal was cleaned, returned to a clean cage with a preheated pad and observed for bleeding or other unusual behavior. The mouse was monitored until recovered completely from the anesthesia.



Metastases development in the bones was monitored by X-ray (Faxitron, SAIF, MD Anderson Cancer Center, Houston, TX) since typically osteolytic metastases are easily recognized appearing as C-like notches, or in the case of C4-2B-luc, by bioluminescence imaging (see “Bioluminescence Imaging” section). The precise location of the bioluminescent areas was then identified by MRI. Animals were euthanized after

four weeks for PC3 and after twelve weeks for C4-2B mice. Bone areas suspicious of tumor content were collected, fixed, decalcified and processed for histologic examination (RHCL, MD Anderson Cancer Center, Houston, TX). Morphological analyses were performed in hematoxylin and eosin (HE)-stained tissue paraffin sections.

In all cases, mice were anesthetized in an induction chamber as previously described prior to imaging, and isoflurane delivery via nosecone maintained throughout image acquisition when available.

### **Bone histomorphometric analysis**

Histomorphometric analysis was performed at the Bone Histomorphometry Core Laboratory, The Bone Disease Program of Texas as previously described (Li et al., 2008). Bone (bone mass, osteoblast and osteoclast) parameters were obtained using tartrate-resistant acid phosphatase (TRAP) stains and Harris Modified hematoxylin counterstains of decalcified bones. Osteoblasts were clearly visible and easily differentiated so an additional toluidine blue stain wasn't needed.

### **Magnetic resonance imaging (MRI)**

MRI was performed with a 4.7-T Biospec small-animal imaging system (Bruker Biospin, SAIF, MD Anderson Cancer Center, Houston, TX). For anatomic tumor imaging, sagittal and axial T2-weighted fast spin-echo sequences with and without fat suppression were used, and tumors were subsequently measured with Image J software (NIH) (Kundra et al., 2007; Yang et al., 2005).

## **Bioluminescence imaging**

Mice were injected (*i.p.*) with 100  $\mu$ L of 15 mg/mL D-Luciferin (Goldbio) in PBS, prior to macroscopic bioluminescence imaging using a Xenogen In Vivo Imaging System (IVIS) 200 (PerkinElmer, SAIF, MD Anderson Cancer Center, Houston, TX) at 3 minutes post-injection. Photon flux emitted by luciferase-expressing cells was then recorded using the Living Image software (PerkinElmer).

## **CLINICAL CORRELATES**

### **Immunohistochemistry (IHC) in tissue specimens obtained from human PCa samples**

IHC analysis of FGFR1 and ladinin 1 expression was performed on 60 samples obtained from human PCa. Thirty tissue specimens were derived from the peripheral zone of non-metastatic, untreated, primary PCa (7, Gleason score 8; 23, Gleason score 9; [10, pT2 and 20, pT3]). Another 30 samples were derived from CRPC bone metastases. Samples were obtained from the Prostate Tissue Bank, Department of Pathology, MD Anderson Cancer Center, Houston, TX, under an Institutional Review Board approved protocol. Fresh cut unstained sections as well as HE-stained slides were provided for each sample. Bone metastases specimens were decalcified and formalin-fixed, paraffin-embedded (FFPE) as previously described (Yang et al., 2001).

Unstained tissue sections were stained with anti-FGFR1 antibody (Abcam, rabbit monoclonal, clone EPR806Y) and anti-LAD1 antibody (Sigma-Aldrich, rabbit polyclonal) as described elsewhere (Wan et al., 2014). Briefly, slides were dried lying flat at 56-60°C overnight prior to staining. After deparaffinization and hydration of sections,

heat-induced antigen retrieval was performed using citrate buffer, pH 6.0, in a water bath, and then 5% normal goat serum (Sigma-Aldrich) was used for blocking. Slides were incubated with diluted primary antibody in a humidity chamber at 4°C overnight. After secondary antibody incubation (goat anti-rabbit IgG biotin-conjugated, Invitrogen) at 37°C for 45 minutes, slides were incubated in Streptavidin HRP ready-to-use (RTU) solution (Vector Laboratories) for 30 minutes at room temperature. NovaRed Peroxidase substrate (Vector Laboratories) chromogen was used for visualization of signal (optimal time was determined by monitoring the chromogenic reaction in corresponding controls at the pilot experiment and kept consistent throughout) and Hematoxylin QS (Vector Laboratories) as counterstain, followed by fast dip in lithium carbonate. After hydration and clearing in HistoClear (National Diagnostics), slides were mounted using non-aqueous permanent Vectamount (Vector Laboratories) and examined under bright-field microscopy. Slides were read independently by 2 investigators and classified according to staining intensity (-, +/-, +, ++, +++), with - being negative stain and +++ the most intense staining. Positive/negative (+/-) expression refers to heterogeneous expression, i.e., some areas positive and some areas negative within the same sample, or very slight staining. Evaluations were concordant in 90% of the readings; differences were resolved by consensus after joint review.

Corresponding controls including no primary antibody and no secondary antibody were processed simultaneously following the exact same procedures.

## STATISTICS

GraphPad Prism (GraphPad software) and Microsoft Excel (Microsoft Office Package) were used for statistical analysis. Data were expressed as means  $\pm$  standard deviation (SD), unless otherwise indicated. Two experimental groups were compared with the two-tailed Student's *t* test for unpaired data, unless otherwise specified. Nonparametric Mantel-Cox tests were carried out when comparing Kaplan-Meier survival curves for mice. Chi-squared test was used to compare the number of bone metastases per group. Fisher's exact test was used to compare immunohistochemical scores in human samples. Chi-squared test with Yates correction was used to assess significance of gene amplification differences between cBioPortal datasets. *P* values < 0.05 were considered statistically significant. For RPPA analyses, an adjusted *P* value was calculated by correcting it by the number of events (n=295 o 447) to eliminate false positives.



## **Chapter 3: RESULTS**

Previous studies conducted in our laboratory suggested that targeting FGF signaling interfered with PCa cells-bone cells interaction (Li et al., 2008), and also implicated the FGF axis, mainly FGFR1, in the progression of PCa in bone (Wan et al., 2014). In this work, we applied *in silico*, *in vitro* and *in vivo* preclinical approaches, complemented with correlative studies using human samples to better elucidate the significance of FGFR1 activation in PCa bone metastasis.

### **Different human PCa tissue samples express different FGFR1 isoforms**

Our previous large-scale RNA sequencing study indicated that FGFR1 has the highest expression among all FGFRs in human PCa samples (Wan et al., 2014). Here, we extended our analysis of this dataset by assessing the expression of FGFR1 isoforms and found different FGFR1 isoforms in different PCa (Appendix II). In a further analysis, we identified eight different protein-coding transcripts to be the most abundantly expressed, three of them with a predicted protein length of 731 to 733 amino acids (aa) and lacking the  $\alpha$  exon (ENST00000326324; ENST00000356207; ENST00000397103). The other five with a predicted protein length of 820 to 853 aa and containing the  $\alpha$  exon (ENST00000397091; ENST00000397108; ENST00000397113; ENST00000425967; ENST00000532791) (Appendix II). Based on the predicted protein lengths of these transcripts and the absence or presence of the  $\alpha$  exon, we focused this study on the two best characterized FGFR1 isoforms,  $\alpha$  (containing the  $\alpha$  exon; NM\_023110.2; 822 aa) and  $\beta$  (lacking the  $\alpha$  exon; NM\_023105.2; 733 aa) (Johnson and Williams, 1993).

## **FGFR1 isoforms are associated with the expression of different genes in human PCa**

The findings outlined above suggest that FGFR1 isoforms expression may at least partly underlie PCa heterogeneity. We thus mined PRAD-TCGA dataset to identify transcripts associated with each FGFR1 isoform,  $\alpha$  and  $\beta$ , and subsequently assessed the expression of genes correlated with each isoform by differential expression analysis. As shown in Fig. 18, we found that each FGFR1 isoform transcript is associated with the expression of different genes. In particular, FGFR1  $\beta$  is associated with a larger number of genes than FGFR1  $\alpha$  (Fig. 18).

Heatmap of top 2,000 genes differentially correlated with  
FGFR1 isoforms

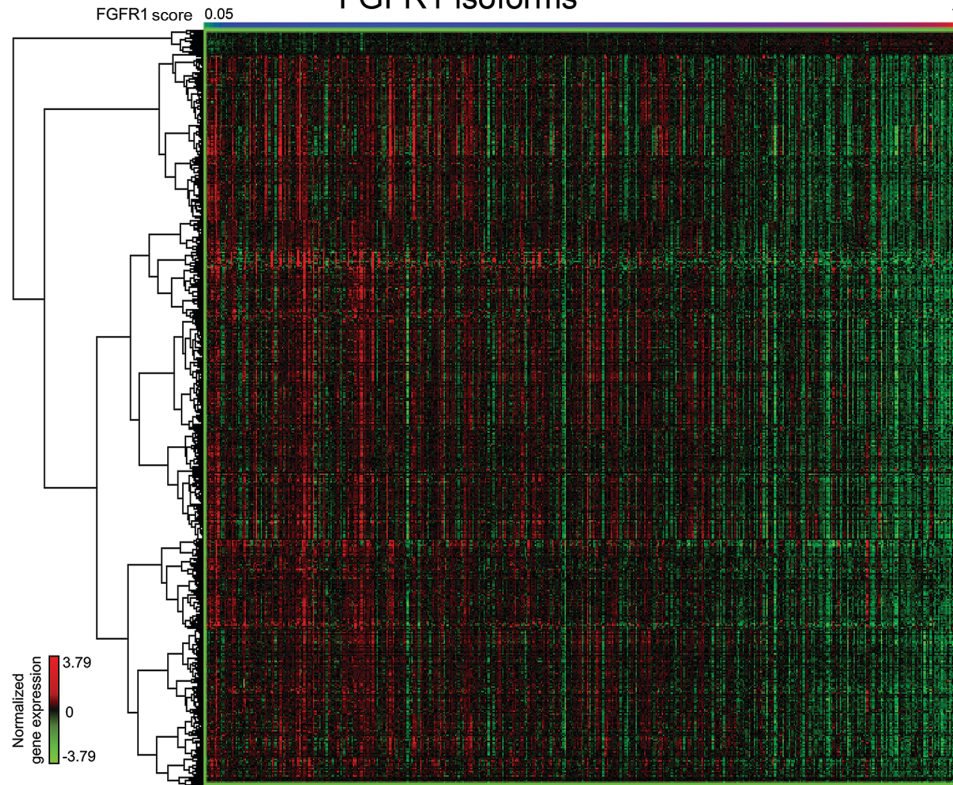


**Figure 18. Heatmap of the 2,000 genes most highly correlated with FGFR1 isoforms  $\alpha$  and  $\beta$  in PRAD-TCGA dataset.** The relative expression of each isoform was defined as the proportion of FGFR1  $\alpha$  to the sum of FGFR1  $\alpha$  + FGFR1  $\beta$  (FGFR1 score) in tumor samples (upper bar) (a high ratio indicates prevalence of the  $\alpha$  isoform, and a low ratio indicates prevalence of  $\beta$  isoform). Rows represent specific genes and columns represent tumor samples arranged in relative levels of FGFR1 isoforms. As the proportion of FGFR1  $\alpha$  increased within the samples, expression of most genes decreased. Red: high normalized gene expression; green: low normalized gene expression (Broom et al., 2017).

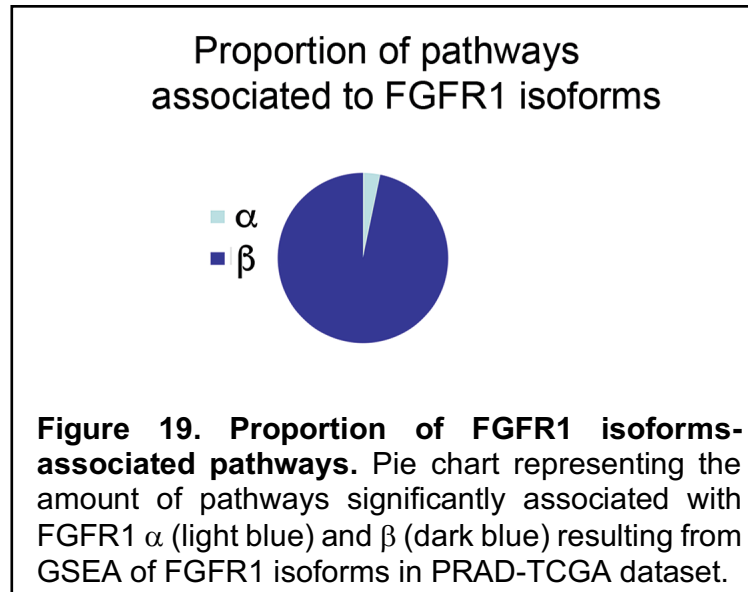
Among the top 20 genes correlated with FGFR1  $\beta$  is *CTSK* (correlation coefficient = 0.539713) (Table 1), coding for cathepsin K, a protease expressed in osteoclasts and involved in bone resorption (Drake et al., 2017).

### Top 20 genes with the highest correlation to FGFR1 isoforms

Genes correlated to FGFR1 $\alpha$			Genes correlated to FGFR1 $\beta$		
gene	correlation	coefficient	gene	correlation	coefficient
PLEKHH1	0.3760326	2.5259998	PMP22	0.5641646	3.928847
THTPA	0.3744982	1.0365405	CORO1C	0.5611298	2.550176
SLC25A42	0.3651624	1.6936021	SERPING1	0.5593268	4.199745
PSD4	0.3630576	1.2315951	FBLN5	0.5554176	4.084689
CANT1	0.3605198	1.3428722	C1S	0.5541675	4.465541
LANCL2	0.3472923	0.8219091	GLT8D2	0.5520242	3.920179
SPTBN2	0.3386063	1.5285074	SYNPO	0.5486689	3.730633
SLC35E1	0.3309034	1.0048222	IGFBP7	0.5479488	3.541869
CNNM3	0.3287317	0.8415453	RAB31	0.5466158	3.504471
ATP13A2	0.3279984	1.0954338	TNFAIP8L3	0.5452566	4.440794
KIAA0319L	0.3274587	1.1546841	RFTN1	0.5434276	3.650135
C15orf37	0.3265595	1.5139643	A2M	0.5428293	4.033372
ALG6	0.3260368	1.2212658	CTSK	0.539713	3.846549
CREB3L4	0.3243941	1.3629656	C3orf59	0.5336978	3.347806
TTLL12	0.3242178	1.2114275	TIMP2	0.5324241	3.359562
INTS5	0.3241892	0.7226837	C1R	0.5310479	4.142481
MOGS	0.3239719	0.8849534	LHFP	0.5270556	3.14607
LOC401588	0.3189179	1.2685184	CLIC2	0.5267913	3.077692
UAP1	0.3173437	1.6361159	CALHM2	0.526377	2.984523
KIAA1543	0.3169949	1.1838213	MFAP4	0.5261008	4.593608

**Table 1. List of the 20 genes most highly correlated with FGFR1  $\alpha$  and  $\beta$  isoforms in PRAD-TCGA dataset.** Gene: gene symbol; correlation: correlation coefficient; coefficient: magnitude of change in gene expression from FGFR1 score 0 (prevalence of FGFR1  $\beta$ ) to 1 (prevalence of FGFR1  $\alpha$ ). The arrow indicates *CTSK*, a gene of particular interest, highly correlated to FGFR1 isoform  $\beta$ .

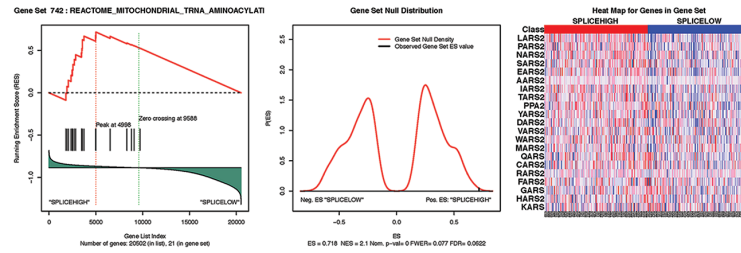
Also, GSEA indicated that FGFR1  $\beta$  isoform is associated with a larger number of pathways than FGFR1  $\alpha$  (FGFR1  $\alpha$   $n = 17$ ; FGFR1  $\beta$   $n = 500$ ) (Fig. 19, Appendix III and IV).



Given the large number of pathways identified, we increased the stringency of prioritized pathways by selecting those with a  $P$  value  $< 0.002$  and normalized enrichment score (NES)  $> 1.78$  for pathways associated with FGFR1  $\alpha$  and  $< -1.78$  for pathways associated with FGFR1  $\beta$  (described in “Methods” section). Using these criteria, we identified only one pathway associated with FGFR1  $\alpha$  (“mitochondrial tRNA aminoacylation”) (Fig. 20A), while FGFR1  $\beta$  was found significantly associated with 50 pathways. Of interest, among those associated with FGFR1  $\beta$  are “MAPK signaling cascade,” “signaling by FGFR in disease,” and “pathways in cancer” (Fig. 20B).

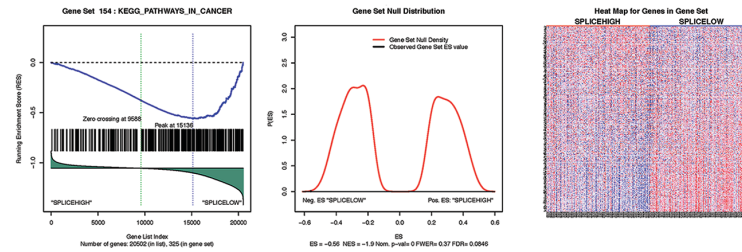
## A Pathway most significantly associated to FGFR1 $\alpha$

Mitochondrial tRNA aminoacylation

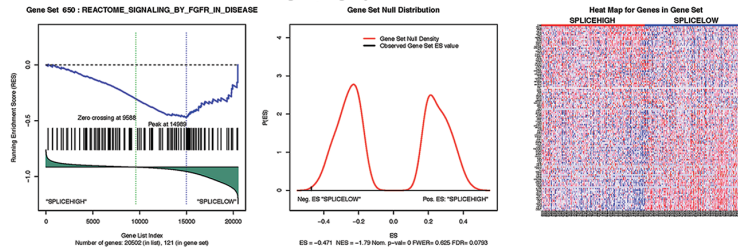


## B Examples of pathways most significantly associated to FGFR1 $\beta$

Pathways in cancer



Signaling by FGFR in disease



MAPK signaling pathway

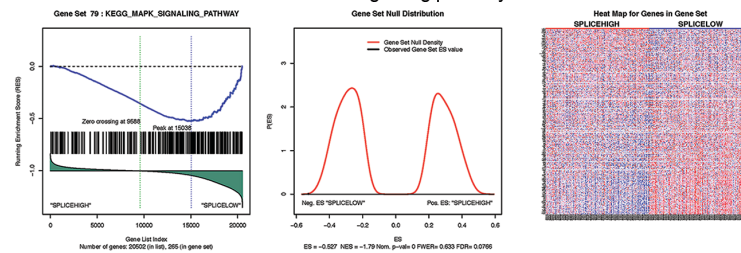


**Figure 20. Most significantly FGFR1  $\alpha$ - and  $\beta$ -associated pathways in PRAD-TCGA dataset.** Pathways most significantly associated with FGFR1  $\alpha$  (A) and FGFR1  $\beta$  (B) identified in GSEA of PRAD-TCGA dataset. The selection criteria were the combined  $P$  value  $< 0.002$  and NES  $> \text{or} < \pm 1.78$ , respectively. Only one pathway significantly associated with FGFR1  $\alpha$  met these criteria; while numerous pathways were found significantly associated with FGFR1  $\beta$  under these criteria. The figure depicts particular pathways of interest selected for  $\beta$ .

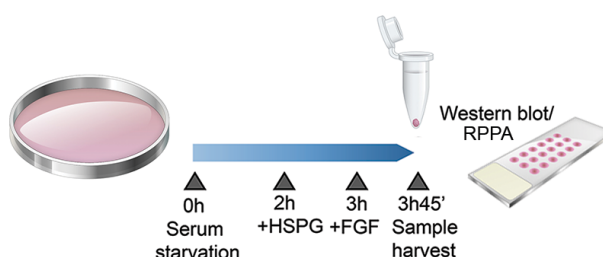
Of note, in PRAD-TCGA dataset analyzed, we found that 11 samples expressed only FGFR1  $\alpha$  (proportion = 1), and one other sample expressed almost only  $\beta$  (proportion = 0.05). The majority of the samples had values between 0.5 and 0.9, indicating a higher proportion of FGFR1  $\alpha$  transcripts than FGFR1  $\beta$  in most PCa.

To further understand the role of FGFR1 isoforms in PCa, we used two different PCa cell lines: PC3, which does not express AR and is therefore hormone insensitive, and C4-2B, an AR-expressing subline of LNCaP obtained from a bone metastasis in mice. Generated PCa cell lines that stably express FGFR1 isoforms (PC3-FGFR1  $\alpha$ ,  $\beta$ ; C4-2B–FGFR1  $\alpha$ ,  $\beta$ ) or empty vector (V) were treated with FGF (Fig. 21A). Western blot analyses showed a greater induction of P-MAPK when cells express FGFR1  $\beta$  isoform (Fig. 21B), which supports our *in silico* findings that the MAPK cascade is significantly associated with the  $\beta$  isoform. RPPA analyses of C4-2B cells that stably express FGFR1 isoforms further confirmed our findings that the MAPK cascade is significantly associated with the  $\beta$  isoform (Fig. 22).



A

## Outline of cell preparation



B

## Western blot analysis

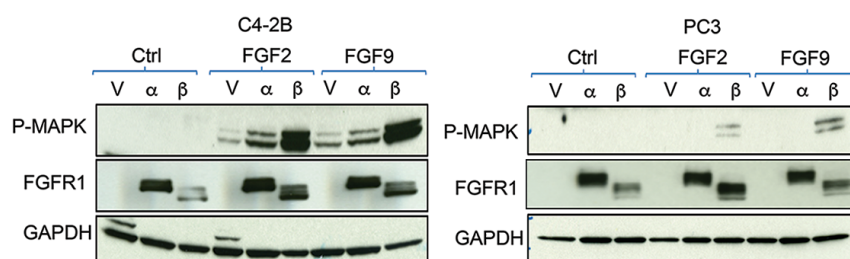
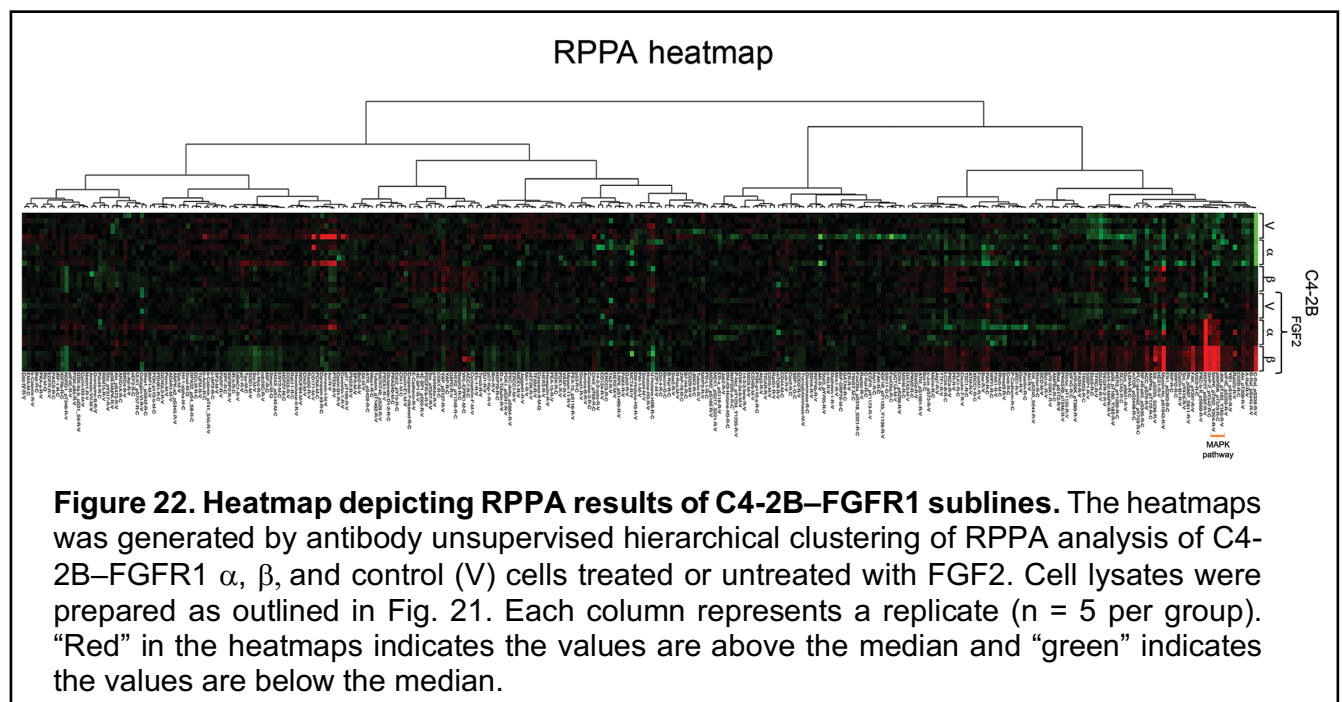
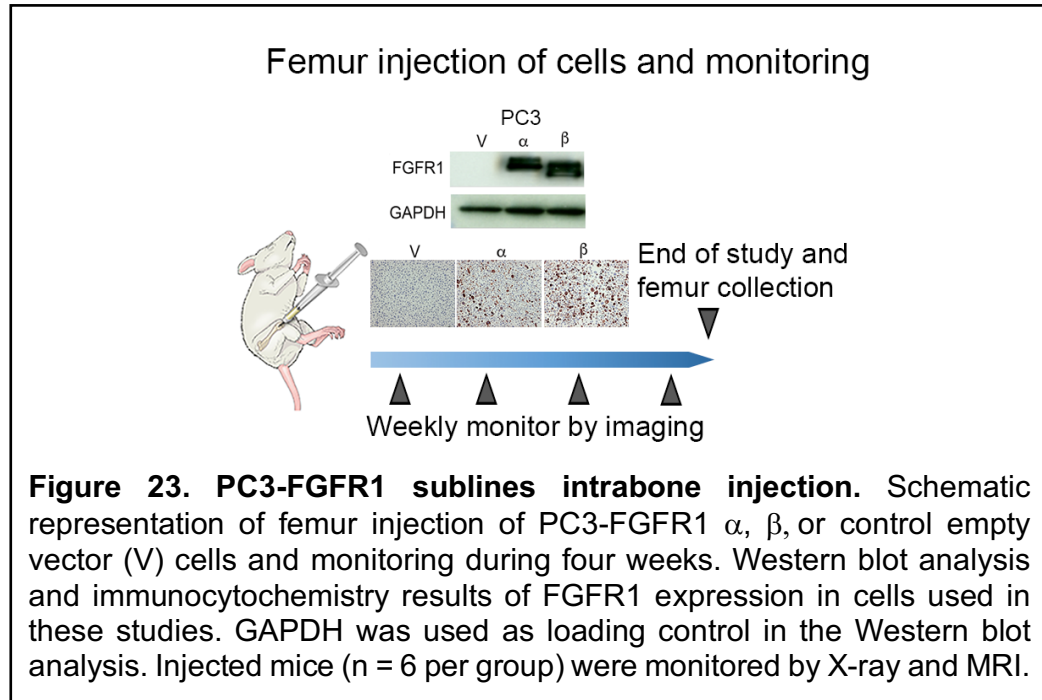


**Figure 21. FGFR1 and P-MAPK expression in PCa cells.** A. Schematic representation of the experimental protocol for cell preparation. PC3- or C4-2B–FGFR1  $\alpha$ ,  $\beta$ , and control (V) cells were cultured in serum-starved conditions for three hours, HSPG (50 ng/mL) was added during the last hour. Subsequently, cells were cultured in the absence or presence of 100 ng/mL FGF2 or FGF9 for 45 minutes. Then, cells were harvested and lysates prepared for Western blot or RPPA (A). B. Western blot analyses of FGFR1 and P-MAPK (Thr202/Tyr204) expression in C4-2B and PC3 cells expressing FGFR1  $\alpha$ ,  $\beta$ , or empty vector (V), untreated or treated with FGF2 and FGF9 as outlined in A. Similar results were obtained in independent experiments. GAPDH was used as loading control.



### FGFR1 alters the bone phenotype induced by PCa cells in tumor-bearing femurs

To understand whether the signaling pathways induced by each isoform in human PCa result in different biological effects, we evaluated tumor growth and bone reaction induced by PC3 cells stably overexpressing FGFR1 isoforms after direct femur injection (Fig. 23).



X-ray analysis of tumor-bearing bones showed several areas of radiolucency that increased overtime, suggesting that these cells induce osteolysis. Quantitative analysis (Bioquant Osteo) of lesions in X-ray images at four weeks after cell injection revealed an increase in radiolucent areas in bones bearing PC3-FGFR1 isoforms tumors compared with PC3-V tumors ( $P = 0.0094$   $\alpha$  vs V;  $P = 0.0001$   $\beta$  vs V) (Fig. 24).

## X-ray analysis of tumor bearing femurs

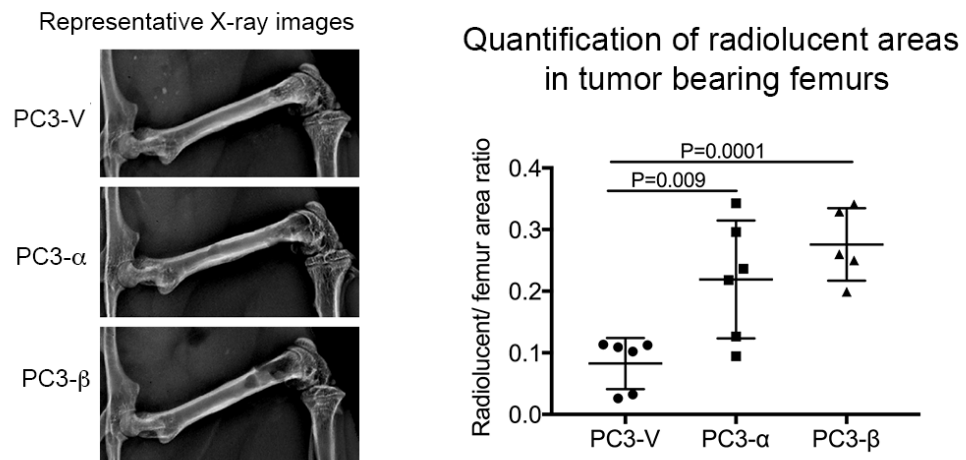


**Figure 24. X-ray analysis of mouse femurs injected with PC3-FGFR1 sublines.** Representative radiographs (left panel) and quantification of radiolucent areas (right panel) of the X-ray analysis of PC3-FGFR1  $\alpha$ ,  $\beta$ , and V tumor-bearing femurs at four weeks after injection. Student's *t* test; error bars indicate SD.

Accordingly, tumor volume, as assessed by MRI analysis, was significantly increased in PC3-FGFR1 isoforms tumors compared to PC3-V tumors ( $P = 0.038$ , Fig. 25).

## MRI analysis of tumor bearing femurs

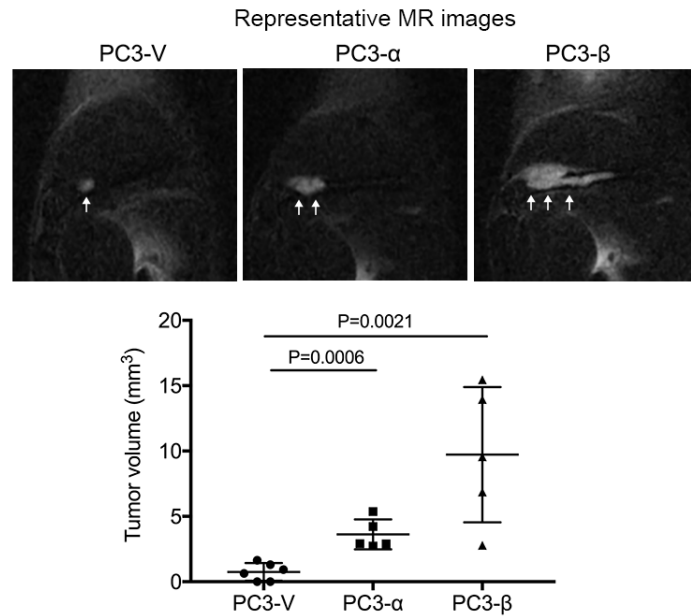
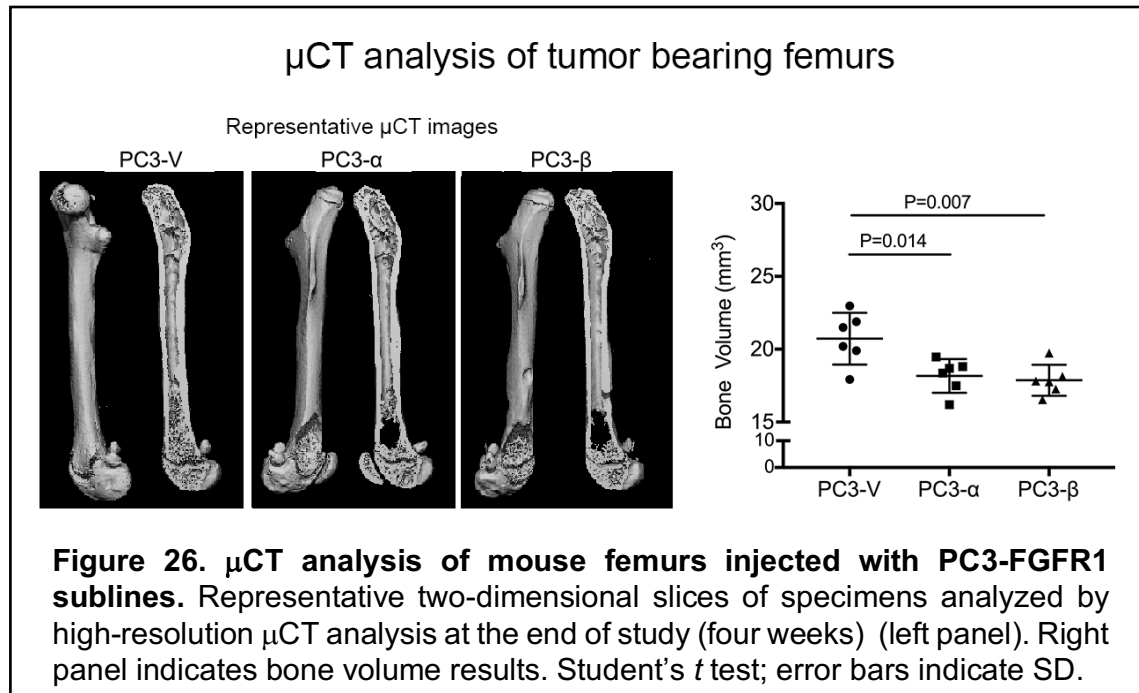


**Figure 25. MRI analysis of mouse femurs injected with PC3-FGFR1 sublines.** Representative sagittal MR images of femurs acquired with a 4.7-T scanner using a T<sub>2</sub>-weighted fast spin (T<sub>2</sub>-FS) echo sequence with fat suppression (upper panel). Arrows indicate tumor, which appears as areas of increased signal on T<sub>2</sub>-weighted images. Tumor volume of PC3-FGFR1  $\alpha$ ,  $\beta$ , or V tumor-bearing femurs assessed by MRI analysis (lower panel). Student's *t* test; error bars indicate SD.

Also, bone volume, as assessed by high resolution  $\mu$ CT analysis, was reduced in femurs injected with PC3-FGFR1  $\alpha$  or  $\beta$  compared with femurs injected with control cells ( $\alpha$   $P = 0.014$ ;  $\beta$   $P = 0.007$ ; Fig. 26).



Together these results indicate that FGFR1 expression in PCa cells induces tumor growth and bone resorption.

In order to understand the cellular changes behind the observed bone phenotype, we performed histomorphometric analyses of tumor-bearing bones. In accordance with the  $\mu$ CT results, we found a reduction of bone mass parameters (bone volume to tissue volume [BV/TV]) in PC3-FGFR1 isoforms tumor-bearing femurs (compared with V controls) (Fig. 27). However, osteoclast parameters (osteoclast surface to bone surface [Oc.S/BS]) were increased in PC3-FGFR1  $\beta$  (but not  $\alpha$ ) compared with PC3-V tumor-bearing femurs (Fig. 27). These results are in accordance with our PRAD-TCGA mining results, where we found an association between FGFR1  $\beta$  and CTSK transcript (a protein predominantly expressed in osteoclasts) (Table 1), as well as with previous reports showing that PCa cells express CTSK (Brubaker et al., 2003; Munari et al., 2017). These evidences indicate that PCa cells expressing FGFR1  $\beta$  are most suited

to activate bone remodeling, which may facilitate tumor growth in bone. This is also in alignment with the greater increase in tumor volume observed in FGFR1  $\beta$  tumors by our MRI analysis (Fig. 25).



## Bone histomorphometry analysis of tumor bearing femurs

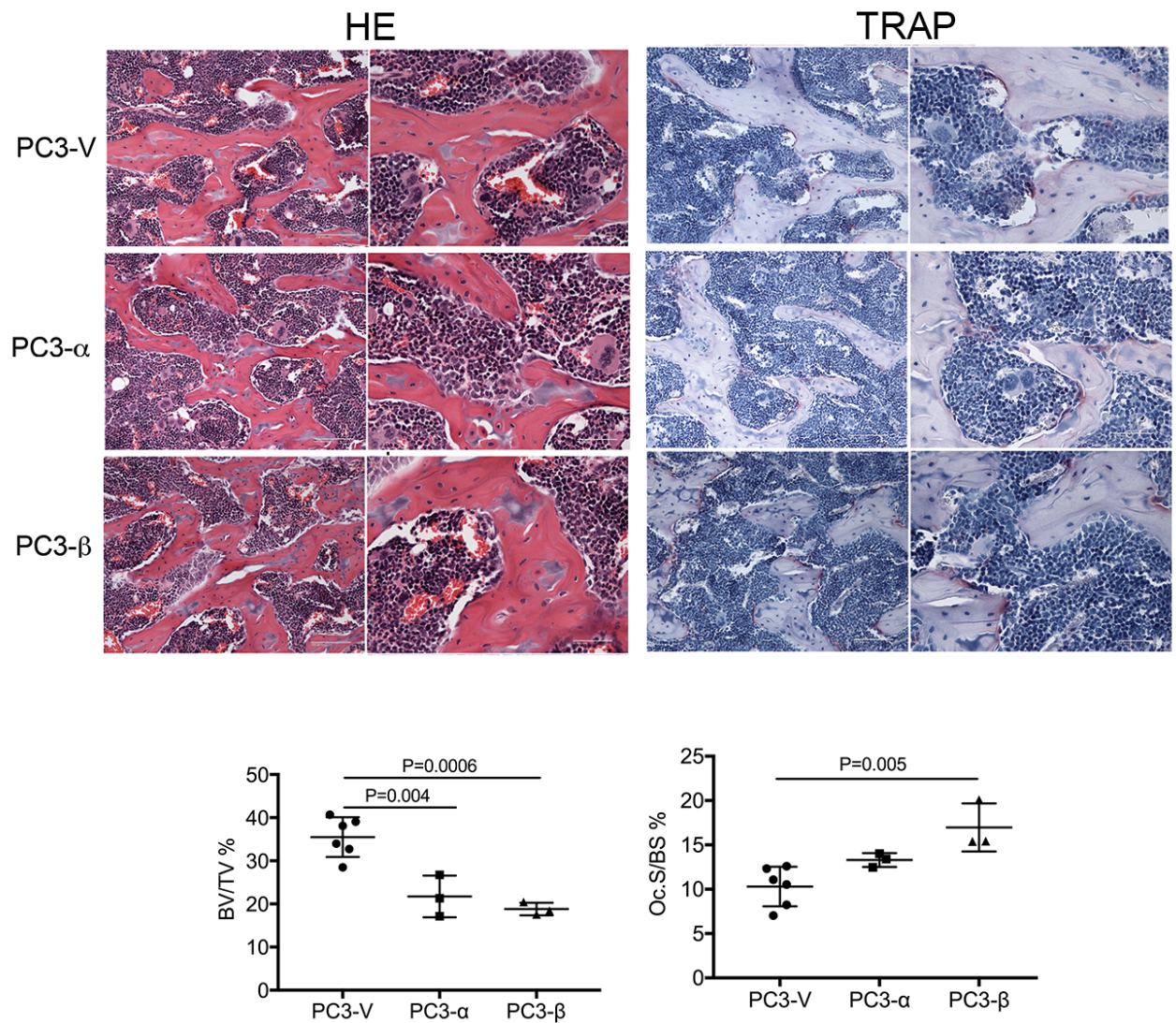
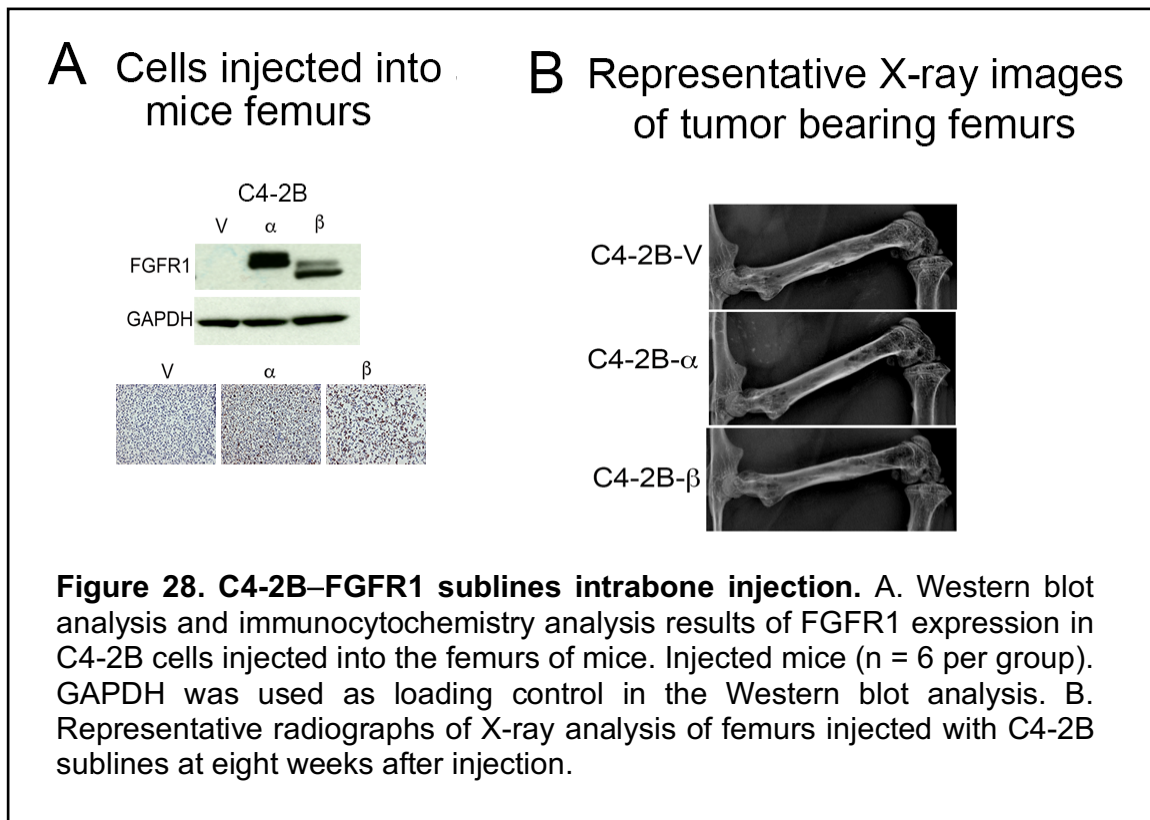


**Figure 27. Bone histomorphometry analysis of mouse femurs injected with PC3-FGFR1 sublines.** Representative photomicrographs of decalcified tumor-bearing femur sections stained with HE (upper left panel) and tartrate-resistant acid phosphatase (TRAP) (upper right panel) (20× magnification, left; 40× magnification, right). Bone histomorphometry analyses indicated a reduced ratio of bone volume to tissue volume (BV/TV) in PC3-FGFR1 tumor-bearing mice (lower left panel). Bone histomorphometry analyses of TRAP-stained sections indicate an increase in osteoclast (Oc) surface to bone surface) in PC3-FGFR1 β tumor-bearing mice (lower right panel). Scale bar, 100μ (20×) o 50μ (40×). Student's *t* test; error bars indicate SD.

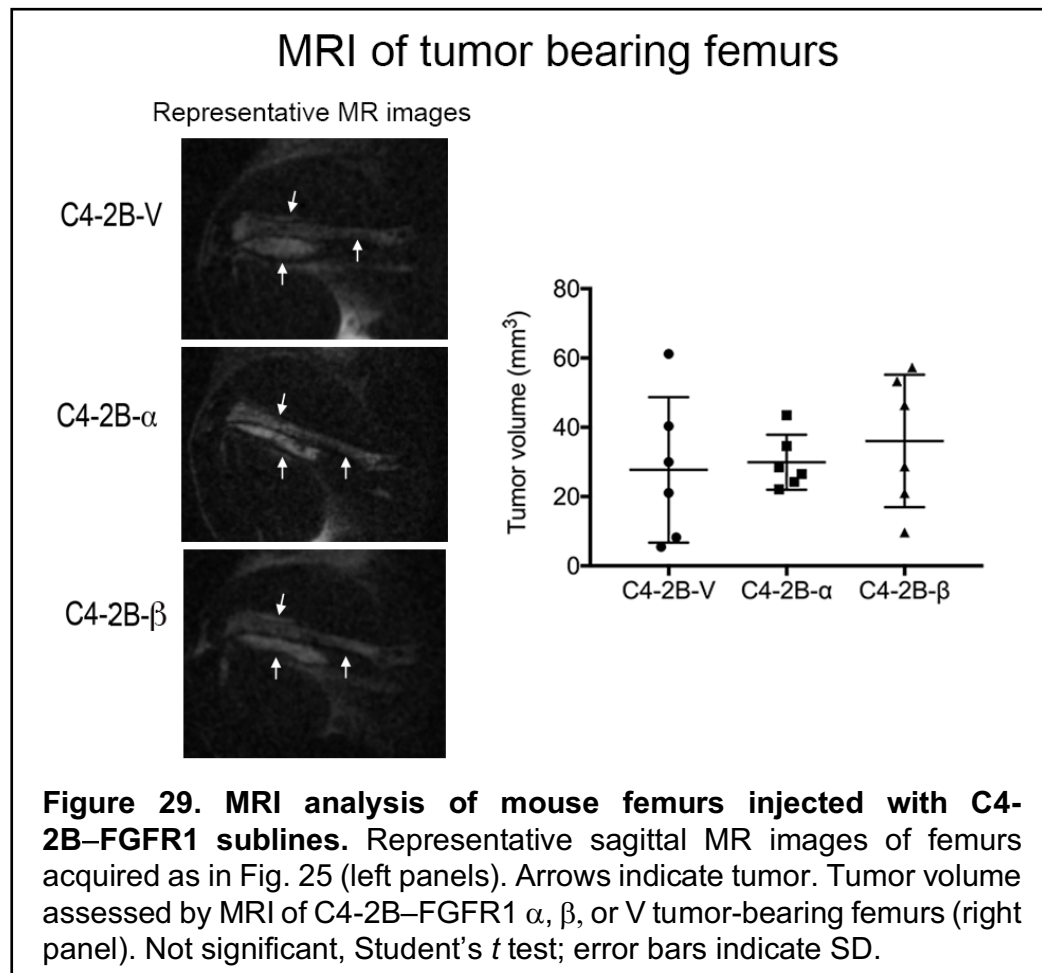


In an independent study, we evaluated the effect of FGFR1 isoform expression in C4-2B cells (Fig. 28A). Again, we monitored tumor growth and bone response of tumor-bearing bones by X-ray. Although we followed the same experimental design as outlined in Fig. 23, in this case we terminated the study at eight weeks given the slow growth rate of this cell line *in vivo*. In agreement with the mixed osteoblastic/osteolytic bone reaction that this cell line typically produces, there were radiolucent and radiopaque areas visible at the X-ray analysis that could not be accurately quantified (Fig. 28B).



All injected mice developed tumor as demonstrated by MR imaging. However, no difference in tumor volume was observed between C4-2B–FGFR1 isoforms and C4-2B-V groups (Fig. 29). Nonetheless, in  $\mu$ CT analysis, we found a decrease in bone volume in the femurs injected with C4-2B–FGFR1  $\beta$  (but not  $\alpha$ ) compared with femurs injected

with C4-2B-V ( $P = 0.024$ ) (Fig. 30).



## μCT analysis of tumor bearing femurs

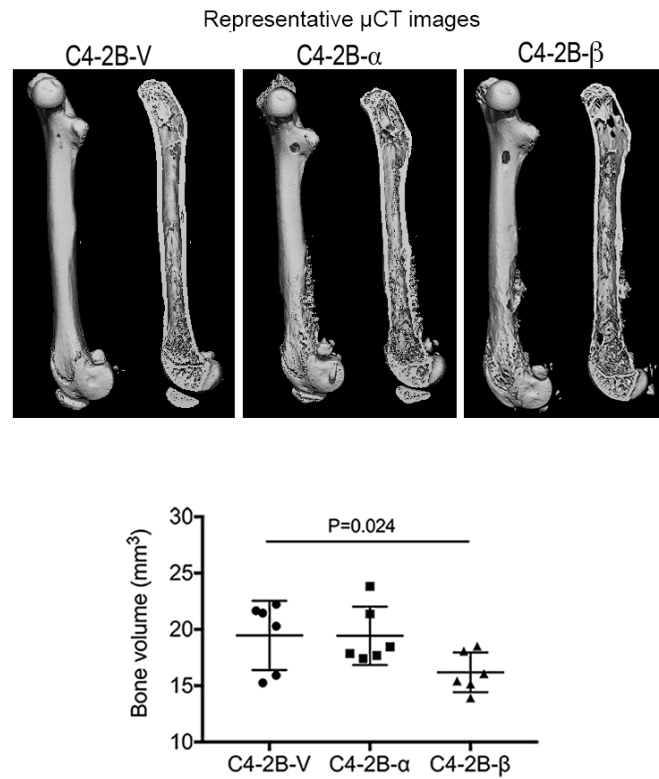
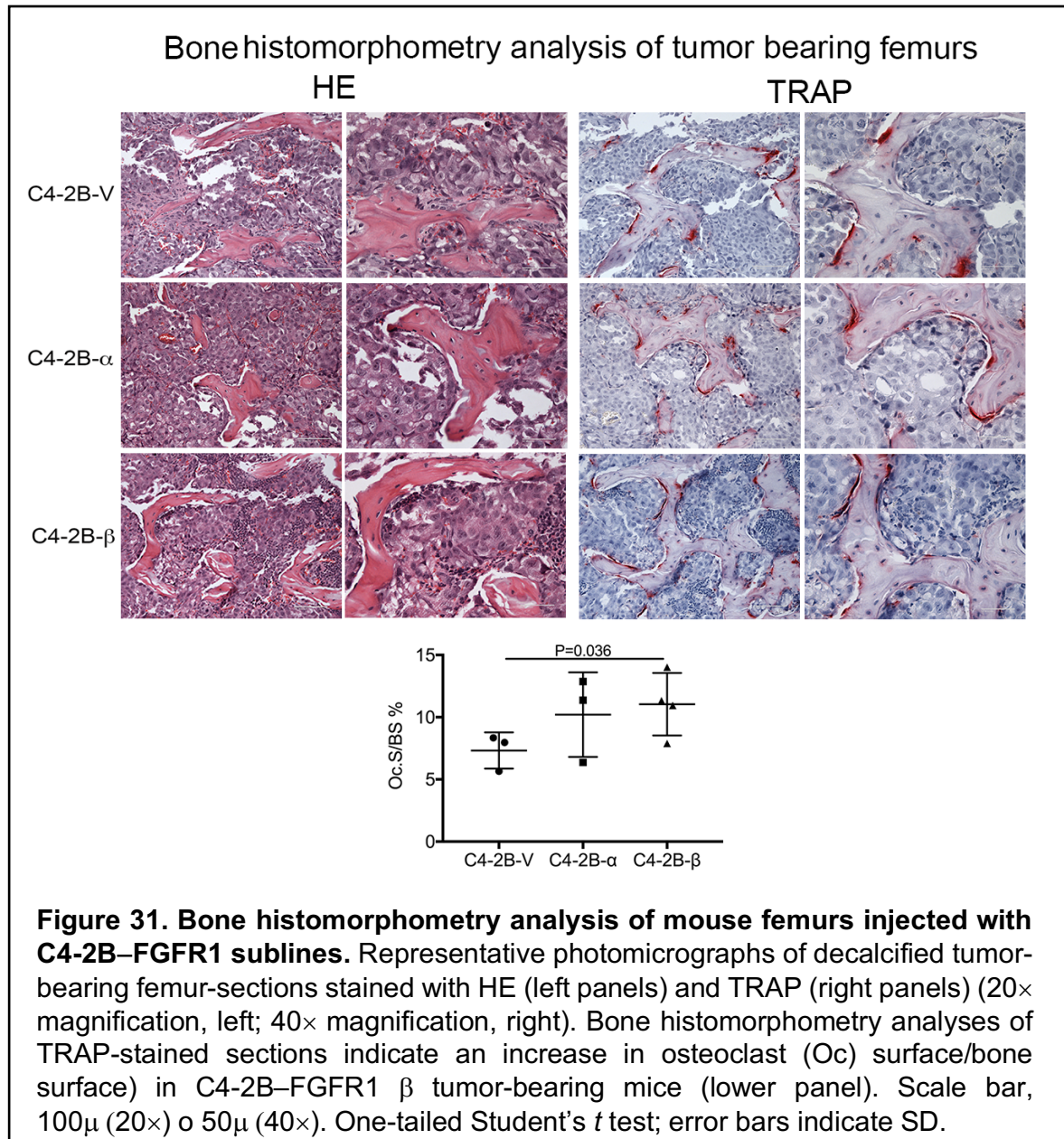


**Figure 30. μCT analysis of mouse femurs injected with C4-2B–FGFR1 sublines.** Representative two-dimensional slices of specimens analyzed by high-resolution μCT analysis at the end of study (upper panel). Lower panel indicates bone volume results. One-tailed Student's *t* test; error bars indicate SD.

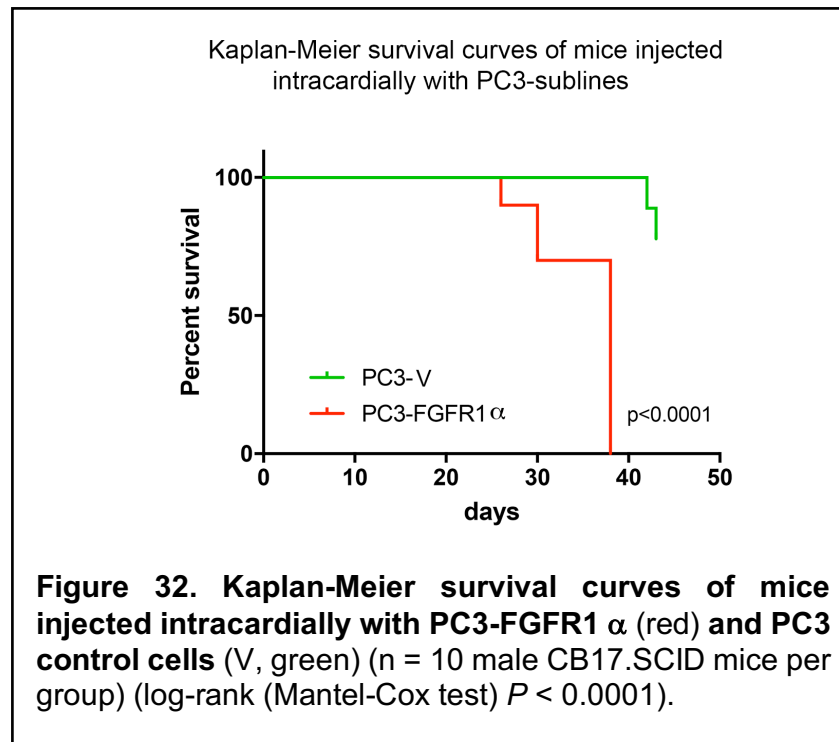
Bone histomorphometry analyses of C4-2B–FGFR1 β (but not α) tumor-bearing mouse bones showed an increase in osteoclast parameters (Oc.S/BS) compared with C4-2B–V mouse bones (Fig. 31). These results support our previous conclusion that PCa cells expressing FGFR1 β are most suited to activate osteoclasts.



### FGFR1 isoforms significantly increase PCa bone metastases *in vivo*

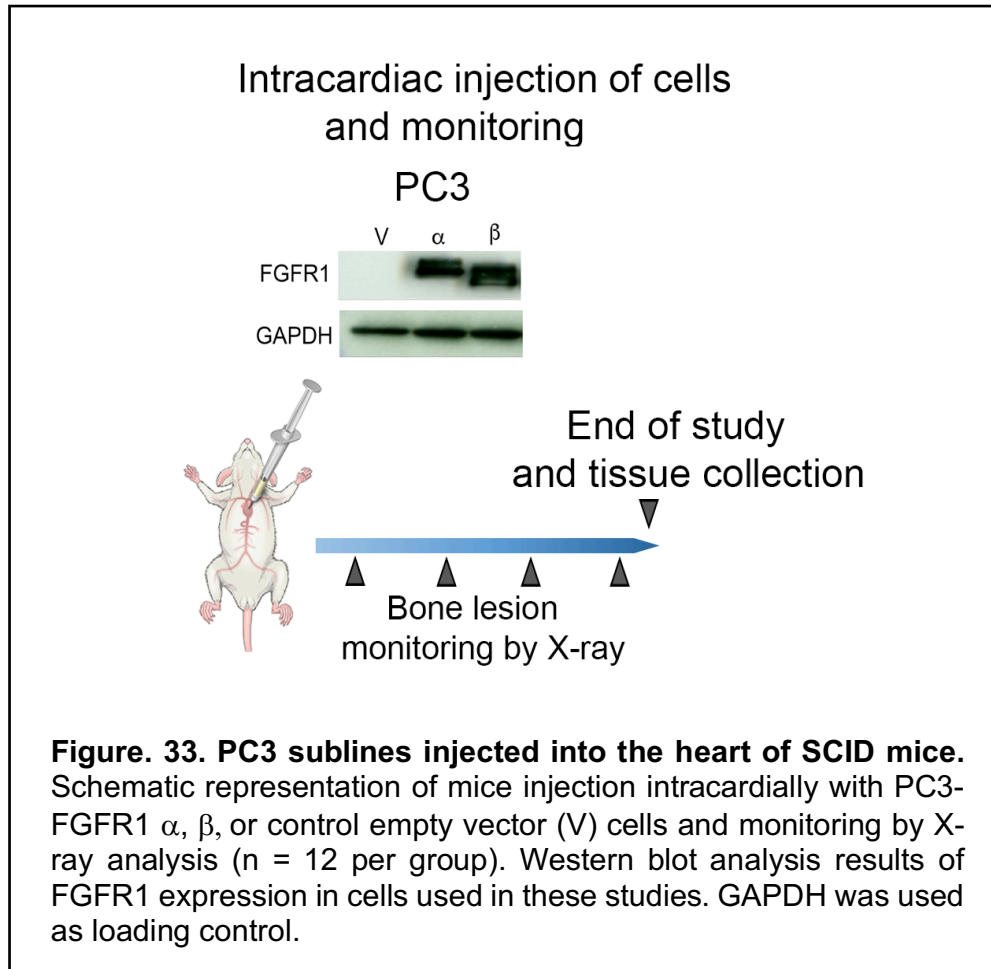
Based on previous reports that FGFR1 is implicated in the pathogenesis of PCa bone metastases (Wan et al., 2014), we then sought to investigate whether FGFR1 isoforms modulate the metastatic potential of PCa cells to bone. In a pilot study we

analyzed the effect of FGFR1 in PC3 cells stably expressing FGFR1  $\alpha$  after intracardiac injection in mice. In animals injected with PC3-FGFR1  $\alpha$ , 3 out of 10 died by four weeks post-injection, and 8 out of 10 died by six weeks post-injection (time in which study was concluded). In contrast, only 1 out of 10 mice injected with PC3-V died before the study was concluded. Statistical analysis indicated that mice injected with PC3-FGFR1  $\alpha$  had significantly reduced survival compared with animals injected with PC3-V ( $P < 0.0001$ ) (Fig. 32).

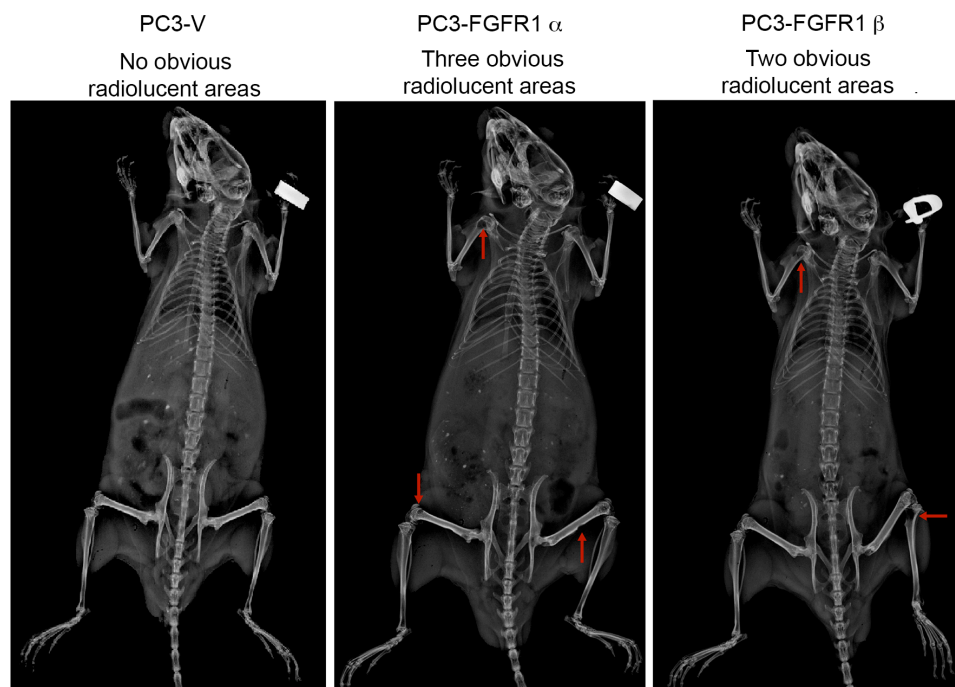


In an independent study, we injected mice intracardially with PC3-FGFR1  $\alpha$ ,  $\beta$ , or V (Fig. 33). Development of bone metastases was monitored by X-ray analysis (Fig. 34). At four weeks post-injection, the study was concluded and necropsy was performed.

We studied radiolucent lesions detected at X-ray imaging for tumor content by morphological analyses of HE-stained tissues (Fig. 35).



Representative X-ray images of mice injected intracardially with PC3 sublines

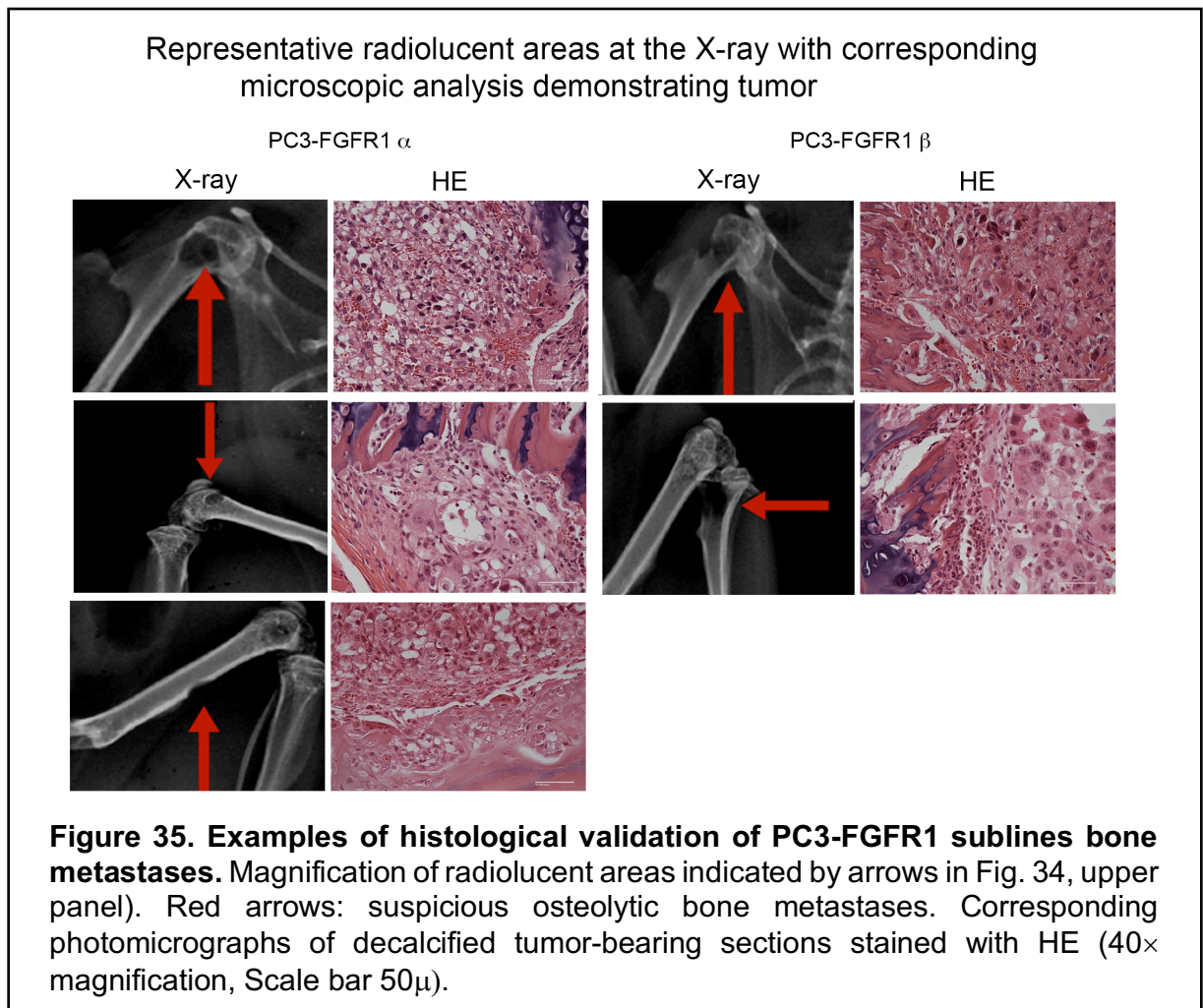


Number of mice with histology confirmed bone metastases

PC3-V	PC3-FGFR1 $\alpha$	PC3-FGFR1 $\beta$
1/12 (8%)	11/12 (92%)	6/12 (50%)

**Figure 34. Rate of bone metastases of PC3-FGFR1 sublines after intracardiac injection into SCID mice.** Representative radiographs of injected whole mice, illustrating radiolucent areas suspicious of osteolytic bone metastases (red arrows) at four weeks post-injection (upper panel). Number of mice with bone metastases after four weeks of intracardiac injection (lower panel).  $P = 0.000045$  FGFR1  $\alpha$  vs V;  $P = 0.02474$  FGFR1  $\beta$  vs V, chi-squared test.



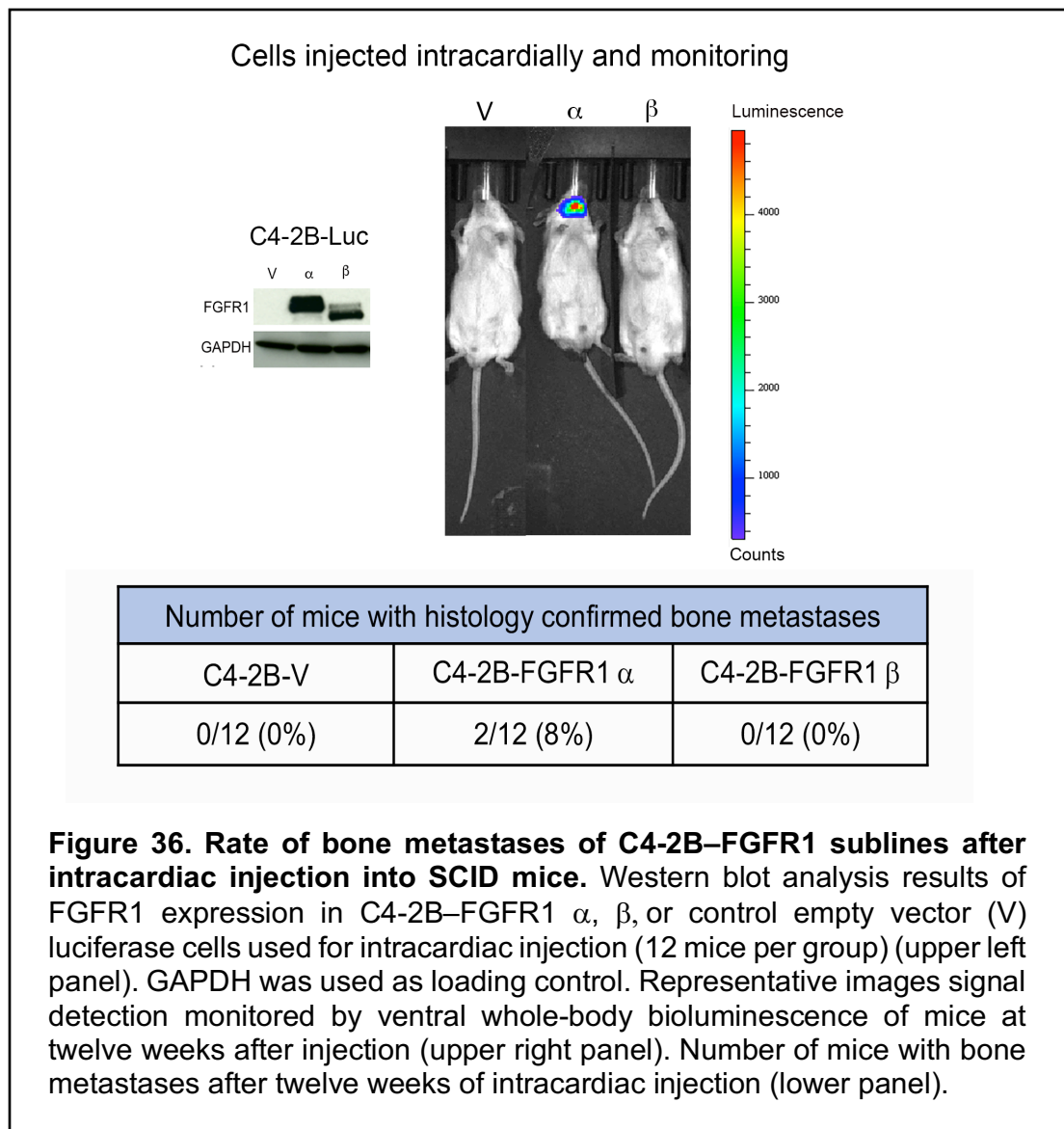


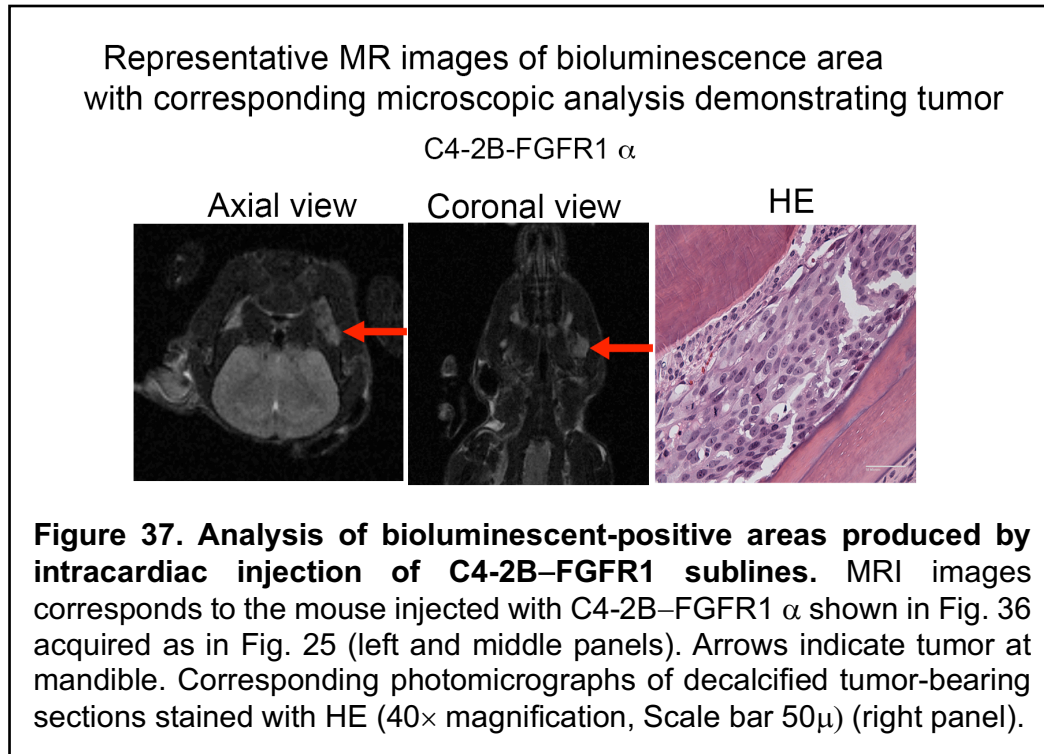
As shown in Fig. 34, significantly more mice injected with PC3-FGFR1  $\alpha$  and PC3-FGFR1  $\beta$  developed bone metastases compared with mice injected with PC3-V ( $P = 0.00005$  and  $P = 0.025$ , respectively). These studies indicate that FGFR1 significantly increases bone metastases in PCa.

To extend our findings, we used C4-2B cells and established FGFR1 isoform sublines (Fig. 36). These lines were made to express luciferase, because C4-2B do not produce clear bone osteolytic lesions, which would allow their identification by direct X-ray analyses. Therefore, metastases were determined by bioluminescence imaging (Fig.



36). We found mice with suspicious lesions, and the precise location of the bioluminescent areas were then identified by MRI (Fig. 37). At necropsy, we harvested suspicious tumors and confirmed, by histology, the presence of mandibular metastases in two mice injected with C4-2B–FGFR1  $\alpha$  (Fig. 37). We did not find bone metastases in mice injected with C4-2B–V or C4-2B–FGFR1  $\beta$  (Fig. 36). Taken together, these results suggest that FGFR1 mediates PCa progression to metastasis and that the penetrance of this effect might be modulated by FGFR1-specific isoforms and by the cellular genetic background.

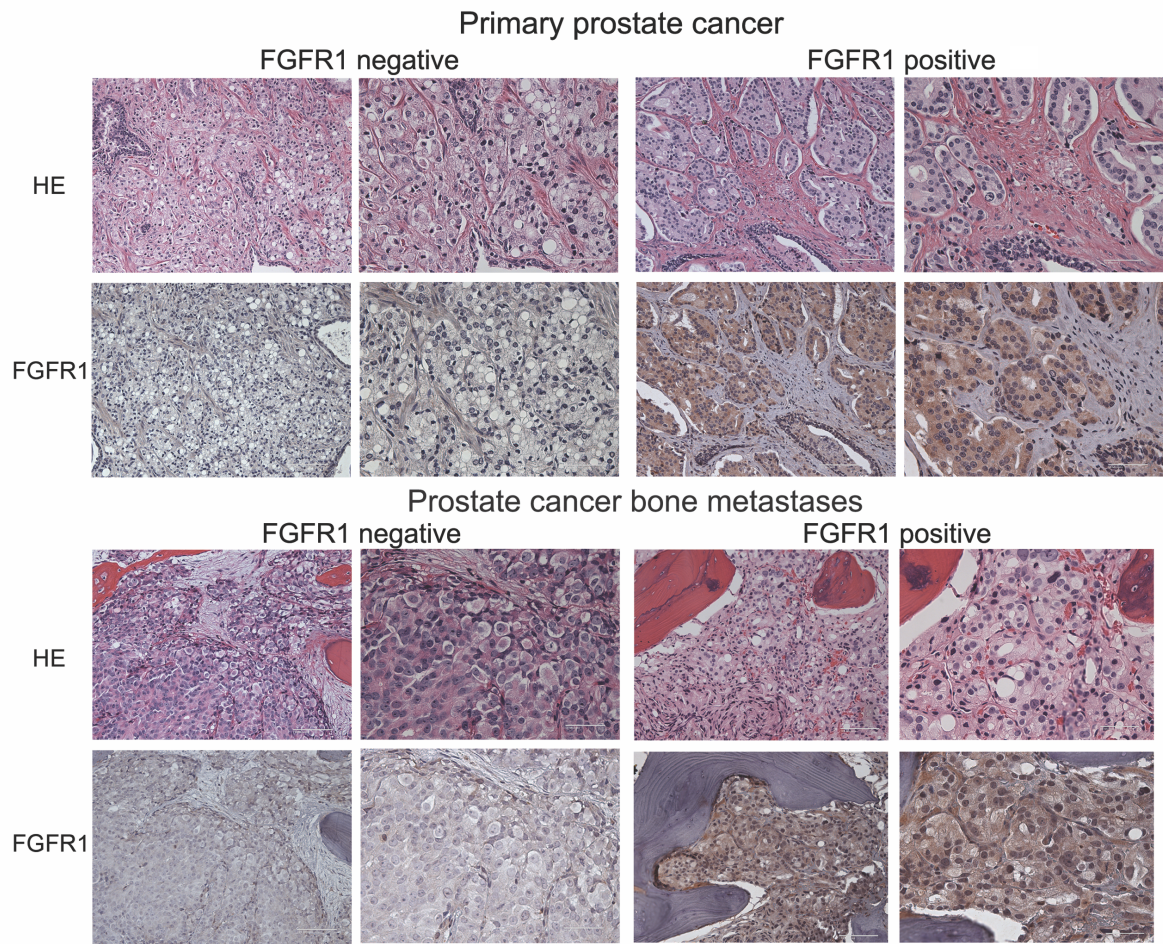




### FGFR1 expression is significantly increased in human PCa bone metastases

To assess the clinical relevance of our findings, we analyzed the expression of FGFR1 in human PCa by IHC analysis. We selected thirty untreated, non-metastatic primary PCa tissue specimens and thirty bone metastatic tissue specimens with CRPC (Fig. 38). Noticeably, we observed a significant enrichment of FGFR1 expression in bone metastases (11/26) versus primary PCa (2/29) ( $P = 0.0007$ ), supporting our postulate that FGFR1 induces the metastatic cascade in PCa. In alignment with our previous RNA sequencing studies in human samples, levels of FGFR1 are heterogenous across samples (Wan et al., 2014).

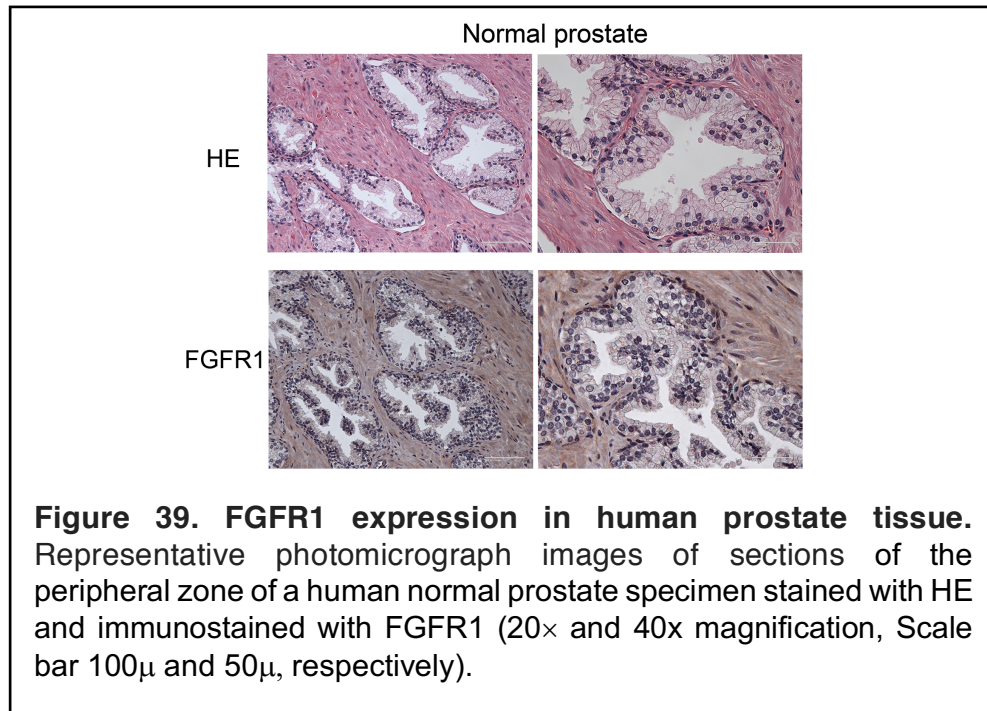
## FGFR1 expression in human prostate cancer



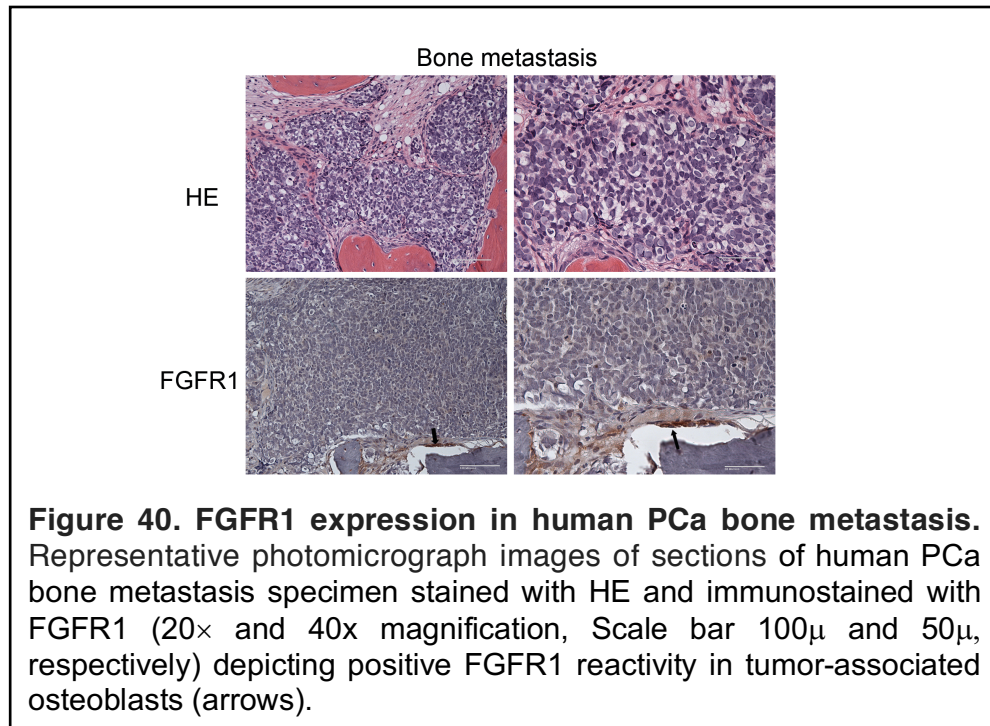
Summary of FGFR1 expression					
Primary prostate cancer (n=29)			Prostate cancer bone metastases (n=26)		
Negative	Positive/negative	Positive	Negative	Positive/negative	Positive
22/29 (76%)	5/29 (17%)	2/29 (7%)	8/26 (31%)	7/26 (27%)	11/26 (42%)

**Figure 38. FGFR1 expression in human PCa.** Representative photomicrograph images of sections stained with HE and immunostained with FGFR1 (20× and 40× magnification, Scale bar 100μ and 50μ, respectively). Table summarizing FGFR1 expression findings in human primary PCa and bone metastatic tissue samples assessed by immunohistochemical analysis (lower panel). Positive/negative (+/-) expression refers to heterogeneous expression, i.e., some areas positive and some areas negative within the same sample, or very slight staining.  $P = 0.0007$ , Fisher's exact test.

As reference for endogenous levels, we assessed the expression of FGFR1 in normal prostate tissue samples (Fig. 39). Additionally, we confirmed our previous report that FGFR1 is expressed in tumor-associated osteoblasts (Wan et al., 2014) in 74% (14/19) of the samples (Fig. 40).

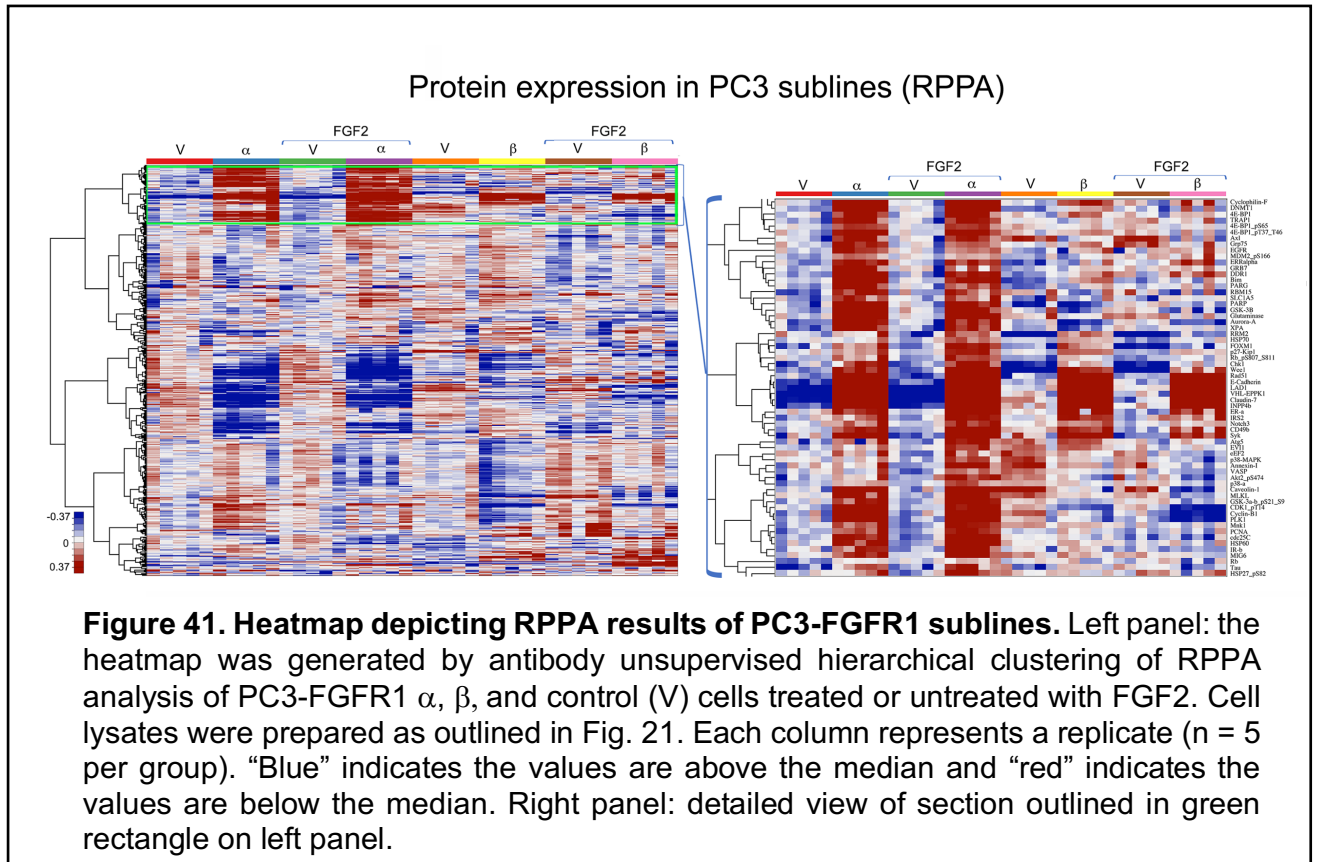




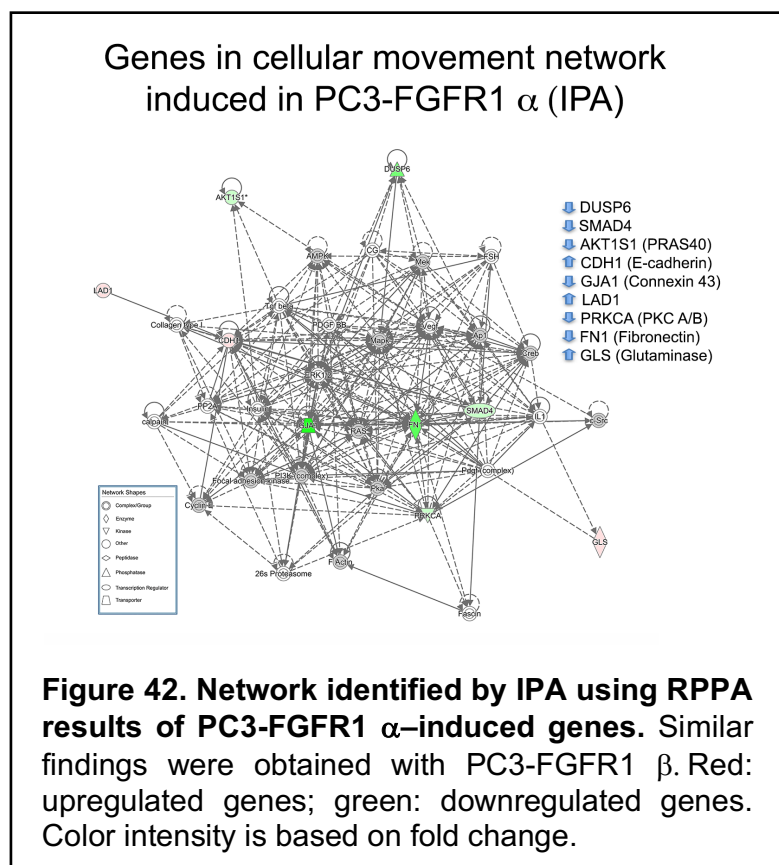


**FGFR1 isoforms induce the expression of ladinin 1, an anchoring filament protein, in PCa PC3 cells.**

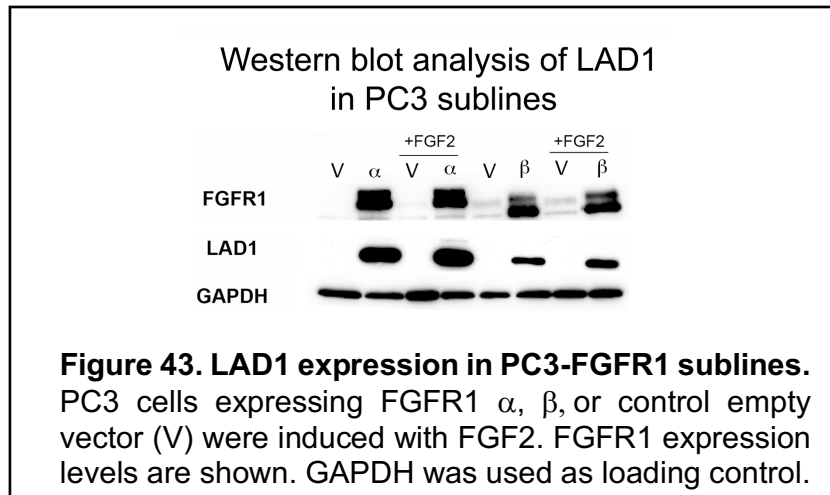
To understand the mechanism of FGFR1-induced metastases, we performed RPPA analysis of PC3 cells stably expressing FGFR1 isoforms (Fig. 41).



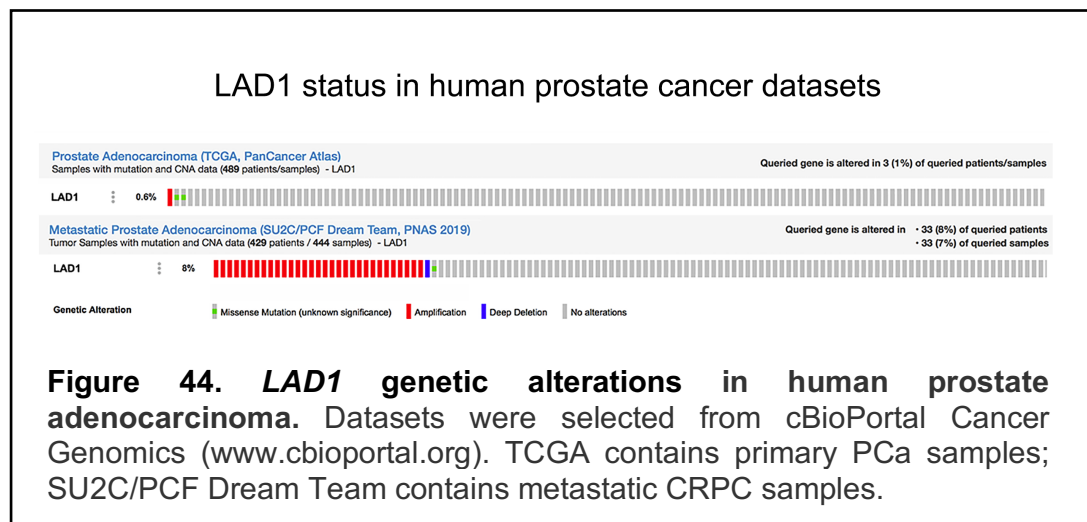
Using Ingenuity Pathway Analysis (IPA) with a fold change of  $\pm 2$ , we found that FGFR1 expression modulates genes in cell movement-associated networks (Fig. 42).



We further prioritized upregulated candidate genes that have been reported to be associated with cancer progression and/or PCa (*LAD1*, *CDH1* and *GLS*) (Putzke et al., 2011; Roth et al., 2018; Santin et al., 2004; Twum-Ampofo et al., 2016; Wang and Guda, 2016). We subsequently confirmed ladinin 1 (*LAD1*) to be upregulated in FGFR1-overexpressing PC3 cells by Western blot analysis (Fig. 43).



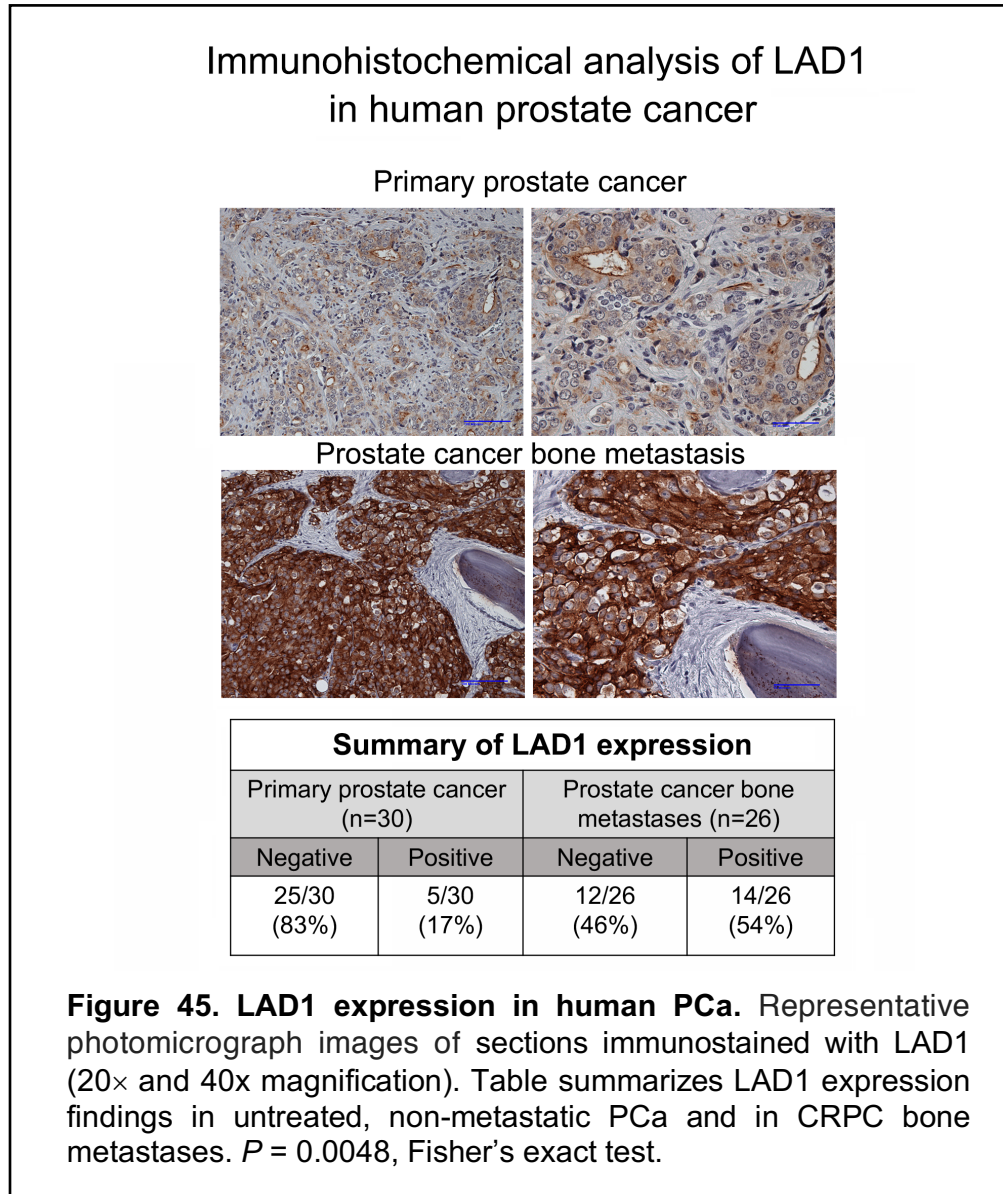
Interestingly, in accordance with our results, *LAD1* gene was significantly amplified in metastatic CRPC (SU2C/PCF Dream Team dataset ((Abida et al., 2019)), compared with cases in PRAD-TCGA dataset (Hoadley et al., 2018), which includes only primary PCa (7% vs 0.2%;  $P < 0.0001$ ) (Fig. 44).



Immunohistochemical analysis of human CRPC bone metastases revealed a significant enrichment of LAD1 expression in bone metastases compared with treatment-



naïve, non-metastatic primary tumors ( $P = 0.0048$ ), supporting the concept that LAD1 mediates, at least in part, the PCa metastatic phenotype (Fig. 45).



## **Chapter 4: DISCUSSION**

Despite effective treatment, no curative therapy is currently available for metastatic PCa. The mechanisms of progression are diverse and include FGF axis activation (Bluemn et al., 2017; Corn et al., 2013; Li et al., 2008; Valta et al., 2008; Wan et al., 2014). Hence, development of FGFR blockade for advanced PCa is critical.

Currently, there are FGFR inhibitors available and clinical trials are ongoing in other malignancies. However, based on prior experience on clinical trials of inhibitors targeting aberrantly activated pathways in CRPC, long-term treatment responses occurred in only a subpopulation of patients, and predictors of treatment response have yet to be validated (Mateo et al., 2015; Saura et al., 2016; Smith et al., 2013; Wan et al., 2014; Zafeiriou et al., 2016). Therefore, it might be expected that a monotherapy with an FGFR inhibitor may not accomplish the desired significant control of PCa progression, and it is essential to identify combination therapies that may optimize efficacy.

Understanding the molecular heterogeneity of tumors led to the successful application of targeted agents in many cancer types (Amirouchene-Angelozzi et al., 2017). As previously mentioned, it is increasingly recognized that PCa is a heterogeneous disease yet available therapies continue to be applied homogeneously. Indeed, the fact that responses to agents with different mechanisms of action were not uniform in PCa patients, is one more evidence of the biological heterogeneity of these tumors and underscore the urgent need to integrate our knowledge of PCa biology into clinical application to address each tumor's unique behavior.

Our comprehensive study of the biological role of two FGFR1 isoforms ( $\alpha$  and  $\beta$ ) and the identification of their different associated signaling pathways in PCa, provides a better understanding of the complexity of this pathway in a clinical context and underlies the importance of defining FGFR1 mediators of PCa progression and markers of FGFR1

signaling. This knowledge brings the relevance of FGFR1 isoforms and their associated gene signatures to the forefront of PCa research and will help develop effective strategies for targeting FGFR1 as PCa therapy.

Our studies also indicate that FGFR1 expression in PCa cells enhances their metastatic behavior. These data are in alignment with our findings of an increase in expression of FGFR1 in CRPC bone metastases compared with primary, untreated PCa. Further, it was previously reported that elevated FGF signaling occurs in a subpopulation of metastatic CRPC (Armstrong et al., 2011; Bluemn et al., 2017) and that it mediates progression under cabozantinib therapy (Varkaris et al., 2016), supporting the concept that, under selective pressure, FGFR1 pathway activation occurs later in the progression of the disease mediating therapy resistance. Considering that many patients progressing under ADT are already metastatic, our observation that FGFR1 further activates the metastatic program of a PCa cell line (PC3) that was already metastatic suggests that FGFR1 mediates not only progression to therapy but also induces secondary metastases. Therefore, the timeframe of initiation of FGFR1 blockade therapy is of utmost relevance as a secondary prevention strategy.

The enhanced metastatic profile of PCa cells expressing FGFR1 was observed in the AR-negative PC3 cell line but was less apparent when we used the AR-positive C4-2B PCa cells, models for AR-negative and AR-positive CRPC, respectively. These results are in agreement with a previous report that FGFR axis mediates the castration-resistance progression of a subpopulation of AR-negative PCa and that AR experimental downregulation results in an increase in FGF signaling (Bluemn et al., 2017). Our results expand on this concept and show that the effects mediated by FGFR1 isoforms are modulated by the genetic background of PCa cells. Indeed, FGFR1 expression in PC3

cells (but not C4-2B) resulted in increased PCa tumor growth in bone. On the other hand, expression of FGFR1  $\beta$  (but not  $\alpha$ ) in both PC3 and C4-2B induced osteoclast parameters in bone after intrafemur injection.

In summary, our studies point to the significance of FGFR1 isoform diversity in PCa and address the need for additional treatment modalities to disrupt the dissemination of PCa cells to bone. Dissecting the role of FGFR1 isoforms in PCa bone metastases will significantly contribute to the identification of men with FGFR1 activation as candidates for FGFR1 blockade.

Another important contribution of our studies was the identification, for the first time, of LAD1 as a downstream target of FGFR1 and its enrichment in CRPC bone metastases.

Constituent of the basement membrane, LAD1 is a relatively uncharacterized protein encoded by the *LAD1* gene, which may be involved in stabilizing the interaction of the epithelium to the mesenchyme (Ishiko et al., 1996). It was recently implicated in actin fiber remodeling, proliferation, and motility of mammary cells (Roth et al., 2018). Further, increased abundance of LAD1 was reported to predict poor prognosis in high-grade breast tumors (Roth et al., 2018), and it was suggested as a new therapy target for triple-negative breast cancer and ovarian cancer (Santin et al., 2004; Wang and Guda, 2016). Further, LAD1 is a downstream target of glucocorticoid receptor (GR) (Chen et al., 2008), which is highly implicated as a resistance mechanism mediating CRPC (Narayanan et al., 2016; Puhr et al., 2018).

Finally, the evidence presented in this report indicates that LAD1 mediates the FGFR1-induced metastases in a subpopulation of cases. The identification of bone metastases specimens that do not express FGFR1 but are positive for LAD1 suggest that

LAD1 may be downstream of other pathways and have a broader role in PCa metastases beyond FGFR1. Hence, the biological implications of LAD1 expression in PCa pathogenesis warrant further investigation.

Overall, here we report for the first time that FGFR1 isoforms are associated with a different gene signature in PCa. The clinical relevance of these results relies on the identification of PCa patient candidates for FGFR1 blockade therapy and the detection of FGFR1 target genes expected to be modulated by FGFR1 targeting. Our findings are also the first to showcase that FGFR1 underlies the metastatic dissemination of PCa, and that LAD1, a relatively uncharacterized anchoring filament protein, is downstream of FGFR1 and enriched in human PCa bone metastases. These results, together with reports indicating that FGFR1 is a major factor involved in disease progression under treatment (Bluemn et al., 2017; Varkaris et al., 2016), suggest that the FGFR1-LAD1 axis mediates progression to metastases and provides a framework of new opportunities for development of FGFR1-LAD1 targeted therapies and/or the identification of markers of progression.

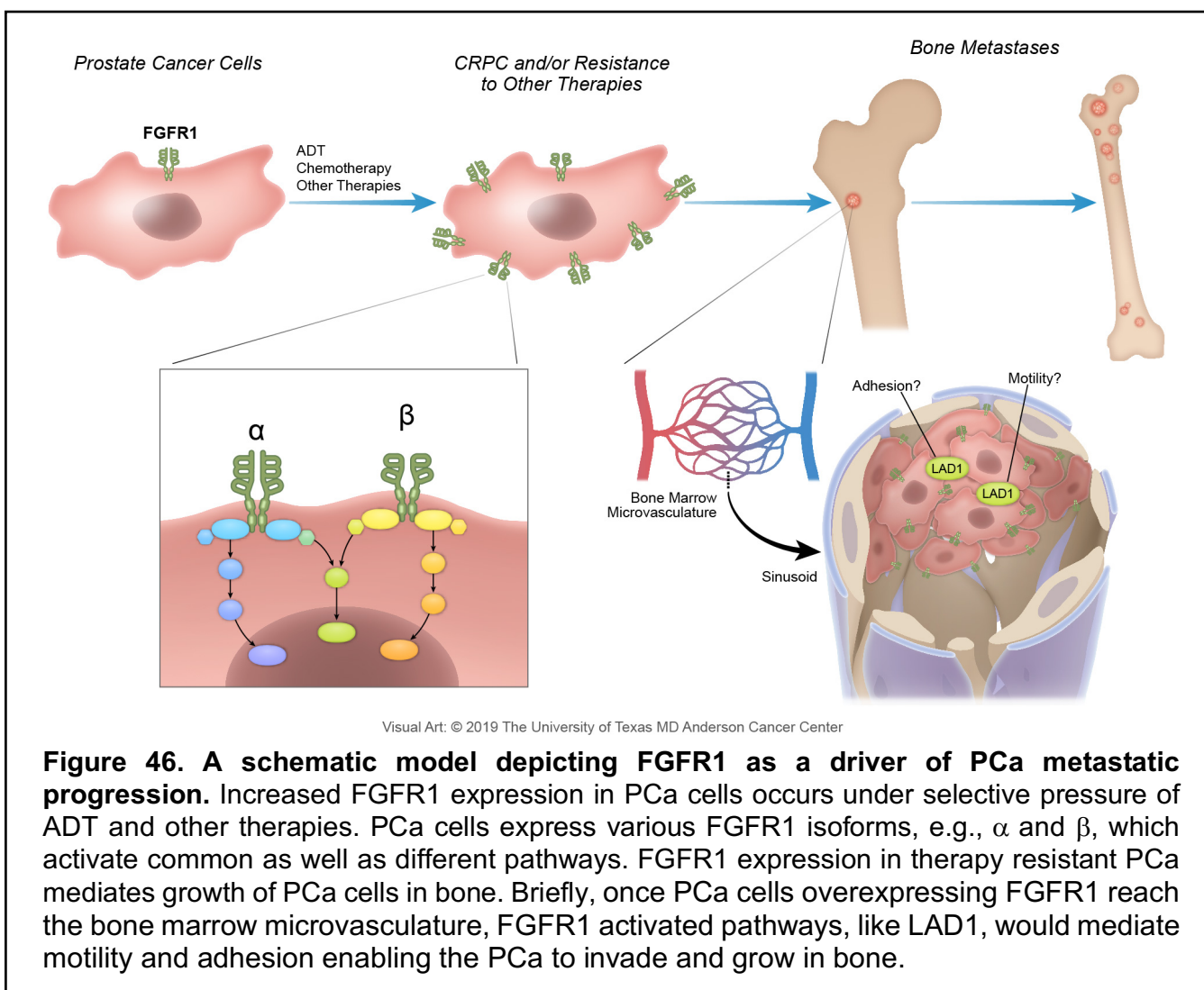


**Figure 46. A schematic model depicting FGFR1 as a driver of PCa metastatic progression.** Increased FGFR1 expression in PCa cells occurs under selective pressure of ADT and other therapies. PCa cells express various FGFR1 isoforms, e.g.,  $\alpha$  and  $\beta$ , which activate common as well as different pathways. FGFR1 expression in therapy resistant PCa mediates growth of PCa cells in bone. Briefly, once PCa cells overexpressing FGFR1 reach the bone marrow microvasculature, FGFR1 activated pathways, like LAD1, would mediate motility and adhesion enabling the PCa to invade and grow in bone.

## Future Directions

In this dissertation, our study has focused on the two best characterized isoforms of FGFR1. It would be of relevant interest to investigate the expression of these isoforms in human tissue, by RNA *in situ* hybridization and study its correlation with PCa clinical stage. Nonetheless, it is worth noting that, as previously described, these are not the only FGFR1 transcripts. Indeed, Ensembl reports more than forty variants for FGFR1, out of

which twenty are protein coding. Hence, we acknowledge that the detection using this technique would include other isoforms as well.

As an initial approach, not described as it is beyond the scope of this dissertation, we have detected expression of some additional variants in PCa and their associated clinical parameters by *in silico* analysis. The clinical relevance as well as the redundancies of all these transcripts and our *in silico* findings remain to be studied in further detail.

Additionally, the existence of different FGFR isoforms resulting from altered splicing can enable stimulation of cancer cells by a broader range of ligands (Brooks et al., 2012). The fact that we have detected numerous isoforms in the bioinformatics approach could be suggestive of this. In fact, in spite of the differences observed, given our findings in which one isoform would support the phenotype/biological effect of the other isoform, our postulate is that presence of both isoforms will be associated with a poorer prognosis or worst outcome. Future directions of interest would be studying the effect of expressing both isoforms simultaneously in the same cell line.

Next steps in this work for an even more in-depth characterization of the isoforms and FGFR1 is immunoprecipitation followed by mass spectrometry. This approach would help in two ways: determine the interacting protein partners, which might aid to better understand the FGFR1-mediated mechanisms of metastasis, as well as the detection of the isoforms at the protein level.

Notably, we also observed FGFR1 staining in tumor-associated osteoblasts in human samples, in line with previous data (Wan et al., 2014); the meaning of this observation and its role in PCa-bone interaction open up an avenue to explore.



On a clinical perspective, this study served as a basis for further studies using a pan-FGFR inhibitor (erdafitinib), of top relevance since it is currently FDA-approved for advanced urothelial bladder cancer (Loriot et al., 2019). Pre-clinical studies in our laboratory with this drug using patient-derived xenografts (PDX) with high and low FGFR1 expression have shown its efficacy and would help define responders to treatment and resistance. The inhibitor targets the tyrosine kinase domain, thus it would be expected that both isoforms will respond the same; however, given their signaling and affinity differences, as well as evidence of diverse responses using another drug in other cancers (Zhao et al., 2019), the experimental study needs to be carried in PCa models.

Furthermore, a more clinically relevant approach would be performing studies using PDX and organoids. In a preliminary screening, we have analyzed the expression of FGFR1 in different PDX by RT-qPCR, Western blot and IHC. We found heterogenous expression, in line with the human sample cohort studies. Of particular interest, the bone metastasis-derived MDA PCa 118b expresses both isoforms, primarily  $\alpha$ . Given this PDX expresses high levels of FGFR1, it will be suitable to genetically (with an inducible system) and pharmacologically disrupt the receptor in this model in order to further analyze its role in the metastatic potential as well as assess modulation of targets that could be driving metastatic progression (i.e. LAD1).

The identification of LAD1 as a novel potential target in PCa progression opens ample opportunities for further studies. Future directions include studying the biological implications of LAD1 expression in PCa pathogenesis by performing *in vitro* and *in vivo* preclinical studies, and correlative analysis with human samples. These involve exploring the invasion potential in cells overexpressing LAD1 and the impact of silencing LAD1

through shRNA or treating with a neutralizing antibody in FGFR1-expressing sublines. This and other future exhaustive studies would help determine the biological mechanisms of LAD1 which, based on our findings and the knowledge available characterizing this protein, could be exerting a dual role, in motility in cancer cells and in adhesion between cancer cells and/or to the stroma. Furthermore, intracardiac injection of FGFR1-expressing cells with LAD1 silencing would help understand the participation of LAD1 in activating the metastatic program of PCa. Again, corresponding studies using PDX with high LAD1 levels would further complement the approach. Complementary non-invasive approaches to monitor patient response to therapy are liquid biopsies, including exosomes, which are extracellular vesicles released from cells containing RNA, DNA and proteins.

With a focus on a metastatic CRPC dataset (cBioPortal SU2C/PCF Dream Team dataset), we report the detection of LAD1 gene amplification in a number of cases; unfortunately, given that the data is recent, expression data is not yet available for the dataset of interest. It is possible that there are a number of cases that are not altered at the DNA level, yet abnormally increased expression will occur at the protein level. Certainly, genetic alterations in PCa are rare, this includes the FGFR1 aberrant expression. For instance, when querying FGFR1 in cBioPortal metastatic dataset with mRNA expression available, a percentage of cases with high mRNA expression lacks genetic alterations. Another important point is to determine what are the relevant levels at the clinical scenario.

Another aspect of relevance for further exploration, based on the evidence presented above, is whether or not there is an interaction between FGFR1-LAD1 axis and

AR, that may influence the outcome of cells expressing FGFR1 and AR. An initial approach would be analyzing the expression of AR by IHC in the human samples used in this work and parallel its status to FGFR1 and LAD1 expression.

Furthermore, as previously mentioned, LAD1 is a downstream target of GR, which is upregulated during resistance to ADT as well as other therapies (Narayanan et al., 2016; Puhr et al., 2018). Since we have detected LAD1 in a substantial amount of human PCa bone metastases cases and propose that the role of this protein might be beyond FGFR1, an additional aspect of interest is to investigate if LAD1 would mediate GR progression to therapy.

Our RPPA analysis has provided a very interesting putative candidate target of FGFR1. The array analysis has resulted in other targets that could be attractive to PCa progression studies. These include the previously mentioned CDH1. Also, a number of DNA-damage response proteins were found upregulated, including Wee1 G2 checkpoint kinase. Again, bioinformatics tools are helpful in this search, for instance, CDH11 (OB-cadherin [osteoblast]) co-expresses with FGFR1 in metastatic CRPC (cBioPortal SU2C/PCF Dream Team).

Our models, intracardiac and intrabone, have allowed the study of the late steps of metastasis, bypassing the first steps. This does not exclude a role for the FGFR1-LAD1 axis in the early steps of metastasis, which might shed light to defining markers of progression and timing therapy regimen. Unfortunately, growth of PCa cells at the orthotopic site does not result in metastatic dissemination to bone, before the health of the mouse is compromised by primary tumor burden. However, metastases to local lymph node would be of interest to study. The use of transgenic mice, such as the well-known

TRAMP model, has proved valuable for the analyses of visceral metastases, since these models have been reported to develop not only lymph node metastases, but also distant metastases to the lungs; although bone metastases occurring in these models are rare (Berish et al., 2018).

Another limitation of our models is the use of immunocompromised mice, which understates the crucial role of the immune system. Specially, in our bioinformatics approach mining molecular correlates to FGFR1 isoforms,  $\beta$  was found associated to many pathways, in particular, many immune-associated pathways. The use of a mouse strain in syngeneic models would compensate this up to certain extent. However, the down-side of using a mouse cell line instead of a human cell line has to be considered to the overall relevance of this model. Considerable efforts have been directed to humanizing mouse models to improve translational outcomes. It is important to highlight that the results obtained in human tissues further validate our findings.

## APPENDIX I

### FGF axis implications in bone metastases of other cancers

Breast Cancer. Breast cancer is the most common malignancy among women worldwide. Breast cancer is classified into different molecular subtypes based on expression of hormone receptors (HR): estrogen receptor and/or progesterone receptor and human epidermal growth factor receptor 2 (HER2), also known as receptor tyrosine-protein kinase erbB-2 (Horton et al., 2018). Among the five major subtypes are estrogen receptor-positive and triple-negative breast cancer (HR-negative and HER2/neu-negative [TNBC]). Breast cancer bone metastases, typically osteolytic, occur in about 70% of cases and are the most common site of disease recurrence. Bone metastases secondary to breast cancer negatively impact patient survival, mobility, and quality of life (Weilbaecher et al., 2011). Breast cancer bone metastases generally produce an osteolytic phenotype by secreting factors that activate the normal bone-resorbing cell, the osteoclast. It has been suggested that FGFs, among other growth factors (e.g., TGF $\beta$ , IGF), are released from the bone matrix during bone resorption, which contributes to the vicious cycle process, originally defined in the context of breast cancer bone metastasis (D'Oronzo et al., 2017; Guise, 2002). FGFR1 gene amplification, which occurs in estrogen receptor-positive breast cancer, represents the most frequent genomic aberration of the FGF axis, whereas amplification of FGFR2-4 genes and FGFR-activating mutations are uncommon (Perez-Garcia et al., 2018). However, whether or not an enrichment of these mutations occurs in bone metastases has not been studied.

Experimental studies indicate that the incidence of bone metastases and growth of osteolytic breast cancer cells is impaired in osteoclast-specific Tgfr2 knockout mice, and this phenotype is rescued by FGF2. Subsequent correlative analysis of human

samples indicate association between the expression of TGFBR2, pSmad-2, and FGFR1 in breast cancer cells and osteoclasts (Meng et al., 2016). Accordingly, it was shown that secreted FGF ligands from breast cancer cells can promote differentiation of osteoclasts, that breast cancer cells enhance osteoclast function in an FGFR-dependent manner, and that this effect is reduced when FGFR is inhibited (Aukes et al., 2017). It is worth noting that the experimental studies outlined below have been done mainly using TNBC cancer models. It remains to be seen if this holds true when using models of other breast cancer subtypes such as estrogen receptor-positive.

Lung Cancer. Of the two main types of lung cancer, small cell lung cancer (SCLC) and non-small cell lung cancer (NSCLC), which accounts for 85% of lung carcinomas, FGFR1 is amplified in 22% of squamous cell lung carcinomas, a subtype of NSCLC (Katoh and Nakagama, 2014). Further, preclinical studies have shown FGFR-altered NSCLC cell lines respond positively to FGFR inhibitors (Hashemi-Sadraei and Hanna, 2017). Lung cancer bone metastases, which occur in 30% to 40% of cases, are typically osteolytic, and the “vicious cycle” defined for other malignancies has also been implicated in this disease (D'Antonio et al., 2014). The release of growth factors from the bone matrix in this context includes FGF ligands.

Bladder Cancer. Urothelial or transitional cell carcinoma is the most common type of bladder cancer, and approximately 30% of its metastases are to the bone (Bellmunt et al., 2010). Alterations in FGFRs are frequent in bladder cancer. Primarily, FGFR3 mutations are found in non-invasive, as well as advanced, metastatic bladder cancer (di Martino et al., 2016). Recently FDA approved an FGFR inhibitor to treat locally advanced or metastatic bladder cancer (Alhalabi et al., 2019).

High levels of FGF-2 have been detected in invasive bladder cancers. Only a correlative study has aimed to explain the molecular mechanism (EMT induction, increased proliferation, and trigger of immune checkpoint) for FGF2-mediated poor prognosis (McNiel and Tschlis, 2017). Once again, it is worth noting that no studies have focused yet on the role of FGF specifically in bone metastases in this disease.

Multiple Myeloma. 70% of patients with multiple myeloma present with bone metastases at diagnosis and 90% will progress and develop bone lesions that are typically osteolytic (Bataille et al., 1989).

Fifteen percent of multiple myeloma patients present with a t(4:14) translocation that results in overexpression of FGFR3. Therefore, clinical trials targeting the FGF pathway have been under study. These included the receptor TKI, dovitinib (TKI258), which showed signs of increased progression-free survival and disease stabilization, but exhibited severe adverse effects on patients (Ghedini et al., 2018; Porta et al., 2017). Other agents that could minimize these off-target effects by being more selective, including monoclonal antibodies (i.e., FGFR3-specific antibody MGFR1877S, hampering receptor dimerization) and more specific inhibitors (i.e., pan-FGFR inhibitor JNJ-42756493 [Janssen pharmaceuticals] and NVP-BGJ398 [Novartis]), are currently under evaluation (Ghedini et al., 2018; Porta et al., 2017). How these agents have direct beneficial effects in bone metastases in particular has not been described in detail, and the bone-specific research area in this context remains relatively unexplored. Thus far, one laboratory based study has shown that the FGFR1 inhibitor NVP-BGJ398 blocked cell growth and blocked the induction of RANKL in co-culture studies of multiple myeloma cells with neonatal mouse calvarie (Suvannasankha et al., 2015).

## APPENDIX II

Most abundant FGFR1 transcript variants expression, grouped by totals levels of expression (reads per kilobase per million (RPKM)). Only RPKM=50 or higher were considered. Transcripts ID are based on ensembl reference annotation.

	# PDXs, human prostate, PCa and normal cells	Total expression on RPKM (Predicted protein length)	ENST00000326324- (731aa)	ENST00000356207 (733aa)	ENST000000397091- (820aa)	ENST00000397103- (733aa)	ENST00000397108- (820aa)	ENST00000397113- (820aa)	ENST00000425967- (853aa)	ENST00000532791- (820aa)
100-200 RPKM	MDA PCa 118b	427.8655514	23.3708	27.7224	48.8548	22.1625	8.54701	55.6413		22.1772
	MDA PCa 155-12	117.4654139				6.78437	9.10308	15.615		5.01488
	PCa 1	118.1781919	10.9309	9.25578	8.30015	10.1135			7.89804	
	PCa 2	113.9026026	9.29076		11.4746	30.2751				
	PCa 3	111.6250986				35.8748				8.01397
	PCa 4	138.9190693	16.6888	13.363	8.52724	23.6115		5.93804		10.9061
	*prsmc	160.7709822	57.5712	32.7191	12.9844					10.9056
	Normal prostate 1	128.4814856		7.53555	12.5837	16.497				
50-100 RPKM	Normal prostate 2	107.782019	20.9962	17.6452	14.0647	7.15797				7.02015
	MDA PCa 146-12	51.20781506						11.0581		
	MDA PCa 150-3	65.7305089						15.2953		
	CWR22	67.34084577		9.21866		12.3439				
	DU145	79.9512445		10.4639	5.22349	13.3995				
	LAPC4	83.00887232				9.44943		7.00601		
	PCa 5	91.47822448	5.54112	5.19175	9.04179	19.898				5.33814
	PCa 6	83.53209378	18.5286		5.15877	7.16404				6.20649
	PCa 7	78.59047831	11.6889			14.2243			7.72551	
	PCa 8	73.44139521	8.78434	7.01864	5.73643	10.1642				
	PCa 9	70.54022119				11.3122		8.57767	5.10366	5.36478
	PCa 10	67.10127222	8.19756		6.81305	9.08281				6.35966
	PCa 11	67.05405656	9.18127		10.1844					
	PCa 12	64.59968344	10.9836			5.86476				
	PCa 13	64.74790703	12.7709		8.5225	6.01785				5.17219
	PCa 14	62.4554847				11.8546				
	PCa 15	62.0401659	5.06302			10.0896			7.10455	
	PCa 16	61.46145327	5.50829			12.7155			5.85344	
	PCa 17	61.58574569	15.5619							5.00763
	PCa 18	58.9497218	8.9148			5.919		5.57059		
	PCa 19	57.65514359	6.12587	7.83535	5.63997	10.925				
	PCa 20	57.2573793						9.42299		
	PCa 21	56.87449593				6.86283			9.85867	
	PCa 22	56.00748482	13.2191		8.9097					
	PCa 23	56.61553416				21.6726		9.17382	6.67297	
	PCa 24	55.9912692				13.1264		7.9531		
	PCa 25	55.22165707	8.53278	7.5201		6.33428				5.15267
	PCa 26	54.14027146				12.3433				
	PCa 27	53.52404405				8.64604			10.8808	
	PCa 28	52.94397734				8.51314			6.61092	
	PCa 29	51.1457494				9.01973				
	PCa 30	50.59670269	6.21757			5.79123				
	PCa 31	50.90175518							11.3804	
	Normal prostate 3	77.37768737				8.15647			14.3598	8.7716
	Normal prostate 4	51.89117413	13.9416		7.89364					
	Normal prostate 5	68.28438842							11.903	
	Normal prostate 6	65.5553075	6.90077	7.14267	6.50364	5.4326				7.37166
	Normal prostate 7	51.4061802				11.0787		5.34857		
	Normal prostate 8	72.38834495	10.5589	7.44605	12.5224	6.67624				7.66432

# PDXs: patient derived xenografts; \*prsmc: human prostate smooth muscle cells



## APPENDIX III

FGFR1 $\alpha$ associated pathways identified in GSEA of TCGA-PRAD dataset. Total number of pathways=22, Total number of pathways with $p < 0.002 = 1$ and selected pathways with $p < 0.002$ and $NES > 1.78 = 1$		
Gene set numbers and names of pathways in KEGG and REACTOME.	Values in each of the parameters associated with the pathways	Pathways that meet selection criteria ( $P < 0.002$ and $NES > 1.78$ )
Gene Set 60 : KEGG_AMINOACYL_TRNA_BIOSYNTHESIS	ES = 0.608 NES = 2.01 Nom. p-val= 0.00956 FWER= 0.16 FDR= 0.0817	
Gene Set 39 : KEGG_GLYCOSYLPHOSPHATIDYLINOSITOL_GPI_ANCHOR_BIOSYNTHESIS	ES = 0.456 NES = 1.67 Nom. p-val= 0.0506 FWER= 0.911 FDR= 0.193	
Gene Set 49 : KEGG_GLYOXYLATE_AND_DICARBOXYLATE_METABOLISM	ES = 0.629 NES = 1.65 Nom. p-val= 0.0363 FWER= 0.935 FDR= 0.211	
Gene Set 73 : KEGG_PROTEIN_EXPORT	ES = 0.604 NES = 1.82 Nom. p-val= 0.0216 FWER= 0.58 FDR= 0.0998	
Gene Set 58 : KEGG_TERPENOID_BACKBONE_BIOSYNTHESIS	ES = 0.696 NES = 1.75 Nom. p-val= 0.0154 FWER= 0.758 FDR= 0.127	
REACTOME_ACTIVATION_OF_THE_MRNA_UPON_BINDING_OF_THE_CAP_BINDING_COMPLEX_AND_EIFS_AND_SUBSEQUENT_BINDING_TO_43S	ES = 0.574 NES = 1.62 Nom. p-val= 0.0747 FWER= 0.962 FDR= 0.235	
Gene Set 1051 : REACTOME_CHOLESTEROL_BIOSYNTHESIS	ES = 0.63 NES = 1.65 Nom. p-val= 0.0455 FWER= 0.93 FDR= 0.21	
REACTOME_FORMATION_OF_TRANSCRIPTION_COUPLED_NER_TC_NER_REPAIR_COMPLEX	ES = 0.567 NES = 1.95 Nom. p-val= 0.00797 FWER= 0.257 FDR= 0.0931	
Gene Set 998 : REACTOME_LATE_PHASE_OF_HIV_LIFE_CYCLE	ES = 0.4 NES = 1.83 Nom. p-val= 0.0388 FWER= 0.559 FDR= 0.104	
Gene Set 566 : REACTOME_METABOLISM_OF_NON_CODING_RNA	ES = 0.53 NES = 1.85 Nom. p-val= 0.0311 FWER= 0.501 FDR= 0.0995	
Gene Set 735 : REACTOME_METABOLISM_OF_POLYAMINES	ES = 0.663 NES = 1.79 Nom. p-val= 0.00591 FWER= 0.663 FDR= 0.113	
Gene Set 742 : REACTOME_MITOCHONDRIAL_TRNA_AMINOACYLATION	ES = 0.718 NES = 2.1 Nom. p-val= 0 FWER= 0.077 FDR= 0.0622	Y
Gene Set 774 : REACTOME_MRNA_PROCESSING	ES = 0.433 NES = 1.93 Nom. p-val= 0.0244 FWER= 0.3 FDR= 0.0672	
Gene Set 989 : REACTOME_NEP_NS2_INTERACTS_WITH_THE_CELLULAR_EXPORT_MACHINERY	ES = 0.556 NES = 1.62 Nom. p-val= 0.0348 FWER= 0.961 FDR= 0.248	
Gene Set 797 : REACTOME_NUCLEOTIDE_EXCISION_REPAIR	ES = 0.427 NES = 1.61 Nom. p-val= 0.0768 FWER= 0.965 FDR= 0.217	
Gene Set 692 : REACTOME_PROCESSING_OF_CAPPED_INTRON_CONTAINING_PRE_MRNA	ES = 0.464 NES = 1.78 Nom. p-val= 0.0318 FWER= 0.707 FDR= 0.118	
Gene Set 1057 : REACTOME_RNA_POL_I_TRANSCRIPTION_INITIATION	ES = 0.551 NES = 1.74 Nom. p-val= 0.0133 FWER= 0.805 FDR= 0.134	
Gene Set 771 : REACTOME_TRANSCRIPTION_COUPLED_NER_TC_NER	ES = 0.522 NES = 1.86 Nom. p-val= 0.0185 FWER= 0.48 FDR= 0.108	
REACTOME_TRANSPORT_OF_MATURE_MRNA_DERIVED_FROM_AN_INTRONLESS_TRANSCRIPT	ES = 0.55 NES = 1.72 Nom. p-val= 0.0114 FWER= 0.844 FDR= 0.149	
Gene Set 706 : REACTOME_TRANSPORT_OF_MATURE_TRANSCRIPT_TO_CYTOPLASM	ES = 0.465 NES = 1.59 Nom. p-val= 0.057 FWER= 0.974 FDR= 0.238	
Gene Set 991 : REACTOME_TRANSPORT_OF_RIBONUCLEOPROTEINS_INTO_THE_HOST_NUCLEUS	ES = 0.552 NES = 1.61 Nom. p-val= 0.0306 FWER= 0.964 FDR= 0.227	
Gene Set 758 : REACTOME_TRNA_AMINOACYLATION	ES = 0.612 NES = 1.94 Nom. p-val= 0.0132 FWER= 0.272 FDR= 0.0752	

ES: enrichment score; Nom. p-val: nominal  $P$  value; FWER: family-wise error rate; FDR: false discovery rate.

## APPENDIX IV

FGFR1  $\beta$  associated pathways identified in GSEA of TCGA-PRAD dataset. Total number of pathways=749, Total number of pathways with  $p < 0.002$ =105 and selected pathways with  $p < 0.002$  and  $NES < -1.78$ =50

Gene set numbers and names of pathways in BIOCARTA, KEGG, NABA, PID, REACTOME, SA, SIG and ST.	Values in each of the parameters associated with the pathways	Pathways that meet selection criteria ( $P < 0.002$ and $NES < -1.78$ )
Gene Set 312 : BIOCARTA_41BB_PATHWAY	ES = -0.534 NES = -1.3 Nom. p-val= 0.194 FWER= 1 FDR= 0.21	
Gene Set 294 : BIOCARTA_ACH_PATHWAY	ES = -0.566 NES = -1.3 Nom. p-val= 0.186 FWER= 1 FDR= 0.21	
Gene Set 327 : BIOCARTA_ACTINY_PATHWAY	ES = -0.476 NES = -1.55 Nom. p-val= 0.0676 FWER= 0.99 FDR= 0.089	
Gene Set 184 : BIOCARTA_AGR_PATHWAY	ES = -0.594 NES = -1.55 Nom. p-val= 0.0404 FWER= 0.991 FDR= 0.0894	
Gene Set 185 : BIOCARTA_AKT_PATHWAY	ES = -0.534 NES = -1.65 Nom. p-val= 0.0282 FWER= 0.924 FDR= 0.0732	
Gene Set 186 : BIOCARTA_ALK_PATHWAY	ES = -0.621 NES = -1.72 Nom. p-val= 0 FWER= 0.785 FDR= 0.0729	
Gene Set 182 : BIOCARTA_AMI_PATHWAY	ES = -0.715 NES = -1.47 Nom. p-val= 0.056 FWER= 0.999 FDR= 0.116	
Gene Set 183 : BIOCARTA_ARAP_PATHWAY	ES = -0.493 NES = -1.57 Nom. p-val= 0.0446 FWER= 0.985 FDR= 0.0841	
Gene Set 187 : BIOCARTA_AT1R_PATHWAY	ES = -0.419 NES = -1.48 Nom. p-val= 0.103 FWER= 0.999 FDR= 0.114	
Gene Set 280 : BIOCARTA_BAD_PATHWAY	ES = -0.531 NES = -1.45 Nom. p-val= 0.0669 FWER= 0.999 FDR= 0.121	
Gene Set 192 : BIOCARTA_BCR_PATHWAY	ES = -0.589 NES = -1.61 Nom. p-val= 0.0175 FWER= 0.964 FDR= 0.0759	
Gene Set 193 : BIOCARTA_BIOPEPTIDES_PATHWAY	ES = -0.433 NES = -1.48 Nom. p-val= 0.0532 FWER= 0.999 FDR= 0.113	
Gene Set 297 : BIOCARTA_BARRESTIN_SRC_PATHWAY	ES = -0.529 NES = -1.54 Nom. p-val= 0.054 FWER= 0.993 FDR= 0.0931	
Gene Set 191 : BIOCARTA_BCELLSURVIVAL_PATHWAY	ES = -0.476 NES = -1.28 Nom. p-val= 0.181 FWER= 1 FDR= 0.218	
Gene Set 214 : BIOCARTA_CALCINEURIN_PATHWAY	ES = -0.551 NES = -1.51 Nom. p-val= 0.0447 FWER= 0.996 FDR= 0.101	
Gene Set 288 : BIOCARTA_CARDIACEGF_PATHWAY	ES = -0.564 NES = -1.36 Nom. p-val= 0.115 FWER= 1 FDR= 0.171	
Gene Set 195 : BIOCARTA_CARM_ER_PATHWAY	ES = -0.449 NES = -1.52 Nom. p-val= 0.0403 FWER= 0.995 FDR= 0.0978	
Gene Set 196 : BIOCARTA_CASPASE_PATHWAY	ES = -0.611 NES = -1.65 Nom. p-val= 0.0301 FWER= 0.927 FDR= 0.0731	
Gene Set 197 : BIOCARTA_CCR3_PATHWAY	ES = -0.639 NES = -1.68 Nom. p-val= 0.00399 FWER= 0.892 FDR= 0.0726	
Gene Set 269 : BIOCARTA_CCR5_PATHWAY	ES = -0.736 NES = -1.57 Nom. p-val= 0.00984 FWER= 0.987 FDR= 0.086	
Gene Set 198 : BIOCARTA_CD40_PATHWAY	ES = -0.599 NES = -1.45 Nom. p-val= 0.0559 FWER= 0.999 FDR= 0.123	
Gene Set 295 : BIOCARTA_CDC42RAC_PATHWAY	ES = -0.535 NES = -1.58 Nom. p-val= 0.0062 FWER= 0.983 FDR= 0.0812	
Gene Set 194 : BIOCARTA_CDMAC_PATHWAY	ES = -0.569 NES = -1.46 Nom. p-val= 0.0651 FWER= 0.999 FDR= 0.119	
Gene Set 209 : BIOCARTA_CELLCYCLE_PATHWAY	ES = -0.504 NES = -1.29 Nom. p-val= 0.208 FWER= 1 FDR= 0.213	
Gene Set 188 : BIOCARTA_CHEMICAL_PATHWAY	ES = -0.452 NES = -1.63 Nom. p-val= 0.0252 FWER= 0.943 FDR= 0.0763	
Gene Set 279 : BIOCARTA_CHREBP2_PATHWAY	ES = -0.334 NES = -1.31 Nom. p-val= 0.171 FWER= 1 FDR= 0.205	
Gene Set 281 : BIOCARTA_CK1_PATHWAY	ES = -0.473 NES = -1.24 Nom. p-val= 0.169 FWER= 1 FDR= 0.248	
Gene Set 204 : BIOCARTA_COMP_PATHWAY	ES = -0.762 NES = -1.61 Nom. p-val= 0.00195 FWER= 0.963 FDR= 0.0763	
Gene Set 321 : BIOCARTA_CREB_PATHWAY	ES = -0.401 NES = -1.24 Nom. p-val= 0.225 FWER= 1 FDR= 0.247	
Gene Set 181 : BIOCARTA_CSK_PATHWAY	ES = -0.698 NES = -1.5 Nom. p-val= 0.048 FWER= 0.997 FDR= 0.107	
Gene Set 207 : BIOCARTA_CTCF_PATHWAY	ES = -0.629 NES = -1.61 Nom. p-val= 0.0139 FWER= 0.964 FDR= 0.0761	
Gene Set 313 : BIOCARTA_CTLA4_PATHWAY	ES = -0.795 NES = -1.39 Nom. p-val= 0.0542 FWER= 1 FDR= 0.153	
Gene Set 208 : BIOCARTA_CXCR4_PATHWAY	ES = -0.5 NES = -1.51 Nom. p-val= 0.0585 FWER= 0.996 FDR= 0.101	
Gene Set 210 : BIOCARTA_CYTOKINE_PATHWAY	ES = -0.672 NES = -1.32 Nom. p-val= 0.129 FWER= 1 FDR= 0.197	
Gene Set 212 : BIOCARTA_DC_PATHWAY	ES = -0.765 NES = -1.47 Nom. p-val= 0.0266 FWER= 0.999 FDR= 0.115	
Gene Set 243 : BIOCARTA_DEATH_PATHWAY	ES = -0.486 NES = -1.73 Nom. p-val= 0.0114 FWER= 0.768 FDR= 0.0725	
Gene Set 218 : BIOCARTA_ECM_PATHWAY	ES = -0.573 NES = -1.72 Nom. p-val= 0.00393 FWER= 0.794 FDR= 0.0731	
Gene Set 271 : BIOCARTA_EDG1_PATHWAY	ES = -0.581 NES = -1.57 Nom. p-val= 0.0298 FWER= 0.987 FDR= 0.0857	
Gene Set 215 : BIOCARTA_EGF_PATHWAY	ES = -0.489 NES = -1.51 Nom. p-val= 0.0617 FWER= 0.996 FDR= 0.101	
Gene Set 217 : BIOCARTA_EPO_PATHWAY	ES = -0.448 NES = -1.46 Nom. p-val= 0.0793 FWER= 0.999 FDR= 0.118	
Gene Set 219 : BIOCARTA_ERK_PATHWAY	ES = -0.487 NES = -1.61 Nom. p-val= 0.0308 FWER= 0.965 FDR= 0.0758	
Gene Set 290 : BIOCARTA_ERK5_PATHWAY	ES = -0.624 NES = -1.72 Nom. p-val= 0.00604 FWER= 0.796 FDR= 0.0736	
Gene Set 220 : BIOCARTA_ERYTH_PATHWAY	ES = -0.716 NES = -1.49 Nom. p-val= 0.0229 FWER= 0.998 FDR= 0.111	
Gene Set 254 : BIOCARTA_ETS_PATHWAY	ES = -0.576 NES = -1.55 Nom. p-val= 0.0199 FWER= 0.99 FDR= 0.0891	
Gene Set 222 : BIOCARTA_FAS_PATHWAY	ES = -0.435 NES = -1.42 Nom. p-val= 0.15 FWER= 1 FDR= 0.137	
Gene Set 223 : BIOCARTA_FCER1_PATHWAY	ES = -0.623 NES = -1.68 Nom. p-val= 0.00402 FWER= 0.891 FDR= 0.0732	
Gene Set 224 : BIOCARTA_FMLP_PATHWAY	ES = -0.494 NES = -1.58 Nom. p-val= 0.0406 FWER= 0.983 FDR= 0.0809	
Gene Set 199 : BIOCARTA_G1_PATHWAY	ES = -0.476 NES = -1.39 Nom. p-val= 0.12 FWER= 1 FDR= 0.153	
Gene Set 225 : BIOCARTA_GATA3_PATHWAY	ES = -0.521 NES = -1.26 Nom. p-val= 0.185 FWER= 1 FDR= 0.239	
Gene Set 206 : BIOCARTA_GCR_PATHWAY	ES = -0.551 NES = -1.51 Nom. p-val= 0.0481 FWER= 0.996 FDR= 0.101	
Gene Set 226 : BIOCARTA_GH_PATHWAY	ES = -0.543 NES = -1.57 Nom. p-val= 0.0305 FWER= 0.986 FDR= 0.0861	

Gene Set 245 : BIOCARTA_GLEEVEC_PATHWAY	ES = -0.456 NES = -1.43 Nom. p-val= 0.109 FWER= 1 FDR= 0.133	
Gene Set 301 : BIOCARTA_GPCR_PATHWAY	ES = -0.373 NES = -1.24 Nom. p-val= 0.224 FWER= 1 FDR= 0.247	
Gene Set 242 : BIOCARTA_GSK3_PATHWAY	ES = -0.599 NES = -1.74 Nom. p-val= 0.002 FWER= 0.757 FDR= 0.0734	
Gene Set 205 : BIOCARTA_HDAC_PATHWAY	ES = -0.467 NES = -1.35 Nom. p-val= 0.146 FWER= 1 FDR= 0.177	
Gene Set 289 : BIOCARTA_HER2_PATHWAY	ES = -0.534 NES = -1.28 Nom. p-val= 0.227 FWER= 1 FDR= 0.221	
Gene Set 227 : BIOCARTA_HIVNEF_PATHWAY	ES = -0.421 NES = -1.62 Nom. p-val= 0.046 FWER= 0.946 FDR= 0.0756	
Gene Set 306 : BIOCARTA_HSP27_PATHWAY	ES = -0.702 NES = -1.54 Nom. p-val= 0.0153 FWER= 0.993 FDR= 0.0927	
Gene Set 232 : BIOCARTA_IGF1_PATHWAY	ES = -0.445 NES = -1.26 Nom. p-val= 0.244 FWER= 1 FDR= 0.233	
Gene Set 299 : BIOCARTA_IL1R_PATHWAY	ES = -0.537 NES = -1.43 Nom. p-val= 0.0757 FWER= 0.999 FDR= 0.129	
Gene Set 234 : BIOCARTA_IL2_PATHWAY	ES = -0.644 NES = -1.51 Nom. p-val= 0.0615 FWER= 0.996 FDR= 0.103	
Gene Set 239 : BIOCARTA_IL2RB_PATHWAY	ES = -0.626 NES = -1.62 Nom. p-val= 0.0229 FWER= 0.958 FDR= 0.0762	
Gene Set 236 : BIOCARTA_IL6_PATHWAY	ES = -0.569 NES = -1.52 Nom. p-val= 0.0444 FWER= 0.995 FDR= 0.0998	
Gene Set 241 : BIOCARTA_IL7_PATHWAY	ES = -0.712 NES = -1.48 Nom. p-val= 0.0331 FWER= 0.999 FDR= 0.113	
Gene Set 237 : BIOCARTA_IL10_PATHWAY	ES = -0.67 NES = -1.43 Nom. p-val= 0.0824 FWER= 1 FDR= 0.133	
Gene Set 238 : BIOCARTA_IL12_PATHWAY	ES = -0.82 NES = -1.48 Nom. p-val= 0.0115 FWER= 0.998 FDR= 0.112	
Gene Set 233 : BIOCARTA_IL17_PATHWAY	ES = -0.76 NES = -1.33 Nom. p-val= 0.0937 FWER= 1 FDR= 0.188	
Gene Set 240 : BIOCARTA_IL22BP_PATHWAY	ES = -0.637 NES = -1.37 Nom. p-val= 0.107 FWER= 1 FDR= 0.163	
Gene Set 211 : BIOCARTA_INFLAM_PATHWAY	ES = -0.704 NES = -1.45 Nom. p-val= 0.0247 FWER= 0.999 FDR= 0.122	
Gene Set 246 : BIOCARTA_INSULIN_PATHWAY	ES = -0.485 NES = -1.41 Nom. p-val= 0.0988 FWER= 1 FDR= 0.141	
Gene Set 247 : BIOCARTA_INTEGRIN_PATHWAY	ES = -0.564 NES = -1.78 Nom. p-val= 0.00394 FWER= 0.655 FDR= 0.0758	
Gene Set 248 : BIOCARTA_INTRINSIC_PATHWAY	ES = -0.672 NES = -1.45 Nom. p-val= 0.0514 FWER= 0.999 FDR= 0.122	
Gene Set 249 : BIOCARTA_KERATINOCYTE_PATHWAY	ES = -0.511 NES = -1.58 Nom. p-val= 0.045 FWER= 0.983 FDR= 0.0811	
Gene Set 201 : BIOCARTA_LAIR_PATHWAY	ES = -0.741 NES = -1.4 Nom. p-val= 0.0502 FWER= 1 FDR= 0.148	
Gene Set 314 : BIOCARTA_LONGEVITY_PATHWAY	ES = -0.476 NES = -1.25 Nom. p-val= 0.2 FWER= 1 FDR= 0.245	
Gene Set 291 : BIOCARTA_MAL_PATHWAY	ES = -0.522 NES = -1.64 Nom. p-val= 0.0269 FWER= 0.934 FDR= 0.0736	
Gene Set 251 : BIOCARTA_MAPK_PATHWAY	ES = -0.351 NES = -1.52 Nom. p-val= 0.0661 FWER= 0.995 FDR= 0.0991	
Gene Set 252 : BIOCARTA_MCALPAIN_PATHWAY	ES = -0.542 NES = -1.53 Nom. p-val= 0.0294 FWER= 0.993 FDR= 0.0953	
Gene Set 292 : BIOCARTA_MEF2D_PATHWAY	ES = -0.484 NES = -1.39 Nom. p-val= 0.119 FWER= 1 FDR= 0.153	
Gene Set 300 : BIOCARTA_MET_PATHWAY	ES = -0.549 NES = -1.67 Nom. p-val= 0.00992 FWER= 0.901 FDR= 0.0725	
Gene Set 213 : BIOCARTA_MTA3_PATHWAY	ES = -0.647 NES = -1.6 Nom. p-val= 0.00954 FWER= 0.97 FDR= 0.0767	
Gene Set 272 : BIOCARTA_MYOSIN_PATHWAY	ES = -0.567 NES = -1.7 Nom. p-val= 0.00784 FWER= 0.828 FDR= 0.0758	
Gene Set 216 : BIOCARTA_NDKDYNAMIN_PATHWAY	ES = -0.53 NES = -1.79 Nom. p-val= 0.0118 FWER= 0.628 FDR= 0.0782	
Gene Set 260 : BIOCARTA_NFAT_PATHWAY	ES = -0.587 NES = -1.7 Nom. p-val= 0 FWER= 0.834 FDR= 0.0759	
Gene Set 262 : BIOCARTA_NFKB_PATHWAY	ES = -0.562 NES = -1.58 Nom. p-val= 0.0273 FWER= 0.985 FDR= 0.0834	
Gene Set 258 : BIOCARTA_NGF_PATHWAY	ES = -0.577 NES = -1.51 Nom. p-val= 0.0562 FWER= 0.996 FDR= 0.103	
Gene Set 278 : BIOCARTA_NKCELLS_PATHWAY	ES = -0.642 NES = -1.41 Nom. p-val= 0.0884 FWER= 1 FDR= 0.144	
Gene Set 298 : BIOCARTA_NKT_PATHWAY	ES = -0.781 NES = -1.48 Nom. p-val= 0.025 FWER= 0.999 FDR= 0.113	
Gene Set 180 : BIOCARTA_NO1_PATHWAY	ES = -0.617 NES = -1.48 Nom. p-val= 0.0546 FWER= 0.998 FDR= 0.112	
Gene Set 264 : BIOCARTA_NO2IL12_PATHWAY	ES = -0.821 NES = -1.36 Nom. p-val= 0.0813 FWER= 1 FDR= 0.168	
Gene Set 261 : BIOCARTA_NTHI_PATHWAY	ES = -0.539 NES = -1.45 Nom. p-val= 0.0868 FWER= 0.999 FDR= 0.122	
Gene Set 266 : BIOCARTA_P38MAPK_PATHWAY	ES = -0.46 NES = -1.69 Nom. p-val= 0.0119 FWER= 0.866 FDR= 0.0763	
Gene Set 267 : BIOCARTA_P53_PATHWAY	ES = -0.496 NES = -1.43 Nom. p-val= 0.12 FWER= 1 FDR= 0.134	
Gene Set 230 : BIOCARTA_P53HYPOXIA_PATHWAY	ES = -0.664 NES = -2.03 Nom. p-val= 0 FWER= 0.126 FDR= 0.0881	Y
Gene Set 315 : BIOCARTA_PAR1_PATHWAY	ES = -0.491 NES = -1.5 Nom. p-val= 0.0592 FWER= 0.996 FDR= 0.106	
Gene Set 268 : BIOCARTA_PDGF_PATHWAY	ES = -0.562 NES = -1.66 Nom. p-val= 0.00198 FWER= 0.919 FDR= 0.0734	
Gene Set 284 : BIOCARTA_PGC1A_PATHWAY	ES = -0.594 NES = -1.49 Nom. p-val= 0.0741 FWER= 0.998 FDR= 0.109	
Gene Set 257 : BIOCARTA_PITX2_PATHWAY	ES = -0.627 NES = -1.61 Nom. p-val= 0.0349 FWER= 0.96 FDR= 0.076	
Gene Set 285 : BIOCARTA_PML_PATHWAY	ES = -0.695 NES = -1.71 Nom. p-val= 0.00758 FWER= 0.826 FDR= 0.0767	
Gene Set 253 : BIOCARTA_PPARA_PATHWAY	ES = -0.493 NES = -1.59 Nom. p-val= 0.0115 FWER= 0.978 FDR= 0.0794	
Gene Set 270 : BIOCARTA_PTDINS_PATHWAY	ES = -0.371 NES = -1.37 Nom. p-val= 0.108 FWER= 1 FDR= 0.162	
Gene Set 275 : BIOCARTA_PTEN_PATHWAY	ES = -0.459 NES = -1.47 Nom. p-val= 0.0905 FWER= 0.999 FDR= 0.114	
Gene Set 250 : BIOCARTA_PYK2_PATHWAY	ES = -0.425 NES = -1.65 Nom. p-val= 0.0198 FWER= 0.925 FDR= 0.0728	
Gene Set 276 : BIOCARTA_RAC1_PATHWAY	ES = -0.673 NES = -1.68 Nom. p-val= 0.00197 FWER= 0.878 FDR= 0.0751	
Gene Set 244 : BIOCARTA_RACCYCD_PATHWAY	ES = -0.374 NES = -1.36 Nom. p-val= 0.154 FWER= 1 FDR= 0.167	
Gene Set 277 : BIOCARTA_RAS_PATHWAY	ES = -0.493 NES = -1.74 Nom. p-val= 0.00794 FWER= 0.755 FDR= 0.0736	
Gene Set 179 : BIOCARTA_RELA_PATHWAY	ES = -0.52 NES = -1.55 Nom. p-val= 0.045 FWER= 0.99 FDR= 0.0897	

Gene Set 286 : BIOCARTA_RHO_PATHWAY	ES = -0.51 NES = -1.83 Nom. p-val= 0.00591 FWER= 0.542 FDR= 0.0817	
Gene Set 303 : BIOCARTA_SHH_PATHWAY	ES = -0.567 NES = -1.4 Nom. p-val= 0.109 FWER= 1 FDR= 0.149	
Gene Set 189 : BIOCARTA_SPPA_PATHWAY	ES = -0.583 NES = -1.56 Nom. p-val= 0.0464 FWER= 0.989 FDR= 0.0881	
Gene Set 304 : BIOCARTA_SPRY_PATHWAY	ES = -0.472 NES = -1.29 Nom. p-val= 0.168 FWER= 1 FDR= 0.214	
Gene Set 305 : BIOCARTA_STATHMIN_PATHWAY	ES = -0.785 NES = -1.77 Nom. p-val= 0 FWER= 0.694 FDR= 0.0716	
Gene Set 283 : BIOCARTA_STEM_PATHWAY	ES = -0.677 NES = -1.37 Nom. p-val= 0.0869 FWER= 1 FDR= 0.166	
Gene Set 308 : BIOCARTA_TALL1_PATHWAY	ES = -0.684 NES = -1.49 Nom. p-val= 0.0276 FWER= 0.998 FDR= 0.111	
Gene Set 307 : BIOCARTA_TCR_PATHWAY	ES = -0.692 NES = -1.68 Nom. p-val= 0.00775 FWER= 0.895 FDR= 0.0724	
Gene Set 322 : BIOCARTA_TFF_PATHWAY	ES = -0.434 NES = -1.38 Nom. p-val= 0.11 FWER= 1 FDR= 0.157	
Gene Set 310 : BIOCARTA_TGFB_PATHWAY	ES = -0.599 NES = -1.73 Nom. p-val= 0 FWER= 0.771 FDR= 0.0724	
Gene Set 311 : BIOCARTA_TH1TH2_PATHWAY	ES = -0.794 NES = -1.48 Nom. p-val= 0.019 FWER= 0.999 FDR= 0.114	
Gene Set 203 : BIOCARTA_TID_PATHWAY	ES = -0.54 NES = -1.46 Nom. p-val= 0.0692 FWER= 0.999 FDR= 0.118	
Gene Set 318 : BIOCARTA_TNFR2_PATHWAY	ES = -0.582 NES = -1.5 Nom. p-val= 0.0453 FWER= 0.997 FDR= 0.107	
Gene Set 296 : BIOCARTA_TOB1_PATHWAY	ES = -0.766 NES = -1.51 Nom. p-val= 0.00582 FWER= 0.996 FDR= 0.102	
Gene Set 319 : BIOCARTA_TOLL_PATHWAY	ES = -0.6 NES = -1.61 Nom. p-val= 0.0196 FWER= 0.96 FDR= 0.0756	
Gene Set 320 : BIOCARTA_TPO_PATHWAY	ES = -0.572 NES = -1.59 Nom. p-val= 0.0245 FWER= 0.976 FDR= 0.0793	
Gene Set 324 : BIOCARTA_UCALPAIN_PATHWAY	ES = -0.623 NES = -1.47 Nom. p-val= 0.0511 FWER= 0.999 FDR= 0.115	
Gene Set 325 : BIOCARTA_VEGF_PATHWAY	ES = -0.56 NES = -1.72 Nom. p-val= 0.02 FWER= 0.784 FDR= 0.0737	
Gene Set 259 : BIOCARTA_VIP_PATHWAY	ES = -0.511 NES = -1.44 Nom. p-val= 0.0946 FWER= 0.999 FDR= 0.127	
Gene Set 326 : BIOCARTA_WNT_PATHWAY	ES = -0.459 NES = -1.62 Nom. p-val= 0.0351 FWER= 0.945 FDR= 0.0757	
Gene Set 65 : KEGG_ABC_TRANSPORTERS	ES = -0.507 NES = -1.38 Nom. p-val= 0.0777 FWER= 1 FDR= 0.157	
Gene Set 166 : KEGG_ACUTE_MYELOID_LEUKEMIA	ES = -0.587 NES = -1.99 Nom. p-val= 0.00197 FWER= 0.186 FDR= 0.102	
Gene Set 109 : KEGG_ADHERENS_JUNCTION	ES = -0.539 NES = -1.9 Nom. p-val= 0 FWER= 0.371 FDR= 0.0821	Y
Gene Set 138 : KEGG_ADIPOCYTOKINE_SIGNALING_PATHWAY	ES = -0.504 NES = -1.61 Nom. p-val= 0.00803 FWER= 0.96 FDR= 0.0758	
Gene Set 15 : KEGG_ALANINE_ASPARTATE_AND_GLUTAMATE_METABOLISM	ES = -0.478 NES = -1.43 Nom. p-val= 0.075 FWER= 1 FDR= 0.133	
Gene Set 142 : KEGG_ALDOSTERONE_REGULATED_SODIUM_REABSORPTION	ES = -0.59 NES = -1.54 Nom. p-val= 0.0116 FWER= 0.992 FDR= 0.0911	
Gene Set 172 : KEGG_ALLOGRAFT_REJECTION	ES = -0.751 NES = -1.52 Nom. p-val= 0.0223 FWER= 0.995 FDR= 0.0997	
Gene Set 145 : KEGG_ALZHEIMERS_DISEASE	ES = -0.31 NES = -1.38 Nom. p-val= 0.0759 FWER= 1 FDR= 0.155	
Gene Set 32 : KEGG_AMINO_SUGAR_AND_NUCLEOTIDE_SUGAR_METABOLISM	ES = -0.443 NES = -1.52 Nom. p-val= 0.0679 FWER= 0.995 FDR= 0.0989	
Gene Set 147 : KEGG_AMYTROPHIC_LATERAL_SCLEROSIS_ALS	ES = -0.499 NES = -1.52 Nom. p-val= 0.0392 FWER= 0.995 FDR= 0.0998	
Gene Set 113 : KEGG_ANTIGEN_PROCESSING_AND_PRESENTATION	ES = -0.586 NES = -1.7 Nom. p-val= 0.0113 FWER= 0.833 FDR= 0.0759	
Gene Set 96 : KEGG_APOPTOSIS	ES = -0.534 NES = -1.84 Nom. p-val= 0 FWER= 0.516 FDR= 0.0875	Y
Gene Set 42 : KEGG_ARACHIDONIC_ACID_METABOLISM	ES = -0.496 NES = -1.29 Nom. p-val= 0.109 FWER= 1 FDR= 0.215	
Gene Set 176 : KEGG_ARRHYTHMOGENIC_RIGHT_VENTRICULAR_CARDIOMYOPATHY_ARVC	ES = -0.648 NES = -1.61 Nom. p-val= 0.00582 FWER= 0.965 FDR= 0.0757	
Gene Set 169 : KEGG_ASTHMA	ES = -0.76 NES = -1.62 Nom. p-val= 0.0075 FWER= 0.958 FDR= 0.0765	
Gene Set 170 : KEGG_AUTOIMMUNE_THYROID_DISEASE	ES = -0.674 NES = -1.63 Nom. p-val= 0.00575 FWER= 0.941 FDR= 0.0749	
Gene Set 104 : KEGG_AXON_GUIDANCE	ES = -0.562 NES = -1.71 Nom. p-val= 0 FWER= 0.823 FDR= 0.0763	
Gene Set 123 : KEGG_B_CELL_RECEPTOR_SIGNALING_PATHWAY	ES = -0.69 NES = -1.84 Nom. p-val= 0.00381 FWER= 0.501 FDR= 0.0866	
Gene Set 162 : KEGG_BASAL_CELL_CARCINOMA	ES = -0.608 NES = -1.55 Nom. p-val= 0.00787 FWER= 0.99 FDR= 0.0896	
Gene Set 164 : KEGG_BLADDER_CANCER	ES = -0.411 NES = -1.34 Nom. p-val= 0.126 FWER= 1 FDR= 0.183	
Gene Set 81 : KEGG_CALCIUM_SIGNALING_PATHWAY	ES = -0.619 NES = -1.65 Nom. p-val= 0 FWER= 0.931 FDR= 0.0739	
Gene Set 97 : KEGG_CARDIAC_MUSCLE_CONTRACTION	ES = -0.625 NES = -1.62 Nom. p-val= 0.0133 FWER= 0.948 FDR= 0.0755	
Gene Set 108 : KEGG_CELL_ADHESION_MOLECULES_CAMS	ES = -0.696 NES = -1.65 Nom. p-val= 0.00192 FWER= 0.924 FDR= 0.0727	
Gene Set 83 : KEGG_CHEMOKINE_SIGNALING_PATHWAY	ES = -0.649 NES = -1.66 Nom. p-val= 0.00388 FWER= 0.921 FDR= 0.0736	
Gene Set 165 : KEGG_CHRONIC_MYELOID_LEUKEMIA	ES = -0.467 NES = -1.83 Nom. p-val= 0 FWER= 0.525 FDR= 0.0873	Y
Gene Set 155 : KEGG_COLORECTAL_CANCER	ES = -0.498 NES = -1.84 Nom. p-val= 0.00203 FWER= 0.507 FDR= 0.0871	
Gene Set 112 : KEGG_COMPLEMENT_AND_COAGULATION_CASCADES	ES = -0.69 NES = -1.61 Nom. p-val= 0 FWER= 0.963 FDR= 0.0756	
Gene Set 82 : KEGG_CYTOKINE_CYTOKINE_RECEPTOR_INTERACTION	ES = -0.691 NES = -1.63 Nom. p-val= 0 FWER= 0.942 FDR= 0.0764	
Gene Set 118 : KEGG_CYTOSOLIC_DNA_SENSING_PATHWAY	ES = -0.621 NES = -1.78 Nom. p-val= 0.00381 FWER= 0.668 FDR= 0.0771	
Gene Set 177 : KEGG_DILATED_CARDIOMYOPATHY	ES = -0.651 NES = -1.6 Nom. p-val= 0.0019 FWER= 0.973 FDR= 0.0783	
Gene Set 100 : KEGG_DORSO_VENTRAL_AXIS_FORMATION	ES = -0.644 NES = -1.64 Nom. p-val= 0.00794 FWER= 0.939 FDR= 0.0746	
Gene Set 62 : KEGG_DRUG_METABOLISM_CYTOCHROME_P450	ES = -0.566 NES = -1.41 Nom. p-val= 0.0395 FWER= 1 FDR= 0.139	
Gene Set 63 : KEGG_DRUG_METABOLISM_OTHER_ENZYMES	ES = -0.529 NES = -1.34 Nom. p-val= 0.106 FWER= 1 FDR= 0.184	
Gene Set 107 : KEGG_ECM_RECEPTOR_INTERACTION	ES = -0.668 NES = -1.7 Nom. p-val= 0 FWER= 0.833 FDR= 0.0763	
Gene Set 93 : KEGG_ENDOCYTOSIS	ES = -0.463 NES = -1.97 Nom. p-val= 0 FWER= 0.218 FDR= 0.102	Y

Gene Set 158 : KEGG ENDOMETRIAL CANCER	ES = -0.456 NES = -1.63 Nom. p-val= 0.0331 FWER= 0.945 FDR= 0.0768	
Gene Set 151 : KEGG EPITHELIAL CELL SIGNALING IN HELICOBACTER PYLORI INFECTION	ES = -0.484 NES = -1.66 Nom. p-val= 0.0195 FWER= 0.922 FDR= 0.073	
Gene Set 80 : KEGG ERBB SIGNALING PATHWAY	ES = -0.449 NES = -1.53 Nom. p-val= 0.026 FWER= 0.993 FDR= 0.0958	
Gene Set 41 : KEGG ETHER LIPID METABOLISM	ES = -0.5 NES = -1.39 Nom. p-val= 0.0712 FWER= 1 FDR= 0.15	
Gene Set 8 : KEGG FATTY ACID METABOLISM	ES = -0.478 NES = -1.4 Nom. p-val= 0.103 FWER= 1 FDR= 0.146	
Gene Set 124 : KEGG FC EPSILON RI SIGNALING PATHWAY	ES = -0.568 NES = -1.68 Nom. p-val= 0.00383 FWER= 0.885 FDR= 0.0754	
Gene Set 125 : KEGG FC GAMMA R MEDIATED PHAGOCYTOSIS	ES = -0.662 NES = -1.93 Nom. p-val= 0 FWER= 0.285 FDR= 0.0951	Y
Gene Set 106 : KEGG FOCAL ADHESION	ES = -0.638 NES = -1.86 Nom. p-val= 0 FWER= 0.462 FDR= 0.0907	Y
Gene Set 6 : KEGG GALACTOSE METABOLISM	ES = -0.467 NES = -1.49 Nom. p-val= 0.0542 FWER= 0.998 FDR= 0.108	
Gene Set 111 : KEGG GAP JUNCTION	ES = -0.532 NES = -1.66 Nom. p-val= 0.00393 FWER= 0.922 FDR= 0.0735	
Gene Set 159 : KEGG GLIOMA	ES = -0.49 NES = -1.65 Nom. p-val= 0.00199 FWER= 0.927 FDR= 0.0728	
Gene Set 27 : KEGG GLUTATHIONE METABOLISM	ES = -0.442 NES = -1.24 Nom. p-val= 0.221 FWER= 1 FDR= 0.249	
Gene Set 37 : KEGG GLYCEROLIPID METABOLISM	ES = -0.492 NES = -1.49 Nom. p-val= 0.0209 FWER= 0.998 FDR= 0.108	
Gene Set 40 : KEGG GLYCEROPHOSPHOLIPID METABOLISM	ES = -0.524 NES = -1.8 Nom. p-val= 0 FWER= 0.619 FDR= 0.0806	Y
Gene Set 1 : KEGG GLYCOLYSIS GLUCONEOGENESIS	ES = -0.478 NES = -1.49 Nom. p-val= 0.0363 FWER= 0.998 FDR= 0.111	
Gene Set 34 : KEGG GLYCOSAMINOGLYCAN BIOSYNTHESIS CHONDROITIN SULFATE	ES = -0.511 NES = -1.42 Nom. p-val= 0.101 FWER= 1 FDR= 0.136	
Gene Set 36 : KEGG GLYCOSAMINOGLYCAN BIOSYNTHESIS HEPARAN SULFATE	ES = -0.482 NES = -1.27 Nom. p-val= 0.163 FWER= 1 FDR= 0.229	
Gene Set 35 : KEGG GLYCOSAMINOGLYCAN BIOSYNTHESIS KERATAN SULFATE	ES = -0.638 NES = -1.48 Nom. p-val= 0.039 FWER= 0.999 FDR= 0.114	
Gene Set 33 : KEGG GLYCOSAMINOGLYCAN DEGRADATION	ES = -0.627 NES = -1.63 Nom. p-val= 0.0117 FWER= 0.945 FDR= 0.0766	
Gene Set 47 : KEGG GLYCOSPHINGOLIPID BIOSYNTHESIS GANGLIO SERIES	ES = -0.668 NES = -1.5 Nom. p-val= 0.0403 FWER= 0.997 FDR= 0.107	
Gene Set 46 : KEGG GLYCOSPHINGOLIPID BIOSYNTHESIS LACTO AND NEOLACTO SERIES	ES = -0.574 NES = -1.39 Nom. p-val= 0.0973 FWER= 1 FDR= 0.153	
Gene Set 135 : KEGG GNRH SIGNALING PATHWAY	ES = -0.431 NES = -1.54 Nom. p-val= 0.0174 FWER= 0.993 FDR= 0.0929	
Gene Set 173 : KEGG GRAFT VERSUS HOST DISEASE	ES = -0.742 NES = -1.5 Nom. p-val= 0.0208 FWER= 0.996 FDR= 0.104	
Gene Set 102 : KEGG HEDGEHOG SIGNALING PATHWAY	ES = -0.582 NES = -1.49 Nom. p-val= 0.016 FWER= 0.998 FDR= 0.108	
Gene Set 120 : KEGG HEMATOPOIETIC CELL LINEAGE	ES = -0.719 NES = -1.56 Nom. p-val= 0.00952 FWER= 0.989 FDR= 0.0885	
Gene Set 21 : KEGG HISTIDINE METABOLISM	ES = -0.499 NES = -1.34 Nom. p-val= 0.104 FWER= 1 FDR= 0.182	
Gene Set 148 : KEGG HUNTINGTONS DISEASE	ES = -0.306 NES = -1.38 Nom. p-val= 0.105 FWER= 1 FDR= 0.158	
Gene Set 175 : KEGG HYPERTROPHIC CARDIOMYOPATHY HCM	ES = -0.674 NES = -1.63 Nom. p-val= 0 FWER= 0.941 FDR= 0.0761	
Gene Set 38 : KEGG INOSITOL PHOSPHATE METABOLISM	ES = -0.456 NES = -1.55 Nom. p-val= 0.023 FWER= 0.99 FDR= 0.0894	
Gene Set 134 : KEGG INSULIN SIGNALING PATHWAY	ES = -0.453 NES = -1.76 Nom. p-val= 0.002 FWER= 0.719 FDR= 0.0731	
Gene Set 127 : KEGG INTESTINAL IMMUNE NETWORK FOR IGA PRODUCTION	ES = -0.784 NES = -1.6 Nom. p-val= 0.00388 FWER= 0.968 FDR= 0.0765	
Gene Set 119 : KEGG JAK STAT SIGNALING PATHWAY	ES = -0.606 NES = -1.68 Nom. p-val= 0 FWER= 0.889 FDR= 0.0734	
Gene Set 153 : KEGG LEISHMANIA INFECTION	ES = -0.702 NES = -1.62 Nom. p-val= 0.00586 FWER= 0.95 FDR= 0.0759	
Gene Set 126 : KEGG LEUKOCYTE TRANSENDOTHELIAL MIGRATION	ES = -0.614 NES = -1.75 Nom. p-val= 0 FWER= 0.727 FDR= 0.0746	
Gene Set 130 : KEGG LONG TERM DEPRESSION	ES = -0.523 NES = -1.56 Nom. p-val= 0.0192 FWER= 0.989 FDR= 0.0872	
Gene Set 128 : KEGG LONG TERM POTENTIATION	ES = -0.451 NES = -1.49 Nom. p-val= 0.0398 FWER= 0.998 FDR= 0.108	
Gene Set 19 : KEGG LYSINE DEGRADATION	ES = -0.342 NES = -1.46 Nom. p-val= 0.0615 FWER= 0.999 FDR= 0.118	
Gene Set 92 : KEGG LYSOSOME	ES = -0.355 NES = -1.47 Nom. p-val= 0.109 FWER= 0.999 FDR= 0.116	
Gene Set 79 : KEGG MAPK SIGNALING PATHWAY	ES = -0.527 NES = -1.79 Nom. p-val= 0 FWER= 0.633 FDR= 0.0766	Y
Gene Set 137 : KEGG MELANOGENESIS	ES = -0.551 NES = -1.63 Nom. p-val= 0.00189 FWER= 0.943 FDR= 0.0763	
Gene Set 163 : KEGG MELANOMA	ES = -0.601 NES = -1.74 Nom. p-val= 0 FWER= 0.741 FDR= 0.0737	
Gene Set 61 : KEGG METABOLISM OF XENOBIOTICS BY CYTOCHROME P450	ES = -0.543 NES = -1.35 Nom. p-val= 0.0707 FWER= 1 FDR= 0.178	
Gene Set 95 : KEGG MTOR SIGNALING PATHWAY	ES = -0.366 NES = -1.41 Nom. p-val= 0.0713 FWER= 1 FDR= 0.14	
Gene Set 121 : KEGG NATURAL KILLER CELL MEDIATED CYTOTOXICITY	ES = -0.62 NES = -1.68 Nom. p-val= 0.0038 FWER= 0.889 FDR= 0.0739	
Gene Set 85 : KEGG NEUROACTIVE LIGAND RECEPTOR INTERACTION	ES = -0.603 NES = -1.61 Nom. p-val= 0 FWER= 0.964 FDR= 0.0762	
Gene Set 129 : KEGG NEUROTROPHIN SIGNALING PATHWAY	ES = -0.466 NES = -1.83 Nom. p-val= 0 FWER= 0.545 FDR= 0.0778	Y
Gene Set 54 : KEGG NICOTINATE AND NICOTINAMIDE METABOLISM	ES = -0.628 NES = -1.65 Nom. p-val= 0.00587 FWER= 0.927 FDR= 0.0733	
Gene Set 116 : KEGG NOD LIKE RECEPTOR SIGNALING PATHWAY	ES = -0.67 NES = -1.62 Nom. p-val= 0.00196 FWER= 0.945 FDR= 0.0759	
Gene Set 168 : KEGG NON SMALL CELL LUNG CANCER	ES = -0.515 NES = -1.76 Nom. p-val= 0.00195 FWER= 0.708 FDR= 0.0729	
Gene Set 88 : KEGG P53 SIGNALING PATHWAY	ES = -0.447 NES = -1.49 Nom. p-val= 0.0532 FWER= 0.998 FDR= 0.11	
Gene Set 157 : KEGG PANCREATIC CANCER	ES = -0.491 NES = -1.75 Nom. p-val= 0.00393 FWER= 0.735 FDR= 0.0728	
Gene Set 55 : KEGG PANTOTHENATE AND COA BIOSYNTHESIS	ES = -0.641 NES = -1.51 Nom. p-val= 0.0366 FWER= 0.996 FDR= 0.102	
Gene Set 146 : KEGG PARKINSONS DISEASE	ES = -0.394 NES = -1.38 Nom. p-val= 0.173 FWER= 1 FDR= 0.158	
Gene Set 152 : KEGG PATHOGENIC ESCHERICHIA COLI INFECTION	ES = -0.456 NES = -1.51 Nom. p-val= 0.0489 FWER= 0.996 FDR= 0.101	
Gene Set 154 : KEGG PATHWAYS IN CANCER	ES = -0.56 NES = -1.9 Nom. p-val= 0 FWER= 0.37 FDR= 0.0846	Y
Gene Set 94 : KEGG PEROXISOME	ES = -0.326 NES = -1.27 Nom. p-val= 0.169 FWER= 1 FDR= 0.229	

Gene Set 23 : KEGG PHENYLALANINE METABOLISM	ES = -0.534 NES = -1.31 Nom. p-val= 0.129 FWER= 1 FDR= 0.204	
Gene Set 84 : KEGG PHOSPHATIDYLINOSITOL SIGNALING SYSTEM	ES = -0.512 NES = -1.66 Nom. p-val= 0.00389 FWER= 0.922 FDR= 0.073	
Gene Set 74 : KEGG_PPAR_SIGNALING_PATHWAY	ES = -0.566 NES = -1.58 Nom. p-val= 0.0157 FWER= 0.983 FDR= 0.0807	
Gene Set 10 : KEGG PRIMARY BILE ACID BIOSYNTHESIS	ES = -0.556 NES = -1.31 Nom. p-val= 0.115 FWER= 1 FDR= 0.2	
Gene Set 174 : KEGG PRIMARY IMMUNODEFICIENCY	ES = -0.792 NES = -1.54 Nom. p-val= 0.0241 FWER= 0.991 FDR= 0.0905	
Gene Set 149 : KEGG PRION DISEASES	ES = -0.646 NES = -1.68 Nom. p-val= 0.00774 FWER= 0.885 FDR= 0.0748	
Gene Set 136 : KEGG PROGESTERONE MEDIATED OOCYTE MATURATION	ES = -0.39 NES = -1.3 Nom. p-val= 0.166 FWER= 1 FDR= 0.212	
Gene Set 160 : KEGG PROSTATE CANCER	ES = -0.482 NES = -1.77 Nom. p-val= 0.00588 FWER= 0.684 FDR= 0.0733	
Gene Set 144 : KEGG PROXIMAL TUBULE BICARBONATE RECLAMATION	ES = -0.637 NES = -1.56 Nom. p-val= 0.00787 FWER= 0.989 FDR= 0.0866	
Gene Set 13 : KEGG PURINE METABOLISM	ES = -0.387 NES = -1.64 Nom. p-val= 0.00406 FWER= 0.938 FDR= 0.0744	
Gene Set 14 : KEGG PYRIMIDINE METABOLISM	ES = -0.29 NES = -1.29 Nom. p-val= 0.153 FWER= 1 FDR= 0.216	
Gene Set 133 : KEGG REGULATION OF ACTIN CYTOSKELETON	ES = -0.584 NES = -1.91 Nom. p-val= 0 FWER= 0.342 FDR= 0.0992	Y
Gene Set 156 : KEGG RENAL CELL CARCINOMA	ES = -0.527 NES = -1.83 Nom. p-val= 0.00199 FWER= 0.529 FDR= 0.0846	
Gene Set 114 : KEGG RENIN ANGIOTENSIN SYSTEM	ES = -0.575 NES = -1.29 Nom. p-val= 0.122 FWER= 1 FDR= 0.215	
Gene Set 56 : KEGG RETINOL METABOLISM	ES = -0.538 NES = -1.34 Nom. p-val= 0.0723 FWER= 1 FDR= 0.184	
Gene Set 117 : KEGG RIG I LIKE RECEPTOR SIGNALING PATHWAY	ES = -0.42 NES = -1.52 Nom. p-val= 0.0455 FWER= 0.995 FDR= 0.0995	
Gene Set 167 : KEGG SMALL CELL LUNG CANCER	ES = -0.532 NES = -1.75 Nom. p-val= 0.00594 FWER= 0.724 FDR= 0.0735	
Gene Set 90 : KEGG SNARE INTERACTIONS IN VESICULAR TRANSPORT	ES = -0.521 NES = -1.96 Nom. p-val= 0 FWER= 0.224 FDR= 0.0967	Y
Gene Set 28 : KEGG STARCH AND SUCROSE METABOLISM	ES = -0.485 NES = -1.26 Nom. p-val= 0.148 FWER= 1 FDR= 0.235	
Gene Set 11 : KEGG STEROID HORMONE BIOSYNTHESIS	ES = -0.545 NES = -1.36 Nom. p-val= 0.0745 FWER= 1 FDR= 0.171	
Gene Set 171 : KEGG SYSTEMIC LUPUS ERYTHEMATOSUS	ES = -0.52 NES = -1.29 Nom. p-val= 0.158 FWER= 1 FDR= 0.215	
Gene Set 122 : KEGG T CELL RECEPTOR SIGNALING PATHWAY	ES = -0.657 NES = -1.67 Nom. p-val= 0.00589 FWER= 0.896 FDR= 0.0722	
Gene Set 103 : KEGG TGF BETA SIGNALING PATHWAY	ES = -0.616 NES = -1.83 Nom. p-val= 0 FWER= 0.546 FDR= 0.0767	Y
Gene Set 161 : KEGG THYROID CANCER	ES = -0.575 NES = -1.8 Nom. p-val= 0.00986 FWER= 0.621 FDR= 0.0793	
Gene Set 110 : KEGG TIGHT JUNCTION	ES = -0.516 NES = -1.77 Nom. p-val= 0 FWER= 0.689 FDR= 0.072	
Gene Set 115 : KEGG TOLL LIKE RECEPTOR SIGNALING PATHWAY	ES = -0.622 NES = -1.75 Nom. p-val= 0.00195 FWER= 0.735 FDR= 0.074	
Gene Set 24 : KEGG TRYPTOPHAN METABOLISM	ES = -0.445 NES = -1.25 Nom. p-val= 0.135 FWER= 1 FDR= 0.24	
Gene Set 140 : KEGG TYPE I DIABETES MELLITUS	ES = -0.713 NES = -1.52 Nom. p-val= 0.0207 FWER= 0.995 FDR= 0.0978	
Gene Set 139 : KEGG TYPE II DIABETES MELLITUS	ES = -0.488 NES = -1.39 Nom. p-val= 0.0772 FWER= 1 FDR= 0.154	
Gene Set 22 : KEGG TYROSINE METABOLISM	ES = -0.463 NES = -1.27 Nom. p-val= 0.144 FWER= 1 FDR= 0.23	
Gene Set 89 : KEGG UBIQUITIN MEDIATED PROTEOLYSIS	ES = -0.212 NES = -1.24 Nom. p-val= 0.209 FWER= 1 FDR= 0.248	
Gene Set 98 : KEGG VASCULAR SMOOTH MUSCLE CONTRACTION	ES = -0.597 NES = -1.76 Nom. p-val= 0 FWER= 0.716 FDR= 0.0736	
Gene Set 143 : KEGG VASOPRESSIN REGULATED WATER REABSORPTION	ES = -0.446 NES = -1.65 Nom. p-val= 0.023 FWER= 0.927 FDR= 0.0733	
Gene Set 105 : KEGG VEGF SIGNALING PATHWAY	ES = -0.51 NES = -1.75 Nom. p-val= 0.00191 FWER= 0.735 FDR= 0.0734	
Gene Set 150 : KEGG VIBRIO CHOLERAE INFECTION	ES = -0.398 NES = -1.46 Nom. p-val= 0.0716 FWER= 0.999 FDR= 0.118	
Gene Set 178 : KEGG VIRAL MYOCARDITIS	ES = -0.73 NES = -1.78 Nom. p-val= 0 FWER= 0.667 FDR= 0.0777	
Gene Set 99 : KEGG WNT SIGNALING PATHWAY	ES = -0.525 NES = -1.77 Nom. p-val= 0 FWER= 0.681 FDR= 0.0739	
Gene Set 1070 : NABA BASEMENT MEMBRANES	ES = -0.684 NES = -1.65 Nom. p-val= 0 FWER= 0.927 FDR= 0.0728	
Gene Set 1063 : NABA COLLAGENS	ES = -0.702 NES = -1.58 Nom. p-val= 0.00781 FWER= 0.983 FDR= 0.0816	
Gene Set 1069 : NABA CORE MATRISOME	ES = -0.684 NES = -1.78 Nom. p-val= 0 FWER= 0.658 FDR= 0.0755	
Gene Set 1066 : NABA ECM AFFILIATED	ES = -0.612 NES = -1.64 Nom. p-val= 0 FWER= 0.94 FDR= 0.0744	
Gene Set 1064 : NABA ECM GLYCOPROTEINS	ES = -0.674 NES = -1.79 Nom. p-val= 0 FWER= 0.629 FDR= 0.0773	Y
Gene Set 1065 : NABA ECM REGULATORS	ES = -0.632 NES = -1.69 Nom. p-val= 0 FWER= 0.869 FDR= 0.0754	
Gene Set 1067 : NABA PROTEOGLYCANS	ES = -0.728 NES = -1.61 Nom. p-val= 0.00385 FWER= 0.963 FDR= 0.0766	
Gene Set 1068 : NABA SECRETED FACTORS	ES = -0.649 NES = -1.66 Nom. p-val= 0 FWER= 0.922 FDR= 0.0732	
Gene Set 516 : PID_A6B1_A6B4_INTEGRIN_PATHWAY	ES = -0.507 NES = -1.5 Nom. p-val= 0.0435 FWER= 0.997 FDR= 0.107	
Gene Set 455 : PID_AJDISS_2PATHWAY	ES = -0.593 NES = -1.79 Nom. p-val= 0.00607 FWER= 0.652 FDR= 0.0762	
Gene Set 482 : PID_ALK1_PATHWAY	ES = -0.616 NES = -1.77 Nom. p-val= 0.00404 FWER= 0.678 FDR= 0.0743	
Gene Set 541 : PID_ALPHA_SYNUCLEIN_PATHWAY	ES = -0.71 NES = -1.9 Nom. p-val= 0 FWER= 0.368 FDR= 0.0873	Y
Gene Set 463 : PID_AMB2_NEUTROPHILS_PATHWAY	ES = -0.716 NES = -1.65 Nom. p-val= 0.00193 FWER= 0.927 FDR= 0.0729	
Gene Set 427 : PID_ANGIOPOIETIN_RECEPTOR_PATHWAY	ES = -0.545 NES = -1.66 Nom. p-val= 0.0098 FWER= 0.916 FDR= 0.0739	
Gene Set 533 : PID_ANTHRAX_PATHWAY	ES = -0.708 NES = -1.5 Nom. p-val= 0.0273 FWER= 0.996 FDR= 0.105	
Gene Set 471 : PID_AP1_PATHWAY	ES = -0.612 NES = -1.66 Nom. p-val= 0.00578 FWER= 0.921 FDR= 0.0734	
Gene Set 499 : PID_AR_NONGENOMIC_PATHWAY	ES = -0.516 NES = -1.7 Nom. p-val= 0.0131 FWER= 0.852 FDR= 0.074	

Gene Set 520 : PID_ARF_3PATHWAY	ES = -0.384 NES = -1.49 Nom. p-val= 0.0442 FWER= 0.998 FDR= 0.108	
Gene Set 443 : PID_ARF6_DOWNSTREAM_PATHWAY	ES = -0.54 NES = -1.63 Nom. p-val= 0.0433 FWER= 0.944 FDR= 0.0764	
Gene Set 422 : PID_ARF6_PATHWAY	ES = -0.534 NES = -1.6 Nom. p-val= 0.016 FWER= 0.971 FDR= 0.0778	
Gene Set 409 : PID_ARF6_TRAFFICKING_PATHWAY	ES = -0.639 NES = -1.91 Nom. p-val= 0 FWER= 0.336 FDR= 0.103	Y
Gene Set 470 : PID_ATF2_PATHWAY	ES = -0.6 NES = -1.63 Nom. p-val= 0.018 FWER= 0.944 FDR= 0.0766	
Gene Set 464 : PID_AVB3_INTEGRIN_PATHWAY	ES = -0.638 NES = -1.73 Nom. p-val= 0 FWER= 0.778 FDR= 0.0728	
Gene Set 406 : PID_AVB3_OPN_PATHWAY	ES = -0.604 NES = -1.64 Nom. p-val= 0.00967 FWER= 0.939 FDR= 0.0746	
Gene Set 368 : PID_BCR_5PATHWAY	ES = -0.623 NES = -1.66 Nom. p-val= 0.0154 FWER= 0.917 FDR= 0.0738	
Gene Set 504 : PID_BETA_CATENIN_NUC_PATHWAY	ES = -0.562 NES = -1.73 Nom. p-val= 0 FWER= 0.765 FDR= 0.0731	
Gene Set 478 : PID_BMP_PATHWAY	ES = -0.571 NES = -1.62 Nom. p-val= 0.0101 FWER= 0.945 FDR= 0.0755	
Gene Set 502 : PID_CASPASE_PATHWAY	ES = -0.516 NES = -1.88 Nom. p-val= 0 FWER= 0.412 FDR= 0.087	Y
Gene Set 538 : PID_CD8_TCR_DOWNSTREAM_PATHWAY	ES = -0.675 NES = -1.62 Nom. p-val= 0.0116 FWER= 0.958 FDR= 0.0762	
Gene Set 424 : PID_CD8_TCR_PATHWAY	ES = -0.744 NES = -1.59 Nom. p-val= 0.00965 FWER= 0.978 FDR= 0.0798	
Gene Set 394 : PID_CD40_PATHWAY	ES = -0.603 NES = -1.65 Nom. p-val= 0.0136 FWER= 0.931 FDR= 0.0741	
Gene Set 418 : PID_CDC42_PATHWAY	ES = -0.347 NES = -1.46 Nom. p-val= 0.0948 FWER= 0.999 FDR= 0.117	
Gene Set 420 : PID_CDC42_REG_PATHWAY	ES = -0.509 NES = -1.58 Nom. p-val= 0.0324 FWER= 0.983 FDR= 0.081	
Gene Set 486 : PID_CMYB_PATHWAY	ES = -0.57 NES = -1.82 Nom. p-val= 0.0019 FWER= 0.56 FDR= 0.0746	
Gene Set 503 : PID_CXCR3_PATHWAY	ES = -0.593 NES = -1.66 Nom. p-val= 0.0154 FWER= 0.922 FDR= 0.0733	
Gene Set 446 : PID_CXCR4_PATHWAY	ES = -0.643 NES = -1.76 Nom. p-val= 0 FWER= 0.711 FDR= 0.0732	
Gene Set 513 : PID_DELTA_NP63_PATHWAY	ES = -0.602 NES = -1.62 Nom. p-val= 0.00806 FWER= 0.959 FDR= 0.0757	
Gene Set 392 : PID_DNA_PK_PATHWAY	ES = -0.518 NES = -1.57 Nom. p-val= 0.0545 FWER= 0.985 FDR= 0.0844	
Gene Set 481 : PID_ECADHERIN_KERATINOCYTE_PATHWAY	ES = -0.422 NES = -1.24 Nom. p-val= 0.256 FWER= 1 FDR= 0.247	
Gene Set 462 : PID_ECADHERIN_NASCENT_AJ_PATHWAY	ES = -0.302 NES = -1.26 Nom. p-val= 0.19 FWER= 1 FDR= 0.237	
Gene Set 509 : PID_ECADHERIN_STABILIZATION_PATHWAY	ES = -0.503 NES = -1.63 Nom. p-val= 0.0202 FWER= 0.943 FDR= 0.0765	
Gene Set 367 : PID_ENDOTHELIN_PATHWAY	ES = -0.608 NES = -1.66 Nom. p-val= 0 FWER= 0.913 FDR= 0.0732	
Gene Set 476 : PID_EPHA_FWDPATHWAY	ES = -0.667 NES = -1.72 Nom. p-val= 0 FWER= 0.794 FDR= 0.0731	
Gene Set 539 : PID_EPHA2_FWD_PATHWAY	ES = -0.482 NES = -1.39 Nom. p-val= 0.139 FWER= 1 FDR= 0.15	
Gene Set 405 : PID_EPHB_FWD_PATHWAY	ES = -0.52 NES = -1.7 Nom. p-val= 0.0134 FWER= 0.849 FDR= 0.0747	
Gene Set 528 : PID_EPHRINB_REV_PATHWAY	ES = -0.654 NES = -1.62 Nom. p-val= 0.00945 FWER= 0.958 FDR= 0.076	
Gene Set 510 : PID_EPO_PATHWAY	ES = -0.553 NES = -1.67 Nom. p-val= 0.00956 FWER= 0.91 FDR= 0.0739	
Gene Set 391 : PID_ER_NONGENOMIC_PATHWAY	ES = -0.594 NES = -1.69 Nom. p-val= 0.002 FWER= 0.865 FDR= 0.076	
Gene Set 491 : PID_ERA_GENOMIC_PATHWAY	ES = -0.434 NES = -1.68 Nom. p-val= 0.0115 FWER= 0.877 FDR= 0.0753	
Gene Set 442 : PID_ERB_GENOMIC_PATHWAY	ES = -0.628 NES = -1.55 Nom. p-val= 0.0498 FWER= 0.99 FDR= 0.0896	
Gene Set 468 : PID_ERBB1_DOWNSTREAM_PATHWAY	ES = -0.39 NES = -1.72 Nom. p-val= 0.0201 FWER= 0.783 FDR= 0.0738	
Gene Set 500 : PID_ERBB1_INTERNALIZATION_PATHWAY	ES = -0.446 NES = -1.6 Nom. p-val= 0.0452 FWER= 0.967 FDR= 0.0764	
Gene Set 448 : PID_ERBB1_RECEPTOR_PROXIMAL_PATHWAY	ES = -0.36 NES = -1.3 Nom. p-val= 0.211 FWER= 1 FDR= 0.21	
Gene Set 474 : PID_ERBB2_ERBB3_PATHWAY	ES = -0.432 NES = -1.59 Nom. p-val= 0.0278 FWER= 0.981 FDR= 0.0807	
Gene Set 371 : PID_ERBB4_PATHWAY	ES = -0.51 NES = -1.45 Nom. p-val= 0.081 FWER= 0.999 FDR= 0.121	
Gene Set 546 : PID_FAK_PATHWAY	ES = -0.51 NES = -1.79 Nom. p-val= 0.008 FWER= 0.647 FDR= 0.0785	
Gene Set 428 : PID_FAS_PATHWAY	ES = -0.54 NES = -1.74 Nom. p-val= 0.00385 FWER= 0.743 FDR= 0.0735	
Gene Set 366 : PID_FCER1_PATHWAY	ES = -0.666 NES = -1.77 Nom. p-val= 0.00196 FWER= 0.698 FDR= 0.0718	
Gene Set 542 : PID_FGF_PATHWAY	ES = -0.586 NES = -1.67 Nom. p-val= 0.00372 FWER= 0.911 FDR= 0.0735	
Gene Set 407 : PID_FRA_PATHWAY	ES = -0.683 NES = -1.61 Nom. p-val= 0.008 FWER= 0.964 FDR= 0.0763	
Gene Set 386 : PID_GLYPICAN_1PATHWAY	ES = -0.702 NES = -1.71 Nom. p-val= 0.00406 FWER= 0.827 FDR= 0.0763	
Gene Set 379 : PID_GMCSF_PATHWAY	ES = -0.582 NES = -1.59 Nom. p-val= 0.0293 FWER= 0.981 FDR= 0.0806	
Gene Set 383 : PID_HDAC_CLASSII_PATHWAY	ES = -0.537 NES = -1.89 Nom. p-val= 0.00769 FWER= 0.38 FDR= 0.0816	
Gene Set 497 : PID_HEDGEHOG_2PATHWAY	ES = -0.633 NES = -1.48 Nom. p-val= 0.0599 FWER= 0.999 FDR= 0.113	
Gene Set 501 : PID_HEDGEHOG_GLI_PATHWAY	ES = -0.417 NES = -1.48 Nom. p-val= 0.0875 FWER= 0.998 FDR= 0.112	
Gene Set 549 : PID_HES_HEY_PATHWAY	ES = -0.409 NES = -1.41 Nom. p-val= 0.0378 FWER= 1 FDR= 0.142	
Gene Set 526 : PID_HIF1_TFPATHWAY	ES = -0.553 NES = -1.77 Nom. p-val= 0.00784 FWER= 0.687 FDR= 0.0732	
Gene Set 477 : PID_HIF1A_PATHWAY	ES = -0.486 NES = -1.55 Nom. p-val= 0.0629 FWER= 0.99 FDR= 0.0896	
Gene Set 393 : PID_HIF2PATHWAY	ES = -0.584 NES = -1.91 Nom. p-val= 0 FWER= 0.342 FDR= 0.0946	Y
Gene Set 488 : PID_HIV_NEF_PATHWAY	ES = -0.542 NES = -1.7 Nom. p-val= 0.00984 FWER= 0.841 FDR= 0.0755	
Gene Set 465 : PID_IFNG_PATHWAY	ES = -0.503 NES = -1.65 Nom. p-val= 0.0174 FWER= 0.924 FDR= 0.0729	
Gene Set 437 : PID_IL1_PATHWAY	ES = -0.513 NES = -1.5 Nom. p-val= 0.0635 FWER= 0.997 FDR= 0.107	

Gene Set 445 : PID_IL2_1PATHWAY	ES = -0.602 NES = -1.65 Nom. p-val= 0.00787 FWER= 0.931 FDR= 0.0738	
Gene Set 456 : PID_IL2_PI3K_PATHWAY	ES = -0.499 NES = -1.45 Nom. p-val= 0.0967 FWER= 0.999 FDR= 0.123	
Gene Set 511 : PID_IL2_STAT5_PATHWAY	ES = -0.661 NES = -1.48 Nom. p-val= 0.0578 FWER= 0.999 FDR= 0.114	
Gene Set 479 : PID_IL3_PATHWAY	ES = -0.577 NES = -1.6 Nom. p-val= 0.02 FWER= 0.967 FDR= 0.0765	
Gene Set 382 : PID_IL4_2PATHWAY	ES = -0.64 NES = -1.64 Nom. p-val= 0.0038 FWER= 0.934 FDR= 0.0738	
Gene Set 480 : PID_IL6_7_PATHWAY	ES = -0.571 NES = -1.55 Nom. p-val= 0.0358 FWER= 0.99 FDR= 0.0895	
Gene Set 524 : PID_IL8_CXCR1_PATHWAY	ES = -0.665 NES = -1.55 Nom. p-val= 0.0115 FWER= 0.99 FDR= 0.0898	
Gene Set 496 : PID_IL8_CXCR2_PATHWAY	ES = -0.674 NES = -1.59 Nom. p-val= 0.0115 FWER= 0.976 FDR= 0.0788	
Gene Set 400 : PID_IL12_2PATHWAY	ES = -0.689 NES = -1.47 Nom. p-val= 0.0564 FWER= 0.999 FDR= 0.116	
Gene Set 550 : PID_IL12_STAT4_PATHWAY	ES = -0.763 NES = -1.51 Nom. p-val= 0.0242 FWER= 0.996 FDR= 0.103	
Gene Set 487 : PID_IL23_PATHWAY	ES = -0.694 NES = -1.41 Nom. p-val= 0.0658 FWER= 1 FDR= 0.144	
Gene Set 388 : PID_IL27_PATHWAY	ES = -0.749 NES = -1.48 Nom. p-val= 0.0189 FWER= 0.999 FDR= 0.113	
Gene Set 413 : PID_ILK_PATHWAY	ES = -0.545 NES = -1.98 Nom. p-val= 0.00192 FWER= 0.196 FDR= 0.097	
Gene Set 521 : PID_INSULIN_GLUCOSE_PATHWAY	ES = -0.423 NES = -1.34 Nom. p-val= 0.159 FWER= 1 FDR= 0.182	
Gene Set 374 : PID_INSULIN_PATHWAY	ES = -0.438 NES = -1.7 Nom. p-val= 0.0156 FWER= 0.85 FDR= 0.0743	
Gene Set 543 : PID_INTEGRIN_A4B1_PATHWAY	ES = -0.667 NES = -1.89 Nom. p-val= 0 FWER= 0.392 FDR= 0.0833	Y
Gene Set 441 : PID_INTEGRIN_A9B1_PATHWAY	ES = -0.661 NES = -1.55 Nom. p-val= 0.012 FWER= 0.99 FDR= 0.089	
Gene Set 396 : PID_INTEGRIN_CS_PATHWAY	ES = -0.753 NES = -1.56 Nom. p-val= 0 FWER= 0.989 FDR= 0.0872	
Gene Set 376 : PID_INTEGRIN1_PATHWAY	ES = -0.694 NES = -1.69 Nom. p-val= 0 FWER= 0.877 FDR= 0.0759	
Gene Set 472 : PID_INTEGRIN2_PATHWAY	ES = -0.756 NES = -1.58 Nom. p-val= 0.0148 FWER= 0.984 FDR= 0.0832	
Gene Set 399 : PID_INTEGRIN3_PATHWAY	ES = -0.701 NES = -1.69 Nom. p-val= 0 FWER= 0.87 FDR= 0.075	
Gene Set 498 : PID_INTEGRIN5_PATHWAY	ES = -0.72 NES = -1.49 Nom. p-val= 0.0233 FWER= 0.998 FDR= 0.111	
Gene Set 508 : PID_KIT_PATHWAY	ES = -0.541 NES = -1.61 Nom. p-val= 0.0193 FWER= 0.96 FDR= 0.0754	
Gene Set 402 : PID_LPA4_PATHWAY	ES = -0.663 NES = -1.45 Nom. p-val= 0.0461 FWER= 0.999 FDR= 0.123	
Gene Set 540 : PID_LYMPH_ANGIOGENESIS_PATHWAY	ES = -0.64 NES = -1.74 Nom. p-val= 0.00192 FWER= 0.755 FDR= 0.0746	
Gene Set 373 : PID_LYSOPHOSPHOLIPID_PATHWAY	ES = -0.513 NES = -1.63 Nom. p-val= 0.0254 FWER= 0.944 FDR= 0.0767	
Gene Set 397 : PID_MET_PATHWAY	ES = -0.382 NES = -1.74 Nom. p-val= 0.012 FWER= 0.755 FDR= 0.074	
Gene Set 408 : PID_MYC_ACTIV_PATHWAY	ES = -0.396 NES = -1.54 Nom. p-val= 0.0631 FWER= 0.991 FDR= 0.09	
Gene Set 525 : PID_MYC_REPRESS_PATHWAY	ES = -0.521 NES = -1.82 Nom. p-val= 0 FWER= 0.553 FDR= 0.0757	Y
Gene Set 532 : PID_NCADHERIN_PATHWAY	ES = -0.582 NES = -1.67 Nom. p-val= 0.00604 FWER= 0.909 FDR= 0.0739	
Gene Set 414 : PID_NECTIN_PATHWAY	ES = -0.408 NES = -1.38 Nom. p-val= 0.171 FWER= 1 FDR= 0.156	
Gene Set 485 : PID_NEPHRIN_NEPH1_PATHWAY	ES = -0.548 NES = -1.74 Nom. p-val= 0.00391 FWER= 0.745 FDR= 0.073	
Gene Set 436 : PID_NETRIN_PATHWAY	ES = -0.637 NES = -1.84 Nom. p-val= 0 FWER= 0.494 FDR= 0.0875	Y
Gene Set 438 : PID_NFAT_3PATHWAY	ES = -0.526 NES = -1.87 Nom. p-val= 0 FWER= 0.423 FDR= 0.0852	Y
Gene Set 404 : PID_NFAT_TFPATHWAY	ES = -0.66 NES = -1.46 Nom. p-val= 0.043 FWER= 0.999 FDR= 0.117	
Gene Set 375 : PID_NOTCH_PATHWAY	ES = -0.427 NES = -1.4 Nom. p-val= 0.0778 FWER= 1 FDR= 0.145	
Gene Set 507 : PID_P38_ALPHA_BETA_DOWNSTREAM_PATHWAY	ES = -0.496 NES = -1.7 Nom. p-val= 0.0202 FWER= 0.845 FDR= 0.0744	
Gene Set 415 : PID_P38_ALPHA_BETA_PATHWAY	ES = -0.623 NES = -1.75 Nom. p-val= 0.00394 FWER= 0.729 FDR= 0.0743	
Gene Set 490 : PID_P38_MK2_PATHWAY	ES = -0.507 NES = -1.52 Nom. p-val= 0.0596 FWER= 0.995 FDR= 0.0976	
Gene Set 458 : PID_P53_DOWNSTREAM_PATHWAY	ES = -0.556 NES = -1.8 Nom. p-val= 0.00192 FWER= 0.614 FDR= 0.0799	
Gene Set 377 : PID_P73PATHWAY	ES = -0.388 NES = -1.34 Nom. p-val= 0.133 FWER= 1 FDR= 0.184	
Gene Set 460 : PID_P75_NTR_PATHWAY	ES = -0.408 NES = -1.56 Nom. p-val= 0.0399 FWER= 0.99 FDR= 0.0888	
Gene Set 494 : PID_PDGFRA_PATHWAY	ES = -0.58 NES = -1.55 Nom. p-val= 0.0501 FWER= 0.99 FDR= 0.0894	
Gene Set 483 : PID_PDGFRA_PATHWAY	ES = -0.504 NES = -1.9 Nom. p-val= 0 FWER= 0.343 FDR= 0.0915	Y
Gene Set 537 : PID_PI3K_PLC_TRK_PATHWAY	ES = -0.628 NES = -2 Nom. p-val= 0 FWER= 0.167 FDR= 0.103	Y
Gene Set 454 : PID_PI3KCI_PATHWAY	ES = -0.683 NES = -1.72 Nom. p-val= 0.00759 FWER= 0.79 FDR= 0.0727	
Gene Set 369 : PID_PRL_SIGNALING_EVENTS_PATHWAY	ES = -0.414 NES = -1.35 Nom. p-val= 0.136 FWER= 1 FDR= 0.173	
Gene Set 412 : PID_PS1_PATHWAY	ES = -0.368 NES = -1.31 Nom. p-val= 0.146 FWER= 1 FDR= 0.2	
Gene Set 398 : PID_PTP1B_PATHWAY	ES = -0.656 NES = -1.79 Nom. p-val= 0 FWER= 0.648 FDR= 0.0766	Y
Gene Set 544 : PID_RAC1_PATHWAY	ES = -0.432 NES = -1.58 Nom. p-val= 0.0441 FWER= 0.984 FDR= 0.0825	
Gene Set 518 : PID_RAC1_REG_PATHWAY	ES = -0.635 NES = -1.63 Nom. p-val= 0.00591 FWER= 0.945 FDR= 0.0761	
Gene Set 535 : PID_RAS_PATHWAY	ES = -0.654 NES = -1.62 Nom. p-val= 0.00377 FWER= 0.953 FDR= 0.0766	
Gene Set 545 : PID_RB_1PATHWAY	ES = -0.52 NES = -1.83 Nom. p-val= 0.00384 FWER= 0.543 FDR= 0.0789	
Gene Set 439 : PID_REG_GR_PATHWAY	ES = -0.446 NES = -1.41 Nom. p-val= 0.084 FWER= 1 FDR= 0.14	
Gene Set 419 : PID_RET_PATHWAY	ES = -0.533 NES = -1.72 Nom. p-val= 0.004 FWER= 0.785 FDR= 0.0734	
Gene Set 495 : PID_RETINOIC_ACID_PATHWAY	ES = -0.494 NES = -1.63 Nom. p-val= 0.016 FWER= 0.943 FDR= 0.0762	



Gene Set 370 : PID_RHOA_PATHWAY	ES = -0.431 NES = -1.51 Nom. p-val= 0.0574 FWER= 0.996 FDR= 0.101	
Gene Set 410 : PID_RHOA_REG_PATHWAY	ES = -0.525 NES = -1.67 Nom. p-val= 0.00765 FWER= 0.91 FDR= 0.0737	
Gene Set 466 : PID_RXR_VDR_PATHWAY	ES = -0.641 NES = -1.8 Nom. p-val= 0 FWER= 0.61 FDR= 0.0792	Y
Gene Set 461 : PID_S1P_META_PATHWAY	ES = -0.627 NES = -1.58 Nom. p-val= 0.0098 FWER= 0.983 FDR= 0.081	
Gene Set 433 : PID_S1P_S1P1_PATHWAY	ES = -0.611 NES = -1.48 Nom. p-val= 0.0425 FWER= 0.999 FDR= 0.114	
Gene Set 534 : PID_S1P_S1P2_PATHWAY	ES = -0.498 NES = -1.43 Nom. p-val= 0.102 FWER= 1 FDR= 0.131	
Gene Set 401 : PID_S1P_S1P3_PATHWAY	ES = -0.624 NES = -1.64 Nom. p-val= 0.00407 FWER= 0.934 FDR= 0.0735	
Gene Set 431 : PID_SHP2_PATHWAY	ES = -0.622 NES = -1.62 Nom. p-val= 0.00398 FWER= 0.958 FDR= 0.0762	
Gene Set 365 : PID_SMAD2_3NUCLEAR_PATHWAY	ES = -0.453 NES = -1.6 Nom. p-val= 0.0176 FWER= 0.971 FDR= 0.0783	
Gene Set 489 : PID_SYNDECAN_1_PATHWAY	ES = -0.704 NES = -1.67 Nom. p-val= 0.00392 FWER= 0.911 FDR= 0.0735	
Gene Set 517 : PID_SYNDECAN_2_PATHWAY	ES = -0.558 NES = -1.73 Nom. p-val= 0 FWER= 0.778 FDR= 0.073	
Gene Set 523 : PID_SYNDECAN_3_PATHWAY	ES = -0.605 NES = -1.55 Nom. p-val= 0.0376 FWER= 0.99 FDR= 0.0897	
Gene Set 469 : PID_SYNDECAN_4_PATHWAY	ES = -0.663 NES = -1.69 Nom. p-val= 0 FWER= 0.866 FDR= 0.0761	
Gene Set 527 : PID_TAP63_PATHWAY	ES = -0.566 NES = -1.66 Nom. p-val= 0.0103 FWER= 0.922 FDR= 0.0731	
Gene Set 426 : PID_TCPTP_PATHWAY	ES = -0.53 NES = -1.55 Nom. p-val= 0.0336 FWER= 0.991 FDR= 0.0897	
Gene Set 512 : PID_TCR_CALCIIUM_PATHWAY	ES = -0.625 NES = -1.43 Nom. p-val= 0.0727 FWER= 1 FDR= 0.133	
Gene Set 387 : PID_TCR_PATHWAY	ES = -0.75 NES = -1.64 Nom. p-val= 0.00771 FWER= 0.939 FDR= 0.0743	
Gene Set 548 : PID_TGFBR_PATHWAY	ES = -0.444 NES = -1.7 Nom. p-val= 0.0167 FWER= 0.844 FDR= 0.0749	
Gene Set 515 : PID_THROMBIN_PAR1_PATHWAY	ES = -0.585 NES = -1.73 Nom. p-val= 0.00189 FWER= 0.765 FDR= 0.0736	
Gene Set 452 : PID_THROMBIN_PAR4_PATHWAY	ES = -0.646 NES = -1.54 Nom. p-val= 0.0263 FWER= 0.991 FDR= 0.0905	
Gene Set 449 : PID_TNF_PATHWAY	ES = -0.454 NES = -1.63 Nom. p-val= 0.0163 FWER= 0.945 FDR= 0.0762	
Gene Set 531 : PID_TOLL_ENDOGENOUS_PATHWAY	ES = -0.711 NES = -1.58 Nom. p-val= 0.0174 FWER= 0.983 FDR= 0.0808	
Gene Set 417 : PID_TRAIL_PATHWAY	ES = -0.473 NES = -1.46 Nom. p-val= 0.0743 FWER= 0.999 FDR= 0.117	
Gene Set 484 : PID_TRKR_PATHWAY	ES = -0.495 NES = -1.7 Nom. p-val= 0.0176 FWER= 0.834 FDR= 0.0755	
Gene Set 430 : PID_TXA2PATHWAY	ES = -0.635 NES = -1.62 Nom. p-val= 0.00579 FWER= 0.955 FDR= 0.076	
Gene Set 473 : PID_UPA_UPAR_PATHWAY	ES = -0.686 NES = -1.61 Nom. p-val= 0.00192 FWER= 0.964 FDR= 0.0758	
Gene Set 514 : PID_VEGFR1_2_PATHWAY	ES = -0.444 NES = -1.68 Nom. p-val= 0.0277 FWER= 0.887 FDR= 0.074	
Gene Set 505 : PID_VEGFR1_PATHWAY	ES = -0.535 NES = -1.5 Nom. p-val= 0.0536 FWER= 0.996 FDR= 0.105	
Gene Set 425 : PID_WNT_CANONICAL_PATHWAY	ES = -0.599 NES = -1.78 Nom. p-val= 0.00379 FWER= 0.668 FDR= 0.0756	
Gene Set 380 : PID_WNT_NONCANONICAL_PATHWAY	ES = -0.625 NES = -1.85 Nom. p-val= 0 FWER= 0.485 FDR= 0.0853	Y
Gene Set 416 : PID_WNT_SIGNALING_PATHWAY	ES = -0.631 NES = -1.52 Nom. p-val= 0.00962 FWER= 0.995 FDR= 0.0986	
REACTOME_A_TETRASACCHARIDE_LINKER_SEQUENCE_IS_REQUIRED_FOR_GAG_SYNTHESIS	ES = -0.599 NES = -1.56 Nom. p-val= 0.0158 FWER= 0.988 FDR= 0.0866	
Gene Set 757 : REACTOME_ABC_FAMILY_PROTEINS_MEDIATED_TRANSPORT	ES = -0.521 NES = -1.34 Nom. p-val= 0.0837 FWER= 1 FDR= 0.18	
Gene Set 583 : REACTOME_ABCA_TRANSPORTERS_IN_LIPID_HOMEOSTASIS	ES = -0.644 NES = -1.53 Nom. p-val= 0.0238 FWER= 0.993 FDR= 0.0959	
Gene Set 756 : REACTOME_ACETYLCHOLINE_BINDING_AND_DOWNSTREAM_EVENTS	ES = -0.643 NES = -1.3 Nom. p-val= 0.136 FWER= 1 FDR= 0.21	
Gene Set 624 : REACTOME_ACTIVATED_NOTCH1_TRANSMITS_SIGNAL_TO_THE_NUCLEUS	ES = -0.466 NES = -1.39 Nom. p-val= 0.0825 FWER= 1 FDR= 0.151	
Gene Set 658 : REACTOME_ACTIVATED_POINT_MUTANTS_OF_FGFR2	ES = -0.682 NES = -1.35 Nom. p-val= 0.0867 FWER= 1 FDR= 0.177	
Gene Set 1018 : REACTOME_ACTIVATED_TLR4_SIGNALLING	ES = -0.497 NES = -1.76 Nom. p-val= 0.00587 FWER= 0.719 FDR= 0.0734	
Gene Set 889 : REACTOME_ACTIVATION_OF_KAINATE_RECEPTORS_UPON_GLUTAMATE_BINDING	ES = -0.642 NES = -1.68 Nom. p-val= 0.0019 FWER= 0.892 FDR= 0.0728	
Gene Set 626 : REACTOME_ACTIVATION_OF_NF_KAPPAB_IN_B_CELLS	ES = -0.398 NES = -1.62 Nom. p-val= 0.0576 FWER= 0.948 FDR= 0.0758	
REACTOME_ACTIVATION_OF_NMDA_RECEPTOR_UPON_GLUTAMATE_BINDING_AND_POSTSYNAPTIC_EVENTS	ES = -0.576 NES = -1.53 Nom. p-val= 0.0212 FWER= 0.993 FDR= 0.093	
Gene Set 655 : REACTOME_ACYL_CHAIN_REMODELLING_OF_PC	ES = -0.54 NES = -1.37 Nom. p-val= 0.0985 FWER= 1 FDR= 0.162	
Gene Set 679 : REACTOME_ACYL_CHAIN_REMODELLING_OF_PE	ES = -0.547 NES = -1.36 Nom. p-val= 0.123 FWER= 1 FDR= 0.172	
Gene Set 678 : REACTOME_ACYL_CHAIN_REMODELLING_OF_PG	ES = -0.569 NES = -1.34 Nom. p-val= 0.115 FWER= 1 FDR= 0.184	
Gene Set 646 : REACTOME_ACYL_CHAIN_REMODELLING_OF_PI	ES = -0.645 NES = -1.46 Nom. p-val= 0.0538 FWER= 0.999 FDR= 0.119	
Gene Set 680 : REACTOME_ACYL_CHAIN_REMODELLING_OF_PS	ES = -0.627 NES = -1.42 Nom. p-val= 0.0609 FWER= 1 FDR= 0.138	
Gene Set 828 : REACTOME_ADHERENS_JUNCTIONS_INTERACTIONS	ES = -0.514 NES = -1.36 Nom. p-val= 0.0789 FWER= 1 FDR= 0.172	
Gene Set 824 : REACTOME_ADP_SIGNALLING_THROUGH_P2RY1	ES = -0.593 NES = -1.62 Nom. p-val= 0.0171 FWER= 0.958 FDR= 0.0759	
Gene Set 873 : REACTOME_ADP_SIGNALLING_THROUGH_P2RY12	ES = -0.608 NES = -1.47 Nom. p-val= 0.0395 FWER= 0.999 FDR= 0.114	
Gene Set 875 : REACTOME_AMINE_COMPOUND_SLC_TRANSPORTERS	ES = -0.53 NES = -1.3 Nom. p-val= 0.1 FWER= 1 FDR= 0.209	
Gene Set 785 : REACTOME_AMINE_LIGAND_BINDING_RECEPTORS	ES = -0.667 NES = -1.56 Nom. p-val= 0.00196 FWER= 0.988 FDR= 0.0865	
Gene Set 851 : REACTOME_AMINO_ACID_AND_OLIGOPEPTIDE_SLC_TRANSPORTERS	ES = -0.54 NES = -1.47 Nom. p-val= 0.0247 FWER= 0.999 FDR= 0.116	
Gene Set 727 : REACTOME_AMINO_ACID_TRANSPORT_ACROSS_THE_PLASMA_MEMBRANE	ES = -0.558 NES = -1.51 Nom. p-val= 0.0209 FWER= 0.996 FDR= 0.101	
REACTOME_ANTIGEN_ACTIVATES_B_CELL_RECEPTOR_LEADING_TO_GENERATION_OF_SECOND_MESSENGERS	ES = -0.697 NES = -1.6 Nom. p-val= 0.0176 FWER= 0.973 FDR= 0.0786	
REACTOME_ANTIGEN_PRESENTATION_FOLDING_ASSEMBLY_AND_PEPTIDE_LOADING_OF_CLASS_I_MHC	ES = -0.476 NES = -1.29 Nom. p-val= 0.232 FWER= 1 FDR= 0.215	

Gene Set 579 : REACTOME ANTIGEN PROCESSING CROSS PRESENTATION	ES = -0.583 NES = -1.9 Nom. p-val= 0.00184 FWER= 0.353 FDR= 0.0868	
: REACTOME ANTIGEN PROCESSING UBIQUITINATION PROTEASOME DEGRADATION	ES = -0.347 NES = -2.13 Nom. p-val= 0 FWER= 0.051 FDR= 0.0441	Y
Gene Set 984 : REACTOME APOPTOSIS	ES = -0.341 NES = -1.68 Nom. p-val= 0.0175 FWER= 0.886 FDR= 0.0743	
Gene Set 930 : REACTOME AQUAPORIN MEDIATED TRANSPORT	ES = -0.594 NES = -1.64 Nom. p-val= 0.0019 FWER= 0.935 FDR= 0.0738	
Gene Set 639 : REACTOME ARMS MEDIATED ACTIVATION	ES = -0.612 NES = -1.75 Nom. p-val= 0.0141 FWER= 0.72 FDR= 0.0728	
REACTOME ASSOCIATION OF TRIC CCT WITH TARGET PROTEINS DURING BIOSYNTHESIS	ES = -0.304 NES = -1.3 Nom. p-val= 0.142 FWER= 1 FDR= 0.209	
Gene Set 798 : REACTOME AXON GUIDANCE	ES = -0.607 NES = -1.94 Nom. p-val= 0 FWER= 0.282 FDR= 0.106	Y
Gene Set 695 : REACTOME BASIGIN INTERACTIONS	ES = -0.575 NES = -1.49 Nom. p-val= 0.031 FWER= 0.998 FDR= 0.111	
Gene Set 611 : REACTOME BETA DEFENSINS	ES = -0.591 NES = -1.55 Nom. p-val= 0.0136 FWER= 0.991 FDR= 0.09	
Gene Set 710 : REACTOME BIOLOGICAL OXIDATIONS	ES = -0.538 NES = -1.5 Nom. p-val= 0.0115 FWER= 0.996 FDR= 0.104	
Gene Set 578 : REACTOME BMAL1_CLOCK NPAS2 ACTIVATES_CIRCADIAN_EXPRESSION	ES = -0.539 NES = -1.55 Nom. p-val= 0.0419 FWER= 0.99 FDR= 0.0897	
Gene Set 593 : REACTOME BOTULINUM NEUROTOXICITY	ES = -0.611 NES = -1.44 Nom. p-val= 0.0524 FWER= 0.999 FDR= 0.128	
Gene Set 744 : REACTOME CA_DEPENDENT_EVENTS	ES = -0.616 NES = -1.63 Nom. p-val= 0.0152 FWER= 0.945 FDR= 0.0764	
Gene Set 826 : REACTOME CD28 CO STIMULATION	ES = -0.622 NES = -1.61 Nom. p-val= 0.0294 FWER= 0.963 FDR= 0.0766	
Gene Set 844 : REACTOME CD28 DEPENDENT PI3K AKT SIGNALING	ES = -0.615 NES = -1.51 Nom. p-val= 0.0549 FWER= 0.996 FDR= 0.101	
Gene Set 582 : REACTOME CELL_CELL_COMMUNICATION	ES = -0.52 NES = -1.68 Nom. p-val= 0.00199 FWER= 0.885 FDR= 0.0752	
Gene Set 840 : REACTOME CELL_CELL_JUNCTION_ORGANIZATION	ES = -0.489 NES = -1.46 Nom. p-val= 0.0176 FWER= 0.999 FDR= 0.117	
Gene Set 724 : REACTOME CELL DEATH SIGNALLING VIA NRAGE NRIF AND NADE	ES = -0.578 NES = -1.82 Nom. p-val= 0.00193 FWER= 0.559 FDR= 0.0754	
Gene Set 874 : REACTOME CELL_JUNCTION_ORGANIZATION	ES = -0.516 NES = -1.58 Nom. p-val= 0.00604 FWER= 0.984 FDR= 0.0833	
Gene Set 643 : REACTOME CELL SURFACE INTERACTIONS AT THE VASCULAR WALL	ES = -0.702 NES = -1.86 Nom. p-val= 0 FWER= 0.437 FDR= 0.0876	Y
Gene Set 922 : REACTOME CGMP_EFFECTS	ES = -0.606 NES = -1.38 Nom. p-val= 0.111 FWER= 1 FDR= 0.157	
Gene Set 746 : REACTOME CHEMOKINE RECEPTORS BIND CHEMOKINES	ES = -0.753 NES = -1.46 Nom. p-val= 0.0269 FWER= 0.999 FDR= 0.119	
Gene Set 663 : REACTOME CHONDROITIN SULFATE BIOSYNTHESIS	ES = -0.69 NES = -1.56 Nom. p-val= 0.0078 FWER= 0.989 FDR= 0.0871	
Gene Set 671 : REACTOME CHONDROITIN SULFATE DERMATAN SULFATE METABOLISM	ES = -0.587 NES = -1.68 Nom. p-val= 0.00594 FWER= 0.885 FDR= 0.0757	
Gene Set 1015 : REACTOME CHYLOMICRON MEDIATED LIPID TRANSPORT	ES = -0.654 NES = -1.35 Nom. p-val= 0.143 FWER= 1 FDR= 0.173	
Gene Set 941 : REACTOME CIRCADIAN CLOCK	ES = -0.507 NES = -1.62 Nom. p-val= 0.0239 FWER= 0.955 FDR= 0.0762	
Gene Set 634 : REACTOME CIRCADIAN REPRESSION OF EXPRESSION BY_REV_ERBA	ES = -0.541 NES = -1.48 Nom. p-val= 0.0787 FWER= 0.999 FDR= 0.114	
Gene Set 736 : REACTOME CLASS A1 RHODOPSIN LIKE RECEPTORS	ES = -0.646 NES = -1.65 Nom. p-val= 0 FWER= 0.927 FDR= 0.0725	
Gene Set 813 : REACTOME CLASS B_2_SECRETIN_FAMILY_RECEPTORS	ES = -0.603 NES = -1.66 Nom. p-val= 0 FWER= 0.916 FDR= 0.0738	
Gene Set 1032 : REACTOME CLASS I MHC MEDIATED ANTIGEN PROCESSING PRESENTATION	ES = -0.443 NES = -2.38 Nom. p-val= 0 FWER= 0.004 FDR= 0.0136	Y
Gene Set 648 : REACTOME COLLAGEN FORMATION	ES = -0.698 NES = -1.65 Nom. p-val= 0.00194 FWER= 0.927 FDR= 0.0726	
Gene Set 1021 : REACTOME COMPLEMENT CASCADE	ES = -0.735 NES = -1.57 Nom. p-val= 0.00604 FWER= 0.987 FDR= 0.0858	
Gene Set 842 : REACTOME COSTIMULATION BY THE CD28 FAMILY	ES = -0.713 NES = -1.69 Nom. p-val= 0.00967 FWER= 0.877 FDR= 0.0759	
Gene Set 866 : REACTOME CREB PHOSPHORYLATION THROUGH THE ACTIVATION OF RAS	ES = -0.542 NES = -1.5 Nom. p-val= 0.034 FWER= 0.996 FDR= 0.105	
REACTOME_CROSS_PRESENTATION_OF_SOLUBLE_EXOGENOUS_ANTIGENS_ENDOSOMES	ES = -0.608 NES = -1.93 Nom. p-val= 0.00373 FWER= 0.284 FDR= 0.101	
Gene Set 849 : REACTOME CTLA4 INHIBITORY SIGNALING	ES = -0.638 NES = -1.68 Nom. p-val= 0.0212 FWER= 0.883 FDR= 0.0757	
Gene Set 715 : REACTOME CYTOCHROME P450 ARRANGED BY SUBSTRATE TYPE	ES = -0.515 NES = -1.26 Nom. p-val= 0.125 FWER= 1 FDR= 0.237	
Gene Set 1029 : REACTOME CYTOKINE SIGNALING IN IMMUNE SYSTEM	ES = -0.574 NES = -1.83 Nom. p-val= 0 FWER= 0.527 FDR= 0.0858	Y
Gene Set 576 : REACTOME DAG AND IP3 SIGNALING	ES = -0.577 NES = -1.6 Nom. p-val= 0.0152 FWER= 0.973 FDR= 0.0784	
Gene Set 745 : REACTOME DARPP_32_EVENTS	ES = -0.359 NES = -1.27 Nom. p-val= 0.186 FWER= 1 FDR= 0.228	
Gene Set 607 : REACTOME DEFENSINS	ES = -0.609 NES = -1.6 Nom. p-val= 0.00189 FWER= 0.971 FDR= 0.0783	
Gene Set 621 : REACTOME DEGRADATION OF THE EXTRACELLULAR MATRIX	ES = -0.641 NES = -1.46 Nom. p-val= 0.0442 FWER= 0.999 FDR= 0.117	
Gene Set 573 : REACTOME DEVELOPMENTAL BIOLOGY	ES = -0.564 NES = -1.95 Nom. p-val= 0 FWER= 0.254 FDR= 0.104	Y
Gene Set 750 : REACTOME DIABETES PATHWAYS	ES = -0.382 NES = -1.68 Nom. p-val= 0.00992 FWER= 0.885 FDR= 0.0744	
Gene Set 647 : REACTOME DOWNREGULATION OF TGF BETA RECEPTOR SIGNALING	ES = -0.467 NES = -1.8 Nom. p-val= 0.00208 FWER= 0.606 FDR= 0.0788	
Gene Set 787 : REACTOME DOWNSTREAM SIGNAL TRANSDUCTION	ES = -0.406 NES = -1.7 Nom. p-val= 0.0102 FWER= 0.845 FDR= 0.0749	
Gene Set 625 : REACTOME DOWNSTREAM SIGNALING EVENTS OF B CELL RECEPTOR BCR	ES = -0.344 NES = -1.71 Nom. p-val= 0.0362 FWER= 0.819 FDR= 0.0759	
Gene Set 882 : REACTOME DOWNSTREAM SIGNALING OF ACTIVATED_FGFR	ES = -0.493 NES = -1.72 Nom. p-val= 0.00572 FWER= 0.794 FDR= 0.073	
Gene Set 694 : REACTOME DOWNSTREAM TCR SIGNALING	ES = -0.728 NES = -1.65 Nom. p-val= 0.00786 FWER= 0.927 FDR= 0.0726	
Gene Set 901 : REACTOME EFFECTS OF PIP2 HYDROLYSIS	ES = -0.68 NES = -1.59 Nom. p-val= 0.008 FWER= 0.981 FDR= 0.0805	
Gene Set 810 : REACTOME EICOSANOID LIGAND BINDING RECEPTORS	ES = -0.771 NES = -1.47 Nom. p-val= 0.00954 FWER= 0.999 FDR= 0.116	
Gene Set 728 : REACTOME ENDOGENOUS STEROLS	ES = -0.646 NES = -1.42 Nom. p-val= 0.0413 FWER= 1 FDR= 0.138	
Gene Set 686 : REACTOME ENOS ACTIVATION AND REGULATION	ES = -0.556 NES = -1.77 Nom. p-val= 0.00818 FWER= 0.694 FDR= 0.0723	
Gene Set 701 : REACTOME ERK MAPK TARGETS	ES = -0.459 NES = -1.45 Nom. p-val= 0.117 FWER= 0.999 FDR= 0.121	
Gene Set 632 : REACTOME EXTRACELLULAR MATRIX ORGANIZATION	ES = -0.678 NES = -1.69 Nom. p-val= 0.00191 FWER= 0.872 FDR= 0.075	
REACTOME_FACTORS_INVOLVED_IN_MEGAKARYOCYTE_DEVELOPMENT_AND_PLATELET_PRODUCTION	ES = -0.382 NES = -1.29 Nom. p-val= 0.139 FWER= 1 FDR= 0.215	

Gene Set 912 : REACTOME FATTY ACID TRIACYLGLYCEROL AND KETONE BODY METABOLISM	ES = -0.394 NES = -1.7 Nom. p-val= 0.00196 FWER= 0.828 FDR= 0.0757	
Gene Set 1050 : REACTOME FGFR LIGAND BINDING AND ACTIVATION	ES = -0.647 NES = -1.42 Nom. p-val= 0.0271 FWER= 1 FDR= 0.139	
Gene Set 856 : REACTOME FORMATION_OF_FIBRIN_CLOT_CLOTTING_CASCADE	ES = -0.645 NES = -1.47 Nom. p-val= 0.043 FWER= 0.999 FDR= 0.116	
Gene Set 878 : REACTOME FRS2 MEDIATED CASCADE	ES = -0.577 NES = -1.49 Nom. p-val= 0.0236 FWER= 0.998 FDR= 0.108	
Gene Set 830 : REACTOME_G_ALPHA_I_SIGNALLING_EVENTS	ES = -0.641 NES = -1.66 Nom. p-val= 0 FWER= 0.918 FDR= 0.0736	
Gene Set 802 : REACTOME_G_ALPHA_Q_SIGNALLING_EVENTS	ES = -0.606 NES = -1.68 Nom. p-val= 0 FWER= 0.885 FDR= 0.0747	
Gene Set 839 : REACTOME_G_ALPHA_S_SIGNALLING_EVENTS	ES = -0.608 NES = -1.7 Nom. p-val= 0 FWER= 0.841 FDR= 0.075	
Gene Set 841 : REACTOME_G_ALPHA_Z_SIGNALLING_EVENTS	ES = -0.591 NES = -1.61 Nom. p-val= 0.00372 FWER= 0.963 FDR= 0.0764	
Gene Set 815 : REACTOME_G_ALPHA1213_SIGNALLING_EVENTS	ES = -0.614 NES = -1.81 Nom. p-val= 0 FWER= 0.586 FDR= 0.0767	Y
Gene Set 835 : REACTOME_G_BETA_GAMMA_SIGNALLING_THROUGH_PI3KGAMMA	ES = -0.69 NES = -1.7 Nom. p-val= 0.00387 FWER= 0.828 FDR= 0.0763	
Gene Set 825 : REACTOME_G_BETA_GAMMA_SIGNALLING_THROUGH_PLG_BETA	ES = -0.664 NES = -1.6 Nom. p-val= 0.0116 FWER= 0.971 FDR= 0.0781	
Gene Set 755 : REACTOME_G_PROTEIN_ACTIVATION	ES = -0.578 NES = -1.45 Nom. p-val= 0.0316 FWER= 0.999 FDR= 0.124	
Gene Set 846 : REACTOME_G_PROTEIN_BETA_GAMMA_SIGNALLING	ES = -0.696 NES = -1.78 Nom. p-val= 0.0019 FWER= 0.668 FDR= 0.0763	
Gene Set 947 : REACTOME GABA_B_RECEPTOR_ACTIVATION	ES = -0.589 NES = -1.54 Nom. p-val= 0.0148 FWER= 0.992 FDR= 0.0912	
Gene Set 955 : REACTOME GABA_RECEPTOR_ACTIVATION	ES = -0.54 NES = -1.43 Nom. p-val= 0.0286 FWER= 0.999 FDR= 0.13	
Gene Set 1055 : REACTOME GAP_JUNCTION_ASSEMBLY	ES = -0.576 NES = -1.28 Nom. p-val= 0.132 FWER= 1 FDR= 0.22	
Gene Set 1052 : REACTOME GAP_JUNCTION_TRAFFICKING	ES = -0.549 NES = -1.36 Nom. p-val= 0.075 FWER= 1 FDR= 0.169	
Gene Set 662 : REACTOME GASTRIN CREB SIGNALLING PATHWAY VIA PKC AND MAPK	ES = -0.595 NES = -1.7 Nom. p-val= 0 FWER= 0.838 FDR= 0.0757	
Gene Set 703 : REACTOME GENERATION_OF_SECOND_MESSENGER_MOLECULES	ES = -0.816 NES = -1.54 Nom. p-val= 0.0132 FWER= 0.993 FDR= 0.0932	
Gene Set 773 : REACTOME GLUCAGON SIGNALING IN METABOLIC REGULATION	ES = -0.587 NES = -1.66 Nom. p-val= 0.00562 FWER= 0.915 FDR= 0.0735	
Gene Set 814 : REACTOME GLUCAGON_TYPE_LIGAND_RECEPTORS	ES = -0.556 NES = -1.41 Nom. p-val= 0.047 FWER= 1 FDR= 0.14	
Gene Set 1025 : REACTOME GLUCOSE METABOLISM	ES = -0.339 NES = -1.27 Nom. p-val= 0.211 FWER= 1 FDR= 0.228	
Gene Set 877 : REACTOME GLUCOSE TRANSPORT	ES = -0.389 NES = -1.38 Nom. p-val= 0.0818 FWER= 1 FDR= 0.155	
Gene Set 700 : REACTOME GLUTAMATE_NEUROTRANSMITTER_RELEASE_CYCLE	ES = -0.606 NES = -1.39 Nom. p-val= 0.0966 FWER= 1 FDR= 0.153	
Gene Set 683 : REACTOME GLYCEROPHOSPHOLIPID BIOSYNTHESIS	ES = -0.504 NES = -1.8 Nom. p-val= 0.00382 FWER= 0.619 FDR= 0.0795	
Gene Set 551 : REACTOME GLYCOGEN_BREAKDOWN_GLYCOGENOLYSIS	ES = -0.601 NES = -1.66 Nom. p-val= 0.0253 FWER= 0.922 FDR= 0.0731	
Gene Set 677 : REACTOME GLYCOSAMINOGLYCAN METABOLISM	ES = -0.589 NES = -1.77 Nom. p-val= 0 FWER= 0.678 FDR= 0.0755	
Gene Set 892 : REACTOME GPCR LIGAND BINDING	ES = -0.631 NES = -1.67 Nom. p-val= 0 FWER= 0.901 FDR= 0.0727	
Gene Set 778 : REACTOME GPVI_MEDIATED_ACTIVATION_CASCADE	ES = -0.72 NES = -1.64 Nom. p-val= 0.00192 FWER= 0.935 FDR= 0.0741	
REACTOME GRB2 SOS PROVIDES LINKAGE TO MAPK SIGNALING FOR INTERGRINS	ES = -0.654 NES = -1.42 Nom. p-val= 0.102 FWER= 1 FDR= 0.138	
Gene Set 580 : REACTOME GROWTH HORMONE RECEPTOR SIGNALING	ES = -0.539 NES = -1.55 Nom. p-val= 0.026 FWER= 0.99 FDR= 0.0894	
Gene Set 716 : REACTOME HDL_MEDIATED_LIPID_TRANSPORT	ES = -0.637 NES = -1.31 Nom. p-val= 0.15 FWER= 1 FDR= 0.204	
Gene Set 986 : REACTOME HEMOSTASIS	ES = -0.568 NES = -1.88 Nom. p-val= 0 FWER= 0.406 FDR= 0.0874	Y
Gene Set 676 : REACTOME HEPARAN SULFATE HEPARIN HS GAG METABOLISM	ES = -0.521 NES = -1.53 Nom. p-val= 0.0259 FWER= 0.993 FDR= 0.0928	
Gene Set 990 : REACTOME HIV INFECTION	ES = -0.403 NES = -2.24 Nom. p-val= 0.00577 FWER= 0.014 FDR= 0.0156	
Gene Set 994 : REACTOME HOST INTERACTIONS OF HIV FACTORS	ES = -0.477 NES = -2.26 Nom. p-val= 0.00192 FWER= 0.011 FDR= 0.021	
Gene Set 674 : REACTOME HS_GAG BIOSYNTHESIS	ES = -0.532 NES = -1.42 Nom. p-val= 0.0527 FWER= 1 FDR= 0.138	
Gene Set 651 : REACTOME HS_GAG DEGRADATION	ES = -0.57 NES = -1.56 Nom. p-val= 0.0207 FWER= 0.99 FDR= 0.0888	
Gene Set 971 : REACTOME IL_2 SIGNALING	ES = -0.64 NES = -1.68 Nom. p-val= 0.00789 FWER= 0.877 FDR= 0.0756	
Gene Set 926 : REACTOME_IL_3_5_AND_GM-CSF_SIGNALING	ES = -0.624 NES = -1.56 Nom. p-val= 0.0299 FWER= 0.989 FDR= 0.0886	
Gene Set 931 : REACTOME_IL_RECEPTOR_SHC_SIGNALING	ES = -0.689 NES = -1.57 Nom. p-val= 0.0159 FWER= 0.987 FDR= 0.0859	
Gene Set 920 : REACTOME IL1 SIGNALING	ES = -0.475 NES = -1.47 Nom. p-val= 0.0866 FWER= 0.999 FDR= 0.114	
REACTOME IMMUNOREGULATORY_INTERACTIONS_BETWEEN_A_LYMPHOID_AND_A_NON_LYMPHOID_CELL	ES = -0.756 NES = -1.54 Nom. p-val= 0.0132 FWER= 0.991 FDR= 0.0909	
Gene Set 1036 : REACTOME INFLAMMASOMES	ES = -0.807 NES = -1.6 Nom. p-val= 0 FWER= 0.967 FDR= 0.0763	
REACTOME INHIBITION OF INSULIN SECRETION BY ADRENALINE NORADRENALINE	ES = -0.587 NES = -1.49 Nom. p-val= 0.0329 FWER= 0.998 FDR= 0.108	
REACTOME INHIBITION OF VOLTAGE GATED CA2 CHANNELS VIA GBETA GAMMA SUBUNITS	ES = -0.592 NES = -1.44 Nom. p-val= 0.0418 FWER= 0.999 FDR= 0.128	
Gene Set 1007 : REACTOME INNATE IMMUNE SYSTEM	ES = -0.587 NES = -1.91 Nom. p-val= 0 FWER= 0.334 FDR= 0.106	Y
Gene Set 638 : REACTOME_INSULIN_RECEPTOR_SIGNALLING_CASCADE	ES = -0.406 NES = -1.47 Nom. p-val= 0.0478 FWER= 0.999 FDR= 0.116	
Gene Set 737 : REACTOME INTEGRATION OF ENERGY METABOLISM	ES = -0.416 NES = -1.48 Nom. p-val= 0.0136 FWER= 0.998 FDR= 0.112	
Gene Set 764 : REACTOME INTEGRIN ALPHAIIIB BETA3 SIGNALING	ES = -0.607 NES = -1.56 Nom. p-val= 0.028 FWER= 0.989 FDR= 0.0872	
Gene Set 713 : REACTOME INTEGRIN_CELL_SURFACE_INTERACTIONS	ES = -0.676 NES = -1.74 Nom. p-val= 0 FWER= 0.755 FDR= 0.0734	
Gene Set 910 : REACTOME INTERACTION BETWEEN L1 AND ANKYRINS	ES = -0.646 NES = -1.44 Nom. p-val= 0.0373 FWER= 0.999 FDR= 0.127	
Gene Set 954 : REACTOME INTERFERON ALPHA BETA SIGNALING	ES = -0.621 NES = -1.61 Nom. p-val= 0.022 FWER= 0.964 FDR= 0.0757	
Gene Set 952 : REACTOME INTERFERON GAMMA SIGNALING	ES = -0.681 NES = -1.62 Nom. p-val= 0.00766 FWER= 0.954 FDR= 0.0766	
Gene Set 959 : REACTOME INTERFERON SIGNALING	ES = -0.577 NES = -1.82 Nom. p-val= 0.002 FWER= 0.55 FDR= 0.0765	
Gene Set 1059 : REACTOME_INTRINSIC_PATHWAY_FOR_APOPTOSIS	ES = -0.386 NES = -1.39 Nom. p-val= 0.132 FWER= 1 FDR= 0.153	

Gene Set 975 : REACTOME_INTRINSIC_PATHWAY	ES = -0.618 NES = -1.39 Nom. p-val= 0.0838 FWER= 1 FDR= 0.151	
Gene Set 1039 : REACTOME_INWARDLY_RECTIFYING_K_CHANNELS	ES = -0.591 NES = -1.47 Nom. p-val= 0.0251 FWER= 0.999 FDR= 0.114	
Gene Set 953 : REACTOME_ION_TRANSPORT_BY_P_TYPE_ATPASES	ES = -0.483 NES = -1.33 Nom. p-val= 0.0884 FWER= 1 FDR= 0.19	
Gene Set 950 : REACTOME_IRON_UPTAKE_AND_TRANSPORT	ES = -0.535 NES = -1.56 Nom. p-val= 0.0314 FWER= 0.989 FDR= 0.0865	
REACTOME_JNK_C_JUN_KINASES_PHOSPHORYLATION_AND_ACTIVATION_MEDIATED_BY_ACTIVATED_HUMAN_TAK1	ES = -0.451 NES = -1.29 Nom. p-val= 0.203 FWER= 1 FDR= 0.212	
Gene Set 668 : REACTOME_KERATAN_SULFATE_BIOSYNTHESIS	ES = -0.673 NES = -1.64 Nom. p-val= 0.00379 FWER= 0.941 FDR= 0.0748	
Gene Set 675 : REACTOME_KERATAN_SULFATE_KERATIN_METABOLISM	ES = -0.659 NES = -1.69 Nom. p-val= 0.00376 FWER= 0.862 FDR= 0.0746	
Gene Set 906 : REACTOME_L1CAM_INTERACTIONS	ES = -0.609 NES = -1.83 Nom. p-val= 0 FWER= 0.542 FDR= 0.0803	Y
REACTOME_LATENT_INFECTION_OF_HOMO_SAPIENS_WITH_MYCOBACTERIUM_TUBERCULOSIS	ES = -0.611 NES = -1.51 Nom. p-val= 0.0422 FWER= 0.996 FDR= 0.103	
Gene Set 985 : REACTOME_LIPID_DIGESTION_MOBILIZATION_AND_TRANSPORT	ES = -0.591 NES = -1.49 Nom. p-val= 0.03 FWER= 0.998 FDR= 0.109	
Gene Set 1012 : REACTOME_LIPOPROTEIN_METABOLISM	ES = -0.624 NES = -1.42 Nom. p-val= 0.0649 FWER= 1 FDR= 0.136	
Gene Set 890 : REACTOME_MAPK_TARGETS_NUCLEAR_EVENTS_MEDIATED_BY_MAP_KINASES	ES = -0.433 NES = -1.43 Nom. p-val= 0.119 FWER= 1 FDR= 0.133	
Gene Set 589 : REACTOME_MEMBRANE_TRAFFICKING	ES = -0.258 NES = -1.32 Nom. p-val= 0.145 FWER= 1 FDR= 0.196	
Gene Set 707 : REACTOME_METABOLISM_OF_AMINO_ACIDS_AND_DERIVATIVES	ES = -0.351 NES = -1.35 Nom. p-val= 0.0543 FWER= 1 FDR= 0.178	
Gene Set 980 : REACTOME_METABOLISM_OF_CARBOHYDRATES	ES = -0.49 NES = -1.87 Nom. p-val= 0 FWER= 0.412 FDR= 0.0843	Y
Gene Set 909 : REACTOME_METABOLISM_OF_LIPIDS_AND_LIPOPROTEINS	ES = -0.411 NES = -1.73 Nom. p-val= 0 FWER= 0.759 FDR= 0.0735	
Gene Set 784 : REACTOME_METABOLISM_OF_NUCLEOTIDES	ES = -0.41 NES = -1.62 Nom. p-val= 0.00768 FWER= 0.958 FDR= 0.0763	
Gene Set 786 : REACTOME_METABOLISM_OF_PROTEINS	ES = -0.257 NES = -1.3 Nom. p-val= 0.17 FWER= 1 FDR= 0.212	
Gene Set 568 : REACTOME_METABOLISM_OF_STEROID_HORMONES_AND_VITAMINS_A_AND_D	ES = -0.523 NES = -1.31 Nom. p-val= 0.0961 FWER= 1 FDR= 0.204	
Gene Set 862 : REACTOME_METAL_ION_SLIC_TRANSPORTERS	ES = -0.455 NES = -1.24 Nom. p-val= 0.186 FWER= 1 FDR= 0.247	
Gene Set 682 : REACTOME_MHC_CLASS_II_ANTIGEN_PRESENTATION	ES = -0.538 NES = -1.77 Nom. p-val= 0.0119 FWER= 0.678 FDR= 0.076	
Gene Set 788 : REACTOME_MUSCLE_CONTRACTION	ES = -0.726 NES = -1.45 Nom. p-val= 0.071 FWER= 0.999 FDR= 0.121	
Gene Set 1006 : REACTOME_MYD88_MAL_CASCADE_INITIATED_ON_PLASMA_MEMBRANE	ES = -0.466 NES = -1.66 Nom. p-val= 0.0137 FWER= 0.913 FDR= 0.0735	
Gene Set 886 : REACTOME_MYOGENESIS	ES = -0.583 NES = -1.45 Nom. p-val= 0.0981 FWER= 0.999 FDR= 0.124	
Gene Set 855 : REACTOME_NA_CL_DEPENDENT_NEUROTRANSMITTER_TRANSPORTERS	ES = -0.595 NES = -1.34 Nom. p-val= 0.0848 FWER= 1 FDR= 0.184	
Gene Set 806 : REACTOME_NCAM_SIGNALING_FOR_NEURITE_OUT_GROWTH	ES = -0.631 NES = -1.77 Nom. p-val= 0 FWER= 0.69 FDR= 0.0718	
Gene Set 804 : REACTOME_NCAM1_INTERACTIONS	ES = -0.686 NES = -1.62 Nom. p-val= 0.00195 FWER= 0.954 FDR= 0.0764	
NEF_MEDIATES_DOWN_MODULATION_OF_CELL_SURFACE_RECEPTORS_BY_RECRUITING_THEM_TO_CLATHRIN_ADAPTERS	ES = -0.603 NES = -1.68 Nom. p-val= 0.0187 FWER= 0.883 FDR= 0.0754	
Gene Set 586 : REACTOME_NEGATIVE_REGULATION_OF_FGFR_SIGNALING	ES = -0.605 NES = -1.55 Nom. p-val= 0.0155 FWER= 0.99 FDR= 0.0896	
Gene Set 960 : REACTOME_NEGATIVE_REGULATORS_OF_RIG_I_MDA5_SIGNALING	ES = -0.466 NES = -1.52 Nom. p-val= 0.095 FWER= 0.996 FDR= 0.101	
Gene Set 925 : REACTOME_NEPHRIN_INTERACTIONS	ES = -0.555 NES = -1.44 Nom. p-val= 0.0867 FWER= 0.999 FDR= 0.127	
Gene Set 908 : REACTOME_NETRIN1_SIGNALING	ES = -0.697 NES = -1.77 Nom. p-val= 0 FWER= 0.688 FDR= 0.0726	
Gene Set 720 : REACTOME_NEURONAL_SYSTEM	ES = -0.542 NES = -1.57 Nom. p-val= 0.00373 FWER= 0.986 FDR= 0.086	
NEUROTRANSMITTER_RECEPTOR_BINDING_AND_DOWNSTREAM_TRANSMISSION_IN_THE_POSTSYNAPTIC_CELL	ES = -0.555 NES = -1.58 Nom. p-val= 0.0038 FWER= 0.983 FDR= 0.0809	
Gene Set 725 : REACTOME_NEUROTRANSMITTER_RELEASE_CYCLE	ES = -0.519 NES = -1.31 Nom. p-val= 0.11 FWER= 1 FDR= 0.2	
REACTOME_NFKB_AND_MAP_KINASES_ACTIVATION_MEDIATED_BY_TLR4_SIGNALING_REPERTOIRE	ES = -0.45 NES = -1.68 Nom. p-val= 0.0117 FWER= 0.889 FDR= 0.074	
Gene Set 644 : REACTOME_NGF_SIGNALING_VIA_TRKA_FROM_THE_PLASMA_MEMBRANE	ES = -0.425 NES = -1.83 Nom. p-val= 0 FWER= 0.531 FDR= 0.0827	Y
Gene Set 927 : REACTOME_NITRIC_OXIDE_STIMULATES_GUANYLATE_CYCLASE	ES = -0.566 NES = -1.32 Nom. p-val= 0.117 FWER= 1 FDR= 0.198	
Gene Set 1028 : REACTOME_NOD1_2_SIGNALING_PATHWAY	ES = -0.45 NES = -1.33 Nom. p-val= 0.167 FWER= 1 FDR= 0.191	
Gene Set 633 : REACTOME_NOTCH1_INTRACELLULAR_DOMAIN_REGULATES_TRANSCRIPTION	ES = -0.416 NES = -1.68 Nom. p-val= 0.0204 FWER= 0.895 FDR= 0.0718	
Gene Set 717 : REACTOME_NRAGE_SIGNALS_DEATH_THROUGH_JNK	ES = -0.637 NES = -1.72 Nom. p-val= 0.00382 FWER= 0.789 FDR= 0.0731	
REACTOME_NUCLEAR_EVENTS_KINASE_AND_TRANSCRIPTION_FACTOR_ACTIVATION	ES = -0.457 NES = -1.54 Nom. p-val= 0.0786 FWER= 0.993 FDR= 0.0929	
Gene Set 765 : REACTOME_NUCLEAR_RECEPTOR_TRANSCRIPTION_PATHWAY	ES = -0.577 NES = -1.59 Nom. p-val= 0.00978 FWER= 0.976 FDR= 0.0791	
Gene Set 616 : REACTOME_NUCLEAR_SIGNALING_BY_ERBB4	ES = -0.545 NES = -1.48 Nom. p-val= 0.0366 FWER= 0.999 FDR= 0.113	
NUCLEOTIDE_BINDING_DOMAIN_LEUCINE_RICH_REPEAT_CONTAINING_RECEPTOR_NLR_SIGNALING_PATHWAYS	ES = -0.61 NES = -1.64 Nom. p-val= 0.00783 FWER= 0.94 FDR= 0.0745	
Gene Set 808 : REACTOME_NUCLEOTIDE_LIKE_PURINERGIC_RECEPTORS	ES = -0.814 NES = -1.59 Nom. p-val= 0 FWER= 0.976 FDR= 0.0791	
Gene Set 601 : REACTOME_O_LINKED_GLYCOSYLATION_OF_MUCINS	ES = -0.509 NES = -1.31 Nom. p-val= 0.141 FWER= 1 FDR= 0.206	
Gene Set 740 : REACTOME_OPIOID_SIGNALING	ES = -0.558 NES = -1.77 Nom. p-val= 0 FWER= 0.678 FDR= 0.0748	
Gene Set 829 : REACTOME_OTHER_SEMAPHORIN_INTERACTIONS	ES = -0.736 NES = -1.62 Nom. p-val= 0.00194 FWER= 0.957 FDR= 0.0765	
REACTOME_OXYGEN_DEPENDENT_PROLINE_HYDROXYLATION_OF_HYPOXIA_INDUCIBLE_FACTOR_ALPHA	ES = -0.578 NES = -1.83 Nom. p-val= 0.00947 FWER= 0.529 FDR= 0.0839	
Gene Set 726 : REACTOME_P75_NTR_RECEPTOR_MEDIATED_SIGNALING	ES = -0.517 NES = -1.82 Nom. p-val= 0.00194 FWER= 0.56 FDR= 0.0736	
Gene Set 751 : REACTOME_P130CAS_LINKAGE_TO_MAPK_SIGNALING_FOR_INTEGRINS	ES = -0.643 NES = -1.41 Nom. p-val= 0.101 FWER= 1 FDR= 0.144	
Gene Set 838 : REACTOME_PD1_SIGNALING	ES = -0.843 NES = -1.47 Nom. p-val= 0.0152 FWER= 0.999 FDR= 0.116	
Gene Set 734 : REACTOME_PEPTIDE_LIGAND_BINDING_RECEPTORS	ES = -0.626 NES = -1.59 Nom. p-val= 0 FWER= 0.976 FDR= 0.0787	
Gene Set 781 : REACTOME_PEROXISOMAL_LIPID_METABOLISM	ES = -0.482 NES = -1.5 Nom. p-val= 0.0786 FWER= 0.996 FDR= 0.106	
Gene Set 1022 : REACTOME_PHASE_II_CONJUGATION	ES = -0.504 NES = -1.42 Nom. p-val= 0.0564 FWER= 1 FDR= 0.139	

Gene Set 722 : REACTOME PHASE1 FUNCTIONALIZATION OF COMPOUNDS	ES = -0.564 NES = -1.42 Nom. p-val= 0.0466 FWER= 1 FDR= 0.134	
Gene Set 888 : REACTOME PHOSPHOLIPASE C MEDIATED CASCADE	ES = -0.602 NES = -1.6 Nom. p-val= 0.00951 FWER= 0.971 FDR= 0.0781	
Gene Set 659 : REACTOME PHOSPHOLIPID METABOLISM	ES = -0.401 NES = -1.65 Nom. p-val= 0.00194 FWER= 0.927 FDR= 0.0734	
Gene Set 699 : REACTOME PHOSPHORYLATION OF CD3 AND TCR ZETA CHAINS	ES = -0.826 NES = -1.45 Nom. p-val= 0.0265 FWER= 0.999 FDR= 0.124	
Gene Set 881 : REACTOME PI_3K CASCADE	ES = -0.505 NES = -1.55 Nom. p-val= 0.0215 FWER= 0.99 FDR= 0.0895	
Gene Set 670 : REACTOME PI METABOLISM	ES = -0.431 NES = -1.45 Nom. p-val= 0.0824 FWER= 0.999 FDR= 0.121	
Gene Set 689 : REACTOME PI3K AKT ACTIVATION	ES = -0.345 NES = -1.36 Nom. p-val= 0.157 FWER= 1 FDR= 0.167	
Gene Set 1060 : REACTOME PI3K CASCADE	ES = -0.438 NES = -1.45 Nom. p-val= 0.0494 FWER= 0.999 FDR= 0.124	
Gene Set 761 : REACTOME PKA MEDIATED PHOSPHORYLATION OF CREB	ES = -0.595 NES = -1.47 Nom. p-val= 0.0574 FWER= 0.999 FDR= 0.115	
Gene Set 1043 : REACTOME PLATELET ACTIVATION SIGNALING AND AGGREGATION	ES = -0.598 NES = -1.83 Nom. p-val= 0 FWER= 0.537 FDR= 0.0825	Y
Gene Set 972 : REACTOME PLATELET AGGREGATION PLUG FORMATION	ES = -0.591 NES = -1.54 Nom. p-val= 0.0208 FWER= 0.991 FDR= 0.0907	
Gene Set 933 : REACTOME PLATELET CALCIUM HOMEOSTASIS	ES = -0.637 NES = -1.39 Nom. p-val= 0.0806 FWER= 1 FDR= 0.152	
Gene Set 928 : REACTOME PLATELET HOMEOSTASIS	ES = -0.584 NES = -1.67 Nom. p-val= 0 FWER= 0.909 FDR= 0.0737	
Gene Set 929 : REACTOME PLATELET SENSITIZATION BY LDL	ES = -0.636 NES = -1.78 Nom. p-val= 0.00197 FWER= 0.67 FDR= 0.0746	
Gene Set 752 : REACTOME PLC BETA MEDIATED EVENTS	ES = -0.588 NES = -1.65 Nom. p-val= 0.00965 FWER= 0.924 FDR= 0.0724	
Gene Set 867 : REACTOME POST NMDA RECEPTOR ACTIVATION EVENTS	ES = -0.516 NES = -1.46 Nom. p-val= 0.0322 FWER= 0.999 FDR= 0.119	
REACTOME POST TRANSLATIONAL MODIFICATION SYNTHESIS OF GPI ANCHORED PROTEINS	ES = -0.336 NES = -1.34 Nom. p-val= 0.123 FWER= 1 FDR= 0.18	
Gene Set 903 : REACTOME POST TRANSLATIONAL PROTEIN MODIFICATION	ES = -0.371 NES = -1.38 Nom. p-val= 0.0812 FWER= 1 FDR= 0.157	
Gene Set 1037 : REACTOME POTASSIUM CHANNELS	ES = -0.573 NES = -1.5 Nom. p-val= 0.00763 FWER= 0.996 FDR= 0.105	
Gene Set 618 : REACTOME PPARA ACTIVATES GENE EXPRESSION	ES = -0.446 NES = -1.68 Nom. p-val= 0.00395 FWER= 0.892 FDR= 0.0726	
Gene Set 630 : REACTOME PRE NOTCH EXPRESSION AND PROCESSING	ES = -0.346 NES = -1.3 Nom. p-val= 0.156 FWER= 1 FDR= 0.209	
Gene Set 620 : REACTOME PRE NOTCH TRANSCRIPTION AND TRANSLATION	ES = -0.404 NES = -1.27 Nom. p-val= 0.241 FWER= 1 FDR= 0.232	
Gene Set 640 : REACTOME PROLONGED ERK ACTIVATION EVENTS	ES = -0.599 NES = -1.79 Nom. p-val= 0.00811 FWER= 0.648 FDR= 0.0776	
Gene Set 934 : REACTOME PROSTACYCLIN SIGNALLING THROUGH PROSTACYCLIN RECEPTOR	ES = -0.687 NES = -1.57 Nom. p-val= 0.0135 FWER= 0.988 FDR= 0.0861	
Gene Set 596 : REACTOME PROTEOLYTIC CLEAVAGE OF SNARE COMPLEX PROTEINS	ES = -0.686 NES = -1.68 Nom. p-val= 0.00577 FWER= 0.892 FDR= 0.0723	
REACTOME PTM GAMMA CARBOXYLATION HYPUSINE FORMATION AND ARYLSULFATASE ACTIVATION	ES = -0.493 NES = -1.3 Nom. p-val= 0.125 FWER= 1 FDR= 0.208	
Gene Set 982 : REACTOME PURINE METABOLISM	ES = -0.474 NES = -1.67 Nom. p-val= 0.0184 FWER= 0.906 FDR= 0.073	
Gene Set 1058 : REACTOME PYRIMIDINE METABOLISM	ES = -0.62 NES = -1.61 Nom. p-val= 0.00759 FWER= 0.963 FDR= 0.0756	
Gene Set 932 : REACTOME RAP1 SIGNALLING	ES = -0.514 NES = -1.27 Nom. p-val= 0.2 FWER= 1 FDR= 0.226	
Gene Set 861 : REACTOME RAS ACTIVATION UOPN CA2 INFUX THROUGH NMDA RECEPTOR	ES = -0.66 NES = -1.5 Nom. p-val= 0.0398 FWER= 0.996 FDR= 0.106	
Gene Set 915 : REACTOME RECYCLING PATHWAY OF L1	ES = -0.544 NES = -1.68 Nom. p-val= 0.00615 FWER= 0.889 FDR= 0.0737	
Gene Set 718 : REACTOME REGULATION OF APOPTOSIS	ES = -0.334 NES = -1.34 Nom. p-val= 0.182 FWER= 1 FDR= 0.184	
REACTOME REGULATION OF GLUCOKINASE BY GLUCOKINASE REGULATORY PROTEIN	ES = -0.361 NES = -1.28 Nom. p-val= 0.191 FWER= 1 FDR= 0.225	
Gene Set 654 : REACTOME REGULATION OF HYPOXIA INDUCIBLE FACTOR HIF BY OXYGEN	ES = -0.45 NES = -1.52 Nom. p-val= 0.0558 FWER= 0.994 FDR= 0.0976	
REACTOME REGULATION OF INSULIN LIKE GROWTH FACTOR IGF ACTIVITY BY INSULIN LIKE GROWTH FACTOR BINDING PROTEINS_IGFBPS	ES = -0.684 NES = -1.53 Nom. p-val= 0.0153 FWER= 0.993 FDR= 0.0952	
: REACTOME REGULATION OF INSULIN SECRETION BY GLUCAGON LIKE PEPTIDE1	ES = -0.509 NES = -1.52 Nom. p-val= 0.0101 FWER= 0.995 FDR= 0.0999	
Gene Set 805 : REACTOME REGULATION OF INSULIN SECRETION	ES = -0.44 NES = -1.45 Nom. p-val= 0.014 FWER= 0.999 FDR= 0.122	
Gene Set 588 : REACTOME REGULATION OF KIT SIGNALING	ES = -0.667 NES = -1.59 Nom. p-val= 0.0134 FWER= 0.976 FDR= 0.0792	
Gene Set 923 : REACTOME REGULATION OF SIGNALING BY CBL	ES = -0.588 NES = -1.39 Nom. p-val= 0.107 FWER= 1 FDR= 0.151	
Gene Set 938 : REACTOME REGULATION OF WATER BALANCE BY RENAL AQUAPORINS	ES = -0.598 NES = -1.7 Nom. p-val= 0.00188 FWER= 0.841 FDR= 0.0746	
Gene Set 705 : REACTOME RESPONSE TO ELEVATED PLATELET CYTOSOLIC CA2	ES = -0.623 NES = -1.75 Nom. p-val= 0 FWER= 0.721 FDR= 0.0726	
: REACTOME RIG I MDA5 MEDIATED INDUCTION OF IFN ALPHA BETA PATHWAYS	ES = -0.423 NES = -1.62 Nom. p-val= 0.0296 FWER= 0.955 FDR= 0.0765	
Gene Set 619 : REACTOME RIP MEDIATED NFKB ACTIVATION VIA DAI	ES = -0.701 NES = -1.57 Nom. p-val= 0.0152 FWER= 0.987 FDR= 0.0857	
Gene Set 627 : REACTOME RORA ACTIVATES CIRCADIAN EXPRESSION	ES = -0.442 NES = -1.25 Nom. p-val= 0.26 FWER= 1 FDR= 0.241	
Gene Set 831 : REACTOME SEMA4D IN SEMAPHORIN SIGNALING	ES = -0.574 NES = -1.65 Nom. p-val= 0.0118 FWER= 0.924 FDR= 0.0726	
: REACTOME SEMA4D INDUCED CELL MIGRATION AND GROWTH CONE COLLAPSE	ES = -0.51 NES = -1.67 Nom. p-val= 0.0359 FWER= 0.896 FDR= 0.072	
Gene Set 832 : REACTOME SEMAPHORIN INTERACTIONS	ES = -0.577 NES = -1.76 Nom. p-val= 0.00193 FWER= 0.709 FDR= 0.0728	
Gene Set 895 : REACTOME SHC MEDIATED CASCADE	ES = -0.622 NES = -1.46 Nom. p-val= 0.0273 FWER= 0.999 FDR= 0.117	
Gene Set 858 : REACTOME SIGNAL AMPLIFICATION	ES = -0.575 NES = -1.59 Nom. p-val= 0.0113 FWER= 0.979 FDR= 0.0798	
Gene Set 911 : REACTOME SIGNAL TRANSDUCTION BY L1	ES = -0.54 NES = -1.69 Nom. p-val= 0.012 FWER= 0.867 FDR= 0.0757	
Gene Set 642 : REACTOME SIGNALING BY BMP	ES = -0.51 NES = -1.39 Nom. p-val= 0.102 FWER= 1 FDR= 0.151	
Gene Set 610 : REACTOME SIGNALING BY EGFR IN CANCER	ES = -0.393 NES = -1.74 Nom. p-val= 0.00594 FWER= 0.748 FDR= 0.0736	
Gene Set 604 : REACTOME SIGNALING BY ERBB2	ES = -0.386 NES = -1.54 Nom. p-val= 0.0394 FWER= 0.993 FDR= 0.0931	
Gene Set 599 : REACTOME SIGNALING BY ERBB4	ES = -0.382 NES = -1.46 Nom. p-val= 0.0717 FWER= 0.999 FDR= 0.118	
Gene Set 650 : REACTOME SIGNALING BY FGFR IN DISEASE	ES = -0.471 NES = -1.79 Nom. p-val= 0 FWER= 0.625 FDR= 0.0793	Y
Gene Set 681 : REACTOME SIGNALING_BY_FGFR_MUTANTS	ES = -0.53 NES = -1.5 Nom. p-val= 0.0305 FWER= 0.998 FDR= 0.108	

Gene Set 722 : REACTOME PHASE1 FUNCTIONALIZATION OF COMPOUNDS	ES = -0.564 NES = -1.42 Nom. p-val= 0.0466 FWER= 1 FDR= 0.134	
Gene Set 888 : REACTOME PHOSPHOLIPASE C MEDIATED CASCADE	ES = -0.602 NES = -1.6 Nom. p-val= 0.00951 FWER= 0.971 FDR= 0.0781	
Gene Set 659 : REACTOME PHOSPHOLIPID METABOLISM	ES = -0.401 NES = -1.65 Nom. p-val= 0.00194 FWER= 0.927 FDR= 0.0734	
Gene Set 699 : REACTOME PHOSPHORYLATION OF CD3 AND TCR ZETA CHAINS	ES = -0.826 NES = -1.45 Nom. p-val= 0.0265 FWER= 0.999 FDR= 0.124	
Gene Set 881 : REACTOME PI_3K CASCADE	ES = -0.505 NES = -1.55 Nom. p-val= 0.0215 FWER= 0.99 FDR= 0.0895	
Gene Set 670 : REACTOME PI METABOLISM	ES = -0.431 NES = -1.45 Nom. p-val= 0.0824 FWER= 0.999 FDR= 0.121	
Gene Set 689 : REACTOME PI3K AKT ACTIVATION	ES = -0.345 NES = -1.36 Nom. p-val= 0.157 FWER= 1 FDR= 0.167	
Gene Set 1060 : REACTOME PI3K CASCADE	ES = -0.438 NES = -1.45 Nom. p-val= 0.0494 FWER= 0.999 FDR= 0.124	
Gene Set 761 : REACTOME PKA MEDIATED PHOSPHORYLATION OF CREB	ES = -0.595 NES = -1.47 Nom. p-val= 0.0574 FWER= 0.999 FDR= 0.115	
Gene Set 1043 : REACTOME PLATELET ACTIVATION SIGNALING AND AGGREGATION	ES = -0.598 NES = -1.83 Nom. p-val= 0 FWER= 0.537 FDR= 0.0825	Y
Gene Set 972 : REACTOME PLATELET AGGREGATION PLUG FORMATION	ES = -0.591 NES = -1.54 Nom. p-val= 0.0208 FWER= 0.991 FDR= 0.0907	
Gene Set 933 : REACTOME PLATELET CALCIUM HOMEOSTASIS	ES = -0.637 NES = -1.39 Nom. p-val= 0.0806 FWER= 1 FDR= 0.152	
Gene Set 928 : REACTOME PLATELET HOMEOSTASIS	ES = -0.584 NES = -1.67 Nom. p-val= 0 FWER= 0.909 FDR= 0.0737	
Gene Set 929 : REACTOME PLATELET SENSITIZATION BY LDL	ES = -0.636 NES = -1.78 Nom. p-val= 0.00197 FWER= 0.67 FDR= 0.0746	
Gene Set 752 : REACTOME PLC BETA MEDIATED EVENTS	ES = -0.588 NES = -1.65 Nom. p-val= 0.00965 FWER= 0.924 FDR= 0.0724	
Gene Set 867 : REACTOME POST NMDA RECEPTOR ACTIVATION EVENTS	ES = -0.516 NES = -1.46 Nom. p-val= 0.0322 FWER= 0.999 FDR= 0.119	
REACTOME POST TRANSLATIONAL MODIFICATION SYNTHESIS OF GPI ANCHORED PROTEINS	ES = -0.336 NES = -1.34 Nom. p-val= 0.123 FWER= 1 FDR= 0.18	
Gene Set 903 : REACTOME POST TRANSLATIONAL PROTEIN MODIFICATION	ES = -0.371 NES = -1.38 Nom. p-val= 0.0812 FWER= 1 FDR= 0.157	
Gene Set 1037 : REACTOME POTASSIUM CHANNELS	ES = -0.573 NES = -1.5 Nom. p-val= 0.00763 FWER= 0.996 FDR= 0.105	
Gene Set 618 : REACTOME PPARA ACTIVATES GENE EXPRESSION	ES = -0.446 NES = -1.68 Nom. p-val= 0.00395 FWER= 0.892 FDR= 0.0726	
Gene Set 630 : REACTOME PRE NOTCH EXPRESSION AND PROCESSING	ES = -0.346 NES = -1.3 Nom. p-val= 0.156 FWER= 1 FDR= 0.209	
Gene Set 620 : REACTOME PRE NOTCH TRANSCRIPTION AND TRANSLATION	ES = -0.404 NES = -1.27 Nom. p-val= 0.241 FWER= 1 FDR= 0.232	
Gene Set 640 : REACTOME PROLONGED ERK ACTIVATION EVENTS	ES = -0.599 NES = -1.79 Nom. p-val= 0.00811 FWER= 0.648 FDR= 0.0776	
Gene Set 934 : REACTOME PROSTACYCLIN SIGNALLING THROUGH PROSTACYCLIN RECEPTOR	ES = -0.687 NES = -1.57 Nom. p-val= 0.0135 FWER= 0.988 FDR= 0.0861	
Gene Set 596 : REACTOME PROTEOLYTIC CLEAVAGE OF SNARE COMPLEX PROTEINS	ES = -0.686 NES = -1.68 Nom. p-val= 0.00577 FWER= 0.892 FDR= 0.0723	
REACTOME PTM GAMMA CARBOXYLATION HYPUSINE FORMATION AND ARYLSULFATASE ACTIVATION	ES = -0.493 NES = -1.3 Nom. p-val= 0.125 FWER= 1 FDR= 0.208	
Gene Set 982 : REACTOME PURINE METABOLISM	ES = -0.474 NES = -1.67 Nom. p-val= 0.0184 FWER= 0.906 FDR= 0.073	
Gene Set 1058 : REACTOME PYRIMIDINE METABOLISM	ES = -0.62 NES = -1.61 Nom. p-val= 0.00759 FWER= 0.963 FDR= 0.0756	
Gene Set 932 : REACTOME RAP1 SIGNALLING	ES = -0.514 NES = -1.27 Nom. p-val= 0.2 FWER= 1 FDR= 0.226	
Gene Set 861 : REACTOME RAS ACTIVATION UOPN CA2 INFUX THROUGH NMDA RECEPTOR	ES = -0.66 NES = -1.5 Nom. p-val= 0.0398 FWER= 0.996 FDR= 0.106	
Gene Set 915 : REACTOME RECYCLING PATHWAY OF L1	ES = -0.544 NES = -1.68 Nom. p-val= 0.00615 FWER= 0.889 FDR= 0.0737	
Gene Set 718 : REACTOME REGULATION OF APOPTOSIS	ES = -0.334 NES = -1.34 Nom. p-val= 0.182 FWER= 1 FDR= 0.184	
REACTOME REGULATION OF GLUCOKINASE BY GLUCOKINASE REGULATORY PROTEIN	ES = -0.361 NES = -1.28 Nom. p-val= 0.191 FWER= 1 FDR= 0.225	
Gene Set 654 : REACTOME REGULATION OF HYPOXIA INDUCIBLE FACTOR HIF BY OXYGEN	ES = -0.45 NES = -1.52 Nom. p-val= 0.0558 FWER= 0.994 FDR= 0.0976	
REACTOME REGULATION OF INSULIN LIKE GROWTH FACTOR IGF ACTIVITY BY INSULIN LIKE GROWTH FACTOR BINDING PROTEINS IGFBPS	ES = -0.684 NES = -1.53 Nom. p-val= 0.0153 FWER= 0.993 FDR= 0.0952	
: REACTOME REGULATION OF INSULIN SECRETION BY GLUCAGON LIKE PEPTIDE1	ES = -0.509 NES = -1.52 Nom. p-val= 0.0101 FWER= 0.995 FDR= 0.0999	
Gene Set 805 : REACTOME REGULATION OF INSULIN SECRETION	ES = -0.44 NES = -1.45 Nom. p-val= 0.014 FWER= 0.999 FDR= 0.122	
Gene Set 588 : REACTOME REGULATION OF KIT SIGNALING	ES = -0.667 NES = -1.59 Nom. p-val= 0.0134 FWER= 0.976 FDR= 0.0792	
Gene Set 923 : REACTOME REGULATION OF SIGNALING BY CBL	ES = -0.588 NES = -1.39 Nom. p-val= 0.107 FWER= 1 FDR= 0.151	
Gene Set 938 : REACTOME REGULATION OF WATER BALANCE BY RENAL AQUAPORINS	ES = -0.598 NES = -1.7 Nom. p-val= 0.00188 FWER= 0.841 FDR= 0.0746	
Gene Set 705 : REACTOME RESPONSE TO ELEVATED PLATELET CYTOSOLIC CA2	ES = -0.623 NES = -1.75 Nom. p-val= 0 FWER= 0.721 FDR= 0.0726	
: REACTOME RIG I MDA5 MEDIATED INDUCTION OF IFN ALPHA BETA PATHWAYS	ES = -0.423 NES = -1.62 Nom. p-val= 0.0296 FWER= 0.955 FDR= 0.0765	
Gene Set 619 : REACTOME RIP MEDIATED NFKB ACTIVATION VIA DAI	ES = -0.701 NES = -1.57 Nom. p-val= 0.0152 FWER= 0.987 FDR= 0.0857	
Gene Set 627 : REACTOME RORA ACTIVATES CIRCADIAN EXPRESSION	ES = -0.442 NES = -1.25 Nom. p-val= 0.26 FWER= 1 FDR= 0.241	
Gene Set 831 : REACTOME SEMA4D IN SEMAPHORIN SIGNALING	ES = -0.574 NES = -1.65 Nom. p-val= 0.0118 FWER= 0.924 FDR= 0.0726	
: REACTOME SEMA4D INDUCED CELL MIGRATION AND GROWTH CONE COLLAPSE	ES = -0.51 NES = -1.67 Nom. p-val= 0.0359 FWER= 0.896 FDR= 0.072	
Gene Set 832 : REACTOME SEMAPHORIN INTERACTIONS	ES = -0.577 NES = -1.76 Nom. p-val= 0.00193 FWER= 0.709 FDR= 0.0728	
Gene Set 895 : REACTOME SHC MEDIATED CASCADE	ES = -0.622 NES = -1.46 Nom. p-val= 0.0273 FWER= 0.999 FDR= 0.117	
Gene Set 858 : REACTOME SIGNAL AMPLIFICATION	ES = -0.575 NES = -1.59 Nom. p-val= 0.0113 FWER= 0.979 FDR= 0.0798	
Gene Set 911 : REACTOME SIGNAL TRANSDUCTION BY L1	ES = -0.54 NES = -1.69 Nom. p-val= 0.012 FWER= 0.867 FDR= 0.0757	
Gene Set 642 : REACTOME SIGNALING BY BMP	ES = -0.51 NES = -1.39 Nom. p-val= 0.102 FWER= 1 FDR= 0.151	
Gene Set 610 : REACTOME SIGNALING BY EGFR IN CANCER	ES = -0.393 NES = -1.74 Nom. p-val= 0.00594 FWER= 0.748 FDR= 0.0736	
Gene Set 604 : REACTOME SIGNALING BY ERBB2	ES = -0.386 NES = -1.54 Nom. p-val= 0.0394 FWER= 0.993 FDR= 0.0931	
Gene Set 599 : REACTOME SIGNALING BY ERBB4	ES = -0.382 NES = -1.46 Nom. p-val= 0.0717 FWER= 0.999 FDR= 0.118	
Gene Set 650 : REACTOME SIGNALING BY FGFR IN DISEASE	ES = -0.471 NES = -1.79 Nom. p-val= 0 FWER= 0.625 FDR= 0.0793	Y
Gene Set 681 : REACTOME SIGNALING BY FGFR MUTANTS	ES = -0.53 NES = -1.5 Nom. p-val= 0.0305 FWER= 0.998 FDR= 0.108	

Gene Set 1054 : REACTOME SIGNALING BY FGFR	ES = -0.492 NES = -1.79 Nom. p-val= 0 FWER= 0.625 FDR= 0.0782	Y
Gene Set 669 : REACTOME SIGNALING BY FGFR1 FUSION MUTANTS	ES = -0.412 NES = -1.28 Nom. p-val= 0.199 FWER= 1 FDR= 0.224	
Gene Set 664 : REACTOME SIGNALING BY FGFR1_MUTANTS	ES = -0.526 NES = -1.41 Nom. p-val= 0.0787 FWER= 1 FDR= 0.14	
Gene Set 907 : REACTOME SIGNALING BY ILS	ES = -0.596 NES = -1.71 Nom. p-val= 0.00786 FWER= 0.81 FDR= 0.0755	
Gene Set 981 : REACTOME SIGNALING BY INSULIN RECEPTOR	ES = -0.394 NES = -1.47 Nom. p-val= 0.0426 FWER= 0.999 FDR= 0.116	
Gene Set 575 : REACTOME SIGNALING BY NODAL	ES = -0.539 NES = -1.38 Nom. p-val= 0.0668 FWER= 1 FDR= 0.157	
Gene Set 973 : REACTOME SIGNALING BY NOTCH	ES = -0.356 NES = -1.56 Nom. p-val= 0.0276 FWER= 0.989 FDR= 0.0873	
Gene Set 636 : REACTOME SIGNALING BY NOTCH1	ES = -0.397 NES = -1.58 Nom. p-val= 0.0217 FWER= 0.983 FDR= 0.0811	
Gene Set 775 : REACTOME SIGNALING BY PDGF	ES = -0.53 NES = -1.94 Nom. p-val= 0 FWER= 0.282 FDR= 0.114	Y
Gene Set 564 : REACTOME SIGNALING BY RHO GTPASES	ES = -0.568 NES = -1.78 Nom. p-val= 0 FWER= 0.669 FDR= 0.0754	
Gene Set 843 : REACTOME SIGNALING BY ROBO RECEPTOR	ES = -0.49 NES = -1.46 Nom. p-val= 0.0827 FWER= 0.999 FDR= 0.117	
Gene Set 572 : REACTOME SIGNALING BY SCF KIT	ES = -0.487 NES = -1.82 Nom. p-val= 0.00385 FWER= 0.56 FDR= 0.0724	
Gene Set 1016 : REACTOME SIGNALING BY_TGF_BETA_RECEPTOR_COMPLEX	ES = -0.335 NES = -1.34 Nom. p-val= 0.198 FWER= 1 FDR= 0.185	
Gene Set 631 : REACTOME SIGNALING BY THE B CELL RECEPTOR BCR	ES = -0.519 NES = -2.11 Nom. p-val= 0.00384 FWER= 0.06 FDR= 0.0433	
Gene Set 569 : REACTOME SIGNALLING BY NGF	ES = -0.455 NES = -1.92 Nom. p-val= 0 FWER= 0.315 FDR= 0.102	Y
Gene Set 645 : REACTOME SIGNALLING TO ERKS	ES = -0.432 NES = -1.59 Nom. p-val= 0.0464 FWER= 0.978 FDR= 0.0793	
Gene Set 652 : REACTOME SIGNALLING TO P38 VIA RIT AND RIN	ES = -0.69 NES = -1.77 Nom. p-val= 0.00407 FWER= 0.681 FDR= 0.0733	
Gene Set 641 : REACTOME SIGNALLING TO RAS	ES = -0.524 NES = -1.79 Nom. p-val= 0.0118 FWER= 0.633 FDR= 0.0775	
Gene Set 823 : REACTOME_SLC_MEDIATED_TRANSMEMBRANE_TRANSPORT	ES = -0.431 NES = -1.45 Nom. p-val= 0.0181 FWER= 0.999 FDR= 0.121	
: REACTOME_SMAD2_SMAD3_SMAD4_HETEROTRIMER_REGULATES_TRANSCRIPTION	ES = -0.458 NES = -1.34 Nom. p-val= 0.19 FWER= 1 FDR= 0.184	
Gene Set 864 : REACTOME_SMOOTH_MUSCLE_CONTRACTION	ES = -0.643 NES = -1.41 Nom. p-val= 0.104 FWER= 1 FDR= 0.142	
Gene Set 760 : REACTOME STEROID HORMONES	ES = -0.559 NES = -1.37 Nom. p-val= 0.0571 FWER= 1 FDR= 0.165	
Gene Set 783 : REACTOME STRIATED MUSCLE CONTRACTION	ES = -0.754 NES = -1.33 Nom. p-val= 0.156 FWER= 1 FDR= 0.184	
Gene Set 567 : REACTOME SYNTHESIS OF BILE ACIDS AND BILE SALTS	ES = -0.496 NES = -1.24 Nom. p-val= 0.155 FWER= 1 FDR= 0.247	
Gene Set 660 : REACTOME SYNTHESIS OF PA	ES = -0.63 NES = -1.67 Nom. p-val= 0.0057 FWER= 0.91 FDR= 0.0738	
Gene Set 673 : REACTOME SYNTHESIS OF PC	ES = -0.46 NES = -1.26 Nom. p-val= 0.194 FWER= 1 FDR= 0.236	
Gene Set 665 : REACTOME SYNTHESIS OF PIPS AT THE PLASMA MEMBRANE	ES = -0.502 NES = -1.4 Nom. p-val= 0.11 FWER= 1 FDR= 0.144	
REACTOME_TAK1_ACTIVATES_NFKB_BY_PHOSPHORYLATION_AND_ACTIVATION_OF_IKKS_COMPLEX	ES = -0.552 NES = -1.53 Nom. p-val= 0.0313 FWER= 0.993 FDR= 0.0931	
Gene Set 693 : REACTOME_TCR_SIGNALING	ES = -0.738 NES = -1.66 Nom. p-val= 0.00581 FWER= 0.913 FDR= 0.0734	
Gene Set 606 : REACTOME TERMINATION OF O GLYCAN BIOSYNTHESIS	ES = -0.589 NES = -1.24 Nom. p-val= 0.195 FWER= 1 FDR= 0.248	
Set 657 : REACTOME_TGF_BETA_RECEPTOR_SIGNALING_ACTIVATES_SMADS	ES = -0.442 NES = -1.82 Nom. p-val= 0.00416 FWER= 0.548 FDR= 0.0763	
REACTOME_THE_ROLE_OF_NEF_IN_HIV1_REPLICATION_AND_DISEASE_PATHOGENESIS	ES = -0.716 NES = -1.76 Nom. p-val= 0.00572 FWER= 0.701 FDR= 0.0715	
REACTOME_THROMBIN_SIGNALING_THROUGH_PROTEINASE_ACTIVATED_RECEPTORS_PARS	ES = -0.6 NES = -1.71 Nom. p-val= 0 FWER= 0.817 FDR= 0.0762	
Gene Set 872 : REACTOME THROMBOXANE SIGNALING THROUGH TP RECEPTOR	ES = -0.633 NES = -1.55 Nom. p-val= 0.0288 FWER= 0.99 FDR= 0.0898	
Gene Set 702 : REACTOME_TIE2_SIGNALING	ES = -0.632 NES = -1.58 Nom. p-val= 0.0116 FWER= 0.983 FDR= 0.0812	
Gene Set 845 : REACTOME TIGHT JUNCTION INTERACTIONS	ES = -0.467 NES = -1.25 Nom. p-val= 0.187 FWER= 1 FDR= 0.247	
Gene Set 1023 : REACTOME TOLL RECEPTOR CASCADES	ES = -0.577 NES = -1.85 Nom. p-val= 0 FWER= 0.473 FDR= 0.0913	Y
REACTOME_TRAF6_MEDIATED_INDUCION_OF_NFKB_AND_MAP_KINASES_UPON_TLR7_8_OR_9_ACTIVATION	ES = -0.406 NES = -1.55 Nom. p-val= 0.0316 FWER= 0.99 FDR= 0.0892	
Gene Set 942 : REACTOME TRAF6 MEDIATED NFKB ACTIVATION	ES = -0.457 NES = -1.31 Nom. p-val= 0.171 FWER= 1 FDR= 0.203	
Gene Set 803 : REACTOME TRAFFICKING OF AMPA RECEPTORS	ES = -0.547 NES = -1.39 Nom. p-val= 0.0916 FWER= 1 FDR= 0.15	
Set 817 : REACTOME TRAFFICKING OF GLUR2 CONTAINING AMPA RECEPTORS	ES = -0.669 NES = -1.41 Nom. p-val= 0.0881 FWER= 1 FDR= 0.142	
REACTOME_TRANSCRIPTIONAL_ACTIVITY_OF_SMAD2_SMAD3_SMAD4_HETEROTRIMER	ES = -0.405 NES = -1.27 Nom. p-val= 0.247 FWER= 1 FDR= 0.229	
REACTOME_TRANSCRIPTIONAL_REGULATION_OF_WHITE_ADIPOCYTE_DIFFERENTIATION	ES = -0.52 NES = -1.85 Nom. p-val= 0 FWER= 0.48 FDR= 0.0864	Y
Gene Set 962 : REACTOME TRANSFERRIN ENDOCYTOSIS AND RECYCLING	ES = -0.49 NES = -1.3 Nom. p-val= 0.211 FWER= 1 FDR= 0.209	
Gene Set 763 : REACTOME TRANSMEMBRANE TRANSPORT OF SMALL MOLECULES	ES = -0.46 NES = -1.57 Nom. p-val= 0 FWER= 0.987 FDR= 0.0858	
Gene Set 711 : REACTOME TRANSMISSION ACROSS CHEMICAL SYNAPSES	ES = -0.542 NES = -1.58 Nom. p-val= 0.00558 FWER= 0.984 FDR= 0.0829	
REACTOME_TRANSPORT_OF_GLUCOSE_AND_OTHER_SUGARS_BILE_SALTS_AND_ORGANIC_ACIDS_METAL_IONS_AND_AMINE_COMPOUNDS	ES = -0.478 NES = -1.38 Nom. p-val= 0.033 FWER= 1 FDR= 0.157	
REACTOME_TRANSPORT_OF_INORGANIC_CATIONS_ANIONS_AND_AMINO_ACIDS_OLIGOPEPTIDES	ES = -0.458 NES = -1.38 Nom. p-val= 0.0342 FWER= 1 FDR= 0.156	
Gene Set 581 : REACTOME TRIF MEDIATED TLR3 SIGNALING	ES = -0.435 NES = -1.61 Nom. p-val= 0.00994 FWER= 0.964 FDR= 0.0756	
Gene Set 637 : REACTOME TRIGLYCERIDE BIOSYNTHESIS	ES = -0.429 NES = -1.44 Nom. p-val= 0.0568 FWER= 0.999 FDR= 0.127	
REACTOME_UNBLOCKING_OF_NMDA_RECEPTOR_GLUTAMATE_BINDING_AND_ACTIVATION	ES = -0.631 NES = -1.34 Nom. p-val= 0.111 FWER= 1 FDR= 0.184	
Gene Set 1027 : REACTOME VOLTAGE GATED POTASSIUM CHANNELS	ES = -0.635 NES = -1.5 Nom. p-val= 0.0152 FWER= 0.996 FDR= 0.105	
Gene Set 629 : REACTOME YAP1 AND WWTR1 TAZ STIMULATED GENE EXPRESSION	ES = -0.581 NES = -1.68 Nom. p-val= 0.0058 FWER= 0.895 FDR= 0.0722	
Gene Set 331 : SA_B_CELL_RECEPTOR_COMPLEXES	ES = -0.539 NES = -1.58 Nom. p-val= 0.0365 FWER= 0.984 FDR= 0.0825	
Gene Set 335 : SA_CASPASE_CASCADE	ES = -0.631 NES = -1.57 Nom. p-val= 0.041 FWER= 0.986 FDR= 0.086	

Gene Set 357 : SA MMP CYTOKINE CONNECTION	ES = -0.765 NES = -1.44 Nom. p-val= 0.0373 FWER= 0.999 FDR= 0.126	
Gene Set 361 : SA PTEN PATHWAY	ES = -0.443 NES = -1.26 Nom. p-val= 0.225 FWER= 1 FDR= 0.233	
Gene Set 362 : SA TRKA RECEPTOR	ES = -0.671 NES = -1.69 Nom. p-val= 0.0155 FWER= 0.867 FDR= 0.076	
Gene Set 353 : SIG BCR SIGNALING PATHWAY	ES = -0.605 NES = -1.62 Nom. p-val= 0.0386 FWER= 0.948 FDR= 0.076	
Gene Set 333 : SIG CD40PATHWAYMAP	ES = -0.414 NES = -1.47 Nom. p-val= 0.061 FWER= 0.999 FDR= 0.116	
Gene Set 339 : SIG CHEMOTAXIS	ES = -0.558 NES = -1.63 Nom. p-val= 0.00994 FWER= 0.941 FDR= 0.0753	
Gene Set 341 : SIG IL4RECEPTOR IN B LYPHOCYTES	ES = -0.55 NES = -1.56 Nom. p-val= 0.0383 FWER= 0.989 FDR= 0.0876	
Gene Set 350 : SIG INSULIN RECEPTOR PATHWAY IN CARDIAC MYOCYTES	ES = -0.377 NES = -1.43 Nom. p-val= 0.0943 FWER= 1 FDR= 0.134	
Gene Set 352 : SIG PIP3 SIGNALING IN B LYMPHOCYTES	ES = -0.611 NES = -1.59 Nom. p-val= 0.01 FWER= 0.978 FDR= 0.08	
Gene Set 334 : SIG PIP3 SIGNALING IN CARDIAC MYOCYTES	ES = -0.47 NES = -1.73 Nom. p-val= 0.0039 FWER= 0.768 FDR= 0.0731	
Gene Set 343 : SIG REGULATION OF THE ACTIN CYTOSKELETON BY RHO GTPASES	ES = -0.605 NES = -1.73 Nom. p-val= 0.00385 FWER= 0.762 FDR= 0.0737	
Gene Set 345 : ST ADRENERGIC	ES = -0.551 NES = -1.52 Nom. p-val= 0.0191 FWER= 0.995 FDR= 0.0979	
Gene Set 354 : ST B CELL ANTIGEN RECEPTOR	ES = -0.536 NES = -1.6 Nom. p-val= 0.0475 FWER= 0.971 FDR= 0.0778	
Gene Set 329 : ST DIFFERENTIATION PATHWAY IN PC12 CELLS	ES = -0.541 NES = -1.6 Nom. p-val= 0.0224 FWER= 0.97 FDR= 0.0767	
Gene Set 332 : ST ERK1 ERK2 MAPK PATHWAY	ES = -0.465 NES = -1.64 Nom. p-val= 0.0294 FWER= 0.94 FDR= 0.0743	
Gene Set 359 : ST FAS SIGNALING PATHWAY	ES = -0.478 NES = -1.85 Nom. p-val= 0 FWER= 0.476 FDR= 0.0899	Y
Gene Set 338 : ST G ALPHA I PATHWAY	ES = -0.525 NES = -1.53 Nom. p-val= 0.0205 FWER= 0.993 FDR= 0.094	
Gene Set 337 : ST G ALPHA S PATHWAY	ES = -0.676 NES = -1.75 Nom. p-val= 0.00571 FWER= 0.733 FDR= 0.0741	
Gene Set 336 : ST GA12 PATHWAY	ES = -0.701 NES = -1.74 Nom. p-val= 0.00592 FWER= 0.743 FDR= 0.073	
Gene Set 348 : ST GA13 PATHWAY	ES = -0.445 NES = -1.42 Nom. p-val= 0.0733 FWER= 1 FDR= 0.135	
Gene Set 347 : ST GAQ PATHWAY	ES = -0.384 NES = -1.3 Nom. p-val= 0.18 FWER= 1 FDR= 0.212	
Gene Set 344 : ST GRANULE CELL SURVIVAL PATHWAY	ES = -0.507 NES = -1.47 Nom. p-val= 0.0484 FWER= 0.999 FDR= 0.114	
Gene Set 346 : ST INTEGRIN SIGNALING PATHWAY	ES = -0.585 NES = -1.9 Nom. p-val= 0 FWER= 0.346 FDR= 0.0887	Y
Gene Set 355 : ST INTERLEUKIN 4 PATHWAY	ES = -0.563 NES = -1.55 Nom. p-val= 0.0301 FWER= 0.99 FDR= 0.0893	
Gene Set 358 : ST JNK MAPK PATHWAY	ES = -0.431 NES = -1.34 Nom. p-val= 0.174 FWER= 1 FDR= 0.183	
Gene Set 360 : ST MYOCYTE AD PATHWAY	ES = -0.602 NES = -1.52 Nom. p-val= 0.0281 FWER= 0.995 FDR= 0.098	
Gene Set 363 : ST PHOSPHOINOSITIDE 3 KINASE PATHWAY	ES = -0.55 NES = -1.81 Nom. p-val= 0.00199 FWER= 0.571 FDR= 0.0744	
Gene Set 351 : ST T CELL SIGNAL TRANSDUCTION	ES = -0.716 NES = -1.64 Nom. p-val= 0.0117 FWER= 0.935 FDR= 0.074	
Gene Set 330 : ST TUMOR NECROSIS FACTOR PATHWAY	ES = -0.467 NES = -1.49 Nom. p-val= 0.0822 FWER= 0.998 FDR= 0.109	
Gene Set 356 : ST WNT BETA CATENIN PATHWAY	ES = -0.603 NES = -1.66 Nom. p-val= 0.0172 FWER= 0.918 FDR= 0.0738	
Gene Set 342 : WNT SIGNALING	ES = -0.584 NES = -1.85 Nom. p-val= 0 FWER= 0.48 FDR= 0.0886	Y

ES: enrichment score; Nom. p-val: nominal *P* value; FWER: family-wise error rate; FDR: false discovery rate.



## Bibliography

- Abida, W., J. Cyrta, G. Heller, D. Prandi, J. Armenia, I. Coleman, M. Cieslik, M. Benelli, D. Robinson, E.M. Van Allen, A. Sboner, T. Fedrizzi, J.M. Mosquera, B.D. Robinson, N. De Sarkar, L.P. Kunju, S. Tomlins, Y.M. Wu, D. Nava Rodrigues, M. Loda, A. Gopalan, V.E. Reuter, C.C. Pritchard, J. Mateo, D. Bianchini, S. Miranda, S. Carreira, P. Rescigno, J. Filipenko, J. Vinson, R.B. Montgomery, H. Beltran, E.I. Heath, H.I. Scher, P.W. Kantoff, M.E. Taplin, N. Schultz, J.S. deBono, F. Demichelis, P.S. Nelson, M.A. Rubin, A.M. Chinnaiyan, and C.L. Sawyers. 2019. Genomic correlates of clinical outcome in advanced prostate cancer. *Proc Natl Acad Sci U S A*. 116:11428-11436.
- Alhalabi, O., H. Rafei, A. Shah, A. Siefker-Radtke, M. Campbell, and J. Gao. 2019. Targeting advanced urothelial carcinoma-developing strategies. *Curr Opin Oncol*. 31:207-215.
- Amirouchene-Angelozzi, N., C. Swanton, and A. Bardelli. 2017. Tumor Evolution as a Therapeutic Target. *Cancer Discovery*. 7:805.
- Armstrong, K., I. Ahmad, G. Kalna, S.S. Tan, J. Edwards, C.N. Robson, and H.Y. Leung. 2011. Upregulated FGFR1 expression is associated with the transition of hormone-naive to castrate-resistant prostate cancer. *Br J Cancer*. 105:1362-1369.
- Aukes, K., C. Forsman, N.J. Brady, K. Astleford, N. Blixt, D. Sachdev, E.D. Jensen, K.C. Mansky, and K.L. Schwertfeger. 2017. Breast cancer cell-derived fibroblast growth factors enhance osteoclast activity and contribute to the formation of metastatic lesions. *PLoS One*. 12:e0185736.

- Balk, S.P., Y.J. Ko, and G.J. Bubley. 2003. Biology of prostate-specific antigen. *J Clin Oncol.* 21:383-391.
- Bataille, R., D. Chappard, C. Marcelli, P. Dessauw, J. Sany, P. Baldet, and C. Alexandre. 1989. Mechanisms of bone destruction in multiple myeloma: the importance of an unbalanced process in determining the severity of lytic bone disease. *J Clin Oncol.* 7:1909-1914.
- Bellmunt, J., T.K. Choueiri, R. Fougerey, F.A. Schutz, Y. Salhi, E. Winkist, S. Culine, H. von der Maase, D.J. Vaughn, and J.E. Rosenberg. 2010. Prognostic factors in patients with advanced transitional cell carcinoma of the urothelial tract experiencing treatment failure with platinum-containing regimens. *J Clin Oncol.* 28:1850-1855.
- Beltran, H., S. Tomlins, A. Aparicio, V. Arora, D. Rickman, G. Ayala, J. Huang, L. True, M.E. Gleave, H. Soule, C. Logothetis, and M.A. Rubin. 2014. Aggressive variants of castration-resistant prostate cancer. *Clin Cancer Res.* 20:2846-2850.
- Benayahu, D., Y. Wiesenfeld, and R. Sapir-Koren. 2019. How is mechanobiology involved in mesenchymal stem cell differentiation toward the osteoblastic or adipogenic fate? *J Cell Physiol.*
- Berendsen, A.D., and B.R. Olsen. 2015. Bone development. *Bone.* 80:14-18.
- Berish, R.B., A.N. Ali, P.G. Telmer, J.A. Ronald, and H.S. Leong. 2018. Translational models of prostate cancer bone metastasis. *Nature Reviews Urology.* 15:403-421.
- Bluemn, E.G., I.M. Coleman, J.M. Lucas, R.T. Coleman, S. Hernandez-Lopez, R. Tharakan, D. Bianchi-Frias, R.F. Dumpit, A. Kaipainen, A.N. Corella, Y.C. Yang, M.D. Nyquist, E. Mostaghel, A.C. Hsieh, X. Zhang, E. Corey, L.G. Brown, H.M. Nguyen, K. Pienta, M. Ittmann, M. Schweizer, L.D. True, D. Wise, P.S. Rennie, R.L. Vessella, C. Morrissey, and P.S. Nelson. 2017. Androgen Receptor Pathway-

- Independent Prostate Cancer Is Sustained through FGF Signaling. *Cancer Cell*. 32:474-489.e476.
- Bray, F., J. Ferlay, I. Soerjomataram, R.L. Siegel, L.A. Torre, and A. Jemal. 2018. Global cancer statistics 2018: GLOBOCAN estimates of incidence and mortality worldwide for 36 cancers in 185 countries. *CA Cancer J Clin*. 68:394-424.
- Brooks, A.N., E. Kilgour, and P.D. Smith. 2012. Molecular Pathways: Fibroblast Growth Factor Signaling: A New Therapeutic Opportunity in Cancer. *Clinical Cancer Research*. 18:1855.
- Broom, B.M., M.C. Ryan, R.E. Brown, F. Ikeda, M. Stucky, D.W. Kane, J. Melott, C. Wakefield, T.D. Casasent, R. Akbani, and J.N. Weinstein. 2017. A Galaxy Implementation of Next-Generation Clustered Heatmaps for Interactive Exploration of Molecular Profiling Data. *Cancer Research*. 77:e23.
- Brubaker, K.D., R.L. Vessella, L.D. True, R. Thomas, and E. Corey. 2003. Cathepsin K mRNA and protein expression in prostate cancer progression. *J Bone Miner Res*. 18:222-230.
- Bruno, I.G., W. Jin, and G.J. Cote. 2004. Correction of aberrant FGFR1 alternative RNA splicing through targeting of intronic regulatory elements. *Hum Mol Genet*. 13:2409-2420.
- Bubendorf, L., A. Schopfer, U. Wagner, G. Sauter, H. Moch, N. Willi, T.C. Gasser, and M.J. Mihatsch. 2000. Metastatic patterns of prostate cancer: an autopsy study of 1,589 patients. *Human pathology*. 31:578-583.
- Catalona, W.J. 1994. Management of Cancer of the Prostate. *The New England Journal of Medicine*. 331:996-1004.
- Cerami, E., J. Gao, U. Dogrusoz, B.E. Gross, S.O. Sumer, B.A. Aksoy, A. Jacobsen, C.J. Byrne, M.L. Heuer, E. Larsson, Y. Antipin, B. Reva, A.P. Goldberg, C. Sander, and

- N. Schultz. 2012. The cBio cancer genomics portal: an open platform for exploring multidimensional cancer genomics data. *Cancer Discovery*. 2:401-404.
- Charoenlarp, P., A.K. Rajendran, and S. Iseki. 2017. Role of fibroblast growth factors in bone regeneration. *Inflammation and Regeneration*. 37:10.
- Chen, W., T. Dang, R.D. Blind, Z. Wang, C.N. Cavasotto, A.B. Hittelman, I. Rogatsky, S.K. Logan, and M.J. Garabedian. 2008. Glucocorticoid receptor phosphorylation differentially affects target gene expression. *Mol Endocrinol*. 22:1754-1766.
- Chen, X., Z. Wang, N. Duan, G. Zhu, E.M. Schwarz, and C. Xie. 2018. Osteoblast-osteoclast interactions. *Connective tissue research*. 59:99-107.
- Cook, G.B., and F.R. Watson. 1968. Events in the natural history of prostate cancer: using salvage curves, mean age distributions and contingency coefficients. *J Urol*. 96: 87-96.
- Corn, P.G., F. Wang, W.L. McKeegan, and N. Navone. 2013. Targeting fibroblast growth factor pathways in prostate cancer. *Clinical cancer research*. 19:5856-5866.
- Crockford, A., M. Jamal-Hanjani, J. Hicks, and C. Swanton. 2014. Implications of intratumour heterogeneity for treatment stratification. *J Pathol*. 232:264-273.
- Croucher, P.I., M.M. McDonald, and T.J. Martin. 2016. Bone metastasis: the importance of the neighbourhood. *Nature reviews. Cancer*. 16:373-386.
- Cuzick, J., M.A. Thorat, G. Andriole, O.W. Brawley, P.H. Brown, Z. Culig, R.A. Eeles, L.G. Ford, F.C. Hamdy, L. Holmberg, D. Ilic, T.J. Key, C.L. Vecchia, H. Lilja, M. Marberger, F.L. Meyskens, L.M. Minasian, C. Parker, H.L. Parnes, S. Perner, H. Rittenhouse, J. Schalken, H.-P. Schmid, B.J. Schmitz-Dräger, F.H. Schröder, A. Stenzl, B. Tombal, T.J. Wilt, and A. Wolk. 2014. Prevention and early detection of prostate cancer. *The Lancet Oncology*. 15:e484-e492.

- D'Antonio, C., A. Passaro, B. Gori, E. Del Signore, M.R. Migliorino, S. Ricciardi, A. Fulvi, and F. de Marinis. 2014. Bone and brain metastasis in lung cancer: recent advances in therapeutic strategies. *Ther Adv Med Oncol*. 6:101-114.
- D'Oronzo, S., J. Brown, and R. Coleman. 2017. The role of biomarkers in the management of bone-homing malignancies. *J Bone Oncol*. 9:1-9.
- Dagogo-Jack, I., and A.T. Shaw. 2017. Tumour heterogeneity and resistance to cancer therapies. *Nature Reviews Clinical Oncology*. 15:81.
- de Bruin, E.C., N. McGranahan, R. Mitter, M. Salm, D.C. Wedge, L. Yates, M. Jamal-Hanjani, S. Shafi, N. Murugaesu, A.J. Rowan, E. Gronroos, M.A. Muhammad, S. Horswell, M. Gerlinger, I. Varela, D. Jones, J. Marshall, T. Voet, P. Van Loo, D.M. Rassl, R.C. Rintoul, S.M. Janes, S.M. Lee, M. Forster, T. Ahmad, D. Lawrence, M. Falzon, A. Capitanio, T.T. Harkins, C.C. Lee, W. Tom, E. Teefe, S.C. Chen, S. Begum, A. Rabinowitz, B. Phillimore, B. Spencer-Dene, G. Stamp, Z. Szallasi, N. Matthews, A. Stewart, P. Campbell, and C. Swanton. 2014. Spatial and temporal diversity in genomic instability processes defines lung cancer evolution. *Science (New York, N.Y.* 346:251-256.
- De Marzo, A.M., M.C. Haffner, T.L. Lotan, S. Yegnasubramanian, and W.G. Nelson. 2016. Premalignancy in Prostate Cancer: Rethinking What we Know. *Cancer prevention research (Philadelphia, Pa.)*. 9:648-656.
- Decker, A.M., Y. Jung, F. Cackowski, and R.S. Taichman. 2016. The role of hematopoietic stem cell niche in prostate cancer bone metastasis. *J Bone Oncol*. 5:117-120.
- Deweerd, S. 2015. Prognosis: Proportionate response. *Nature*. 528:S124.
- di Martino, E., D.C. Tomlinson, S.V. Williams, and M.A. Knowles. 2016. A place for precision medicine in bladder cancer: targeting the FGFRs. *Future Oncology*. 12:2243-2263.

- Drake, M.T., B.L. Clarke, M.J. Oursler, and S. Khosla. 2017. Cathepsin K Inhibitors for Osteoporosis: Biology, Potential Clinical Utility, and Lessons Learned. *Endocr Rev.* 38:325-350.
- Ell, B., and Y. Kang. 2012. SnapShot: Bone Metastasis. *Cell.* 151:690-690 e691.
- Feng, J.Q., E.L. Clinkenbeard, B. Yuan, K.E. White, and M.K. Drezner. 2013. Osteocyte regulation of phosphate homeostasis and bone mineralization underlies the pathophysiology of the heritable disorders of rickets and osteomalacia. *Bone.* 54:213-221.
- Freeman, A.K., V.P. Sumathi, and L. Jeys. 2015. Metastatic tumours of bone. *Surgery - Oxford International Edition.* 33:34-39.
- Furuya, M., J. Kikuta, S. Fujimori, S. Seno, H. Maeda, M. Shirazaki, M. Uenaka, H. Mizuno, Y. Iwamoto, A. Morimoto, K. Hashimoto, T. Ito, Y. Isogai, M. Kashii, T. Kaito, S. Ohba, U.I. Chung, A.C. Lichtler, K. Kikuchi, H. Matsuda, H. Yoshikawa, and M. Ishii. 2018. Direct cell-cell contact between mature osteoblasts and osteoclasts dynamically controls their functions in vivo. *Nat Commun.* 9:300.
- Gao, J., B.A. Aksoy, U. Dogrusoz, G. Dresdner, B. Gross, S.O. Sumer, Y. Sun, A. Jacobsen, R. Sinha, E. Larsson, E. Cerami, C. Sander, and N. Schultz. 2013. Integrative analysis of complex cancer genomics and clinical profiles using the cBioPortal. *Science signaling.* 6:pl1.
- Ghedini, G.C., R. Ronca, M. Presta, and A. Giacomini. 2018. Future applications of FGF/FGFR inhibitors in cancer. *Expert Review of Anticancer Therapy.* 18:861-872.
- Gilbert, S. 2000. Osteogenesis: The Development of Bones. *In Developmental Biology.* Sinauer Associates, Sunderland (MA)
- Gleason, D.F. 1966. Classification of prostatic carcinomas. *Cancer Chemother Rep.* 50:125-128.

- Gómez-Cuadrado, L., N. Tracey, R. Ma, B. Qian, and V.G. Brunton. 2017. Mouse models of metastasis: progress and prospects. *Disease Models & Mechanisms*. 10:1061.
- Gong, S.G. 2014. Isoforms of receptors of fibroblast growth factors. *Journal of cellular physiology*. 229:1887-1895.
- Guise, T.A. 2002. The vicious cycle of bone metastases. *J Musculoskelet Neuronal Interact*. 2:570-572.
- Haffner, M.C., C. Weier, M.M. Xu, A. Vaghasia, B. Gurel, B. Gumuskaya, D.M. Esopi, H. Fedor, H.L. Tan, I. Kulac, J. Hicks, W.B. Isaacs, T.L. Lotan, W.G. Nelson, S. Yegnasubramanian, and A.M. De Marzo. 2016. Molecular evidence that invasive adenocarcinoma can mimic prostatic intraepithelial neoplasia (PIN) and intraductal carcinoma through retrograde glandular colonization. *The Journal of pathology*. 238:31-41.
- Hagedorn, E.J., J.W. Ziel, M.A. Morrissey, L.M. Linden, Z. Wang, Q. Chi, S.A. Johnson, and D.R. Sherwood. 2013. The netrin receptor DCC focuses invadopodia-driven basement membrane transmigration in vivo. *The Journal of Cell Biology*. 201:903.
- Han, X., Z. Xiao, and L.D. Quarles. 2015. Membrane and integrative nuclear fibroblastic growth factor receptor (FGFR) regulation of FGF-23. *The Journal of biological chemistry*. 290:10447-10459.
- Hart, I.R., and I.J. Fidler. 1980. Role of organ selectivity in the determination of metastatic patterns of B16 melanoma. *Cancer Res*. 40:2281-2287.
- Hashemi-Sadraei, N., and N. Hanna. 2017. Targeting FGFR in Squamous Cell Carcinoma of the Lung. *Target Oncol*. 12:741-755.
- Hess, K.R., G.R. Varadhachary, S.H. Taylor, W. Wei, M.N. Raber, R. Lenzi, and J.L. Abbruzzese. 2006. Metastatic patterns in adenocarcinoma. *Cancer*. 106:1624-1633.

- Hoadley, K.A., C. Yau, T. Hinoue, D.M. Wolf, A.J. Lazar, E. Drill, R. Shen, A.M. Taylor, A.D. Cherniack, V. Thorsson, R. Akbani, R. Bowlby, C.K. Wong, M. Wiznerowicz, F. Sanchez-Vega, A.G. Robertson, B.G. Schneider, M.S. Lawrence, H. Noushmehr, T.M. Malta, N. Cancer Genome Atlas, J.M. Stuart, C.C. Benz, and P.W. Laird. 2018. Cell-of-Origin Patterns Dominate the Molecular Classification of 10,000 Tumors from 33 Types of Cancer. *Cell*. 173:291-304 e296.
- Hodson, R. 2015. Small organ, big reach. *Nature*. 528:S118.
- Hong, M.K., G. Macintyre, D.C. Wedge, P. Van Loo, K. Patel, S. Lunke, L.B. Alexandrov, C. Sloggett, M. Cmero, F. Marass, D. Tsui, S. Mangiola, A. Lonie, H. Naeem, N. Sapre, P.M. Phal, N. Kurganovs, X. Chin, M. Kerger, A.Y. Warren, D. Neal, V. Gnanapragasam, N. Rosenfeld, J.S. Pedersen, A. Ryan, I. Haviv, A.J. Costello, N.M. Corcoran, and C.M. Hovens. 2015. Tracking the origins and drivers of subclonal metastatic expansion in prostate cancer. *Nature communications*. 6:6605.
- Horton, J.K., R. Jagsi, W.A. Woodward, and A. Ho. 2018. Breast Cancer Biology: Clinical Implications for Breast Radiation Therapy. *Int J Radiat Oncol Biol Phys*. 100:23-37.
- Huang, W.C., Z. Xie, H. Konaka, J. Sodek, H.E. Zhau, and L.W. Chung. 2005. Human osteocalcin and bone sialoprotein mediating osteomimicry of prostate cancer cells: role of cAMP-dependent protein kinase A signaling pathway. *Cancer Res*. 65:2303-2313.
- Huang, Y., C. Jin, T. Hamana, J. Liu, C. Wang, L. An, W.L. McKeehan, and F. Wang. 2015. Overexpression of FGF9 in prostate epithelial cells augments reactive stroma formation and promotes prostate cancer progression. *International journal of biological sciences*. 11:948-960.



- Ishiko, A., H. Shimizu, T. Masunaga, T. Hashimoto, M. Dmochowski, F. Wojnarowska, B.S. Bhogal, M.M. Black, and T. Nishikawa. 1996. 97-kDa linear IgA bullous dermatosis (LAD) antigen localizes to the lamina lucida of the epidermal basement membrane. *The Journal of investigative dermatology*. 106:739-743.
- J. Gordon Betts, K.A.Y., James A. Wise, Eddie Johnson, Brandon Poe, Dean H. Kruse, Oksana Korol, Jody E. Johnson, Mark Womble, Peter DeSaix. 2013. Bone Tissue and the Skeletal System. *In Anatomy & Physiology*. Vol. <http://cnx.org/contents/14fb4ad7-39a1-4eee-ab6e-3ef2482e3e22@8.24>. O. College, editor. OpenStax CNX, Houston, Texas.
- Jacob, A.L., C. Smith, J. Partanen, and D.M. Ornitz. 2006. Fibroblast growth factor receptor 1 signaling in the osteo-chondrogenic cell lineage regulates sequential steps of osteoblast maturation. *Dev Biol*. 296:315-328.
- Johnson, D.E., and L.T. Williams. 1993. Structural and functional diversity in the FGF receptor multigene family. *Advances in cancer research*. 60:1-41.
- Kahkonen, T.E., K.K. Ivaska, M. Jiang, K.G. Buki, H.K. Vaananen, and P.L. Harkonen. 2018. Role of fibroblast growth factor receptors (FGFR) and FGFR like-1 (FGFRL1) in mesenchymal stromal cell differentiation to osteoblasts and adipocytes. *Mol Cell Endocrinol*. 461:194-204.
- Karuppaiah, K., K. Yu, J. Lim, J. Chen, C. Smith, F. Long, and D.M. Ornitz. 2016. FGF signaling in the osteoprogenitor lineage non-autonomously regulates postnatal chondrocyte proliferation and skeletal growth. *Development*. 143:1811-1822.
- Katoh, M., and H. Nakagama. 2014. FGF receptors: cancer biology and therapeutics. *Med Res Rev*. 34:280-300.
- Kim, J., and G.A. Coetzee. 2004. Prostate specific antigen gene regulation by androgen receptor. *Journal of cellular biochemistry*. 93:233-241.

- Kohrman, A.Q., and D.Q. Matus. 2017. Divide or Conquer: Cell Cycle Regulation of Invasive Behavior. *Trends in Cell Biology*. 27:12-25.
- Kozlow, W., and T.A. Guise. 2005. Breast Cancer Metastasis to Bone: Mechanisms of Osteolysis and Implications for Therapy. *Journal of Mammary Gland Biology and Neoplasia*. 10:169-180.
- Kramer, A., J. Green, J. Pollard, Jr., and S. Tugendreich. 2014. Causal analysis approaches in Ingenuity Pathway Analysis. *Bioinformatics (Oxford, England)*. 30:523-530.
- Kundra, V., C.S. Ng, J. Ma, J.A. Bankson, R.E. Price, D.D. Cody, K.A. Do, L. Han, and N.M. Navone. 2007. In vivo imaging of prostate cancer involving bone in a mouse model. *The Prostate*. 67:50-60.
- Kwabi-Addo, B., M. Ozen, and M. Ittmann. 2004. The role of fibroblast growth factors and their receptors in prostate cancer. *Endocr Relat Cancer*. 11:709-724.
- Lee, Y.-C., M.S. Gajdosik, D. Josic, J.G. Clifton, C. Logothetis, L.-Y. Yu-Lee, G.E. Gallick, S.N. Maity, and S.-H. Lin. 2015a. Secretome Analysis of an Osteogenic Prostate Tumor Identifies Complex Signaling Networks Mediating Cross-talk of Cancer and Stromal Cells Within the Tumor Microenvironment. *Molecular & Cellular Proteomics*. 14:471.
- Lee, Y.-C., S.-C. Lin, G. Yu, C.-J. Cheng, B. Liu, H.-C. Liu, D.H. Hawke, N.U. Parikh, A. Varkaris, P. Corn, C. Logothetis, R.L. Satcher, L.-Y. Yu-Lee, G.E. Gallick, and S.-H. Lin. 2015b. Identification of Bone-Derived Factors Conferring De Novo Therapeutic Resistance in Metastatic Prostate Cancer. *Cancer Research*. 75:4949.
- Li, X., J.A. Sterling, K.H. Fan, R.L. Vessella, Y. Shyr, S.W. Hayward, L.M. Matrisian, and N.A. Bhowmick. 2012. Loss of TGF-beta responsiveness in prostate stromal cells

- alters chemokine levels and facilitates the development of mixed osteoblastic/osteolytic bone lesions. *Molecular cancer research*. 10:494-503.
- Li, X., C. Wang, J. Xiao, W.L. McKeegan, and F. Wang. 2016. Fibroblast growth factors, old kids on the new block. *Seminars in cell & developmental biology*. 53:155-167.
- Li, Z.G., P. Mathew, J. Yang, M.W. Starbuck, A.J. Zurita, J. Liu, C. Sikes, A.S. Multani, E. Efstathiou, A. Lopez, J. Wang, T.V. Fanning, V.G. Prieto, V. Kundra, E.S. Vazquez, P. Troncoso, A.K. Raymond, C.J. Logothetis, S.H. Lin, S. Maity, and N.M. Navone. 2008. Androgen receptor-negative human prostate cancer cells induce osteogenesis in mice through FGF9-mediated mechanisms. *J Clin Invest*. 118:2697-2710.
- Lin, Y., and F. Wang. 2010. FGF signalling in prostate development, tissue homeostasis and tumorigenesis. *Biosci Rep*. 30:285-291.
- Liu, J., P. You, G. Chen, X. Fu, X. Zeng, C. Wang, Y. Huang, L. An, X. Wan, N. Navone, C.L. Wu, W.L. McKeegan, Z. Zhang, W. Zhong, and F. Wang. 2016. Hyperactivated FRS2alpha-mediated signaling in prostate cancer cells promotes tumor angiogenesis and predicts poor clinical outcome of patients. *Oncogene*. 35:1750-1759.
- Loberg, R.D., C.J. Logothetis, E.T. Keller, and K.J. Pienta. 2005. Pathogenesis and Treatment of Prostate Cancer Bone Metastases: Targeting the Lethal Phenotype. *Journal of Clinical Oncology*. 23:8232-8241.
- Logothetis, C., M.J. Morris, R. Den, and R.E. Coleman. 2018. Current perspectives on bone metastases in castrate-resistant prostate cancer. *Cancer Metastasis Rev*. 37:189-196.

- Logothetis, C.J., G.E. Gallick, S.N. Maity, J. Kim, A. Aparicio, E. Efstathiou, and S.H. Lin. 2013. Molecular classification of prostate cancer progression: foundation for marker-driven treatment of prostate cancer. *Cancer Discov.* 3:849-861.
- Logothetis, C.J., N.M. Navone, and S.-H. Lin. 2008. Understanding the Biology of Bone Metastases: Key to the Effective Treatment of Prostate Cancer. *Clinical Cancer Research.* 14:1599.
- Loriot, Y., A. Necchi, S.H. Park, J. Garcia-Donas, R. Huddart, E. Burgess, M. Fleming, A. Rezazadeh, B. Mellado, S. Varlamov, M. Joshi, I. Duran, S.T. Tagawa, Y. Zakharia, B. Zhong, K. Stuyckens, A. Santiago-Walker, P. De Porre, A. O'Hagan, A. Avadhani, and A.O. Siefker-Radtke. 2019. Erdafitinib in Locally Advanced or Metastatic Urothelial Carcinoma. *The New England Journal of Medicine.* 381:338-348.
- Lu, X., N. Su, J. Yang, W. Huang, C. Li, L. Zhao, Q. He, X. Du, Y. Shen, B. Chen, and L. Chen. 2009. Fibroblast growth factor receptor 1 regulates the differentiation and activation of osteoclasts through Erk1/2 pathway. *Biochem Biophys Res Commun.* 390:494-499.
- Luqmani Y.A., C. Mortimer, C. Yiangou, C.L. Johnston, G.S. Bansal, D. Sinnett, M. Law, R.C. Coombes. 1995. Expression of 2 variant forms of fibroblast growth factor receptor 1 in human breast. *Int J Cancer.* 64:274-279.
- Martin, A., S. Liu, V. David, H. Li, A. Karydis, J.Q. Feng, and L.D. Quarles. 2011. Bone proteins PHEX and DMP1 regulate fibroblastic growth factor Fgf23 expression in osteocytes through a common pathway involving FGF receptor (FGFR) signaling. *FASEB J.* 25:2551-2562.
- Massague, J., and A.C. Obenauf. 2016. Metastatic colonization by circulating tumour cells. *Nature.* 529:298-306.

- Mateo, J., S. Carreira, S. Sandhu, S. Miranda, H. Mossop, R. Perez-Lopez, D. Nava Rodrigues, D. Robinson, A. Omlin, N. Tunariu, G. Boysen, N. Porta, P. Flohr, A. Gillman, I. Figueiredo, C. Paulding, G. Seed, S. Jain, C. Ralph, A. Protheroe, S. Hussain, R. Jones, T. Elliott, U. McGovern, D. Bianchini, J. Goodall, Z. Zafeiriou, C.T. Williamson, R. Ferraldeschi, R. Riisnaes, B. Ebbs, G. Fowler, D. Roda, W. Yuan, Y.M. Wu, X. Cao, R. Brough, H. Pemberton, R. A'Hern, A. Swain, L.P. Kunju, R. Eeles, G. Attard, C.J. Lord, A. Ashworth, M.A. Rubin, K.E. Knudsen, F.Y. Feng, A.M. Chinnaiyan, E. Hall, and J.S. de Bono. 2015. DNA-Repair Defects and Olaparib in Metastatic Prostate Cancer. *The New England Journal of Medicine*. 373:1697-1708.
- Matus, D.Q., X.-Y. Li, S. Durbin, D. Agarwal, Q. Chi, S.J. Weiss, and D.R. Sherwood. 2010. In Vivo Identification of Regulators of Cell Invasion Across Basement Membranes. *Science Signaling*. 3:ra35.
- Matus, D. Q., L. L. Lohmer, L.C. Kelley, A.J. Schindler, A.Q. Kohrman, M. Barkoulas, W. Zhang, Q. Chi, and D.R. Sherwood. 2015. Invasive Cell Fate Requires G1 Cell-Cycle Arrest and Histone Deacetylase-Mediated Changes in Gene Expression. *Developmental Cell*. 35:162-174.
- McNiel, E.A., and P.N. Tschlis. 2017. Analyses of publicly available genomics resources define FGF-2-expressing bladder carcinomas as EMT-prone, proliferative tumors with low mutation rates and high expression of CTLA-4, PD-1 and PD-L1. *Signal Transduction and Targeted Therapy*. 2:16045.
- Meng, X., A. Vander Ark, P. Daft, E. Woodford, J. Wang, Z. Madaj, and X. Li. 2018. Loss of TGF-beta signaling in osteoblasts increases basic-FGF and promotes prostate cancer bone metastasis. *Cancer Letters*. 418:109-118.

- Meng, X., A. Vander Ark, P. Lee, G. Hostetter, N.A. Bhowmick, L.M. Matrisian, B.O. Williams, C.K. Miranti, and X. Li. 2016. Myeloid-specific TGF-beta signaling in bone promotes basic-FGF and breast cancer bone metastasis. *Oncogene*. 35:2370-2378.
- Miraoui, H., and P.J. Marie. 2010. Fibroblast growth factor receptor signaling crosstalk in skeletogenesis. *Science signaling*. 3:re9.
- Montero, A., Y. Okada, M. Tomita, M. Ito, H. Tsurukami, T. Nakamura, T. Doetschman, J.D. Coffin, and M.M. Hurley. 2000. Disruption of the fibroblast growth factor-2 gene results in decreased bone mass and bone formation. *J Clin Invest*. 105:1085-1093.
- Munari, E., L. Cima, F. Massari, F. Bertoldo, A.B. Porcaro, A. Calio, G. Riva, E. Ciocchetta, C. Ciccarese, A. Modena, R. Iacovelli, T. Sava, A. Eccher, C. Ghimenton, G. Tortora, W. Artibani, G. Novella, G. Bogina, G. Zamboni, F. Sanguedolce, A. D'Amuri, G. Martignoni, and M. Brunelli. 2017. Cathepsin K expression in castration-resistant prostate carcinoma: a therapeutical target for patients at risk for bone metastases. *Int J Biol Markers*. 32:e243-e247.
- Murali, S.K., P. Roschger, U. Zeitz, K. Klaushofer, O. Andrukhova, and R.G. Erben. 2016. FGF23 Regulates Bone Mineralization in a 1,25(OH)<sub>2</sub> D<sub>3</sub> and Klotho-Independent Manner. *Journal of bone and mineral research : the official journal of the American Society for Bone and Mineral Research*. 31:129-142.
- Narayanan, S., S. Srinivas, and D. Feldman. 2016. Androgen-glucocorticoid interactions in the era of novel prostate cancer therapy. *Nature reviews. Urology*. 13:47-60.
- Navone, N.M., and E. Labanca. 2017. Modeling Cancer Metastasis. In *Patient-Derived Xenograft Models of Human Cancer*. Y. Wang, D. Lin, and P.W. Gout, editors. Springer International Publishing, Cham. 93-114.

- Neben, C.L., C.T. Tuzon, X. Mao, F.D. Lay, and A.E. Merrill. 2017. FGFR2 mutations in bent bone dysplasia syndrome activate nucleolar stress and perturb cell fate determination. *Human molecular genetics*. 26:3253-3270.
- Ornitz, D.M., and N. Itoh. 2015. The Fibroblast Growth Factor signaling pathway. *Wiley Interdisciplinary Reviews. Developmental Biology*. 4:215-266.
- Ornitz, D.M., and P.J. Marie. 2015. Fibroblast growth factor signaling in skeletal development and disease. *Genes Dev*. 29:1463-1486.
- Ottewill, P.D., N. Wang, J. Meek, C.A. Fowles, P.I. Croucher, C.L. Eaton, and I. Holen. 2014. Castration-induced bone loss triggers growth of disseminated prostate cancer cells in bone. *Endocr Relat Cancer*. 21:769-781.
- Panaroni, C., A.J. Yee, and N.S. Raje. 2017. Myeloma and Bone Disease. *Curr Osteoporos Rep*. 15:483-498.
- Parker, C., S. Nilsson, D. Heinrich, S.I. Helle, J.M. O'Sullivan, S.D. Fosså, A. Chodacki, P. Wiechno, J. Logue, M. Seke, A. Widmark, D.C. Johannessen, P. Hoskin, D. Bottomley, N.D. James, A. Solberg, I. Syndikus, J. Kliment, S. Wedel, S. Boehmer, M. Dall'Oglio, L. Franzén, R. Coleman, N.J. Vogelzang, C.G. O'Bryan-Tear, K. Staudacher, J. Garcia-Vargas, M. Shan, Ø.S. Bruland, and O. Sartor. 2013. Alpha Emitter Radium-223 and Survival in Metastatic Prostate Cancer. *The New England Journal of Medicine*. 369:213-223.
- Pecqueux, C., A. Arslan, M. Heller, M. Falkenstein, A. Kaczorowski, Y. Tolstov, H. Sultmann, C. Grulich, E. Herpel, A. Duensing, G. Kristiansen, M. Hohenfellner, N.M. Navone, and S. Duensing. 2018. FGF-2 is a driving force for chromosomal instability and a stromal factor associated with adverse clinico-pathological features in prostate cancer. *Urol Oncol*. 36:365 e315-365 e326.

- Perez-Garcia, J., E. Munoz-Couselo, J. Soberino, F. Racca, and J. Cortes. 2018. Targeting FGFR pathway in breast cancer. *Breast*. 37:126-133.
- Pin, E., G. Federici, and E.F. Petricoin, 3rd. 2014. Preparation and use of reverse protein microarrays. *Curr Protoc Protein Sci*. 75:Unit 27.27.
- Porta, R., R. Borea, A. Coelho, S. Khan, A. Araújo, P. Reclusa, T. Franchina, N. Van Der Steen, P. Van Dam, J. Ferri, R. Sirera, A. Naing, D. Hong, and C. Rolfo. 2017. FGFR a promising druggable target in cancer: Molecular biology and new drugs. *Critical Reviews in Oncology / Hematology*. 113:256-267.
- Proulx, H.R., and W.G. Donald. 2019. Bone. *In* Encyclopædia Britannica. Encyclopædia Britannica, inc.
- Puhr, M., J. Hoefer, A. Eigentler, C. Ploner, F. Handle, G. Schaefer, J. Kroon, A. Leo, I. Heidegger, I. Eder, Z. Culig, G. Van der Pluijm, and H. Klocker. 2018. The Glucocorticoid Receptor Is a Key Player for Prostate Cancer Cell Survival and a Target for Improved Antiandrogen Therapy. *Clinical cancer research*. 24:927-938.
- Putzke, A.P., A.P. Ventura, A.M. Bailey, C. Akture, J. Opoku-Ansah, M. Celiktaş, M.S. Hwang, D.S. Darling, I.M. Coleman, P.S. Nelson, H.M. Nguyen, E. Corey, M. Tewari, C. Morrissey, R.L. Vessella, and B.S. Knudsen. 2011. Metastatic progression of prostate cancer and e-cadherin regulation by zeb1 and SRC family kinases. *Am J Pathol*. 179:400-410.
- Quarles, L.D. 2012. Skeletal secretion of FGF-23 regulates phosphate and vitamin D metabolism. *Nature Reviews Endocrinology*. 8:276.
- Rane, J.K., D. Pellacani, and N.J. Maitland. 2012. Advanced prostate cancer--a case for adjuvant differentiation therapy. *Nature reviews. Urology*. 9:595-602.
- Rodan, G.A. 2003. The development and function of the skeleton and bone metastases. *Cancer*. 97:726-732.



- Roth, L., S. Srivastava, M. Lindzen, A. Sas-Chen, M. Sheffer, M. Lauriola, Y. Erika, A. Noronha, M. Mancini, S. Lavi, G. Tarcic, G. Pines, N. Nevo, O. Heyman, T. Ziv, O.M. Rueda, D. Gnocchi, E. Pikarsky, A. Admon, C. Caldas, and Y. Yarden. 2018. SILAC identifies LAD1 as a filamin-binding regulator of actin dynamics in response to EGF and a marker of aggressive breast tumors. *Science signaling*. 11.
- Ryan, M.C., J. Cleland, R. Kim, W.C. Wong, and J.N. Weinstein. 2012. SpliceSeq: a resource for analysis and visualization of RNA-Seq data on alternative splicing and its functional impacts. *Bioinformatics (Oxford, England)*. 28:2385-2387.
- Santin, A.D., F. Zhan, S. Bellone, M. Palmieri, S. Cane, E. Bignotti, S. Anfossi, M. Gokden, D. Dunn, J.J. Roman, T.J. O'Brien, E. Tian, M.J. Cannon, J. Shaughnessy, Jr., and S. Pecorelli. 2004. Gene expression profiles in primary ovarian serous papillary tumors and normal ovarian epithelium: identification of candidate molecular markers for ovarian cancer diagnosis and therapy. *Int J Cancer*. 112:14-25.
- Saura, C., D. Roda, S. Rosello, M. Oliveira, T. Macarulla, J.A. Perez-Fidalgo, R. Morales-Barrera, J.M. Sanchis-Garcia, L. Musib, N. Budha, J. Zhu, M. Nannini, W.Y. Chan, S.M. Sanabria Bohorquez, R.D. Meng, K. Lin, Y. Yan, P. Patel, J. Baselga, J. Tabernero, and A. Cervantes. 2016. A First-in-Human Phase I Study of the ATP-Competitive AKT Inhibitor Ipatasertib Demonstrates Robust and Safe Targeting of AKT in Patients with Solid Tumors. *Cancer Discovery*.
- Sethi, N., and Y. Kang. 2011. Unravelling the complexity of metastasis - molecular understanding and targeted therapies. *Nat Rev Cancer*. 11:735-748.
- Shahi, M., A. Peymani, and M. Sahmani. 2017. Regulation of Bone Metabolism. *Reports of biochemistry & molecular biology*. 5:73-82.
- Shiozawa, Y., E.A. Pedersen, A.M. Havens, Y. Jung, A. Mishra, J. Joseph, J.K. Kim, L.R. Patel, C. Ying, A.M. Ziegler, M.J. Pienta, J. Song, J. Wang, R.D. Loberg, P.H.

- Krebsbach, K.J. Pienta, and R.S. Taichman. 2011. Human prostate cancer metastases target the hematopoietic stem cell niche to establish footholds in mouse bone marrow. *J Clin Invest.* 121:1298-1312.
- Siegel, R.L., K.D. Miller, and A. Jemal. 2017. Cancer statistics, 2017. *CA: A Cancer Journal for Clinicians.* 67:7-30.
- Siegel, R.L., K.D. Miller, and A. Jemal. 2018. Cancer statistics, 2018. *CA Cancer J Clin.* 68:7-30.
- Sims, N.A., and T.J. Martin. 2014. Coupling the activities of bone formation and resorption: a multitude of signals within the basic multicellular unit. *BoneKEY reports.* 3:481.
- Smith, D.C., M.R. Smith, C. Sweeney, A.A. Elfiky, C. Logothetis, P.G. Corn, N.J. Vogelzang, E.J. Small, A.L. Harzstark, M.S. Gordon, U.N. Vaishampayan, N.B. Haas, A.I. Spira, P.N. Lara, Jr., C.C. Lin, S. Srinivas, A. Sella, P. Schoffski, C. Scheffold, A.L. Weitzman, and M. Hussain. 2013. Cabozantinib in patients with advanced prostate cancer: results of a phase II randomized discontinuation trial. *J Clin Oncol.* 31:412-419.
- Su, N., M. Jin, and L. Chen. 2014. Role of FGF/FGFR signaling in skeletal development and homeostasis: learning from mouse models. *Bone Research.* 2:14003.
- Subramanian, A., P. Tamayo, V.K. Mootha, S. Mukherjee, B.L. Ebert, M.A. Gillette, A. Paulovich, S.L. Pomeroy, T.R. Golub, E.S. Lander, and J.P. Mesirov. 2005. Gene set enrichment analysis: a knowledge-based approach for interpreting genome-wide expression profiles. *Proceedings of the National Academy of Sciences of the United States of America.* 102:15545-15550.
- Suominen, M.I., K.M. Fagerlund, J.P. Rissanen, Y.M. Konkol, J.P. Morko, Z. Peng, E.J. Alhoniemi, S.K. Laine, E. Corey, D. Mumberg, K. Ziegelbauer, S.-M. Käkönen, J.M. Halleen, R.L. Vessella, and A. Scholz. 2017. Radium-223 Inhibits Osseous

- Prostate Cancer Growth by Dual Targeting of Cancer Cells and Bone Microenvironment in Mouse Models. *Clinical Cancer Research*. 23:4335.
- Suvannasankha, A., D.R. Tompkins, D.F. Edwards, K.V. Petyaykina, C.D. Crean, P.G. Fournier, J.M. Parker, G.E. Sandusky, S. Ichikawa, E.A. Imel, and J.M. Chirgwin. 2015. FGF23 is elevated in multiple myeloma and increases heparanase expression by tumor cells. *Oncotarget*. 6:19647-19660.
- Taichman, R.S., Z. Wang, Y. Shiozawa, Y. Jung, J. Song, A. Balduino, J. Wang, L.R. Patel, A.M. Havens, M. Kucia, M.Z. Ratajczak, and P.H. Krebsbach. 2010. Prospective identification and skeletal localization of cells capable of multilineage differentiation in vivo. *Stem Cells Dev*. 19:1557-1570.
- Takarada, T., R. Nakazato, A. Tsuchikane, K. Fujikawa, T. Iezaki, Y. Yoneda, and E. Hinoi. 2016. Genetic analysis of Runx2 function during intramembranous ossification. *Development*. 143:211-218.
- Talmadge, J.E., and I.J. Fidler. 2010. AACR centennial series: the biology of cancer metastasis: historical perspective. *Cancer Res*. 70:5649-5669.
- Teishima, J., T. Hayashi, H. Nagamatsu, K. Shoji, H. Shikuma, R. Yamanaka, Y. Sekino, K. Goto, S. Inoue, and A. Matsubara. 2019. Fibroblast Growth Factor Family in the Progression of Prostate Cancer. *J Clin Med*. 8.
- Teven, C.M., E.M. Farina, J. Rivas, and R.R. Reid. 2014. Fibroblast growth factor (FGF) signaling in development and skeletal diseases. *Genes Dis*. 1:199-213.
- Tibes, R., Y. Qiu, Y. Lu, B. Hennessey, M. Andreeff, G.B. Mills, and S.M. Kornblau. 2006. Reverse phase protein array: validation of a novel proteomic technology and utility for analysis of primary leukemia specimens and hematopoietic stem cells. *Molecular cancer therapeutics*. 5:2512-2521.

- Toivanen, R., and M.M. Shen. 2017. Prostate organogenesis: tissue induction, hormonal regulation and cell type specification. *Development*. 144:1382.
- Tomlinson, D.C., and M.A. Knowles. 2010. Altered splicing of FGFR1 is associated with high tumor grade and stage and leads to increased sensitivity to FGF1 in bladder cancer. *Am J Pathol*. 177:2379-2386.
- Turajlic, S., and C. Swanton. 2016. Metastasis as an evolutionary process. *Science (New York, N.Y.)*. 352:169-175.
- Twum-Ampofo, J., D.X. Fu, A. Passaniti, A. Hussain, and M.M. Siddiqui. 2016. Metabolic targets for potential prostate cancer therapeutics. *Curr Opin Oncol*. 28:241-247.
- Valastyan, S., and R.A. Weinberg. 2011. Tumor metastasis: molecular insights and evolving paradigms. *Cell*. 147:275-292.
- Valta, M.P., T. Hentunen, Q. Qu, E.M. Valve, A. Harjula, J.A. Seppanen, H.K. Vaananen, and P.L. Harkonen. 2006. Regulation of osteoblast differentiation: a novel function for fibroblast growth factor 8. *Endocrinology*. 147:2171-2182.
- Valta, M.P., J. Tuomela, A. Bjartell, E. Valve, H.K. Vaananen, and P. Harkonen. 2008. FGF-8 is involved in bone metastasis of prostate cancer. *Int J Cancer*. 123:22-31.
- Varkaris, A., P.G. Corn, N.U. Parikh, E. Efstathiou, J.H. Song, Y.C. Lee, A. Aparicio, A.G. Hoang, S. Gaur, L. Thorpe, S.N. Maity, M. Bar Eli, B.A. Czerniak, Y. Shao, M. Alauddin, S.H. Lin, C.J. Logothetis, and G.E. Gallick. 2016. Integrating Murine and Clinical Trials with Cabozantinib to Understand Roles of MET and VEGFR2 as Targets for Growth Inhibition of Prostate Cancer. *Clinical Cancer Research*. 22:107-121.
- Vickers SM, H.Z., MacMillan-Crow L, Greendorfer JS, Thompson JA. 2002. Ligand activation of alternatively spliced fibroblast growth factor receptor-1 modulates pancreatic adenocarcinoma cell malignancy. *J Gastrointest Surg*. 6:546-553.

- Wan, X., P.G. Corn, J. Yang, N. Palanisamy, M.W. Starbuck, E. Efstathiou, E.M. Li Ning Tapia, A.J. Zurita, A. Aparicio, M.K. Ravoori, E.S. Vazquez, D.R. Robinson, Y.M. Wu, X. Cao, M.K. Iyer, W. McKeegan, V. Kundra, F. Wang, P. Troncoso, A.M. Chinnaiyan, C.J. Logothetis, and N.M. Navone. 2014. Prostate cancer cell-stromal cell crosstalk via FGFR1 mediates antitumor activity of dovitinib in bone metastases. *Sci Transl Med.* 6:252ra122.
- Wang, C., Z. Liu, Y. Ke, and F. Wang. 2019. Intrinsic FGFR2 and Ectopic FGFR1 Signaling in the Prostate and Prostate Cancer. *Frontiers in genetics.* 10:12.
- Wang, G., D. Zhao, D.J. Spring, and R.A. DePinho. 2018. Genetics and biology of prostate cancer. *Genes Dev.* 32:1105-1140.
- Wang, X., and C. Guda. 2016. Integrative exploration of genomic profiles for triple negative breast cancer identifies potential drug targets. *Medicine (Baltimore).* 95:e4321.
- Watson, P.A., V.K. Arora, and C.L. Sawyers. 2015. Emerging mechanisms of resistance to androgen receptor inhibitors in prostate cancer. *Nature reviews. Cancer.* 15:701-711.
- Weilbaeher, K.N., T.A. Guise, and L.K. McCauley. 2011. Cancer to bone: a fatal attraction. *Nat Rev Cancer.* 11:411-425.
- Wendt, M.K., M.A. Taylor, B.J. Schiemann, K. Sossey-Alaoui, and W.P. Schiemann. 2014. Fibroblast growth factor receptor splice variants are stable markers of oncogenic transforming growth factor beta1 signaling in metastatic breast cancers. *Breast Cancer Res.* 16:R24.
- Wesche, J., K. Haglund, and E.M. Haugsten. 2011. Fibroblast growth factors and their receptors in cancer. *The Biochemical journal.* 437:199-213.

- Witte, J.S. 2009. Prostate cancer genomics: towards a new understanding. *Nature Reviews Genetics*. 10:77-82.
- Xiao, L., C. Homer-Bouthiette, and M.M. Hurley. 2018. FGF23 Neutralizing Antibody Partially Improves Bone Mineralization Defect of HMWFGF2 Isoforms in Transgenic Female Mice. *Journal of bone and mineral research: the official journal of the American Society for Bone and Mineral Research*.
- Xiao, L., T. Naganawa, J. Lorenzo, T.O. Carpenter, J.D. Coffin, and M.M. Hurley. 2010. Nuclear isoforms of fibroblast growth factor 2 are novel inducers of hypophosphatemia via modulation of FGF23 and KLOTHO. *J Biol Chem*. 285:2834-2846.
- Xiao, Z., J. Huang, L. Cao, Y. Liang, X. Han, and L.D. Quarles. 2014. Osteocyte-specific deletion of Fgfr1 suppresses FGF23. *PLoS One*. 9:e104154.
- Yang, D., L. Han, and V. Kundra. 2005. Exogenous gene expression in tumors: noninvasive quantification with functional and anatomic imaging in a mouse model. *Radiology*. 235:950-958.
- Yang, J., K. Fizazi, S. Peleg, C.R. Sikes, A.K. Raymond, N. Jamal, M. Hu, M. Olive, L.A. Martinez, C.G. Wood, C.J. Logothetis, G. Karsenty, and N.M. Navone. 2001. Prostate cancer cells induce osteoblast differentiation through a Cbfa1-dependent pathway. *Cancer Res*. 61:5652-5659.
- Zafeiriou, Z., A. Jayaram, A. Sharp, and J.S. de Bono. 2016. Managing Metastatic Castration-Resistant Prostate Cancer in the Pre-chemotherapy Setting: A Changing Approach in the Era of New Targeted Agents. *Drugs*. 76:421-430.
- Zhang, Y., N. Su, F. Luo, X. Wen, Y. Tang, J. Yang, S. Chen, W. Jiang, X. Du, and L. Chen. 2014. Deletion of Fgfr1 in osteoblasts enhances mobilization of EPCs into peripheral blood in a mouse endotoxemia model. *Int J Biol Sci*. 10:1064-1071.

- Zhao, M., M.L. Zhuo, X. Zheng, X. Su, and F. Meric-Bernstam. 2019. FGFR1beta is a driver isoform of FGFR1 alternative splicing in breast cancer cells. *Oncotarget*. 10:30-44.
- Zhou, M. 2018. High-grade prostatic intraepithelial neoplasia, PIN-like carcinoma, ductal carcinoma, and intraductal carcinoma of the prostate. *Modern pathology: an official journal of the United States and Canadian Academy of Pathology, Inc.* 31:S71-79.

## **Vita**

Estefania Labanca was born in Buenos Aires, Argentina, the daughter of Elba and Ricardo Labanca. After completing her work at St. Nicholas' English School, Buenos Aires, Argentina in 2007, she entered the Universidad de Buenos Aires in Buenos Aires, Argentina. She received the degree of Bachelor of Science with a major in molecular biology from the Universidad de Buenos Aires in April, 2014. After college, she joined the Department of Genitourinary Oncology at MD Anderson Cancer Center. In August of 2015 she entered The University of Texas MD Anderson Cancer Center UTHealth Graduate School of Biomedical Sciences.